

Lactam-based π -conjugated semiconducting polymers

Citation for published version (APA):

Pruissen, van, G. W. P. (2015). *Lactam-based π -conjugated semiconducting polymers*. [Phd Thesis 1 (Research TU/e / Graduation TU/e), Chemical Engineering and Chemistry]. Technische Universiteit Eindhoven.
<https://doi.org/10.6100/IR783942>

DOI:

[10.6100/IR783942](https://doi.org/10.6100/IR783942)

Document status and date:

Published: 01/01/2015

Document Version:

Publisher's PDF, also known as Version of Record (includes final page, issue and volume numbers)

Please check the document version of this publication:

- A submitted manuscript is the version of the article upon submission and before peer-review. There can be important differences between the submitted version and the official published version of record. People interested in the research are advised to contact the author for the final version of the publication, or visit the DOI to the publisher's website.
- The final author version and the galley proof are versions of the publication after peer review.
- The final published version features the final layout of the paper including the volume, issue and page numbers.

[Link to publication](#)

General rights

Copyright and moral rights for the publications made accessible in the public portal are retained by the authors and/or other copyright owners and it is a condition of accessing publications that users recognise and abide by the legal requirements associated with these rights.

- Users may download and print one copy of any publication from the public portal for the purpose of private study or research.
- You may not further distribute the material or use it for any profit-making activity or commercial gain
- You may freely distribute the URL identifying the publication in the public portal.

If the publication is distributed under the terms of Article 25fa of the Dutch Copyright Act, indicated by the "Taverne" license above, please follow below link for the End User Agreement:

www.tue.nl/taverne

Take down policy

If you believe that this document breaches copyright please contact us at:

openaccess@tue.nl

providing details and we will investigate your claim.

Lactam-based π -conjugated semiconducting polymers

PROEFSCHRIFT

ter verkrijging van de graad van doctor aan de Technische Universiteit Eindhoven, op
gezag van de rector magnificus prof.dr.ir. C.J. van Duijn, voor een commissie aangewezen
door het College voor Promoties, in het openbaar te verdedigen op donderdag 15 januari

2015 om 16:00 uur

door

Gijsbrecht Willem Philippus van Pruissen

geboren te Tilburg

Dit proefschrift is goedgekeurd door de promotoren en de samenstelling van de promotiecommissie is als volgt:

voorzitter:	prof.dr.ir. J.C. Schouten
1 ^e promotor:	prof.dr.ir. R.A.J. Janssen
copromotor:	dr.ir. M.M. Wienk
leden:	prof.dr. D. Vanderzande (Universiteit Hasselt) prof.dr. A.E. Rowan (Radboud Universiteit) prof.dr. M. Heeney (Imperial College London) prof.dr. A.P.H.J. Schenning
adviseur:	dr. J.A.J.M. Vekemans

A catalogue record is available from the Eindhoven University of Technology Library

ISBN: 978-90-386-3762-4

Printed by Gildeprint, Enschede



This work was funded by:



The work was supported by the *Europees Fonds voor Regionale Ontwikkeling* (EFRO) in the Interreg IV A project Organext. The research forms part of the Solliance OPV programme and has received funding from the Ministry of Education, Culture and Science (Gravity program 024.001.035).

Table of Contents

Table of Contents	5
Chapter 1. Introduction	7
1.1 Background	8
1.2 Organic photovoltaics	9
1.3 Field-effect transistors	16
1.4 Designing polymers.....	18
1.5 Outline of this thesis	21
1.6 References	23
Chapter 2. Increasing fused ring systems in isoindigo-based π-conjugated polymers	27
2.1 Introduction	28
2.2 Aim	30
2.3 Results and discussion	31
2.4 Conclusion.....	39
2.5 Experimental.....	40
2.6 Acknowledgements	44
2.7 References	45
Chapter 3. Thienoisindigo for small band gap polymers	47
3.1 Introduction	48
3.2 Aim	49
3.3 Results and discussion	49
3.4 Conclusion.....	54
3.5 Experimental.....	55
3.6 Acknowledgements	59
3.7 References	60
Chapter 4. High ambipolar charge carrier mobility in benzodipyrrolidone conjugated polymers	63
4.1 Introduction	64
4.2 Aim	66
4.3 Results and discussion	66
4.4 Conclusions	79
4.5 Experimental.....	79
4.6 Acknowledgements	82
4.7 References	83

Chapter 5. The effects of cross conjugation in copolymers of isoindigo and thienothiophene	85
5.1 Introduction	86
5.2 Aim	87
5.3 Results and discussion	88
5.4 Conclusions	100
5.5 Experimental.....	101
5.6 References	106
Chapter 6. Pentacyclic lactam as a building block for wide band gap materials	109
6.1 Introduction	110
6.2 Aim	111
6.3 Results and discussion	112
6.4 Conclusion.....	120
6.5 Experimental.....	120
6.6 Acknowledgements	123
6.7 References	124
Chapter 7. Wide band gap TPD materials for tandem solar cells	125
7.1 Introduction	126
7.2 Aim	127
7.3 Results and discussion	128
7.4 Conclusions	137
7.5 Experimental.....	138
7.6 Acknowledgements	141
7.7 References	142
Summary	145
Samenvatting	148
Curriculum Vitae	153
List of publications.....	155
Dankwoord.....	157

Chapter 1.

Introduction

1.1 Background

The world population increased over the past decades to seven billion,¹ which, combined with an economic uprise of developing countries, poses a major claim on earth's limited resources. Fossil fuels for energy production and metals and rare earth elements for construction and production of luxury goods are mined excessively. Devastation by mining activities and global warming arising from emission of greenhouse gasses are worldwide threats to the environment. In addition, the foreseen depletion of some of these resources in the short term and midterm,² make it inevitable to change the way energy and goods are produced. Given that the *homo sapiens* population is estimated to grow to ten billion by 2050,¹ a sustainable and peaceful future global society involves production in an energy and material efficient way, with abundant materials and from sustainable resources.

Organic materials based on carbon, hydrogen, nitrogen, oxygen, and, to a lesser extend sulfur and phosphorus, form an interesting alternative. Nature shows the versatility of these elements with countless different molecules that have biological and physical function and organic chemistry extends the possibilities with the synthesis of new materials such as pharmaceuticals, dyes, and plastics. Since the discovery that plastics based on conjugated polymers can have semiconducting and metallic properties,³ they have attracted attention for application in organic photovoltaics (OPVs)⁴⁻⁷ field-effect transistors (OFETs)⁸⁻¹⁰ and light-emitting diodes (OLEDs).^{11,12} OPV and OLED devices can contribute to a more sustainable future by converting sunlight into electricity (OPV) and offering energy efficient lighting and display applications (OLED). The possibility to process these materials from inks allows for flexible, cheap, roll-to-roll printing with minimal energy and material usage.

The research in OLED technology has already resulted in brightly colored displays and lighting applications that are commercially available in mobile phones, tablets, televisions, and in designer lighting. For OPV and OFET however, there is still a need for better performing materials, i.e. higher power conversion efficiency (PCE) for OPV and better charge mobility for OFET applications.

A promising and relatively new class of semiconducting polymers for both OPV and FET applications is formed by polymers based on diketopyrrolopyrrole (DPP). As a result there is a fast-growing interest in DPP-based polymers as evidenced from the yearly number of publications (Figure 1.1). Ketopyrrole, or lactam, is the defining chemical structure in this type of polymers. The lactams make conjugated systems highly colored

due to the push-pull interaction of the nitrogen and carbonyl moieties with the conjugated π -electrons. Furthermore they are electron deficient, flat, and are likely enhancing stacking via dipole interactions. There are many ways imaginable to incorporate lactams in conjugated polymers (Figure 1.1) and derivatives such as isoindigo and thienopyrroledione have been investigated from 2010 onwards. For the design of high performing materials it is of interest to explore the synthesis, properties, and application in (opto)electronic devices of novel lactam-based π -conjugated polymers. This is the prime objective of this thesis.

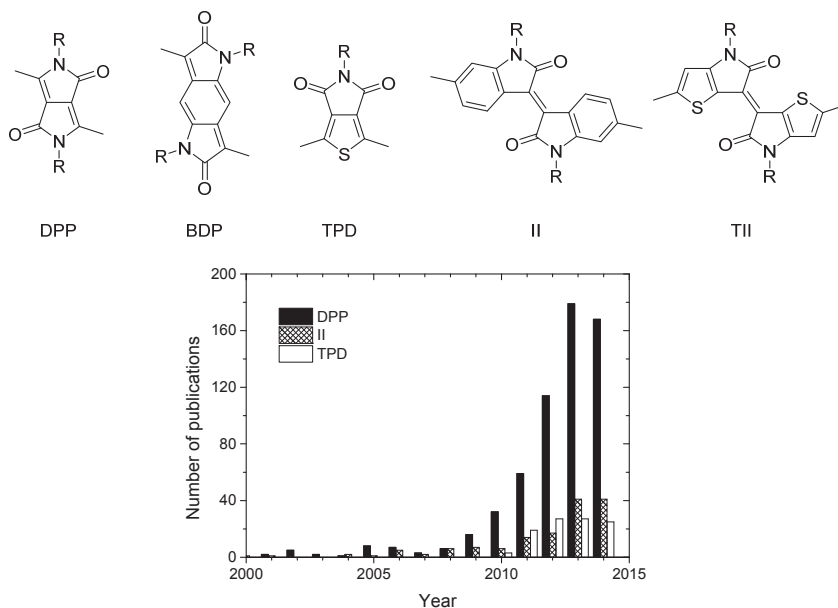


Figure 1.1 – Top: Structures of pyrrolo[3,4-*c*]pyrrole-1,4-dione (or diketopyrrolopyrrole, DPP), benzo[1,2-*b*:4,5-*b'*]dipyrrole-2,6(1*H*,5*H*)-dione (BDP), thieno[3,4-*c*]pyrrole-4,6-dione (TPD), isoindigo (II) and thienoisindigo (TII). Bottom: Number of publications per year on diketopyrrolopyrrole (DPP, black), isoindigo (II, hatched) and thienopyrroledione (TPD, white) as found by a search on Web of Science (September 2014) with these search terms.

1.2 Organic photovoltaics

1.2.1 Historic overview

That light can have electrical effects in materials was first recognized in 1839 by Becquerel.¹³ The so called photovoltaic effect was used more than a century later, in 1954

by Chapin *et al.*¹⁴ in Bell Laboratories, to make the first silicon-based solar cell. This marks the start of the silicon solar cell technology that currently dominates the commercial market. Nowadays an efficiency of 25.6% can be realized with single crystal silicon,¹⁵ which is approaching the Shockley – Queisser limit of ~30% for a single junction solar cell with a 1.1 eV band gap absorber.¹⁶ In this theoretical study the maximum achievable efficiency is approximated assuming that every photon from the AM1.5G solar spectrum with energy higher than the band gap, contributes one electron to the photocurrent at a voltage similar to the band gap.

Many other materials and techniques have been developed in the past decades based on III-V materials such as gallium arsenide (GaAs, 28.8%), chalcogenides such as copper indium gallium selenide (CIGS, 20.5%) and cadmium telluride (CdTe, 19.6%), hybrid organic inorganic dye sensitized solar cells (11.9%), perovskites (17.9%),¹⁷ and organic photovoltaics (9.5%).¹⁸ The high price of scarce elements such as indium and gallium or the public's opinion on the use of toxic elements such as cadmium or lead (perovskites) can threaten the wide application of these high performing techniques. For organic-based techniques commercialization only becomes viable when higher efficiencies can be realized.

1.2.2 Working principle

The development of OPV starts with the Nobel Prize winning discovery of conjugated (semi) conducting polymers.³ The first solar cells based on conjugated molecules however showed really low performance <1%.¹⁹ Absorption of light in organic molecules excites an electron from the highest occupied molecular orbital (HOMO) to the lowest unoccupied molecular orbital (LUMO). Due to the low dielectric constant of organic materials this results in strong Coulombically bound electron-hole pairs known as excitons (Figure 1.2, step 1). This in contrast to the inorganic semiconductors where light absorption results in the excitation of an electron from the valence band to the conduction band, where the electron and hole are only weakly bound ($< kT$) and easy to separate by a p-n junction. To separate the charges of the strongly bound exciton an additional driving force is needed. An effective way to provide this driving force is to place a different molecule with stronger electron affinity, i.e. a lower LUMO, in close vicinity of the exciton so that it can diffuse to the interface (step 2). At the interface an energetically more favorable state is present for the electron, i.e. the LUMO of the acceptor. This results in charge (electron) transfer from the donor molecule to the acceptor molecule (step 3). In 1986 Tang was the first to

demonstrate this by applying a bilayer of copper phthalocyanine (donor) and a perylene tetracarboxylic derivative (acceptor) as active layer in a solar cell with $PCE = 1\%$.²⁰ Later the same photoinduced electron transfer was shown for conjugated polymers and fullerenes.²¹ The hole and electron are now spatially separated and can move independently through the donor phase and acceptor phase as free charges (Step 4). Charges are transported to their electrodes under influence of an internal electric field that arises from the different work functions of the electrodes (step 5) where they are finally collected to deliver power to an external circuit (step 6). Note that the complementary process, i.e. absorption in the acceptor and hole transfer to the donor, is equivalent and results in the same charge transfer state (step 3).

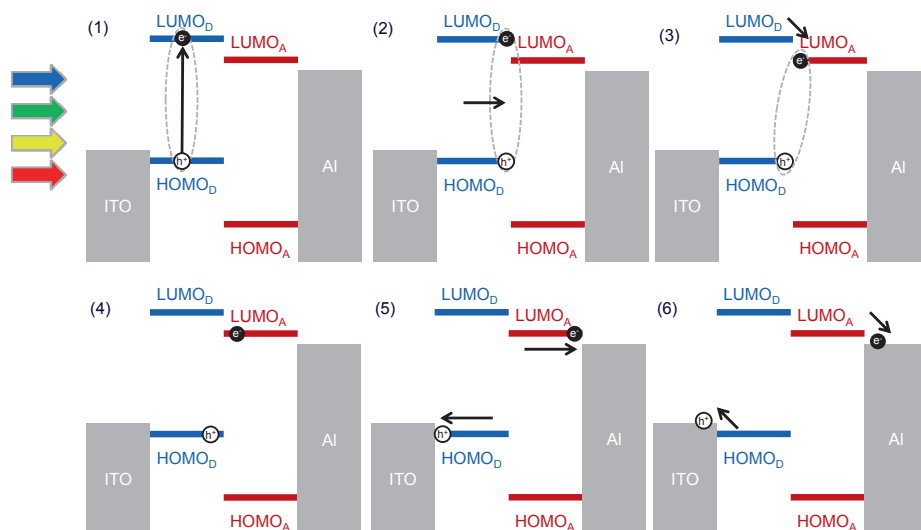


Figure 1.2 – Schematic energy diagrams for the basic operation steps in OPV. (1) Excitation of an electron by the absorption of light and formation of an exciton. (2) Diffusion of the exciton to a donor – acceptor interface. (3) Charge transfer by hopping of the electron to the lower LUMO of the acceptor. (4) Charges are separated as free charges. (5) Transport of charges to their respective electrodes. (6) Charge collection at the electrodes, delivering power to an external circuit.

1.2.3 Morphology

In order to achieve a good efficiency every exciton should reach an interface where it dissociates in free charges that can contribute to the photocurrent. Decay via radiative and non-radiative processes make that excited states have a limited lifetime and therefore can only diffuse a maximum distance of about 5–10 nm.²²⁻²⁴ This implies a maximum layer thickness of 10–20 nm. This is, however, insufficient to absorb all the light. The bulk heterojunction (BHJ) concept, intimately mixing conjugated polymers as donor with C₆₀ fullerene acceptors (see magnification Figure 1.3), was introduced in 1995.²⁵⁻²⁷ The BHJ is now widely applied with a better soluble C₆₀ derivative [6,6]-phenyl-C₆₁-buteric acid methyl ester (PC₆₀BM)²⁸ and its PC₇₀BM derivative for better light absorption properties (Scheme 1.1).²⁹

The mixing of donor and acceptor materials is a crucial parameter for the PCE as a 10–20 nm thick intertwining network with good percolation to the electrodes has to be created. Molecular properties such as molecular weight,³⁰ polydispersity,³¹ regio-chemistry,^{32,33} and purity³⁴⁻³⁶ determined during synthesis play an important role, but processing conditions such as concentration, solvent choice,³⁷ co-solvent,³⁸⁻⁴¹ and drying time^{42,43} also have strong influence on the initial morphology formation, while post processing techniques such as thermal annealing⁴⁴ or solvent annealing⁴⁵ can further manipulate the morphology.

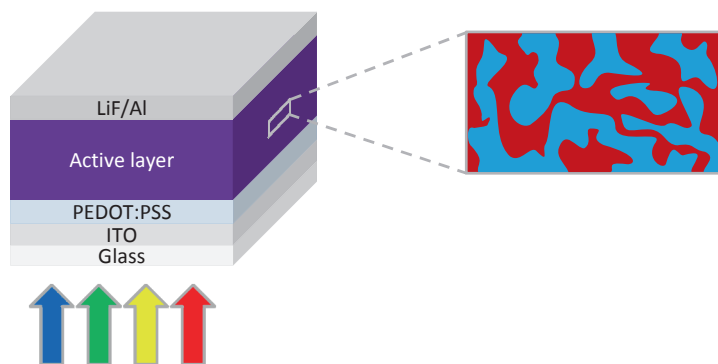


Figure 1.3 - Schematic device layout of OPV devices: glass substrate, transparent indium tin oxide (ITO) contact, transparent hole conducting layer of poly(3,4-ethylenedioxythiophene):poly(styrene sulfonate) (PEDOT:PSS), bulk heterojunction active layer schematically represented in the magnification, top electrode with lithium fluoride and aluminum.

1.2.4 Characterization

To characterize the performance of solar cells a current density – voltage ($J - V$) curve is measured, sweeping the voltage while the sample is illuminated with 100 mW/cm^2 simulated AM1.5G solar spectrum. This is a standard spectrum and intensity that represents the light of one sun that has passed through 1.5 times the thickness of the earth's atmosphere. The resulting curve is described by a few characteristic points that are described in Figure 1.4. The voltage at zero current density is called open-circuit voltage V_{oc} and similarly the current density at zero voltage is called short-circuit current density J_{sc} . These represent the maximum photocurrent density and the maximum photovoltage that can be obtained from the solar cell without external bias. The power density delivered by the cell is given by equation 1.

$$P_{out} = V \times J \quad (1)$$

Therefore the power density is zero when the cell operates at V_{oc} or J_{sc} , but moving along the $J - V$ curve the product of current density and voltage somewhere reaches a maximum. This point is called the maximum power point (MPP) and the corresponding voltage and current density are denoted as V_{mpp} and J_{mpp} .

$$P_{mpp} = V_{mpp} \times J_{mpp} \quad (2)$$

To express the maximum power output of the cell in terms of easy measurable quantities like V_{oc} and J_{sc} the fill factor (FF) is defined as the ratio between the maximum power and the virtual power when the maximum current density would be achieved at the maximum voltage. The FF is the ratio between the areas of the two rectangles in Figure 1.4.

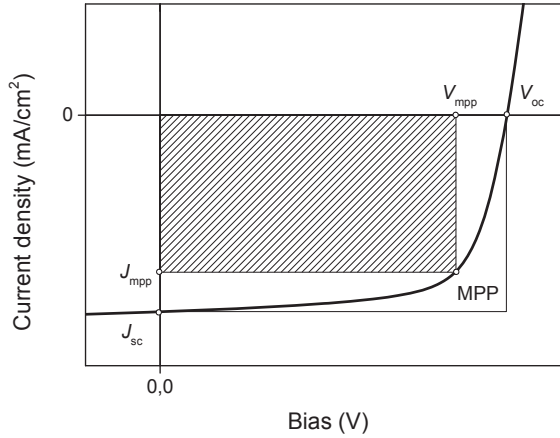


Figure 1.4 – Typical $J - V$ characteristic of an OPV device under illumination with performance parameters indicated.

$$FF = \frac{J_{mpp} \times V_{mpp}}{J_{sc} \times V_{oc}} \quad (3)$$

The efficiency of a cell can now be denoted in terms of V_{oc} , J_{sc} , and FF. The power conversion efficiency (PCE) is the ratio of the power that is delivered by the cell and the input power from the solar radiation.

$$\eta = \frac{P_{mpp}}{P_{in}} = \frac{J_{sc} \times V_{oc} \times FF}{P_{in}} = \text{PCE} \quad (4)$$

Since it is experimentally challenging to exactly simulate the AM1.5G spectrum and measure precisely at 100 mW/cm^2 , the measured $J - V$ curve has to be corrected for spectral and light intensity mismatches. Therefore the spectral response of the cell is measured and compared to that of a calibrated reference cell to determine the external quantum efficiency (EQE) of the cell. The EQE is the efficiency by which the cell converts photons of a specific wavelength that arrive at the front side of the cell into electrons in the external circuit. By integrating the product of the EQE and the spectral irradiance of the AM1.5G spectrum over all wavelengths, the correct J_{sc} can be estimated and used to determine the PCE of the cell under standardized conditions.

$$J_{sc} = \frac{e}{hc} \int \text{EQE}(\lambda) \text{AM1.5G}(\lambda) \lambda d\lambda \quad (5)$$

1.2.5 Design rules for optimization

The efficiency limits for a traditional solar cell were outlined by Shockley and Queisser from a detailed balance analyses assuming that every photon with an energy higher than the optical band gap ($E > E_g$) is absorbed and contributes one electron to the photocurrent at a voltage similar to the band gap.¹⁶ Based on these assumptions an optimum band gap for solar cells can be determined based on the AM1.5G spectrum. A high band gap will result in low currents as most of the photons will be lost as they have insufficient energy to excite an electron. A smaller band gap increases the number of absorbed photons, and therefore the current. However it decreases the voltage and all high energy photons will lose a significant part of their energy via thermalization to the lowest excited state (Figure 1.5). This set of assumptions and the thermodynamic limits have been translated to the operation principle of organic solar cells both empirically and fundamentally, as reviewed by Janssen and Nelson.⁴⁶

Scharber *et al.* were the first to formulate clear design rules for donor polymers in polymer/PCBM BHJ solar cells.⁴⁷ Based on the empirical relation between V_{oc} and the difference between the HOMO level of the donor and LUMO level of the acceptor (ΔE_{HL}).

$$qV_{oc} = \Delta E_{HL} - 0.3q = \left| E_{\text{HOMO}_{\text{donor}}} - E_{\text{LUMO}_{\text{acceptor}}} \right| - 0.3q \quad (6)$$

The 0.3 eV loss is attributed to losses in the transport and charge collection at the electrodes. Furthermore a minimum required LUMO – LUMO offset (ΔE_{Ll}) and HOMO – HOMO offset (ΔE_{Hh}) of 0.3 eV were assumed for efficient charge transfer. Equivalently, the V_{oc} can be directly related to E_g describing the total energy loss. In this description, all losses larger than 0.6 eV can be considered as avoidable.

$$E_g - qV_{oc} \geq 0.6 \text{ eV} \quad (7)$$

To predict power conversion efficiencies an EQE of 0.65 and a FF of 0.65 were taken as realistic estimates. Such analysis shows that theoretical efficiencies over 10% can be expected for polymers with a band gap of ~ 1.5 eV and $\Delta E_{LL} = 0.3$ eV.^{46,47}

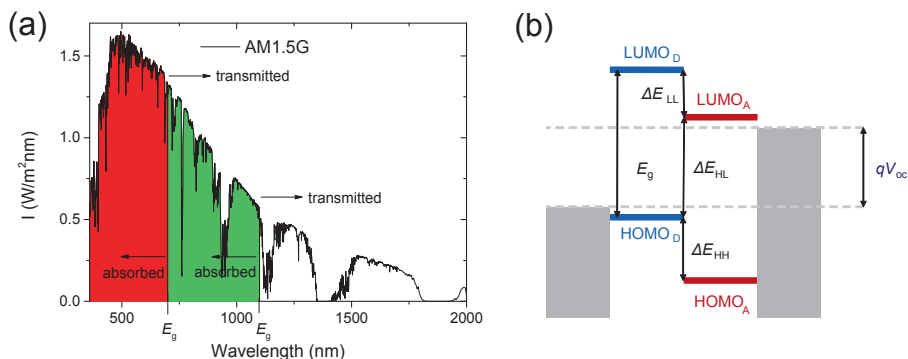


Figure 1.5 – (a) Absorption and transmission of photons from the AM1.5G spectrum for different E_g and (b) energy level diagram of a donor-acceptor solar cell and the important offsets in material optimization.

Thermodynamic losses can be reduced using a tandem or multi-junction device layout. Absorption of high energy photons with a wide band gap material reduces thermal losses while transmitted photons can be absorbed by a second small band gap material and still contribute to the output power. The same design rules used for single junction cells can be applied to tandem solar cells, leading to predicted efficiencies of about 15% for a tandem with band gaps of ~ 1.6 eV and ~ 1.3 eV.⁴⁸

1.3 Field-effect transistors

Field-effect transistors form the main electronic component in virtually all modern electronic circuits. In their most fundamental form they consist of a metal electrode that is separated from a semiconductor by an insulator (MISFET). Despite the wide application of silicon-based FETs, there is an interesting niche market for printable and flexible applications that has been explored extensively over the past decades.^{10,49} Here π -conjugated organic materials can function as the semiconducting active layer in these devices as was shown already in the 1980s for organic thin film transistors (OTFT).⁵⁰⁻⁵²

By applying a voltage to the gate electrode a thin layer of charges, either electrons or holes, can be induced in the active layer. If a voltage over the source and drain is present, a

current will flow between the source and drain that can be modulated by the gate voltage, allowing for more or less charges in the active layer. Key property for high performance are the mobility μ of the charges in the active layer and the on/off ratio of the transistor. The current – voltage relation is given by the following two equations.

$$I_{SD} = \frac{\mu CW}{L} \left((V_{GS} - V_{th})V_{DS} - \frac{V_{DS}^2}{2} \right) \quad (8)$$

for $V_{GS} - V_{th} > V_{DS}$ (linear regime)

$$I_{SD} = \frac{\mu CW}{2L} (V_{GS} - V_{th})^2 \quad (9)$$

for $V_{DS} > V_{GS} - V_{th} > 0$ (saturated regime)

Here I_{SD} is the source-drain current, μ is the charge mobility, C is the capacitance of the gate dielectric that separates the gate electrode from the semiconductor channel, W and L are respectively the width and length of the channel, and V_{GS} , V_{th} , and V_{DS} are the voltages between gate and source, the threshold voltage, and voltage between source and drain, respectively.

The charge mobility μ can vary over several decades for different materials but also depends on specific device architecture. Four different device layouts are commonly used: i.e. bottom-gate bottom-contact (coplanar), bottom-gate top-contact (staggered), top-gate bottom-contact (staggered), and top-gate top-contact (coplanar) (Figure 1.6). Each has its own advantages and disadvantages but generally higher mobilities are measured in devices with a staggered structure, because the electric field over the active layer can enhance charge injection compared to coplanar architectures.⁵³

For most conjugated polymers only hole transport is measured, while electron transport is less common but dominates in e.g. fullerenes. Recently, ambipolar materials have been developed by decreasing the band gap that can be operated as electron or hole conducting device.⁵⁴

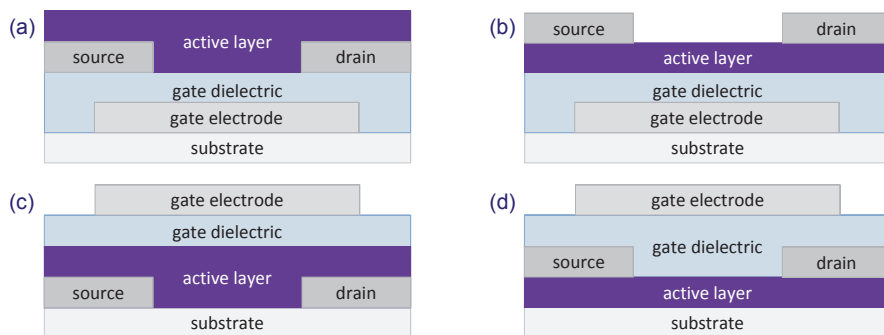


Figure 1.6 – Different organic thin film transistor device architectures. (a) Bottom-gate bottom-contact device layout. (b) Bottom-gate top-contact device layout. (c) Top-gate bottom-contact device layout and (d) top-gate top-contact device layout.

1.4 Designing polymers

The archetype polymers for organic electronics are poly(*p*-phenylenevinylene)⁵⁵ and poly(3-alkylthiophene) (P3HT)⁵⁶ (Scheme 1.1). These are however poorly adjusted to the design rules outlined in previous paragraphs, mainly due to their wide band gaps. In designing new conjugated polymers, several parameters must be considered. The most relevant electronic parameters are the optical band gap, redox levels, and charge carrier mobility, but materials properties such as solubility, molecular weight, and tendency to form ordered aggregates or semi-crystalline domains are likewise important.

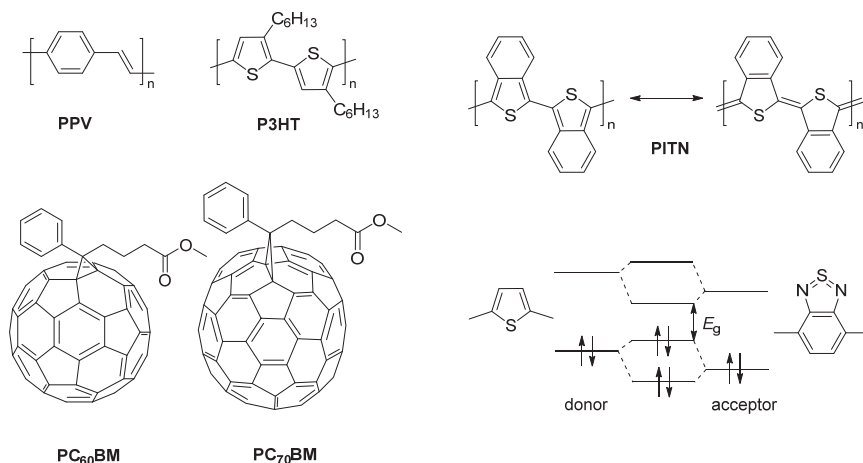
One design strategy to lower the band gap, i.e. reduce the bond length alternation, is to stabilize the quinoid resonance structure. Introduction of fused rings to the polymer backbone that are not in the main chain and that gain aromaticity when the polymer adopts a quinoid form, effectively reduces the energy difference between both states and results in small band gap materials such as polyisothianaphthalenes (Scheme 1.1).⁵⁷

The leading design motif for controlling the optical band gap and energy levels of conjugated semiconducting polymers is the alternation of electron rich and electron deficient units along the chain as pioneered by Havinga^{58,59} and Tanaka.⁶⁰ To first order this can be explained by a simple molecular orbital representation. Hybridization of the frontier orbital levels of the donor and acceptor monomers results in new molecular orbitals with a significant decrease of the band gap (Scheme 1.1). In these push-pull systems the LUMO of the acceptor primarily determines the LUMO of the resulting polymer whereas the HOMO is mainly determined by the HOMO of the donor. This gives

easy control because individual orbital levels can now be adjusted by exchange with a stronger or weaker donor or acceptor monomer.

For the electron rich unit conjugated oligomers are often used. These commonly combine benzene, thiophene, pyrrole, furan, or combinations thereof as building blocks, sometimes in fused ring configurations. Fusing rings enhances co-planarity which is favorable for good π - π stacking and π -conjugation along the backbone.

For the electron deficient unit, aromatic heterocycles such as quinoxalines,⁶¹ thienopyrazines,⁶² thieno(3,4-*b*)thiophenes,^{63, 64} and benzothiadiazole that contain electron withdrawing nitrogen atoms have been effective.^{7,65,66} Note that most of these acceptors also have fused rings to stabilize quinoid resonance structures. In recent years, the incorporation of cyclic amides or imids has been established as a very effective way to combine strong electron accepting properties with a tendency to provide close intermolecular packing. This favors small optical band gaps and high charge carrier mobilities and has resulted in exceptionally good performance in OFETs and OPV cells.^{67, 68} Examples of these new acceptor units are diketopyrrolopyrrole,^{69 - 71} benzodipyrrolidiones,⁷² thienopyrroledione,⁷³⁻⁷⁵ and isoindigo⁷⁶⁻⁷⁹ as shown in Figure 1.1.

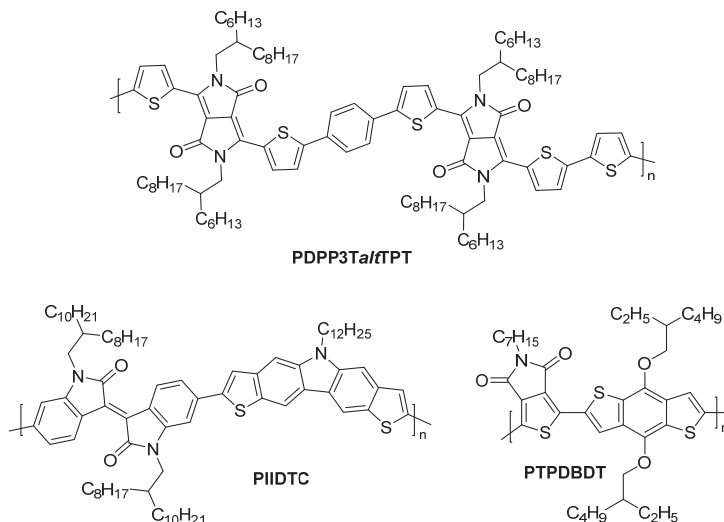


Scheme 1.1 – Chemical structures of poly(*p*-phenylenevinylene) (PPV) and poly(3-hexylthiophene) (P3HT) as archetype wide band gap conjugated polymers. Polyisothianaphthalene (PITN) in its ground state with non-aromatic benzene and its quinoid resonance structure with aromatic benzene rings. Structure of electron acceptor PC₆₀BM and PC₇₀BM. Schematic energy level diagram of the recombination of molecular orbital levels in a donor-acceptor system. Thiophene and benzothiadiazole are shown as typical example.

1.4.1 Current top materials based on lactam acceptors

The fast development of new lactam-based materials in the past 4 – 5 years (Figure 1.1) is accompanied with many milestone achievements. A thorough review on the many amide and imide derived materials was recently published, giving an excellent overview.⁸⁰ Some of the highlights for different acceptors are summarized here.

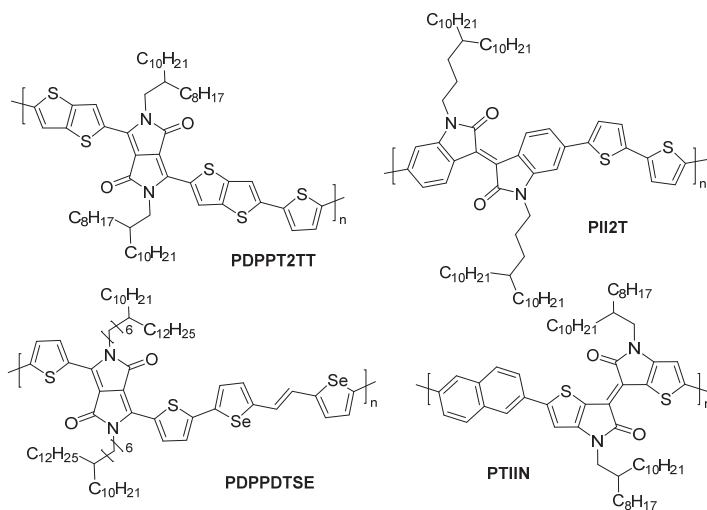
Careful fine tuning of the frontier orbital levels in DPP-based terpolymers with two different donor segments resulted in devices with PCE of 8% (Scheme 1.2).³⁰ Isoindigo-based materials recently also surpassed the 8% PCE mark with a copolymer incorporating a dithienocarbazole (DTC) donor unit.⁸¹ For polymers with thienopyrroledione (TPD) and benzodithiophene a PCE of 8.5% has been achieved after careful optimization of the side chain length and branching point.⁸²



Scheme 1.2 – Lactam-based materials that all show over 8% PCE in OPV devices.

Also the application of lactam-based materials in OFETs has seen major improvements over the past years. With development of new materials, mobilities in the order of 1–10 cm²/Vs have been achieved.⁸³ For a DPP-based polymer with flanking thienothiophenes a hole mobility (μ_h) of 1.95 cm²/Vs was achieved (Scheme 1.3).⁸⁴ Further fine tuning of co-monomer and side chain branching point have resulted in a DPP polymer with $\mu_h = 12$ cm²/Vs.⁸⁵ That tuning the branching point can help improve the hole mobility was also shown in isoindigo-based materials were in a PII2T polymer $\mu_h = 3.62$ cm²/Vs was measured when the branching point was at the fourth carbon in the side chain.⁸⁶ That the

isoindigo motif is a promising structure was further shown for a thienoisindigo that, when copolymerized with naphthalene affords mobilities as high as $\mu_h = 14.4 \text{ cm}^2/\text{Vs}$.⁸⁷



Scheme 1.3 – Lactam-based materials with high hole mobilities with PDPPDTSE and PTIIN even surpassing $10 \text{ cm}^2/\text{Vs}$.

1.5 Outline of this thesis

Inspired by the good performance of DPP-based materials in optoelectronic devices, it is the aim of this thesis to explore different electron-deficient lactam-based units in donor-acceptor conjugated polymers and assess their properties and performance in OPV and OFET devices.

The influence of increasing donor blocks on solubility and OPV device performance is assessed for isoindigo-based polymers in Chapter 2. Synthesis of a thiophene-flanked isoindigo monomer and polymerization with thiophene, thieno[3,2-*b*]thiophene, and benzo[1,2-*b*:4,5-*b'*]dithiophene is presented. The influence of aggregation and solubility on processing conditions and device performance are investigated.

In Chapter 3 thienoisindigo is developed as a structural derivative of isoindigo. The properties of different copolymers with thienoisindigo are compared with their isoindigo analogs and tested in OFET devices to assess their conducting properties.

In the next chapter benzodipyrrolidone (BDP) is developed as a lactam acceptor unit with a quinoid ground state. The combination of these features make BDP a strong

acceptor that can be used in ambipolar OFETs. Here the influence of different oligothiophene (nT) donors on electron and hole mobility in OFETs is investigated in copolymers with BDP.

The donor – acceptor and aromatic – quinoid approach are generally used design principles to obtain small band gap materials and influence the HOMO and LUMO levels. In Chapter 5 the influence of cross conjugation in conjugated donor – acceptor polymers is investigated as an additional tool to manipulate optical and electrochemical properties. The influence of cross conjugation on optical and electrochemical properties of four isomeric isoindigo and thienothiophene model polymers is investigated both experimentally and theoretically with density functional theory (DFT) calculations to obtain insight in the underlying principles at work.

In Chapter 6 a new lactam-based acceptor with five fused heterocycles is explored that is a promising candidate for wide band gap materials in tandem solar cell front cells. To reduce the high energy loss that these polymers exhibit, the pentacyclic lactam acceptor is combined with co-monomers that have different electron affinity. Polymerization with strong donors (thiophene, thieno[3,2-*b*]thiophene, and dithiophene), weak donors (benzene and benzo[1,2-*b*:4,5-*b'*]dithiophene) and a strong acceptor (benzothiadiazole), was performed and the resulting polymers were assessed in OPV devices.

The last chapter explores thienopyrroledione (TPD) acceptors for wide band gap materials in tandem front cells. Three new copolymers with thiophene, thienothiophene, and benzene were made with a thiophene-flanked TPD monomer and applied in single junction devices. Furthermore a different TPD polymer with benzodithiophene was adapted from literature and applied in a tandem solar cell that was modeled and measured experimentally.

1.6 Reference

- ¹ United Nations, Department of Economic and Social Affairs, Population Division (2014). World Population Prospects: The 2012 Revision, Methodology of the United Nations Population Estimates and Projections. ESA/P/WP.235.
- ² A. Valero and A. Valero, *Resour. Conserv. Recy.*, **2010**, *54*, 1074-1083.
- ³ H. Shirakawa, E. J. Louis, A. G. Macdiarmid, C. K. Chiang, and A. J. Heeger, *J. Chem. Soc. Chem. Commun.* **1977**, 578-580.
- ⁴ S. Günes, H. Neugebauer, and N. S. Sariciftci, *Chem. Rev.*, **2007**, *107*, 1324-1338.
- ⁵ H. Zhou, L. Yang, and W. You, *Macromolecules*, **2012**, *45*, 607-632.
- ⁶ R. S. Kularatne, H. D. Magurudeniya, P. Sista, M. C. Biewer, and M. C. Stefan, *J. Polym. Sci. A.*, **2013**, *51*, 743-768.
- ⁷ C. Duan, F. Huang and Y. Cao, *J. Mater. Chem.*, **2012**, *22*, 10416-10434.
- ⁸ C. D. Dimitrakopoulos and P. R. L. Malenfant, *Adv. Mater.*, **2002**, *14*, 99-117.
- ⁹ W. Wu, Y. Liu, and D. Zhu, *Chem. Soc. Rev.*, **2010**, *39*, 1489-1502.
- ¹⁰ G. Horowitz, *Adv. Mater.*, **1998**, *10*, 365-337.
- ¹¹ R. H. Friend, R. W. Gymer, A. B. Holmes, J. H. Burroughes, R. N. Marks, C. Taliani, D. D. C. Bradley, D. A. D. Santos, J. L. Bredas, M. Logdlund, and W. R. Salaneck, *Nature*, **1999**, *397*, 121-128.
- ¹² A. Kraft, A. C. Grimsdale, and A. B. Holmes, *Angew. Chem., Int. Ed.*, **1998**, *37*, 402-428.
- ¹³ A. E. Becquerel, *Comptes Rendus*, **1839**, *9*, 561-567.
- ¹⁴ D. M. Chapin, C. S. Fuller, and G. L. Pearson, *J. Appl. Phys.*, **1954**, *25*, 676-677.
- ¹⁵ Panasonic Press Release, 10 April 2014. Panasonic HIT® solar cell achieves world's highest energy conversion efficiency of 25.6% at research level. (<http://panasonic.co.jp/corp/news/official.data/data.dir/2014/04/en140410-4/en140410-4.html>; accessed 25 September 2014).
- ¹⁶ W. Shockley and H. J. Queisser, *J. Appl. Phys.*, **1961**, *32*, 510-519.
- ¹⁷ M. A. Green, K. Emery, Y. Hishikawa, W. Warta, and E. D. Dunlop, *Prog. Photovoltaics Res. Appl.*, **2014**, *22*, 701-710.
- ¹⁸ L. Ye, S. Zhang, W. Zhao, H. Yao, and J. Hou, *Chem. Mater.*, **2014**, *26*, 3603-3605.
- ¹⁹ G. A. Chamberlain, *Sol. Cells*, **1983**, *8*, 47-83.
- ²⁰ C. W. Tang, *Appl. Phys. Lett.*, **1986**, *48*, 183-185.
- ²¹ N. S. Sariciftci, L. Smilowitz, A. J. Heeger, and F. Wudl, *Science* **1992**, *258*, 1474-1476.
- ²² A. Haugeneder, M. Neges, C. Kallinger, W. Spirkl, U. Lemmer, J. Feldmann, U. Scherf, E. Harth, A. Gügel, and K. Müllen, *Phys. Rev. B*, **1999**, *59*, 15346-15351.
- ²³ M. Theander, A. Yartsev, D. Zigmantas, V. Sundström, W. Mammo, M. R. Andersson, and O. Inganäs, *Phys. Rev. B*, **2000**, *61*, 12957-12963.
- ²⁴ D. E. Markov, E. Amsterdam, P. W. M. Blom, A. B. Sieval, and J. C. Hummelen, *J. Phys. Chem. A*, **2005**, *109*, 5266-5274.
- ²⁵ N. S. Sariciftci and A. J. Heeger, University of California, US Patent, 5331183, **1994**.
- ²⁶ J. J. M. Halls, C. A. Walsh, N. C. Greenham, E. A. Marseglia, R. H. Friend, S. C. Moratti, and A. B. Holmes, *Nature*, **1995**, *376*, 498-500.
- ²⁷ G. Yu, J. Gao, J. C. Hummelen, F. Wudl, and A. J. Heeger, *Science*, **1995**, *270*, 1789-1791.
- ²⁸ J. C. Hummelen, B. W. Knight, F. LePeq, F. Wudl, J. Yao, and C. L. Wilkins, *J. Org. Chem.*, **1995**, *60*, 532-538.
- ²⁹ M. M. Wienk, J. M. Kroon, W. J. H. Verhees, J. Knol, J. C. Hummelen, P. A. van Hal, and R. A. J. Janssen, *Angew. Chem., Int. Ed.*, **2003**, *42*, 3371-3375.
- ³⁰ K. H. Hendriks, G. H. L. Heintges, V. S. Gevaerts, M. M. Wienk, and R. A. J. Janssen, *Angew. Chem., Int. Ed.*, **2013**, *52*, 8341-8344.

- ³¹ M. Koppe, C. J. Brabec, S. Heiml, A. Schausberger, W. Duffy, M. Heeney, and I. McCulloch, *Macromolecules*, **2009**, *42*, 4661-4666.
- ³² Y. Kim, S. Cook, S. M. Tuladhar, S. A. Choulis, J. Nelson, J. R. Durrant, D. D. C. Bradley, M. Giles, I. McCulloch, C. S. Ha, and M. Ree, *Nat. Mater.*, **2006**, *5*, 197-203.
- ³³ K. H. Hendriks, W. Li, G. H. L. Heintges, G. W. P. van Pruissen, M. M. Wienk, and R. A. J. Janssen, *J. Am. Chem. Soc.*, **2014**, *136*, 11128-11133.
- ³⁴ J. Kettle, M. Horie, L. A. Majewski, B. R. Saunders, S. Tuladhar, J. Nelson, and M. L. Turner, *Sol. Energy Mater. Sol. Cells*, **2011**, *95*, 2186-2193.
- ³⁵ S. Van Mierloo, A. Hadipour, M.-J. Spijkman, N. Van den Brande, B. Ruttens, J. Kesters, J. D'Haen, G. Van Assche, D. M. de Leeuw, T. Aernouts, J. Manca, L. Lutsen, D. J. Vanderzande, and W. Maes, *Chem. Mater.*, **2012**, *24*, 587-593.
- ³⁶ W. R. Mateker, J. D. Douglas, C. Cabanetos, I. T. Sachs-Quintana, J. A. Bartelt, E. T. Hoke, A. El Labban, P. M. Beaujuge, J. M. J. Frechet, and M. D. McGehee, *Energy Environ. Sci.*, **2013**, *6*, 2529-2537.
- ³⁷ S. E. Shaheen, C. J. Brabec, N. S. Sariciftci, F. Padinger, T. Fromherz, and J. C. Hummelen, *Appl. Phys. Lett.*, **2001**, *78*, 841-843.
- ³⁸ A. J. Moulé and K. Meerholz, *Adv. Mater.*, **2008**, *20*, 240-245.
- ³⁹ W. Wang, H. Wu, C. Yang, C. Luo, Y. Zhang, J. Chen, and Y. Cao, *Appl. Phys. Lett.*, **2007**, *90*, 183512.
- ⁴⁰ F. Zhang, K. G. Jespersen, C. Björström, M. Svensson, M. R. Andersson, V. Sundström, K. Magnusson, E. Moons, A. Yartsev, and O. Inganäs, *Adv. Funct. Mater.*, **2006**, *16*, 667-674.
- ⁴¹ J. Peet, J. Y. Kim, N. E. Coates, W. L. Ma, D. Moses, A. J. Heeger, and G. C. Bazan, *Nat. Mater.*, **2007**, *6*, 497-500.
- ⁴² G. Li, V. Shrotriya, J. Huang, Y. Yao, T. Moriarty, K. Emery, and Y. Yang, *Nat. Mater.*, **2005**, *4*, 864-868.
- ⁴³ B. Schmidt-Hansberg, M. Sanyal, M. F. G. Klein, M. Pfaff, N. Schnabel, S. Jaiser, A. Vorobiev, E. Müller, A. Colmann, P. Scharfer, D. Gerthsen, U. Lemmer, E. Barrena, and W. Schabel, *ACS Nano*, **2011**, *5*, 8579-8590.
- ⁴⁴ F. Padinger, R. S. Rittberger, and N. S. Sariciftci, *Adv. Funct. Mater.*, **2003**, *13*, 85-88.
- ⁴⁵ M. Campoy-Quiles, T. Ferenczi, T. Agostinelli, P. G. Etchegoin, Y. Kim, T. D. Anthopoulos, P. N. Stavrinou, D. D. C. Bradley, and J. Nelson, *Nat. Mater.*, **2008**, *7*, 158-164.
- ⁴⁶ R. A. Janssen and J. Nelson, *Adv. Mater.*, **2013**, *25*, 1847-1858.
- ⁴⁷ M. C. Scharber, D. Mühlbacher, M. Koppe, P. Denk, C. Waldauf, A. J. Heeger, and C. J. Brabec, *Adv. Mater.*, **2006**, *18*, 789-794.
- ⁴⁸ G. Dennler, M. C. Scharber, T. Ameri, P. Denk, K. Forberich, C. Waldauf, and C. J. Brabec, *Adv. Mater.*, **2008**, *20*, 579-583.
- ⁴⁹ H. Klauk, *Chem. Soc. Rev.*, **2010**, *39*, 2643-2666.
- ⁵⁰ A. Tsumura, H. Koezuka, and T. Ando, *Appl. Phys. Lett.*, **1986**, *49*, 1210-1212.
- ⁵¹ K. Kudo, M. Yamashina, and T. Moriizumi, *Jpn. J. Appl. Phys.*, **1984**, *23*, 130-130.
- ⁵² C. Clarisse, M. T. Riou, M. Gauneau, and M. I. Contellec, *Electron. Lett.*, **1988**, *24*, 674-675.
- ⁵³ K. Chang Hyun, Y. Bonnassieux, and G. Horowitz, *Electron Dev. Lett., IEEE*, **2011**, *32*, 1302-1304.
- ⁵⁴ T. D. Anthopoulos, S. Setayesh, E. Smits, M. Cölle, E. Cantatore, B. de Boer, P. W. M. Blom, and D. M. de Leeuw, *Adv. Mater.*, **2006**, *18*, 1900-1904.
- ⁵⁵ H. Becker, H. Spreitzer, W. Kreuder, E. Kluge, H. Schenk, I. Parker, and Y. Cao, *Adv. Mater.*, **2000**, *12*, 42-48.
- ⁵⁶ A. Marrocchi, D. Lanari, A. Facchetti, and L. Vaccaro, *Energy Environ. Sci.*, **2012**, *5*, 8457-8474.
- ⁵⁷ F. Wudl, M. Kobayashi, and A. J. Heeger, *J. Org. Chem.*, **1984**, *49*, 3382-3384.
- ⁵⁸ E. E. Havinga, W. Ten Hoeve, and H. Wynberg, *Polym. Bull.*, **1992**, *29*, 119-126.
- ⁵⁹ E. E. Havinga, W. Ten Hoeve, and H. Wynberg, *Synth. Met.*, **1993**, *55*, 299-306.

- ⁶⁰ C. Kitamura, S. Tanaka, and Y. Yamashita, *Chem. Mater.*, **1996**, *8*, 570-578.
- ⁶¹ A. Gadisa, W. Mammo, L. M. Andersson, S. Admassie, F. Zhang, M. R. Andersson, and O. Inganäs, *Adv. Funct. Mater.*, **2007**, *17*, 3836-3842.
- ⁶² Y. Zhu, R. D. Champion, and S. A. Jenekhe, *Macromolecules*, **2006**, *39*, 8712-8719.
- ⁶³ Y. Y. Liang, Z. Xu, J. B. Xia, S. T. Tsai, Y. Wu, G. Li, C. Ray, and L. P. Yu, *Adv. Mater.*, **2010**, *22*, E135-E138.
- ⁶⁴ Y. Liang, D. Feng, Y. Wu, S.-T. Tsai, G. Li, C. Ray, and L. Yu, *J. Am. Chem. Soc.*, **2009**, *131*, 7792-7799.
- ⁶⁵ J. Chen and Y. Cao, *Acc. Chem. Res.*, **2009**, *42*, 1709-1718.
- ⁶⁶ Y.-J. Cheng, S.-H. Yang and C.-S. Hsu, *Chem. Rev.*, **2009**, *109*, 5868-5923.
- ⁶⁷ L. Biniek, B. C. Schroeder, C. B. Nielsen, and I. McCulloch, *J. Mater. Chem.*, **2012**, *22*, 14803-14813.
- ⁶⁸ P.-L. T. Boudreault, A. Najari, and M. Leclerc, *Chem. Mater.*, **2011**, *23*, 456-469.
- ⁶⁹ L. Bürgi, M. Turbiez, R. Pfeiffer, F. Bienewald, H. J. Kirner, and C. Winnewisser, *Adv. Mater.*, **2008**, *20*, 2217-2224.
- ⁷⁰ M. M. Wienk, M. Turbiez, J. Gilot, and R. A. J. Janssen, *Adv. Mater.*, **2008**, *20*, 2556-2560.
- ⁷¹ J. C. Bijleveld, A. P. Zoombelt, S. G. J. Mathijssen, M. M. Wienk, M. Turbiez, D. M. de Leeuw, and R. A. J. Janssen, *J. Am. Chem. Soc.*, **2009**, *131*, 16616-16617.
- ⁷² W. Cui, J. Yuen, and F. Wudl, *Macromolecules*, **2011**, *44*, 7869-7873.
- ⁷³ Y. Zhang, S. K. Hau, H.-L. Yip, Y. Sun, O. Acton, and A. K.-Y. Jen, *Chem. Mater.*, **2010**, *22*, 2696-2698.
- ⁷⁴ Y. Zou, A. Najari, P. Berrouard, S. Beaupré, B. Réda Aïch, Y. Tao, and M. Leclerc, *J. Am. Chem. Soc.*, **2010**, *132*, 5330-5331.
- ⁷⁵ C. Piliago, T. W. Holcombe, J. D. Douglas, C.H. Woo, P. M. Beaujuge, and J. M. J. Fréchet, *J. Am. Chem. Soc.*, **2010**, *132*, 7595-7597.
- ⁷⁶ J. Mei, K. R. Graham, R. Stalder, and J. R. Reynolds, *Org. Lett.* **2010**, *12*, 660-663.
- ⁷⁷ R. Stalder, J. Mei, and J. R. Reynolds, *Macromolecules*, **2010**, *43*, 8348-8352.
- ⁷⁸ E. Wang, Z. Ma, Z. Zhang, P. Henriksson, O. Inganäs, F. Zhang, and M. R. Andersson, *Chem. Commun.*, **2011**, *47*, 4908-4910.
- ⁷⁹ E. G. Wang, Z. Ma, Z. Zhang, K. Vandewal, P. Henriksson, O. Inganäs, F. Zhang, and M. R. Andersson, *J. Am. Chem. Soc.* **2011**, *133*, 14244-14247.
- ⁸⁰ X. Guo, A. Facchetti, and T. J. Marks, *Chem. Rev.*, **2014**, *114*, 8943-9021.
- ⁸¹ Y. Deng, J. Liu, J. Wang, L. Liu, W. Li, H. Tian, X. Zhang, Z. Xie, Y. Geng, and F. Wang, *Adv. Mater.*, **2014**, *26*, 471-476.
- ⁸² C. Cabanetos, A. El Labban, J. A. Bartelt, J. D. Douglas, W. R. Mateker, J. M. J. Fréchet, M. D. McGehee, and P. M. Beaujuge, *J. Am. Chem. Soc.*, **2013**, *135*, 4656-4659.
- ⁸³ I. McCulloch, M. Heeney, M. L. Chabiny, D. DeLongchamp, R. J. Kline, M. Cölle, W. Duffy, D. Fischer, D. Gundlach, B. Hamadani, R. Hamilton, L. Richter, A. Salleo, M. Shkunov, D. Sparrowe, S. Tierney, and W. Zhang, *Adv. Mater.*, **2009**, *21*, 1091-1109.
- ⁸⁴ H. Bronstein, Z. Chen, R. S. Ashraf, W. Zhang, J. Du, J. R. Durrant, P. Shakya Tuladhar, K. Song, S. E. Watkins, Y. Geerts, M. M. Wienk, R. A. J. Janssen, T. Anthopoulos, H. Sirringhaus, M. Heeney, and I. McCulloch, *J. Am. Chem. Soc.*, **2011**, *133*, 3272-3275.
- ⁸⁵ I. Kang, H.-J. Yun, D. S. Chung, S.-K. Kwon, and Y.-H. Kim, *J. Am. Chem. Soc.*, **2013**, *135*, 14896-14899.
- ⁸⁶ T. Lei, J.-H. Dou, and J. Pei, *Adv. Mater.*, **2012**, *24*, 6457-6461.
- ⁸⁷ G. Kim, S.-J. Kang, G. K. Dutta, Y.-K. Han, T. J. Shin, Y.-Y. Noh, and C. Yang, *J. Am. Chem. Soc.*, **2014**, *136*, 9477-9483.

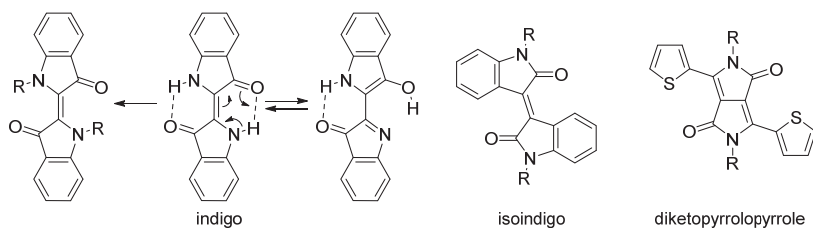
Chapter 2.

Increasing fused ring systems in isoindigo-based π -conjugated polymers

Isoindigo (II) has recently emerged as a successful electron deficient unit in conjugated polymers for organic photovoltaics. High performing materials with suitable frontier orbital energy levels and excellent electronic properties have been obtained when II alternates with oligothiophenes (nT). Here we assess the influence of incorporating fused aromatic ring systems (X = thiophene, thieno[3,2-b]thiophene, or benzo[1,2-b:4,5-b']dithiophene) as electron rich unit in alternating copolymers with II as electron deficient unit. These polymers show increased aggregation behavior and decreased solubility when increasing the fused ring system. The polymers were used as electron donor in polymer solar cells in combination with PC₇₀BM. Power conversion efficiencies up to 5.6% were achieved for a polymer with thieno[3,2-b]thiophene.

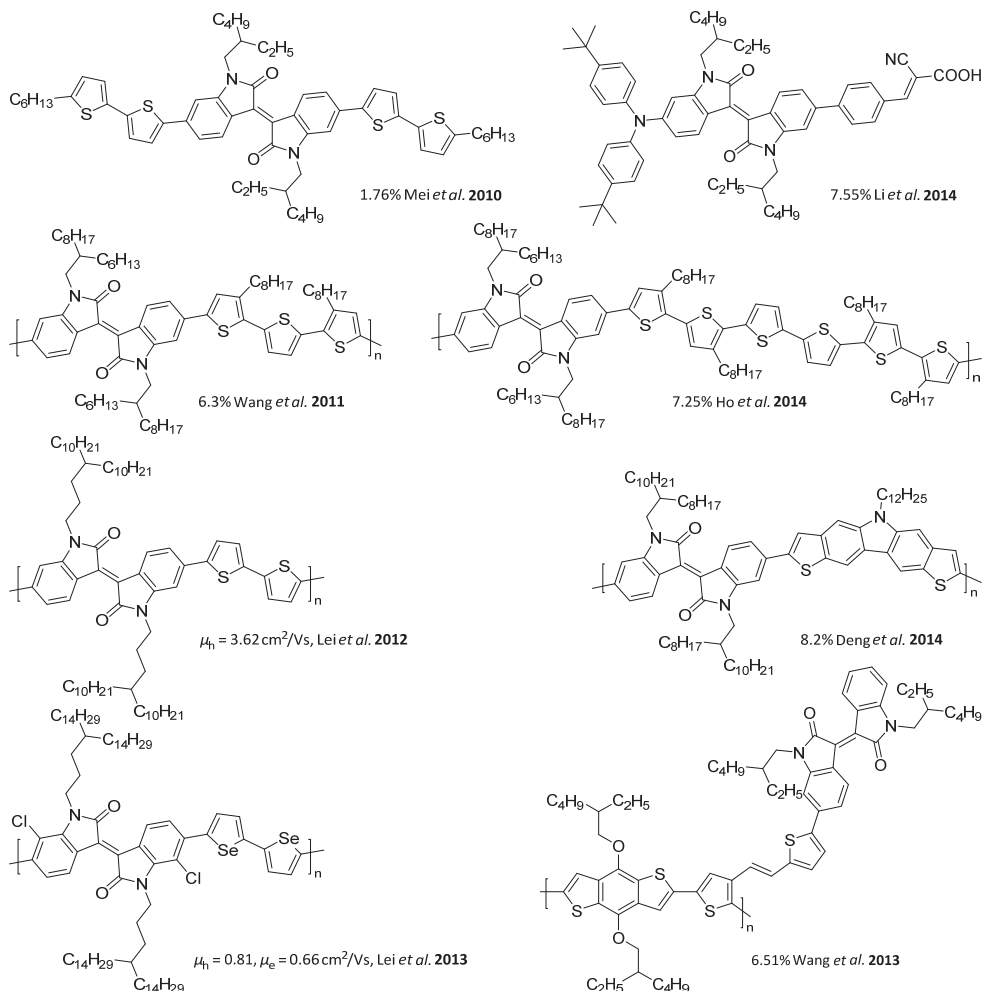
2.1 Introduction

Already in ancient times mankind made use of the natural blue pigment indigo and nowadays it is still used as the blue dye coloring denim.¹ Indigo has a strong red-shifted absorption because of the conjugated system of donor (NR₃) and acceptor groups (C=O) linked by the central double bond.² The benzene rings can be π -conjugated to this chromophore via tautomerization (Scheme 2.1).³ Such conjugation is needed for electronic interaction over this unit in π -conjugated polymers. However *N*-alkylation for solubilizing side chains hampers the tautomerization, and hence breaks the conjugation along the polymer backbone. To meet both requirements, solubility and conjugation along the chain, without using *N*-alkylation is synthetically challenging. A structural isomer of indigo, isoindigo (II), is already fully conjugated without tautomerization, leaving the possibility for *N*-alkylation and hence incorporation in soluble conjugated polymers. Isoindigo was first synthesized and patented as a dye in 1921 by Stollé.^{4,5}



Scheme 2.1 – From left to right structures of: the cross-conjugated alkylated indigo; the natural pigment indigo; the tautomerized fully conjugated indigo; isoindigo (II); and diketopyrrolopyrrole (DPP).

The lactam rings of II, are similar to those in the successful electron acceptor diketopyrrolopyrrole (DPP),⁶ which performs excellent in donor-acceptor (D-A) conjugated polymers for various organic electronic applications.⁷ The first application of II in organic photovoltaics (OPV) made use of D-A-D conjugated molecules.⁸ These triads (Scheme 2.2) showed reasonable good power conversion efficiencies (PCE) up to 1.76% demonstrating the feasibility of II-based materials. Later, efficiency of OPV devices with small molecules incorporating II gradually increased to a present maximum of 3.3%.⁹⁻¹⁶



Scheme 2.2 – First isoindigo-based D-A-D small molecule (top left) and subsequent high performing isoindigo-based materials for DSSC (top right), bulk heterojunction polymer/PCBM OPV and OFET.

Polymer-based materials generally show a higher PCEs in OPV owing to some inherent features such as a long conjugation length, higher viscosity which helps in the formation a good blend morphology, and good interconnectivity between crystalline domains. The first D-A copolymers combining II with different donors were synthesized shortly after the first small molecules.¹⁷ The vast number of possible donors resulted in many more examples of II-based polymers that were tested in OPV.¹⁸⁻³⁶

Polymers incorporating thiophene donors stand out with excellent PCEs that go up from 6.3% for a PII3T²⁵ and to 7.25% for a PII6T.³⁷ Interesting chemical modifications such as the introduction of polystyrene side chains³⁸ and halogenations of II³⁹ yielded polymers that also performed over 7%. Alternating the II unit with a different acceptor in D-A₁-D-A₂ systems also showed good results^{40,41} and, interestingly, a polymer using II as conjugated side chains to the conjugated backbone was able to give a 6.51% PCE.⁴² The ultimate II copolymer so far is achieved when II is combined with a dithienocarbazole (DTC) to give 7.2% PCE in a regular device and a PCE of 8.2% in an inverted geometry (Scheme 2.2).⁴³

Not only has II proven its value in bulk heterojunction solar cells, but also dye sensitized solar cells (DSSC) have benefited from new sensitizing dyes based on II,⁴⁴⁻⁴⁶ showing a very promising 7.55% PCE for II with a diphenylamine donor.⁴⁷

Besides the use in OPV materials, II has also been applied to OFET devices⁴⁸⁻⁵⁶ where it gives high and balanced ambipolar charge mobility in a polymer with chlorinated II ($\mu_h = 0.81$ and $\mu_e = 0.66$ cm²/Vs).⁵⁷ Furthermore it was shown that the hole mobility can be increased to 3.62 cm²/Vs by systematically moving the branching point in the alkyl side chains further away from the polymer backbone (Scheme 2.2).⁵⁸

2.2 Aim

The work in this chapter is largely based on the early high PCE polymer PII3T that is a promising candidate for further development and fine tuning. Besides well-tuned band gap and frontier orbital energy levels, it was already shown that good performing materials need a balance between high molecular weight, which requires solubility during polymerization and processing, and good π - π stacking with minimum electronically insulating alkyl side chains. We investigate this by systematically increasing the donor block from a central thiophene via thieno[3,2-b]thiophene, of which a promising 4.7% example has been published meanwhile,⁵⁹ to a benzo[1,2-*b*:4,5-*b'*]dithiophene core and evaluating the effect on OPV performance.

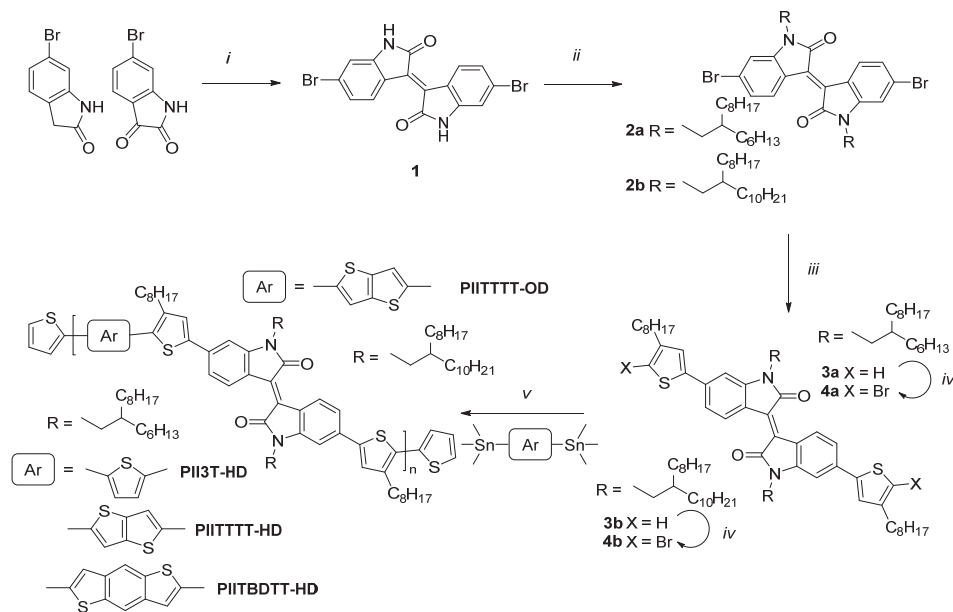
2.3 Results and discussion

2.3.1 Synthesis of isoindigo polymers

II can be synthesized from the 6-bromoisatin and 6-bromooxindole by an Aldol condensation under acidic conditions.⁶⁰ This affords unsubstituted II **1** (Scheme 2.3) in good yield. From the possible *E* and *Z* isomers only the *E* isomer is formed as is evidenced by IR and ¹³C NMR. Alkyl side chains are attached at the amide nitrogen of the poorly soluble **1** using branched alkyl bromides with different length. For good solubility of the polymers, 2-hexyldecyl or even longer 2-octyldecyl side chains are used to give **2a** and **2b** respectively. The isoindigo is then extended using 4,4,5,5-tetramethyl-2-(4-octylthiophen-2-yl)-1,3,2-dioxaborolane via a Suzuki cross coupling reaction to give **3a** and **3b** that were both brominated with *N*-bromosuccinimide (NBS) resulting in extended isoindigo monomers **4a** and **4b**, similar to the method used by Wang *et al.*²⁵ For **4a** and **4b** a silica column and subsequent recrystallization from ethanol gives the required purity for polymerizations.

Using the extended II monomers various alternating co-polymers were synthesized using donor blocks with increasing size: thiophene (T), thieno[3,2-*b*]thiophene (TT), and benzo[1,2-*b*:4,5-*b'*]dithiophene (BDT). For convenience the polymers are named PII3T-HD, PIITTTT-HD, PIITTTT-OD, and PIITBDTT-HD, where HD and OD are respectively the 2-hexyldecyl and 2-octyldecyl side chains on the II (Scheme 2.3). Prior to polymerization all monomers were recrystallized to ensure the highest possible purity. Stille coupling was used with tris(dibenzylideneacetone)dipalladium(0) (Pd₂dba₃) and triphenylphosphine (PPh₃) (1:4) as catalyst in toluene/dimethylformamide (DMF) to afford purple polymers. These were purified using Soxhlet extraction to remove residual catalyst and low molecular weight fractions and finally precipitated in methanol.

Already during product collection after Soxhlet extraction some differences in solubility became apparent. Both PII3T-HD and PIITTTT-OD could be collected in hot chloroform, but for PIITTTT-HD and PIITBDTT-HD chlorinated solvents with higher boiling point were needed such as *ortho*-dichlorobenzene (ODCB) and 1,1,2,2-tetrachloroethane (TCE) respectively.



Scheme 2.3 – Synthesis of thiophene-extended isoindigo monomers and polymers. (i) HCl, AcOH, 120 °C, 15-18 h, 94%. (ii) 2-hexyldecyl-1-bromide or 2-octyldecyl-1-bromide, K₂CO₃, DMF, 100 °C, 15-18 h, 80%. (iii) 4,4,5,5-tetramethyl-2-(4-octylthiophen-2-yl)-1,3,2-dioxaborolane, K₃PO₄, Pd₂dba₃, PPh₃, Aliquat 336, toluene/water (9/1), 115 °C, 15-18 h, 59-86%. (iv) NBS, dichloromethane (DCM), 0 °C to room temperature, to completion, typical ~85%, (v) Equimolar quantities of 2,5-bis(trimethylstannyl)thiophene, or 2,5-bis(trimethylstannyl)thieno[3,2-*b*]thiophene, or 2,6-bis(trimethylstannyl)benzo[1,2-*b*:4,5-*b'*]dithiophene and 4, Pd₂dba₃, PPh₃, toluene/DMF (9/1), 115 °C, overnight.

2.3.2 Characterization of isoindigo polymers

From the UV-vis-NIR absorption spectra, measured for chloroform solution and thin films on glass, the optical band gaps of these polymers are determined. The polymers with thiophene and thieno[3,2-*b*]thiophene show very similar absorption spectra with band gaps of 1.58 eV for PII3T-HD and PIITTTT-HD and 1.62 eV for PIITTTT-OD, while the benzo[1,2-*b*:4,5-*b'*]dithiophene copolymer has a somewhat larger band gap of 1.67 eV (Figure 2.1 and Table 2.1). The spectra in solution and thin film look very similar for all polymers, indicating strong aggregation in solution. PIITTTT-HD and PIITBDTT-HD show clear vibrational features as shoulders on both sides of the peak maximum. This is indicative for the anticipated better π - π stacking for polymers with extended aromatic

electron-rich co-monomers. The other polymers show less distinguished features. The clear difference between PIITTTT-HD and PIITTTT-OD demonstrates that solubility is another key parameter governing the stacking behavior.

The strong tendency of these polymers to aggregate in solution makes it challenging to determine the correct molecular weight via gel permeation chromatography (GPC). At room temperature some materials are insoluble, others are eluded as aggregates at short retention volumes, overestimating the molecular weight. However, these aggregates can be molecularly dissolved by raising the temperature. Figure 2.2 a shows the chromatograms of PIITTTT-HD recorded at different temperatures, using chloroform as eluent. At low temperature, two distinct peaks are obtained; the one at low retention volume is attributed to polymer aggregates, as it reduces in relative intensity with increasing temperatures. At a temperature as high as 145 °C, only the peak of the molecularly dissolved polymer chain remains.⁶¹ PIITTTT-OD displays very similar temperature dependent behavior. The main difference is the retention volume for the aggregate peak, which is, in contrast to the peak of the molecularly dissolved material, substantially larger than for PIITTTT-HD. This indicates that the aggregates of the better soluble PIITTTT-OD are significantly smaller than that of PIITTTT-HD. However, no quantification of the size of the aggregates can be made, since the elution volumes are outside the range of reliable weight determination for this column.

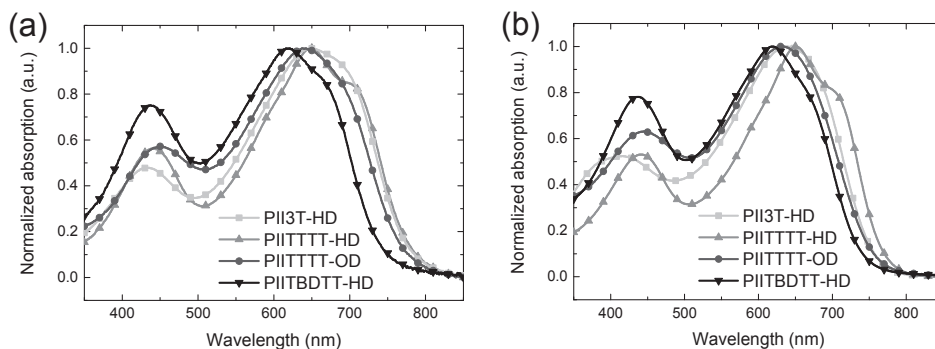


Figure 2.1 – UV-vis-NIR absorption of isoindigo polymers (a) as thin films on glass and (b) in chloroform solutions.

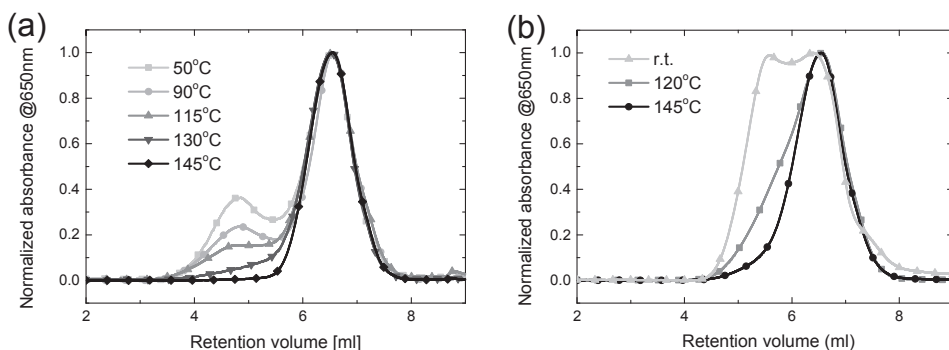


Figure 2.2 – Gel permeation chromatography of PIITTTT-HD (a) and PIITTTT-OD (b) in CHCl_3 at different temperatures showing the breakup of aggregates. From the different onsets of aggregate elution larger aggregates for PIITTTT-HD can be expected.

For a quantitative comparison of all PIIX materials, GPC measurements were carried out at a fixed elevated (140 °C) temperature, using ODCB as eluent. The polymers show number average molecular weights of 97.7, 33.4, 45.0, and 21.5 kg/mol for PII3T-HD, PIITTTT-HD, PIITTTT-OD, and PIITBDTT-HD, respectively. The lower molecular weight for the poorly soluble polymers is most likely the result of precipitation during the polymerization reaction. As soon as the polymer precipitates its elongation is terminated.

Cyclic voltammetry was used to determine the onsets of oxidation and reduction potentials of the respective PIIX polymers versus the ferrocene/ferrocenium redox couple. Using these redox potentials the HOMO and LUMO levels were estimated using $E = -5.23 - qE_{\text{redox}}$ (Table 2.1).⁶² For PII3T the HOMO is determined to be at -5.43 eV and the LUMO at -3.90 eV versus the vacuum level. This implies that the offset to the LUMO of [6,6]-phenyl- C_{71} -butyric acid methyl ester (PC_{70}BM) (-4.15 eV), which is commonly used as acceptor in polymer solar cells, is slightly less than the minimum of 0.3 eV, required for photoinduced electron transfer. For PIITTTT-HD and PIITTTT-OD very similar HOMO (-5.42 and -5.41 eV) and LUMO levels (-3.76 and -3.78 eV) are found. The slightly higher LUMO can increase the driving force for charge separation and increase J_{sc} while similar V_{oc} can be expected based on the HOMO levels. For PIITBDTT-HD a significantly lower HOMO is found at -5.53 eV, which should lead to higher V_{oc} but since the LUMO level is lowered to -3.94 eV the LUMO-LUMO offset with PC_{70}BM drops well below 0.25 eV.

Table 2.1 – Characteristics of PIIX polyisoindigo polymers

Polymer	M_n kg/mol	PDI	$\lambda_{\max}^{\text{film}}$ nm	E_g^{sol} eV	E_g^{film} eV	E_{HOMO}^a eV	E_{LUMO}^a eV	$E_g^{\text{cv}b}$ eV
PII3T-HD	97.7	4.2	648	1.63	1.58	-5.43	-3.90	1.53
PIITTTT-HD	33.4	2.0	647	1.61	1.58	-5.42	-3.76	1.66
PIITTTT-OD	45.0	2.7	642	1.64	1.62	-5.41	-3.78	1.62
PIITBDDT-HD	21.5	2.0	621	1.69	1.67	-5.53	-3.94	1.59

^a Onset potentials vs. Fc/Fc^+ converted via: $E = -5.23 - qE_{\text{redox}}$. ^b $E_g^{\text{cv}} = q(E_{\text{ox}} - E_{\text{red}})$.

2.3.3 Organic photovoltaics

The HOMO and LUMO levels and related band gaps of the PIIX isoindigo polymers make them very suitable candidates to be combined with PC_{70}BM as electron acceptor in junction solar cells.⁶³ Photovoltaic cells were made and optimized in a regular polarity device architecture with a stack design of glass/ITO(115 nm)/PEDOT:PSS(35 nm)/active layer(80–120 nm)/LiF(1 nm)/Al(100 nm). Although these polymers are electronically very similar, device optimization led to quite different optimal processing conditions for all polymers. Their different solubility requires different solvent combinations and temperatures to achieve optimal film morphology blends with PC_{70}BM . The current density – voltage (J - V) characteristics and external quantum efficiency (EQE) of all optimized devices are shown in Figure 2.3 and the relevant solar cell parameters are collected in Table 2.2.

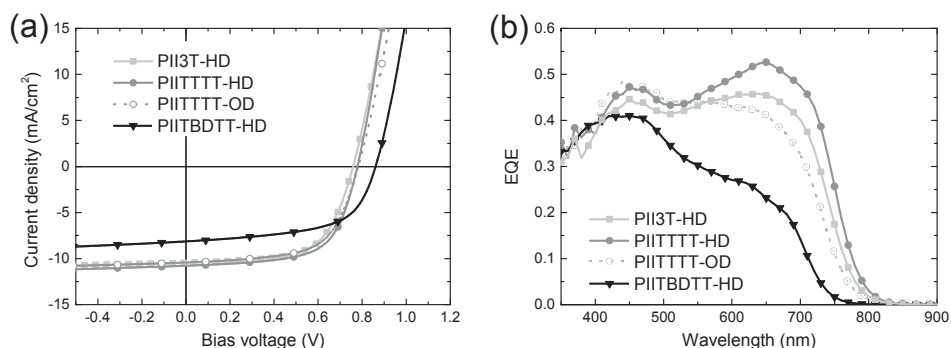


Figure 2.3 – J – V Characteristics of optimized solar cells (a) and the corresponding EQE of the devices (b).

The processing conditions for PII3T-HD were optimized by spin coating the photoactive blend from chloroform or ODCB, using diiodooctane (DIO) or ODCB as co-solvents, respectively. Also the PII3T-HD concentration, polymer:PC₇₀BM ratio, and active layer thickness were optimized. This led to a maximum PCE of 4.8% for a cell processed from ODCB:DIO (2.5% v/v), a PII3T-HD:PCBM weight ratio of 1:1.5, and a layer thickness of 100 nm. These are exactly the same conditions as found by Wang *et al.*²² for this polymer. Device performance however lagged somewhat compared to this literature example mainly due to a significantly lower short-circuit current density (J_{sc}) of 10.0 mA/cm² versus a reported 13.1 mA/cm² and the lower fill factor (FF) of 0.63 versus 0.69. Only the open-circuit voltage (V_{oc}) of 0.76 V is higher compared to the reported 0.70 V. The high current density and a maximum EQE > 50% indicate that the LUMO-LUMO energy offset between this polymer and PC₇₀BM is still large enough for efficient charge carrier generation, in spite of the relatively small estimate of ~0.3 eV indicated by the CV measurements.

Table 2.2 – Characteristics of optimized PIIX:PC₇₀BM solar cells

Polymer	Polymer: PC ₇₀ BM	Solvent	J_{sc} mA/cm ²	V_{oc} V	FF	PCE %
PII3T-HD	1:1.5	ODCB:DIO 2.5% (v/v)	10.0	0.76	0.63	4.8
PIITTTT-HD	1:1.5	TCE:ODCB 10% (v/v)	11.2	0.78	0.64	5.6
PIITTTT-OD	1:1.5	CHCl ₃ :DIO 4% (v/v)	9.5	0.77	0.62	4.5
PIITBDTT-HD	1:1.5	TCE:ODCB 10% (v/v)	6.4	0.86	0.59	3.3

For PIITTTT-HD the low solubility in chloroform and ODCB prevented processing from these solvents. Solubility in 1,1,2,2-tetrachloroethane (TCE), on the other hand, was sufficient to spin coat layers. To reach a layer thickness of around 100 nm a concentration of 10 mg/ml was needed, over to the solubility limit as evidenced from small chunks of polymer that were observed in the spin coated layers. Despite the poor film quality, the performance of the devices was remarkably good albeit with low short circuit current densities (J_{sc} = 3.6 mA/cm²). Adding ODCB (10% v/v optimized) as a co-solvent increased J_{sc} to 11.2 mA/cm², giving a maximum PCE of 5.6% with a V_{oc} of 0.78 V and a FF of 0.64. A maximum EQE of 0.54 was measured at 650 nm, indicating efficient charge collection from absorbed photons in the polymer. Compared to PII3T-HD both the J_{sc} and the FF improved, pointing at improved charge carrier collection.

Device optimization for the PIITBDTT-HD polymer suffered from the low solubility of this material and even films spun from TCE showed substantial scattering after drying,

indicating the formation of large domains. Spin coating from hot solutions hardly improved this but cells from TCE with 10% ODCB (v/v) showed a $V_{oc} = 0.86$ V, which is almost 0.1 V higher than for any of the other PIIX polymers, with $J_{sc} = 6.4$ mA/cm², FF= 0.59, and hence a PCE of 3.3%. The higher V_{oc} can be explained by a 0.1 eV lower lying HOMO. The observed low current density and corresponding low EQE of this cell could be the result of the bad film morphology due to the partially dissolved polymer and/or to the relatively low lying LUMO energy level and hence lower driving force for electron transfer from the polymer to the PC₇₀BM. This hypothesis is supported by the spectrally resolved EQE data. Particularly in the spectral region above 550 nm where the polymer absorbs the EQE is comparatively low, whereas it remains high at shorter wavelengths where PC₇₀BM is the main absorber, indicating that photoinduced hole transfer from the fullerene to the polymer is still efficient.

Overall, increasing the size of the aromatic electron rich co-monomer improved the optimized efficiency, going from a single thiophene to a thieno[3,2-*b*]thiophene ring. This is tentatively assigned to improved solid state electronic properties as a result of enhanced π - π stacking. Further increasing the size of the aromatic co-monomer to a benzo[1,2-*b*:4,5-*b'*]dithiophene unit rendered a material which turned out to be too insoluble to allow further efficiency improvements.

As the best material in hand, PIITTT-HD relied on quite harsh processing conditions a more soluble PIITTTT-OD was synthesized, which has somewhat larger solubilizing alkyl side chains. This polymer displayed a promising high molecular weight, with good solubility in chloroform and ODCB. However, processing optimization yielded devices with $J_{sc} = 9.5$ mA/cm², $V_{oc} = 0.77$, FF = 0.62, and a PCE of only 4.5% using active layers spin coated from chloroform with DIO (4% v/v). External quantum efficiency (EQE) measurements revealed that the lower J_{sc} is mainly caused by a lower contribution of PIITTTT-OD in the region 500 – 800 nm compared to PIITTTT-HD (Figure 2.3). This may be due to a somewhat large fraction of the PC₇₀BM molecules molecularly mixed in the polymer rich domains, facilitated by the larger side chains. Excitation of the polymer near such isolated acceptor molecules could yield charge separated states from which the electron will be very hard to extract.

2.3.3.1 *Mixing PIITTTT-HD and PIITTTT-OD*

Since the active layers of PIITTTT-HD were coarsened by chunks of undissolved material as a result of the low solubility, we hypothesized that blending this polymer with

the more soluble PIITTTT-OD with higher molecular weight might improve the layer quality. Cells with mixed polymer layers were made, using PIITTTT-HD/OD ratios of 1:3, 1:1, and 3:1 and compared with the pure PIITTTT-HD and PIITTTT-OD devices. For all cells TCE with 10% ODCB was used as processing solvents, because the optimal solvent combination for PIITTTT-OD (chloroform:DIO) is unable to dissolve the PIITTTT-HD.

Figure 2.4 shows the resulting $J - V$ characteristics and the relevant parameters are collected in Table 2.3. The best results were obtained with pure PIITTTT-HD. Owing to the unfavorable processing solvent, PIITTTT-OD gave the lowest performance which was considerably poorer than when processed from chloroform:DIO, as shown above. The performance of the mixed polymer devices varies more or less linearly with the polymer ratio, decreasing with increasing PIITTTT-OD content. Despite the improved layer formation the best blend, with the highest PIITTTT-HD content, performs less than the 100% PIITTTT-HD device.

Table 2.3 – Characteristics of (PIITTTT-HD/PIITTTT-OD):PC₇₀BM solar cells

HD/OD ratio	PIITTTT:PC ₇₀ BM ratio	J_{sc} mA/cm ²	V_{oc} V	FF	PCE %
0/1	1:1.5	1.4	0.77	0.47	0.5
1/3	1:1.5	2.3	0.77	0.57	1.0
1/1	1:1.5	3.3	0.77	0.61	1.5
3/1	1:1.5	7.4	0.77	0.62	3.5
1/0	1:1.5	11.2	0.78	0.64	5.6

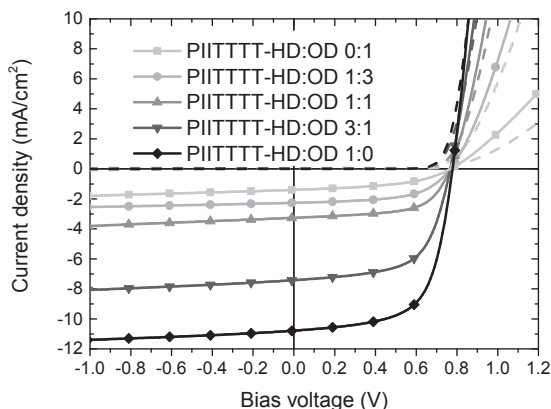


Figure 2.4 – $J - V$ Characteristics of (PIITTTT-HD/PIITTTT-OD):PC₇₀BM solar cells with PIITTTT-HD and PIITTTT-OD in different ratios.

2.4 Conclusion

A series of isoindigo conjugated polymers of the form PIITXT was synthesized where X was varied from thiophene to thieno[3,2-*b*]thiophene and benzo[1,2-*b*:4,5-*b'*]dithiophene. Increasing the rigid blocks by fusion of more π -conjugated rings together, leaving the length of solubilizing side chains constant, gradually decreases the solubility of these polymers. Concomitantly, the molecular weights along this series of polymers reduced, likely due to earlier precipitation during polymerization. After optimization of the processing conditions of the polymers in combination with PC₇₀BM the highest efficiency of 5.6% was achieved for PIITTTT-HD. This is attributed to the property of this material to possess the most balanced solubility; sufficiently poor to enhance π - π stacking and improve the electronic properties of the material and generate a favorable morphology, yet sufficiently good to allow processing, albeit from hot TCE. A minimal increase of the solubilizing side chains from PIITTTT-HD to PIITTTT-OD increased the solubility and afforded a higher molecular weight (M_n from 33.4 kg/mol to 45.0 kg/mol). However, despite the higher M_n the improved solubility rendered less efficient optimized devices. Possibly, the increased solubility and/or the bulkier side chains hamper the aggregation of the polymer in the solid state which is needed for optimal electronic properties.

2.5 Experimental

2.5.1 General procedures

All starting materials and reagents were purchased from commercial suppliers unless stated otherwise. All ^1H NMR and ^{13}C NMR spectra were recorded on a 400 MHz Varian Mercury Spectrometer using CDCl_3 as solvent with tetramethylsilane (TMS) as internal standard. The given values are in ppm relative to TMS (0 ppm). UV-vis-NIR optical absorption spectra were recorded on a Perkin-Elmer Lambda 900 spectrometer in a chloroform solution in a quartz cell or a thin film spin coated on a glass substrate. Cyclic voltammetry (CV) was conducted under inert atmosphere using an Autolab PGSTAT30 with a three electrode setup equipped with a platinum disc working electrode, silver counter electrode and a silver electrode coated with silver chloride (Ag/AgCl) as quasi reference electrode in combination with ferrocene/ferrocenium (Fc/Fc^+) as internal standard. A 1 M solution of tetrabutylammonium hexafluorophosphate (TBAPF_6) in *ortho*-dichlorobenzene (ODCB) was used as the electrolyte. Matrix-assisted laser desorption ionization time-of-flight (MALDI-TOF) was measured on a PerSeptive Biosystems Voyager – DE PRO spectrometer using either α -cyano-4-hydroxycinnamic acid (CHCA) and/or trans-2-[3-(4-*tert*-butylphenyl)-2-methyl-2-propenylidene]malononitrile (DCTB) as matrices. Molecular weights for the polymers were determined with two high temperature GPC setups, a Shimadzu LC-20AD Prominence Liquid Chromatograph equipped with a SPD-20A UV-Vis detector and a RID-10A refractive index detector and a Mixed-D (200-400.000 Da versus polystyrene standards) column running on chloroform at 110 °C and an Agilent high temperature GPC equipped with a PDA detector, RI detector and LS detector and with a μgel 10 μm Mixed B column using ODCB at 140 °C as eluent.

2.5.2 Solar cell fabrication and characterization

Photovoltaic devices with an active area of 0.09 and 0.16 cm^2 were fabricated by spin coating poly(ethylenedioxythiophene):poly(styrene sulfonate) (PEDOT:PSS) (Clevios P, VP Al4083) (40 nm) on pre-cleaned, patterned indium tin oxide (ITO) glass substrates (Naranjo Substrates). The back electrode consisted of LiF (1 nm) and Al (100 nm) which were deposited by evaporation under high vacuum (3×10^{-7} mbar). J - V characteristics were measured with a Keithley 2400 source meter under ~ 100 mW/cm^2 white light illumination from a tungsten-halogen lamp filtered by a Schott GG385 UV filter and a Hoya LB120 daylight filter. Short-circuit current densities under AM1.5G conditions were estimated by integrating the EQE with the solar spectrum. EQE measurements were conducted under 1 sun operating conditions by using a 532 nm solid state laser (Edmund Optics) for bias illumination. The device was kept in a nitrogen filled box behind a quartz window and irradiated with modulated monochromatic light, from a 50 W tungsten-halogen lamp (Philips focusline) and monochromator (Oriel, Cornerstone 130) with the use of a mechanical chopper. The response was recorded as a voltage over a 50 Ω resistor using a lock-in amplifier (Stanford research Systems SR830). A calibrated silicon cell was

used as reference. The thickness of the active layers was determined on a Veeco Dektak150 profilometer.

2.5.3 Synthesis

(E)-6,6'-dibromo-[3,3'-biindolinylidene]-2,2'-dione (1).

6-Bromo-2-oxindol (1.000 g, 4.72 mmol) and 6-bromoisatin (1.067 g, 4.72 mmol) were dissolved in a mixture of AcOH (30 ml) and concentrated HCl (0.2 ml) and heated to 120 °C for 24h. After cooling down to room temperature the reaction mixture was filtered. The solid phase was washed with water, EtOH, EtOAc and dried under vacuum to give the essentially pure product (1.865 g, 4.44 mmol, 94%). ^1H NMR (400 MHz, DMSO- d_6 , ppm): δ 7.00 (d, J = 2.0, 2H), 7.19 (dd, J = 2.0, 8.6, 2H), 9.00 (d, J = 8.6, 2H), 11.11 (s, 2H). ^{13}C NMR (100 MHz, DMSO- d_6 , ppm): δ 112.88, 121.29, 124.46, 126.12, 131.36, 133.10, 145.97, 171.74.

(E)-6,6'-dibromo-1,1'-bis(2-hexyldecyl)-[3,3'-biindolinylidene]-2,2'-dione (2a).

In dry DMF (9.5 ml) **1** (1.032 g, 2.46 mmol) was dissolved together with K_2CO_3 (1.70 g, 12.3 mmol) under argon atmosphere. After stirring for 30 min, 1-bromo-2-hexyldecane (1.646 g, 5.41 mmol) was added and the reaction was heated to 100 °C for 15h. After cooling down, diethyl ether was added and the organic phase was washed three times with water and brine and dried over MgSO_4 . The solvent was removed under reduced pressure and the crude product was purified by silica column chromatography using a heptane/DCM (80/20) to give the pure product (1.754 g, 2.02 mmol, 82%). ^1H NMR (400 MHz, CDCl_3 , ppm): δ 9.06 (d, J = 8.6, 2H), 7.15 (dd, J = 2.0, 8.6, 2H), 6.88 (d, J = 2.0, 2H), 3.60 (d, J = 7.4, 4H), 1.87 (s, 2H), 1.27 (m, 48H), 0.86 (t, J = 7.4, 12H). ^{13}C NMR (100 MHz, CDCl_3 , ppm): δ 168.07, 146.18, 132.53, 131.01, 126.64, 125.06, 120.36, 111.51, 44.67, 36.07, 31.85, 31.78, 31.48, 29.96, 29.62, 29.52, 29.27, 26.34, 26.31, 22.65, 22.62, 14.10, 14.07.

(E)-6,6'-dibromo-1,1'-bis(2-octyldodecyl)-[3,3'-biindolinylidene]-2,2'-dione (2b).

The same procedure as for **2a** but using an equivalent amount of 1-bromo-2-octyldodecane instead of 1-bromo-2-hexyldecane. ^1H NMR (400 MHz, CDCl_3 , ppm): δ 9.07 (d, J = 8.6, 2H), 7.16 (dd, J = 1.6, 9.0, 2H), 6.90 (d, J = 1.2, 2H), 3.62 (d, J = 7.4, 4H), 1.88 (s, 2H), 1.27 (m, 64H), 0.86 (m, 12H). ^{13}C NMR (100 MHz, CDCl_3 , ppm): δ 168.11, 146.20, 132.58, 131.00, 126.65, 125.09, 120.37, 111.55, 44.68, 36.07, 35.41, 31.90, 31.87, 31.86, 31.47, 29.97, 29.62, 29.61, 29.58, 29.53, 29.34, 29.27, 29.02, 26.34, 22.65, 22.68, 14.12, 14.10.

(E)-1,1'-bis(2-hexyldecyl)-6,6'-bis(4-octylthiophen-2-yl)-[3,3'-biindolinylidene]-2,2'-dione (3a).

Toluene (4.6 ml), water (0.58 ml) and one droplet of Aliquat 336 were added to a mixture of **2a** (0.390 g, 460 μmol), 4,4,5,5-tetramethyl-2-(4-octylthiophen-2-yl)-1,3,2-dioxaborolane (0.445 g, 1.38 mmol) and K_3PO_4 (0.488 g, 2.3 mmol) under argon atmosphere. The mixture was degassed for 30 min with argon before adding Pd_2dba_3 (21 mg, 23 μmol) and PPh_3 (15.2 mg, 58 μmol). The solution was heated to 115 °C and stirred overnight. After cooling down, CHCl_3 was added and the organic phase was washed 3 times with water, brine, and dried over MgSO_4 . The solvent was evaporated under reduced pressure and the crude product was purified by silica column chromatography

using a heptane/CHCl₃ gradient (100/0 → 50/50) to give the product (0.297 g, 270 μmol, 59 %). ¹H NMR (400 MHz, CHCl₃, ppm): δ 9.15 (d, *J* = 8.6, 2H), 7.26 (m, 4H), 6.95 (s, 4H), 3.69 (s, 4H), 2.63 (t, *J* = 7.4, 4H), 1.92 (s, 2H), 1.67 (m, 4H), 1.13-1.47 (m, 68H), 0.86 (m, 18H). ¹³C NMR (100 MHz, CDCl₃, ppm): δ 168.64, 144.69, 131.90, 130.10, 125.56, 125.54, 120.92, 120.85, 119.06, 119.04, 44.44, 36.41, 31.89, 31.87, 31.79, 31.77, 30.64, 30.48, 30.02, 29.68, 29.61, 29.46, 29.40, 29.39, 29.32, 29.30, 26.66, 26.65, 22.69, 22.65, 14.12, 14.09, MALDI-TOF *m/z*: 1098.85 (M⁺, 100%).

(*E*)-1,1'-bis(2-octyldodecyl)-6,6'-bis(4-octylthiophen-2-yl)-[3,3'-biindolinylidene]-2,2'-dione (3b).

The same procedure as for **3a** but using an equivalent amount of **2b** instead of **2a**. ¹H NMR (400 MHz, CHCl₃, ppm): δ 9.15 (d, *J* = 8.2, 2H), 7.26 (t, *J* = 7, 4H), 6.95 (d, *J* = 6.2, 4H), 3.69 (d, *J* = 7.4, 4H), 2.63 (t, *J* = 7.4, 4H), 1.93 (s, 2H), 1.65 (m, 4H), 1.20-1.43 (m, 84H), 0.86 (m, 18H). ¹³C NMR (100 MHz, CDCl₃, ppm): δ 168.88, 145.66, 144.67, 143.67, 138.00, 131.92, 131.24, 130.07, 125.54, 120.83, 113.24, 104.92, 31.91, 31.88, 31.75, 30.64, 30.62, 30.47, 30.10, 30.00, 29.45, 29.41, 29.37, 29.36, 29.31, 29.28, 29.02, 26.64, 24.77, 24.74, 22.68, 22.67, 14.11, 14.10. MALDI-TOF *m/z*: 1210.93 (M⁺, 100 %).

(*E*)-6,6'-bis(5-bromo-4-octylthiophen-2-yl)-1,1'-bis(2-hexyldodecyl)-[3,3'-biindolinylidene]-2,2'-dione (4a).

In DCM (10 ml) **3** (0.226 g, 0.206 mmol) was dissolved and cooled to 0 °C. NBS (0.073 g, 0.411 mmol) was added to the solution in portions and the solution was stirred at room temperature until TLC indicated that the reaction was completed. Diethyl ether was added and the organic phase was washed three times with water, brine and dried over MgSO₄. The solvent was removed under reduced pressure and the crude product was recrystallized from EtOH to give the pure product (0.221 g, 176 μmol, 85 %). ¹H NMR (400 MHz, CDCl₃, ppm): δ 9.16 (d, *J* = 8.2, 2H), 7.18 (d, *J* = 8.2, 2H), 7.09 (s, 2H), 6.86 (s, 2H), 3.69 (d, *J* = 6.3, 4H), 2.58 (t, *J* = 7.4, 4H), 1.91 (s, 2H), 1.63 (m, 4H), 1.14-1.47 (m, 68H), 0.78-0.96 (m, 18H). ¹³C NMR (100 MHz, CDCl₃, ppm) δ 168.52, 145.74, 143.56, 143.23, 137.05, 131.93, 130.24, 124.94, 121.15, 118.63, 109.90, 104.50, 44.42, 36.37, 31.87, 31.74, 29.99, 29.75, 29.70, 29.66, 29.59, 29.38, 29.30, 29.24, 26.61, 22.65, 22.63, 14.09. MALDI-TOF *m/z*: 1256.64 (M⁺, 100%).

(*E*)-6,6'-bis(5-bromo-4-octylthiophen-2-yl)-1,1'-bis(2-octyldodecyl)-[3,3'-biindolinylidene]-2,2'-dione (4b).

The same procedure as for **4a** but using an equivalent amount of **3b** instead of **3a**. ¹H NMR (400 MHz, CDCl₃, ppm): δ 9.16 (d, *J* = 8.2, 2H), 7.19 (dd, *J* = 1.2, 8.6, 2H), 7.09 (s, 2H), 6.87 (s, 2H), 3.70 (d, *J* = 7.4, 4H), 2.58 (t, *J* = 7.4, 4H), 1.92 (s, 2H), 1.63 (m, 4H), 1.18-1.43 (m, 84H), 0.86 (m, 18H). ¹³C NMR (100 MHz, CDCl₃, ppm): δ 168.88, 145.98, 144.80, 143.67, 139.10, 135.55, 124.98, 121.19, 113.70, 111.66, 108.13, 104.43, 31.91, 31.87, 31.74, 31.16, 30.58, 30.00, 29.65, 29.63, 29.59, 29.38, 29.31, 29.28, 29.25, 26.62, 22.68, 22.66, 14.09. MALDI-TOF *m/z*: 1369.74 (M⁺, 100 %).

PII3T-HD.

To a mixture of **4a** (48.29 mg, 38.4 μmol) and 2,5-bis(trimethylstannyl)thiophene (15.74 mg, 38.4 μmol) dry toluene (0.9 ml) and DMF (0.1 ml) were added under argon atmosphere and argon was bubbled through the reaction mixture. After 30 min. Pd₂dba₃ (0.703 mg, 0.768 μmol) and PPh₃ (0.802 mg, 3.07 μmol) were added and the reaction

mixture was heated to 115 °C for 18 h. Trimethyl(thiophen-2-yl)stannane (49 μ l, 153.6 μ mol) and 2-bromothiophene (30 μ l, 307 μ mol) were added with an interval of 30 min. to end cap the polymer. After 30 min. the reaction was allowed to cool to room temperature and was precipitated in methanol and filtered through a Soxhlet thimble. The polymer was extracted with acetone, hexanes and chloroform and the chloroform fraction was purified by passing it through a short silica plug and precipitated in methanol. The polymer was filtered over a PTFE filter and dried overnight in a vacuum oven at 40 °C to give 39 mg of the polymer. GPC (140 °C ODCB): M_n = 97.7 kg/mol and PDI = 4.2. λ_{max} = 639 nm.

PIITTTT-HD.

To a mixture of **4a** (68.33 mg, 54.3 μ mol) and 2,5-bis(trimethylstannyl)thieno[3,2-*b*]thiophene (25.31 mg, 54.3 μ mol) dry toluene/DMF (9/1) (1 ml) were added under argon atmosphere and argon was bubbled through for 15 min. Then Pd₂dba₃ (0.99 mg, 1.09 μ mol) and PPh₃ (1.14 mg, 4.35 μ mol) were added and the reaction mixture was heated to 115 °C overnight. Trimethyl(thiophen-2-yl)stannane (69 μ l, 217 μ mol) and 2-bromothiophene (42 μ l, 435 μ mol) were added with an interval of 30 min. to end cap the polymer. After 30 min. the reaction was allowed to cool to room temperature and was precipitated in methanol and filtered through a Soxhlet thimble. The polymer was extracted with acetone, hexanes, chloroform, and chlorobenzene. The chlorobenzene fraction was evaporated to a minimal amount and precipitated in methanol. The polymer was filtered over a PTFE filter and dried overnight in a vacuum oven at 40 °C to give 45 mg of the polymer. GPC (ODCB, 140 °C): M_n = 33.4 kg/mol and PDI = 2.0. λ_{max} = 651 nm.

PIITTTT-OD.

To a mixture of **4b** (49.98 mg, 36.5 μ mol) and 2,5-bis(trimethylstannyl)thieno[3,2-*b*]thiophene (17.00 mg, 36.5 μ mol) dry toluene (0.9 ml) and DMF (0.1 ml) were added under argon atmosphere and the reaction mixture was bubbled through with argon. After 30 min Pd₂dba₃ (0.668 mg, 0.73 μ mol) and PPh₃ (0.76 mg, 2.92 μ mol) were added and the reaction mixture was heated to 115 °C for 64 h. Trimethyl(thiophen-2-yl)stannane (69 μ l, 217 μ mol) and 2-bromothiophene (42 μ l, 0.435 mmol) were added with an interval of 30 min. to end cap the polymer. After 30 min. the reaction was allowed to cool to room temperature and was precipitated in methanol and filtered through a Soxhlet thimble. The polymer was extracted with acetone, hexanes, chloroform and chlorobenzene. The chlorobenzene fraction was evaporated to a minimal amount and precipitated in methanol. The polymer was filtered over a PTFE filter and dried overnight in a vacuum oven at 40 °C to give 46 mg of the polymer. GPC (ODCB, 80 °C): M_n = 45.0 kg/mol and PDI = 2.7. λ_{max} = 651 nm.

PIITBDTT-HD.

In a Schlenk tube **4a** (97.5 mg, 77.5 μ mol) and 2,6-bis(trimethylstannyl)benzo[1,2-*b*:4,5-*b'*]dithiophene (40.0 mg, 77.5 μ mol) together with Pd₂dba₃ (1.42 mg, 1.55 μ mol) and PPh₃ (1.63 mg, 6.20 μ mol) were put under argon and dissolved in a toluene/DMF (9/1) mixture (2 ml). Argon was bubbled through the mixture for 15 min. prior heating to 115 °C overnight. The formed polymer was then precipitated in methanol and filtered in a Soxhlet thimble. Subsequently the polymers were extracted with acetone, heptane, dichloromethane, and finally chloroform to afford 57 mg of product after precipitation in

methanol, filtration over a PTFE filter and vacuum drying. GPC (140 °C ODCB): $M_n = 21.5$ kg/mol and PDI = 2.0. $\lambda_{\max} = 621$ nm.

2.6 Acknowledgements

Many of the results described in this chapter were obtained by Jeroen Brebels who worked on the synthesis and analysis of isoindigo polymers as part of his Master graduation project. I thank Xianwen Lou for his work on super heated chloroform GPC.

2.7 References

- ¹ H. Schoots, Celanese International Corporation, USA, **2013**, p. 20pp.
- ² E. Wille and W. Lüttke, *Angew. Chem., Int. Ed.*, **1971**, *10*, 803-804.
- ³ W. Lüttke and M. Klessinger, *Chem. Ber.*, **1964**, *97*, 2342-2357.
- ⁴ R. Stollé, **1921**, Patent DE335673.
- ⁵ R. Stollé, R. Bergdoll, M. Luther, A. Auerhahn, and W. Wacker, *J. Prakt. Chem.*, **1930**, *128*, 1-43.
- ⁶ B. P. Karsten, J. C. Bijleveld, and R. A. J. Janssen, *Macromol. Rapid. Comm.*, **2010**, *31*, 1554-1559.
- ⁷ K. H. Hendriks, G. H. L. Heintges, V. S. Gevaerts, M. M. Wienk, and R. A. J. Janssen, *Angew. Chem., Int. Ed.*, **2013**, *52*, 8341-8344.
- ⁸ J. Mei, K. R. Graham, R. Stalder, and J. R. Reynolds, *Org. Lett.*, **2010**, *12*, 660-663.
- ⁹ K. R. Graham, J. Mei, R. Stalder, J. W. Shim, H. Cheun, F. Steffy, F. So, B. Kippelen, and J. R. Reynolds, *ACS Appl. Mater. Inter.*, **2011**, *3*, 1210-1215.
- ¹⁰ Q. Liu, Z. Du, W. Chen, L. Sun, Y. Chen, M. Sun, and R. Yang, *Synth. Met.*, **2013**, *178*, 38-43.
- ¹¹ A. Yassin, P. Leriche, M. Allain, and J. Roncali, *New J. Chem.*, **2013**, *37*, 502-507.
- ¹² T. Wang, Y. Chen, X. Bao, Z. Du, J. Guo, N. Wang, M. Sun, and R. Yang, *Dyes Pigm.*, **2013**, *98*, 11-16.
- ¹³ M. Yang, X. Chen, Y. Zou, C. Pan, B. Liu, and H. Zhong, *J. Mater. Sci.*, **2013**, *48*, 1014-1020.
- ¹⁴ K. R. Graham, R. Stalder, P. M. Wieruszewski, D. G. Patel, D. H. Salazar, and J. R. Reynolds, *ACS Appl. Mater. Inter.*, **2013**, *5*, 63-71.
- ¹⁵ W. Elsayy, C.-L. Lee, S. Cho, S.-H. Oh, S.-H. Moon, A. Elbarbary, and J.-S. Lee, *Phys. Chem. Chem. Phys.*, **2013**, *15*, 15193-15203.
- ¹⁶ K. R. Graham, P. M. Wieruszewski, R. Stalder, M. J. Hartel, J. Mei, F. So, and J. R. Reynolds, *Adv. Funct. Mater.*, **2012**, *22*, 4801-4813.
- ¹⁷ R. Stalder, J. G. Mei, and J. R. Reynolds, *Macromolecules*, **2010**, *43*, 8348-8352.
- ¹⁸ B. Liu, Y. Zou, B. Peng, B. Zhao, K. Huang, Y. He, and C. Pan, *Polym. Chem.*, **2011**, *2*, 1156-1162.
- ¹⁹ S. Li, J. Yuan, P. Deng, W. Ma, and Q. Zhang, *Dyes Pigm.* **2014**, *106*, 121-127.
- ²⁰ M. Wan, H. Zhu, H. Deng, L. Jin, J. Guo, and Y. Huang, *J. Polym. Sci., Part A: Polym. Chem.* **2013**, *51*, 3477-3485.
- ²¹ X. Sun, W. Chen, Z. Du, X. Bao, G. Song, K. Guo, N. Wang, and R. Yang, *Polym. Chem.* **2013**, *4*, 1317-1322.
- ²² W. Zhuang, M. Bolognesi, M. Seri, P. Henriksson, D. Gedefaw, R. Kroon, M. Jarvid, A. Lundin, E. Wang, M. Muccini, and M. R. Andersson, *Macromolecules*, **2013**, *46*, 8488-8499.
- ²³ E. Wang, Z. Ma, Z. Zhang, P. Henriksson, O. Inganäs, F. Zhang, and M. R. Andersson, *Chem. Commun.*, **2011**, *47*, 4908-4910.
- ²⁴ Z. Ma, E. Wang, K. Vandewal, M. R. Andersson, and F. Zhang, *Appl. Phys. Lett.*, **2011**, *99*, 143302-143303.
- ²⁵ E. Wang, Z. Ma, Z. Zhang, K. Vandewal, P. Henriksson, O. Inganäs, F. Zhang, and M. R. Andersson, *J. Am. Chem. Soc.*, **2011**, *133*, 14244-14247.
- ²⁶ G. Zhang, Y. Fu, Z. Xie, and Q. Zhang, *Macromolecules*, **2011**, *44*, 1414-1420.
- ²⁷ R. Stalder, C. Grand, J. Subbiah, F. So, and J. R. Reynolds, *Polym. Chem.*, **2012**, *3*, 89-92.
- ²⁸ X. Xu, P. Cai, Y. Lu, N. S. Choon, J. Chen, X. Hu, and B. S. Ong, *J. Polym. Sci. Part A: Polym. Chem.*, **2012**, *51*, 424-434.
- ²⁹ K. Cao, Z. Wu, S. Li, B. Sun, G. Zhang, and Q. Zhang, *J. Polym. Sci. Part A: Polym. Chem.*, **2013**, *51*, 94-100.
- ³⁰ S. Li, J. Yuan, P. Deng, W. Ma, and Q. Zhang, *Sol. Energy Mater. Sol. Cells*, **2013**, *118*, 22-29.
- ³¹ K. Mahmood, Z.-P. Liu, C. Li, Z. Lu, T. Fang, X. Liu, J. Zhou, T. Lei, J. Pei, and Z. Bo, *Polym. Chem.*, **2013**, *4*, 3563-3574.
- ³² P. Sonar, H.-S. Tan, S. Sun, Y. M. Lam, and A. Dodabalapur, *Polym. Chem.*, **2013**, *4*, 1983-1994.

- ³³ F. Wu, H. Yang, C. M. Li, and J. Qin, *Polym. Advan. Technol.*, **2013**, 24, 945-950.
- ³⁴ C.-C. Ho, S.-Y. Chang, T.-C. Huang, C.-A. Chen, H.-C. Liao, Y.-F. Chen, and W.-F. Su, *Polym. Chem.*, **2013**, 4, 5351-5360.
- ³⁵ C. Hu, Y. Fu, S. Li, Z. Xie, and Q. Zhang, *Polym. Chem.*, **2012**, 3, 2949-2955.
- ³⁶ D. H. Kim, A. L. Ayzner, A. L. Appleton, K. Schmidt, J. Mei, M. F. Toney, and Z. Bao, *Chem. Mater.*, **2013**, 25, 431-440.
- ³⁷ C.-C. Ho, C.-A. Chen, C.-Y. Chang, S. B. Darling, and W.-F. Su, *J. Mater. Chem. A*, **2014**, 2, 8026-8032.
- ³⁸ L. Fang, Y. Zhou, Y.-X. Yao, Y. Diao, W.-Y. Lee, A. L. Appleton, R. Allen, J. Reinspach, S. C. B. Mannsfeld, and Z. Bao, *Chem. Mater.*, **2013**, 25, 4874-4880.
- ³⁹ Y. Yang, R. Wu, X. Wang, X. Xu, Z. Li, K. Li, and Q. Peng, *Chem. Commun.*, **2014**, 50, 439-441.
- ⁴⁰ W. Sun, Z. Ma, D. Dang, W. Zhu, M. R. Andersson, F. Zhang, and E. Wang, *J. Mater. Chem. A*, **2013**, 1, 11141-11144.
- ⁴¹ D. Dang, W. Chen, R. Yang, W. Zhu, W. Mammo, and E. Wang, *Chem. Commun.*, **2013**, 49, 9335-9337.
- ⁴² C. Wang, B. Zhao, Z. Cao, P. Shen, Z. Tan, X. Li, and S. Tan, *Chem. Commun.*, **2013**, 49, 3857-3859.
- ⁴³ Y. Deng, J. Liu, J. Wang, L. Liu, W. Li, H. Tian, X. Zhang, Z. Xie, Y. Geng, and F. Wang, *Adv. Mater.*, **2014**, 26, 471-476.
- ⁴⁴ G. Wang, H. Tan, Y. Zhang, Y. Wu, Z. Hu, G. Yu, and C. Pan, *Synth. Met.*, **2014**, 187, 17-23.
- ⁴⁵ W. Ying, F. Guo, J. Li, Q. Zhang, W. Wu, H. Tian, and J. Hua, *ACS Appl. Mater. Inter.*, **2012**, 4, 4215-4224.
- ⁴⁶ R. Stalder, D. Xie, A. Islam, L. Han, J. R. Reynolds, and K. S. Schanze, *ACS Appl. Mater. Inter.*, **2014**, 6, 8715-8722.
- ⁴⁷ S.-G. Li, K.-J. Jiang, J.-H. Huang, L.-M. Yang, and Y.-L. Song, *Chem. Commun.*, **2014**, 50, 4309-4311.
- ⁴⁸ J. G. Mei, D. H. Kim, A. L. Ayzner, M. F. Toney, and Z. Bao, *J. Am. Chem. Soc.*, **2011**, 133, 20130-20133.
- ⁴⁹ T. Lei, Y. Cao, X. Zhou, Y. Peng, J. Bian, and J. Pei, *Chem. Mater.*, **2012**, 24, 1762-1770.
- ⁵⁰ J. Shin, H. A. Um, D. H. Lee, T. W. Lee, M. J. Cho, and D. H. Choi, *Polym. Chem.*, **2013**, 4, 5688-5695.
- ⁵¹ S. S. Dharmapurikar, A. Arulkashmir, C. Das, P. Muddellu, and K. Krishnamoorthy, *ACS Appl. Mater. Inter.*, **2013**, 5, 7086-7093.
- ⁵² T. Lei, Y. Cao, Y. Fan, C.-J. Liu, S.-C. Yuan, and J. Pei, *J. Am. Chem. Soc.* **2011**, 133, 6099-6101.
- ⁵³ T. Lei, J.-H. Dou, Z.-J. Ma, C.-H. Yao, C.-J. Liu, J.-Y. Wang, and J. Pei, *J. Am. Chem. Soc.*, **2012**, 134, 20025-20028.
- ⁵⁴ H.-C. Wu, S. J. Benight, A. Chortos, W.-Y. Lee, J. Mei, J. W. F. To, C. Lu, M. He, J. B. H. Tok, W.-C. Chen, and Z. Bao, *Chem. Mater.*, **2014**, 26, 4544-4551.
- ⁵⁵ G. Kim, A. R. Han, H. R. Lee, J. H. Oh, and C. Yang, *Phys. Chem. Chem. Phys.*, **2014**, DOI: 10.1039/C4CP01787K
- ⁵⁶ G. Kim, A. R. Han, H. R. Lee, J. Lee, J. H. Oh, and C. Yang, *Chem. Commun.*, **2014**, 50, 2180-2183.
- ⁵⁷ T. Lei, J.-H. Dou, Z.-J. Ma, C.-J. Liu, J.-Y. Wang, and J. Pei, *Chem. Sci.*, **2013**, 4, 2447-2452.
- ⁵⁸ T. Lei, J.-H. Dou, and J. Pei, *Adv. Mater.*, **2012**, 24, 6457-6461.
- ⁵⁹ X. Xu, P. Cai, Y. Lu, N. S. Choon, J. Chen, X. Hu, and B. S. Ong, *J. Polym. Sci. Part A: Polym. Chem.*, **2012**, 51, 424-434.
- ⁶⁰ C. Papageorgiou and X. Borer, *Helv. Chim. Acta*, **1988**, 71, 1079-1083.
- ⁶¹ X. Lou, J. L. J. van Dongen, Y. Braeken, J. Brebels, G. W. P. van Pruissen, W. Li, M. M. Wienk, and R. A. J. Janssen, *Polym. Chem.*, **2014**, 5, 558-561.
- ⁶² D. Veldman, S. C. J. Meskers, and R. A. J. Janssen, *Adv. Funct. Mater.*, **2009**, 19, 1939-1948.
- ⁶³ M. C. Scharber, D. Mühlbacher, M. Koppe, P. Denk, C. Waldauf, A. J. Heeger, and C. J. Brabec, *Adv. Mater.*, **2006**, 18, 789-794.

Chapter 3.

Thienoisindigo for small band gap polymers*

Using Stille and Suzuki polymerization reactions thienoisindigo was incorporated as an acceptor co-monomer in a series of alternating π -conjugated copolymers with combinations of benzene, thiophene, and carbazole as donor co-monomers. By changing the nature and length of the donor segments, the optical band gap of these soluble TII copolymers can be varied over a large range from 1.52 eV down to 0.87 eV. The semiconducting properties of the TII copolymers were established in bottom-gate bottom-contact field-effect transistors that provide hole mobilities for these materials in the range of 10^{-3} to 10^{-2} cm²/Vs.

* This chapter is based on G.W.P. van Pruissen, F. Gholamrezaie, M.M. Wienk, and R.A.J. Janssen, *J. Mater. Chem.*, **2012**, 22, 20387-20393.

3.1 Introduction

In the previous chapter it was shown that isoindigo (II) based small molecules^{1,2} and polymers³⁻¹⁰ can be used as promising materials in OPV devices. The application in FETs¹¹ and organic memory devices¹² was also shown in literature. Reports on the molecular conformation of different II derivatives in single crystals leave ambiguity on the planarity of these molecules. X-ray diffraction of single crystals of unsubstituted II and *N-N'*-dibutyl substituted II showed fully planar conformations^{13,14} while a 22.3° twist over the central double bond was reported for *N-N'*-dimethyl substituted II.¹⁵ Density functional theory (DFT) based calculations showed that both conformations are energetic minima with very little ($< kT$) difference and that the twisted conformation is the overall minimum.¹⁶ By replacing the benzene ring of II with a stronger electron donating thiophene to give a thienoisindigo (TII) the steric hindrance will be reduced and the internal donor acceptor interactions increased (Figure 3.1, II and TII). This will enhance planarity and reduce the bond length alternation, resulting in lower band gaps, better packing, and higher charge mobilities. For OPV application a TII-based polymer was predicted to give a PCE over 10% in a DFT study¹⁷ based on the Schrabler model for energy levels and efficiency (Figure 3.1, PTII2TPD).¹⁸

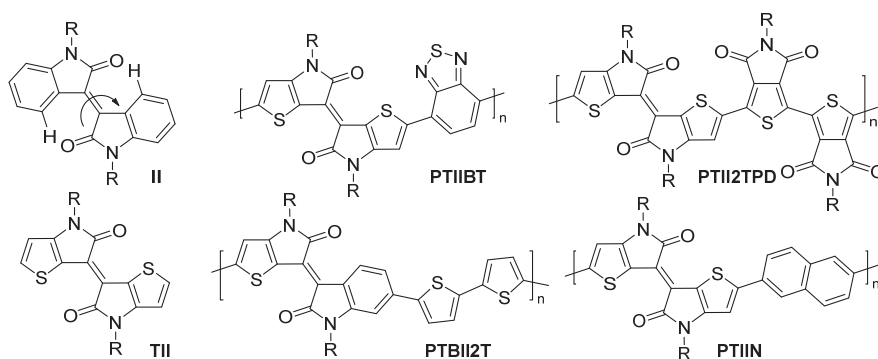


Figure 3.1 – Isoindigo (II) with the steric hindrance of two benzene protons that can cause twisting around the central double bond. Thienoisindigo (TII) without steric hindrance and no twisting. PTII2TPD gives ambipolar charge mobility, see ref. 20. PTII2TPD is predicted to give over 10% PCE in OPV, see ref. 17. PTBII2T combines II and TII, see ref. 22. PTIIN gives record hole mobility of 14.4 cm^2/Vs , see ref. 28.

This appealing structure was first described in a patent¹⁹ that formed the starting point of the work on TII in this chapter. Concurrently the potential of TII-based materials was also subject of investigation in other groups and the first polymer published in scientific literature was a TII and benzothiadiazole (BT) copolymer with high ambipolar charge mobilities (Figure 3.1, PTIIBT).²⁰

After publication of the work described in this chapter,²¹ the control of backbone coplanarity in II received further attention and hybrid isoindigo derivatives with one thiophene ring and one benzene ring (TBII) (Figure 3.1, PTBII2T) were described.²² TII-based materials were subsequently further investigated for their extreme small band gaps to make near infrared absorbing OPVs^{22,23-26} although efficiencies were never over 2%, primarily due to the very short exciton lifetimes in these small band gap TII copolymers.²² The low LUMO and high HOMO of these materials proved more useful in OFETs²⁷ where it can give ambipolar behavior²⁰ and reach a record hole mobility of 14.4 cm²/Vs in a TII copolymer with naphthalene (Figure 3.1, PTIIN).²⁸

3.2 Aim

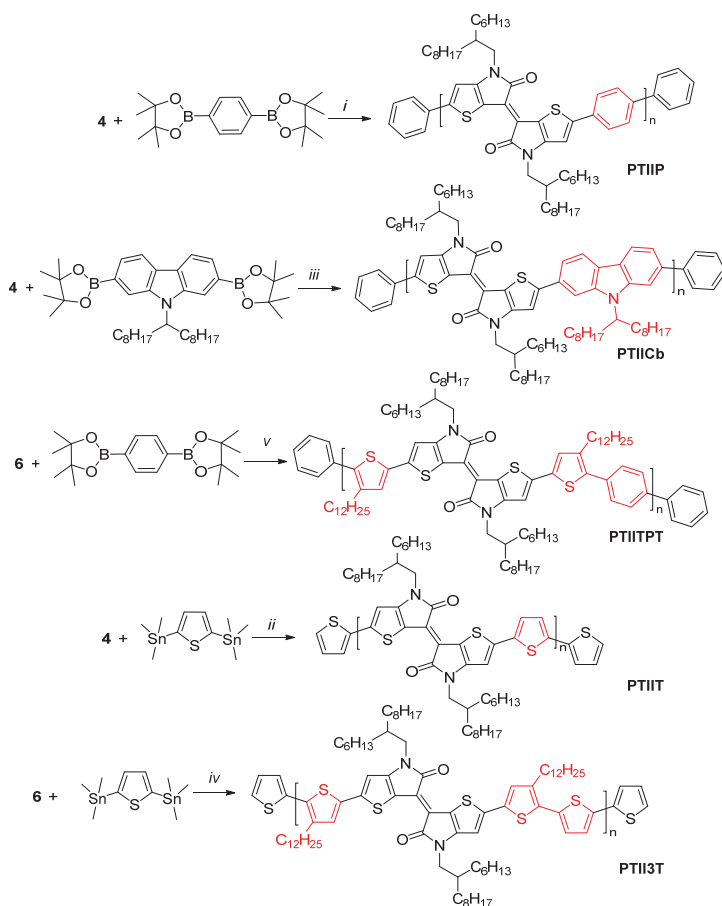
The synthesis of five new TII-copolymers is presented in which TII is alternating with benzene, thiophene, carbazole, and combinations thereof. This new class of TII-based materials is compared to their II counterparts and explored for their semiconducting properties. The TII polymers show band gaps in the range 0.87–1.52 eV and hole mobilities of 10⁻³ to 10⁻² cm²/Vs in bottom-gate bottom-contact FETs.

3.3 Results and discussion

3.3.1 Synthesis

The synthesis of the TII monomer starts with an Ullmann coupling of 3-bromothiophene with 2-hexyldecan-1-amine to give **1** (Scheme 3.1),^{19,20} followed by a Friedel-Crafts reaction with oxalyl chloride to give the thiophene derivative of isatin (**2**). The isatin derivative was dimerized with Lawesson's reagent to give **3**, following a procedure previously used for various pyrrole-2,3-diones.²⁹ This procedure is known to give exclusively the *E* isomer, which is confirmed for **3** by six sp² carbon signals in the ¹³C NMR spectrum indicating a single isomer and a single IR band at 1667 cm⁻¹ of the C=O stretch vibration. For the *Z* isomer symmetrical and anti-symmetrical vibrations would be

In many optoelectronic applications of conjugated copolymers the molecular weight is a critical factor because it controls the morphology and interchain ordering in the material. For PTIITPT, PTIICb, and PTII3T the molecular weight was determined with GPC to be respectively $M_n = 32.4$ kg/mol, 33.1 kg/mol and 13.4 kg/mol versus polystyrene standards with PDIs of 2.5, 2.5, and 4.0 as summarized in Table 3.1. For PTIIT and PTIIP, GPC measurements of the molecular weight gave inconclusive results because these polymers showed a strong interaction with the column material. The three copolymers, PTIITPT, PTIICb, and PTII3T that do not suffer from this problem have extra side chains attached to the donor units probably inhibiting the interaction with the column.



Scheme 3.2 – (ii) and (iv) Pd_2dba_3 , PPh_3 , toluene/DMF, 110 °C; (i), (iii) and (v) Pd_2dba_3 , PPh_3 , K_3PO_4 , Aliquat 336, toluene/ H_2O , 115 °C.

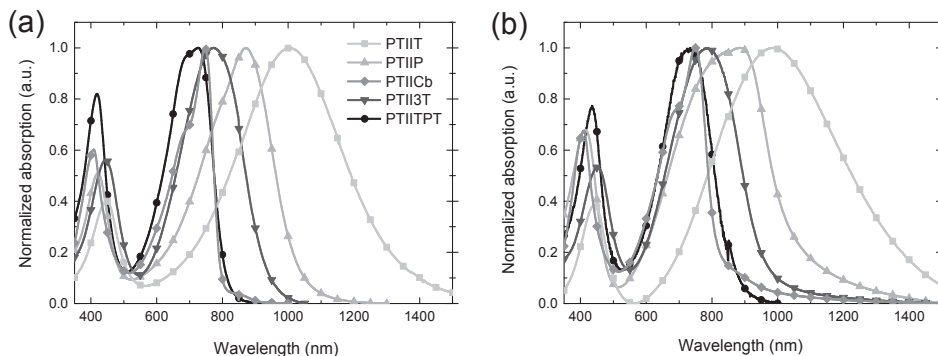


Figure 3.2 – Normalized absorption spectra of TII-based polymers in chloroform solution (a) and as thin films on glass (b).

3.3.2 Optical and electrochemical properties

The absence of a bathochromic shift in the spectra of these polymers between the solution and thin film samples shows that there is a strong tendency to aggregate already in solution. The optical band gaps for these materials, measured as the onset of absorption, range from 0.87 eV for the PTIIT polymer to 1.52 eV for the PTIICb polymer (Table 3.1). Relevant optical data for thienoisoindigo (PTIIX) polymers from this work and isoindigo (PIIX) polymers available from literature are collected in Table 3.1 and reveal that the optical band gaps of PTIIX derivatives are smaller than for PIIX. The difference is very pronounced for PTIIT ($E_g = 0.87$ eV) and PIIT ($E_g = 1.65$ eV).³ For none of these polymers significant fluorescence could be observed.

Cyclic voltammetry (CV) was used to determine the onsets of oxidation and reduction potentials versus the Fc/Fc^+ redox couple of the copolymers in solution. Using the redox potentials the HOMO and LUMO levels were estimated using $E = -5.23 - qE_{\text{redox}}$.³² The results are summarized in Table 3.1. The high HOMO levels for PTIIT (-4.82 eV) and to a lesser extent for PTIIP (-4.99 eV), PTII3T (-5.03 eV), and PTIITPT (-5.03 eV) make these polymers strong electron donors that can easily be oxidized. PTIICb is the only polymer that has a somewhat deeper HOMO (-5.24 eV). Compared to the corresponding isoindigo (II) analogs PIIT (PT-ID1,³ -5.92 eV), PIICb (PCzID,⁶ -5.66 eV) and PII3T (P3TI,³³ -5.71 eV), which were measured as thin films, a large difference of up to 1.1 eV for the HOMO level is observed.

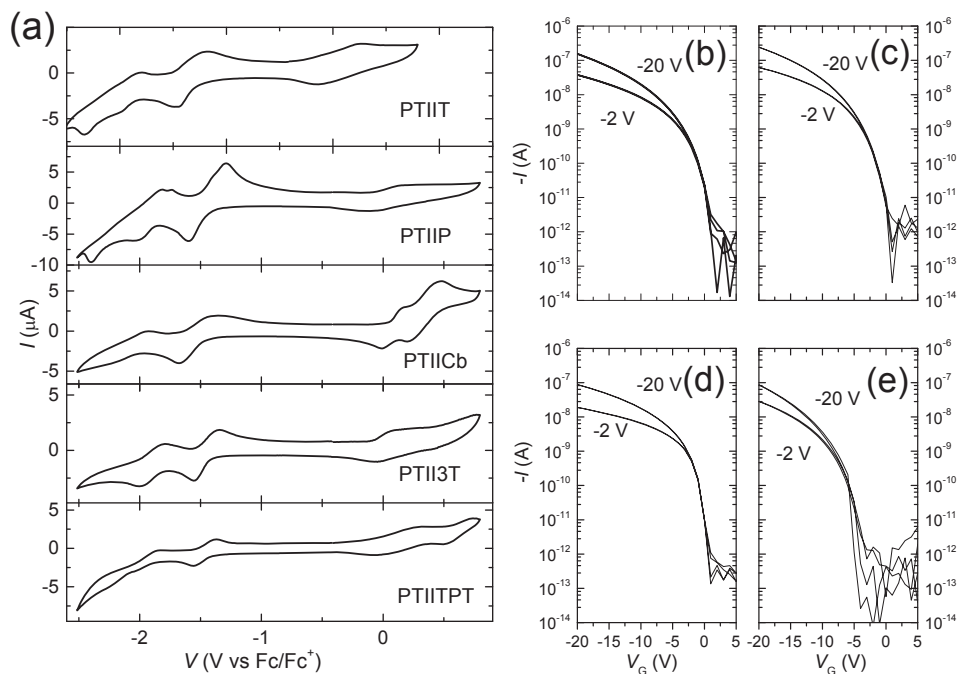


Figure 3.3 – (a) Cyclic voltammetry of TII-based polymers recorded in ODCB with $TBAPF_6$ as supporting electrolyte. Linear ($V_D = -2$ V) and saturated ($V_D = -20$ V) transfer characteristic of spin-coated field-effect transistors. The channel length is $40 \mu m$ and channel width is $1000 \mu m$. To prevent parasitic leakage currents, ring geometry was used in all cases. (b) PTIIP, (c) PTIITPT, (d) PTII3T and (e) PTIICb.

The differences between optical and electrochemical properties of the TII and II polymers are induced by the stronger electron donating properties of the thiophene ring compared to the benzene ring. In addition, co-planarity with the neighboring aromatic units is easier whilst steric hindrance is reduced, especially when a phenyl or carbazole is used as aromatic unit adjacent to II.

3.3.3 Electrical characterization

The electrical transport of conjugated polymers discussed above was investigated in field-effect transistors. In the transfer curves of the polymers PTIIT, PTIIP, PTIITPT, PTII3T, and PTIICb measured immediately after spin-coating, i.e. prior to thermal annealing, a large hysteresis was observed and the threshold voltage was not at zero gate bias. After annealing the transistors at $180^\circ C$ overnight, the performance improved for all polymers

except PTIIT. Note that for small band gap polymers often ambipolar transport is observed and has been reported for a related TII-based conjugated polymer.²⁰ In the FETs of PTII-X hole transport was observed but no electron transport. Figure 3.3 shows the typical transfer characteristics of a ring transistor for the four other polymers measured at room temperature after annealing. The curves for PTIIP, PTIITPT, PTII3T, and PTIICb show almost no hysteresis and have threshold voltages at zero voltage as well as high on-off ratios with a current modulation of almost five to six decades for all these four copolymers. The linear and saturated mobilities are quite similar and are about $5 \times 10^{-3} \text{ cm}^2/\text{Vs}$ for PTIIP, $8 \times 10^{-3} \text{ cm}^2/\text{Vs}$ for PTIITPT, $2 \times 10^{-3} \text{ cm}^2/\text{Vs}$ for PTII3T, and $5 \times 10^{-3} \text{ cm}^2/\text{Vs}$ for PTIICb.

Table 3.1 – Molecular weight, optical and electrochemical data of the TII-based and II-based copolymers.

Polymer	M_n kg/mol	PDI	$\lambda_{\text{max}}^{\text{sol}}$ nm	E_g^{sol} eV	E_g^{film} eV	E_{ox}^a V	E_{red}^a V	$E_g^{\text{cv}b}$ eV	E_{HOMO}^c eV	E_{LUMO}^c eV	Ref
Thienoisindigo polymers (PTII-X)											
PTIIT	n/a	n/a	1006	0.92	0.87	-0.41	-1.45	1.04	-4.82	-3.78	
PTIIP	n/a	n/a	872	1.21	1.18	-0.24	-1.60	1.36	-4.99	-3.63	
PTIICb	33.1	2.5	746	1.57	1.52	0.01	-1.49	1.50	-5.24	-3.74	
PTII3T	13.4	4.0	768	1.36	1.29	-0.20	-1.51	1.31	-5.03	-3.72	
PTIITPT	32.4	2.5	742	1.53	1.45	-0.20	-1.48	1.28	-5.03	-3.75	
Isoindigo polymers (PII-X) ^d											
PIIT (PT-ID1) ^e	17.2	2.1	684	1.68	1.65	0.69	-	-	-5.92	-	3
PIICb (PCzID) ^e	8.9	1.5	576	1.80	1.75	0.43	-1.20	1.63	-5.66	-4.03	6
PII3T (P3TI) ^e	73.0	2.9	645	1.63	1.50	0.48	-1.18	1.66	-5.71	-4.05	33

^a Onsets, potentials vs. Fc/Fc^+ . ^b $E_g^{\text{cv}} = q(E_{\text{ox}} - E_{\text{red}})$. ^c $E = -5.23 - qE_{\text{redox}}$. ^d Values may differ slightly from those stated in the cited papers due to small corrections (e.g. for reference potentials) made to allow direct comparison. ^e The acronyms used in the cited references are included between parentheses. Values for the PII-X polymers were measured for thin films in refs 3, 6 and 33.

3.4 Conclusion

A first series of TII-based π -conjugated polymers has been synthesized, extending the class of polymers incorporating a lactam functionality as an acceptor in its backbone. The TII unit influences the energy levels significantly when compared to PII-X polymers by raising the HOMO levels and therewith lowering the optical band gap to as low as 0.87 eV.

The FET mobilities are in line with other well performing polymers showing that these amide derived materials can be valuable in many organic electronic devices.

3.5 Experimental

3.5.1 General procedures

See paragraph 2.5.1.

3.5.2 OFET fabrication and characterization

OFETs were fabricated on a heavily doped silicon wafer as common gate electrode, covered by 200 nm thermally grown silicon dioxide passivated with HMDS as gate dielectric and gold source and drain electrodes were defined using conventional photolithography and a 10 nm Ti adhesion layer. The polymers were applied via spin coating at 1000 rpm for 30 s with acceleration of 100 rpm/s from chloroform solution and thermally annealed for 24 h at 180 °C in vacuum before measuring. The electrical transport was measured using a HP 4155C semiconductor parameter analyzer in vacuum of 10^{-6} mbar. To compare the current all measurements were done on a 40 μm channel length and channel width is 1000 μm .

3.5.3 Synthesis

2-Hexyldecan-1-amine.

Triphenylphosphine (36.5 g, 139 mmol) and phthalimide (20.5 g, 139 mmol) were suspended in DCM and cooled to 0 °C. Then 2-hexyl-1-decanol (30.6 g, 126.4 mmol) was added and stirred for 30 min. before the dropwise addition of diisopropyl azodicarboxylate (28.1 g, 139 mmol) while keeping the temperature under 10 °C. Upon the complete addition the mixture was stirred for another hour at room temperature before it was concentrated *in vacuo*. After redissolving in hexanes and filtration the resulting oil was subjected to a short silica column and concentrated. Then hydrazine and THF were added and the mixture was refluxed overnight. After cooling 2 M KOH was added and the product was extracted with ethyl acetate, washed with brine and dried over MgSO_4 before the crude oil was subjected to distillation. The product was distilled at 180 °C and 2×10^{-1} mbar to give 17.3 g (57%) 2-hexyldecan-1-amine as a colorless oil. ^1H NMR (400 MHz, CDCl_3 , ppm): δ 2.60 (d, $J = 4.7$ Hz, 2H), 1.36 – 1.18 (m, 25H), 1.08 (s, 2H), 0.88 (t, $J = 6.6$ Hz, 6H). ^{13}C NMR (100 MHz, CDCl_3 , ppm): δ 45.25, 40.93, 31.88, 31.54, 30.09, 29.76, 29.61, 29.32, 26.78, 26.75, 22.66, 14.08.

N-(2-hexyldecyl)thiophen-3-amine (1).

A mixture of 3-bromothiophene (11.023 g, 67.6 mmol), 2-hexyldecan-1-amine (16.3 g, 67.6 mmol), CuI (1.3 g, 6.8 mmol) and grinded K_3PO_4 (43.0 g, 200 mmol) in dimethylaminoethanol (30 ml) was heated to 90 °C for 2 days under an argon atmosphere. The reaction was cooled to room temperature and filtered. The residue was washed with

ethyl acetate and the filtrate concentrated and subjected to silica column chromatography (gradient heptane/DCM 0 - 100%) to give 7.7 g (35.5%) of the desired air sensitive compound. ^1H NMR (400 MHz, CDCl_3 , ppm): δ 7.13 (dd, $J = 5.1, 2.9$ Hz, 1H), 6.61 (dd, $J = 5.1, 1.5$ Hz, 1H), 5.91 (dd, $J = 3.0, 1.5$ Hz, 2H), 3.56 (s, 1H), 2.97 (d, $J = 6.0$ Hz, 2H), 1.70 – 1.52 (m, 1H), 1.45 – 1.12 (m, 24H), 0.88 (t, $J = 6.7$ Hz, 6H). ^{13}C NMR (100 MHz, CDCl_3 , ppm): δ 149.10, 124.94, 119.90, 94.76, 49.87, 37.82, 32.22, 32.21, 31.90, 31.88, 30.07, 29.74, 29.60, 29.33, 26.79, 26.76, 22.69, 22.68, 14.10.

4-(2-hexyldecyl)-4H-thieno[3,2-b]pyrrole-5,6-dione (2).

To a solution of oxalyl chloride (2.6 ml, 30 mmol) in DCM (20 ml) was added dropwise a solution of **1** (7.7 g, 24 mmol) in DCM (40 ml) while cooling the reaction at 0 °C. After 30 min. a solution of Et_3N (6 ml) in DCM (40 ml) was added dropwise after which the reaction was warmed to room temperature and stirred overnight. The mixture was concentrated and purified by silica column chromatography using a heptane/DCM 70/30 mixture as eluent to give 5.9 g of 4-(2-hexyldecyl)-4H-thieno[3,2-b]pyrrole-5,6-dione as an orange oil in 70% yield. ^1H NMR (400 MHz, CDCl_3 , ppm): δ 8.00 (d, $J = 5.0$ Hz, 1H), 6.76 (d, $J = 4.7$ Hz, 1H), 3.53 (d, $J = 7.4$ Hz, 2H), 1.81 – 1.74 (m, 1H), 1.36 – 1.18 (m, 24H), 0.87 (td, $J = 6.8, 2.2$ Hz, 6H). ^{13}C NMR (100 MHz, CDCl_3 , ppm): δ 172.96, 165.50, 161.72, 143.77, 113.11, 111.01, 46.44, 36.96, 31.83, 31.73, 31.38, 29.88, 29.55, 29.47, 29.24, 26.34, 26.31, 22.63, 22.59, 14.08, 14.04.

(E)-4,4'-bis(2-hexyldecyl)-[6,6'-bithieno[3,2-b]pyrrolylidene]-5,5'(4H,4'H)-dione (3).

Lawesson's reagent (1.9 g, 4.72 mmol) was put under argon and a solution of **2** (3.342 g, 9.44 mmol) in dry toluene (20 ml) was added. The reaction was heated to 65 °C and stirred until complete conversion was seen on TLC. After cooling, water was added and the product was extracted with chloroform, washed with brine and dried over MgSO_4 . After removal of the solvent the crude product was subjected to silica column chromatography with hexane/DCM as eluent to give 1.238 g of the title compound in 36.3% yield. ^1H NMR (400 MHz, CDCl_3 , ppm): δ 7.52 (d, $J = 5.1$ Hz, 2H), 6.78 (d, $J = 5.1$ Hz, 2H), 3.69 (d, $J = 7.4$ Hz, 4H), 1.93 – 1.85 (m, 2H), 1.35 – 1.21 (m, 48H), 0.92 – 0.81 (m, 12H). ^{13}C NMR (100 MHz, CDCl_3 , ppm): δ 171.28, 151.51, 134.19, 121.04, 114.20, 111.32, 46.12, 37.13, 31.87, 31.85, 31.76, 31.46, 29.93, 29.60, 29.49, 29.25, 26.40, 26.37, 22.68, 22.64, 22.61, 14.09, 14.05. MALDI-TOF m/e : 722.43 (M^{+} , 100%). FT-IR: 1667 cm^{-1} (C=O).

(E)-2,2'-dibromo-4,4'-bis(2-hexyldecyl)-[6,6'-bithieno[3,2-b]pyrrolylidene]-5,5'(4H,4'H)-dione (4).

A solution of **3** (280 mg, 0.53 mmol) in DCM was added NBS (189 mg, 1.06 mmol) at 0 °C. Upon completion the reaction mixture was washed with water and brine and dried over MgSO_4 before it was purified over silica column with an heptane/chloroform mixture to give 366 mg of the desired monomer (79% yield). ^1H NMR (400 MHz, CDCl_3 , ppm): δ 6.81 (s, 2H), 3.62 (d, $J = 7.4$ Hz, 4H), 1.87 – 1.78 (m, 2H), 1.38 – 1.19 (m, 48H), 0.91 – 0.82 (m, 12H). ^{13}C NMR (100 MHz, CDCl_3 , ppm): δ 170.20, 150.07, 122.97, 119.50, 114.88, 114.62, 46.13, 37.19, 31.86, 31.77, 31.41, 31.38, 29.93, 29.62, 29.50, 29.28, 26.34, 22.66, 22.63, 14.10, 14.07. MALDI-TOF m/z : 880.26 (M^{+} , 100%).

(E)-2,2'-bis(4-dodecylthiophen-2-yl)-4,4'-bis(2-hexyldecyl)-[6,6'-bithieno[3,2-b]pyrrolylidene]-5,5'(4H,4'H)-dione (5).

Under argon atmosphere toluene (3 ml), water (0.3 ml) and one drop of Aliquat 336 were added to **4** (100 mg, 114 μmol), 2-(4-dodecylthiophen-2-yl)-4,4,5,5-tetramethyl-1,3,2-dioxaborolane (171.7 mg, 454 μmol) and K_3PO_4 (106 mg, 500 μmol). Then argon was bubbled through for 30 min. before adding Pd_2dba_3 (4.6 mg, 5 μmol) and PPh_3 (3.3 mg, 12.5 μmol). The reaction mixture was heated to 115 °C and stirred overnight. After extraction with chloroform and water the organic fraction was washed with brine and dried over MgSO_4 before it was subjected to column chromatography using a heptane/chloroform gradient. Product containing fractions were combined to give 123 mg of the title compound (88% yield). ^1H NMR (400 MHz, CDCl_3 , ppm): δ 7.25 (s, 2H), 6.93 (s, 2H), 6.80 (s, 2H), 3.63 (d, $J = 7.4$ Hz, 4H), 2.61 (t, $J = 7.8$ Hz, 4H), 1.87 (s, 2H), 1.64 (q, $J = 7.2$ Hz, 4H), 1.47 – 1.05 (m, 84H), 0.99 – 0.67 (m, 18H). ^{13}C NMR (100 MHz, CDCl_3 , ppm): δ 170.59, 151.36, 145.04, 144.72, 137.40, 125.61, 120.36, 118.81, 113.27, 107.03, 45.77, 37.15, 31.95, 31.91, 31.84, 31.40, 30.46, 30.44, 30.00, 29.72, 29.68, 29.57, 29.52, 29.40, 29.38, 29.36, 26.34, 26.32, 22.70, 22.69, 13.88. MALDI-TOF m/z : 1222.86 (M^{++} , 100%)

(E)-2,2'-bis(5-bromo-4-dodecylthiophen-2-yl)-4,4'-bis(2-hexyldecyl)-[6,6'-bithieno[3,2-b]pyrrolylidene]-5,5'(4H,4'H)-dione (6).

A solution of **5** (123 mg, 100.7 μmol) in dichloromethane (4 ml) was cooled to 0 °C and wrapped in aluminum foil. Then NBS (36.23 mg, 201.3 μmol) was added. When complete conversion was observed by TLC the solvent was removed *in vacuo* and the crude product subjected to silica column chromatography with heptane/DCM 75/25 to give 107 mg of the extended monomer (76.8% yield). ^1H NMR (400 MHz, CDCl_3 , ppm): δ 7.03 (s, 2H), 6.62 (s, 2H), 3.61 (dt, $J = 7.4, 3.9$ Hz, 4H), 2.53 (t, $J = 7.6$ Hz, 4H), 1.80 (p, $J = 6.5$ Hz, 2H), 1.60 (p, $J = 7.2$ Hz, 4H), 1.45 – 1.23 (m, 42H), 0.95 – 0.80 (m, 18H). MALDI-TOF m/z : 1378.66 (M^{++} , 100%)

PTIIT.

To a mixture of monomer **4** (99 mg, 112.7 μmol) and 2,5-bis(trimethylstannyl)thiophene (46.2 mg, 112.7 μmol) under argon atmosphere was added dry toluene (2 ml) and dry dimethylformamide (0.2 ml). Argon was bubbled through for 30 min. before addition of Pd_2dba_3 (4.1 mg, 4.5 μmol) and PPh_3 (2.4 mg, 9 μmol) and heating the reaction mixture to 110 °C. After 2 h subsequently tributyl(thiophen-2-yl)stannane (42 mg, 112.7 μmol) and 2-bromothiophene (37 mg, 225.2 μmol) were added with 30 min. interval to end cap the polymer. After another 30 min. the reaction mixture was cooled, precipitated in acetone and filtered through a Soxhlet thimble. The polymer was extracted with acetone, hexanes, dichloromethane and chloroform. The dichloromethane fraction was concentrated to minimal amount, precipitated in methanol, filtered over a PTFE filter and dried in a vacuum oven at 40 °C to give 85 mg of the title polymer. GPC (both chloroform 110 °C and 80 °C ODCB) was inconclusive as the polymer had interaction with the column. λ_{max} (CHCl_3) = 1006 nm.

PTIIP.

To a mixture of **4** (49.5 mg, 56.4 μmol), 1,4-bis(4,4,5,5-tetramethyl-1,3,2-dioxaborolan-2-yl)benzene (18.6 mg, 56.4 μmol) and K_3PO_4 (48 mg, 225.6 μmol) under argon atmosphere was added toluene (0.8 ml), 0.1 ml demi water (0.1 ml) and a 50:50

mixture of toluene and Aliquat 336 (0.1 ml). Argon was bubbled through this solution for 30 minutes before addition of Pd₂dba₃ (2.75 mg, 3 μmol) and PPh₃ (2 mg, 8 μmol). The reaction was started in a preheated oil bath at 115 °C and stirred at that temperature for 3 h. Then subsequently 4,4,5,5-tetramethyl-2-phenyl-1,3,2-dioxaborolane (46 mg, 225.6 μmol) and bromobenzene (48 μl, 451.2 μmol) were added with 30 min. intervals to end cap the polymer. After another 30 min. the reaction was cooled and quenched by precipitation in methanol (100 ml). The polymer was redissolved in chloroform and stirred overnight with diethylthiocarbamate solution (4 g/l, 50 ml). After extraction the organics were washed with water, concentrated to a minimal amount and precipitated in methanol. The precipitates were filtered through a Soxhlet thimble and extracted under argon with methanol, heptane, dichloromethane and chloroform. The dichloromethane fraction contained most of the polymer and was precipitated in methanol after which the precipitates were filtered over a PTFE filter and dried in a vacuum oven at 40 °C to give 36 mg of dark polymer. GPC (both chloroform 110 °C and 80 °C ODCB) was inconclusive as the polymer had interaction with the column. λ_{max} (CHCl₃) = 872 nm.

PTIICb.

To a mixture of monomer **4** (72 mg, 82.0 μmol), 9-(heptadecan-9-yl)-2,7-bis(4,4,5,5-tetramethyl-1,3,2-dioxaborolan-2-yl)-9H-carbazole (53.9 mg, 82.0 μmol) and K₃PO₄ (87 mg, 410 μmol) was added under argon atmosphere toluene (3 ml) and water (0.3 ml) together with one drop of Aliquat 336. Argon was bubbled through for 30 min. before addition of Pd₂dba₃ (3.0 mg, 3.3 μmol) and PPh₃ (1.7 mg, 6.6 μmol) after which the reaction was heated to 115 °C for 3 h. Then subsequently 4,4,5,5-tetramethyl-2-phenyl-1,3,2-dioxaborolane (16.7 mg, 82.0 μmol) and bromobenzene (17.3 μl, 164 μmol) are added with 30 min. interval to end cap the polymer. After another 30 min. the reaction was cooled and quenched by precipitation in acetone. Filtration through a Soxhlet thimble and subsequent extraction with acetone, hexane and chloroform gave most of the polymer in the chloroform fraction. Reducing the volume and precipitation in methanol followed by filtration over a PTFE filter and drying the polymer in a vacuum oven at 40 °C resulted in 88 mg of the desired polymer. GPC (CHCl₃, 110 °C): M_n = 33.1 kg/mole and PDI = 2.5. GPC (ODCB, 80 °C): M_n = 42.7 kg/mole and PDI = 2.3. λ_{max} (CHCl₃) = 746 nm.

PTII3T.

To monomer **6** (52 mg, 39.2 μmol) and 2,5-bis(trimethylstannyl)thiophene (16.06 mg, 39.2 μmol) under argon atmosphere was added dry toluene (3 ml) and dry DMF (0.6 ml). Argon was bubbled through for 30 min. before Pd₂dba₃ (1.44 mg, 1.57 μmol) and PPh₃ (1.03 mg, 3.9 μmol) were added. The reaction was heated to 110 °C and stirred overnight. Then the polymer was end capped with subsequently tributyl(thiophen-2-yl)stannane (14.9 mg, 40 μmol) and 2-bromothiophene (13 mg, 80 μmol) with 30 min. interval. After another hour the reaction was cooled, precipitated in methanol and filtered through a Soxhlet thimble and washed with acetone. The polymer was subjected to Soxhlet extraction under argon atmosphere with acetone, hexane and chloroform to give 33 mg of the desired polymer. GPC (CHCl₃, 110 °C): M_n = 13.4 kg/mol and PDI = 4.0. GPC (ODCB, 80 °C): M_n = 14.3 kg/mol and PDI = 2.1. λ_{max} (CHCl₃) = 768 nm.

PTIITPT.

To **6** (45.2 mg, 32.7 μmol), 1,4-bis(4,4,5,5-tetramethyl-1,3,2-dioxaborolan-2-yl)benzene (10.8 mg, 32.7 μmol) and K_3PO_4 (27.8 mg, 130.8 μmol) under argon atmosphere was added THF/water 5/1 (3.6 ml). Argon was bubbled through this solution for 15 minutes after which Pd_2dba_3 (1.2 mg, 1.3 μmol) and ${}^t\text{Bu}_3\text{PHBF}_4$ (0.8 mg, 2.6 μmol) were added. The mixture was then heated to 80 $^\circ\text{C}$ and stirred overnight at this temperature. Then bromobenzene (27.5 μl , 261.6 μmol) was added 1 h after the addition of 4,4,5,5-tetramethyl-2-phenyl-1,3,2-dioxaborolane (26.7 mg, 130.8 μmol) to terminate all reactive end groups. After 1 h the reaction was quenched by precipitating the polymer in methanol including the solids that had already formed in the reaction mixture. After filtration the residue was subjected to Soxhlet extraction with acetone, heptane, dichloromethane, chloroform, chlorobenzene and *ortho*-dichlorobenzene. Approximately 20 mg of the polymer remained as solids in the Soxhlet timble. The chloroform fraction was concentrated to give 2 mg of the desired polymer. (CHCl_3 , 110 $^\circ\text{C}$): $M_n = 29.5$ kg/mol and PDI = 2.5. GPC (ODCB, 80 $^\circ\text{C}$): $M_n = 32.4$ kg/mol and PDI = 2.5. $\lambda_{\text{max}}(\text{CHCl}_3) = 737$ nm.

3.6 Acknowledgements

I thank Dr. J.-C. Flores and Dr. M. Turbiez (BASF Switzerland) for helpful discussions and Dr. F. Gholamrezaie for assistance with the OFET preparation and mobility measurements.

3.7 References

- ¹ J. Mei, K. R. Graham, R. Stalder, and J. R. Reynolds, *Org. Lett.*, **2010**, *12*, 660-663.
- ² K. R. Graham, J. Mei, R. Stalder, J. W. Shim, H. Cheun, F. Steffy, F. So, B. Kippelen, and J. R. Reynolds, *ACS Appl. Mater. Interfaces*, **2011**, *3*, 1210-1215.
- ³ R. Stalder, J. G. Mei, and J. R. Reynolds, *Macromolecules*, **2010**, *43*, 8348-8352.
- ⁴ G. Zhang, Y. Fu, Z. Xie, and Q. Zhang, *Macromolecules*, **2011**, *44*, 1414-1420.
- ⁵ Z. Ma, E. Wang, K. Vandewal, M. R. Andersson, and F. Zhang, *Appl. Phys. Lett.*, **2011**, *99*, 143302.
- ⁶ B. Liu, Y. Zou, B. Peng, B. Zhao, K. Huang, Y. He, and C. Pan, *Polym. Chem.*, **2011**, *2*, 1156-1162.
- ⁷ R. Stalder, J. Mei, J. Subbiah, C. Grand, L. A. Estrada, F. So, and J. R. Reynolds, *Macromolecules*, **2011**, *44*, 6303-6310.
- ⁸ J. Mei, D. H. Kim, A. L. Ayzner, M. F. Toney, and Z. Bao, *J. Am. Chem. Soc.*, **2011**, *133*, 20130-20133.
- ⁹ R. Stalder, C. Grand, J. Subbiah, F. So, and J. R. Reynolds, *Polym. Chem.* **2012**, *3*, 89-92.
- ¹⁰ Z. Ma, E. Wang, M. E. Jarvid, P. Henriksson, O. Inganäs, F. Zhang, and M. R. Andersson, *J. Mater. Chem.*, **2012**, *22*, 2306-2314.
- ¹¹ T. Lei, Y. Cao, Y. Fan, C.-J. Liu, S.-C. Yuan, and J. Pei, *J. Am. Chem. Soc.* **2011**, *133*, 6099-6101.
- ¹² J. Xu, L. D. Li, B. Liu, and Y. P. Zou, *Appl. Phys. Lett.* **2011**, *98*, 063303.
- ¹³ H. Von Eller-Pandraud, *Acta Crystallogr.*, **1960**, *13*, 936-938.
- ¹⁴ M.-S. Yuan, Q. Fang, L. Ji, and W.-T. Yu, *Acta Crystallogr. E*, **2007**, *63*, o4342.
- ¹⁵ Y. K. Voronina, D. B. Krivolapov, A. V. Bogdanov, V. F. Mironov, and I. A. Litvinov, *J. Struct. Chem.*, **2012**, *53*, 413-416.
- ¹⁶ L. A. Estrada, R. Stalder, K. A. Abboud, C. Risko, J.-L. Brédas, and J. R. Reynolds, *Macromolecules*, **2013**, *46*, 8832-8844.
- ¹⁷ N. Bérubé, V. Gosselin, J. Gaudreau, and M. Cote, *J. Phys. Chem. C*, **2013**, *117*, 7964-7972.
- ¹⁸ M. C. Scharber, D. Mühlbacher, M. Koppe, P. Denk, C. Waldauf, A. J. Heeger, and C. J. Brabec, *Adv. Mater.*, **2006**, *18*, 789-794.
- ¹⁹ J.-C. Flores, U. Berens, F. Bienewald, H. J. Kirner, and M. G. R. Turbiez, *PCT Int. Appl.* **2009**, WO2009053291A1.
- ²⁰ R. S. Ashraf, A. J. Kronemeijer, D. I. James, H. Siringhaus, and I. McCulloch, *Chem. Commun.*, **2012**, *48*, 3939-3941.
- ²¹ G. W. P. Van Puijssen, F. Gholamrezaie, M. M. Wienk, and R. A. J. Janssen, *J. Mater. Chem.*, **2012**, *22*, 20387-20393.
- ²² M. S. Chen, J. R. Niskala, D. A. Unruh, C. K. Chu, O. P. Lee, and J. M. J. Fréchet, *Chem. Mater.*, **2013**, *25*, 4088-4096.
- ²³ M. Ide, Y. Koizumi, A. Saeki, Y. Izumiya, H. Ohkita, S. Ito, and S. Seki, *J. Phys. Chem. C*, **2013**, *117*, 26859-26870.
- ²⁴ M. Ide, Y. Koizumi, A. Saeki, and S. Seki, *J. Photopolym. Sci. Technol.*, **2013**, *26*, 217-221.
- ²⁵ M. Karakawa, and Y. Aso, *Macromol. Chem. Phys.*, **2013**, *214*, 2388-2397.
- ²⁶ Y. Chen, Z. Du, W. Chen, L. Han, Q. Liu, M. Sun, and R. Yang, *Synth. Met.*, **2014**, *187*, 24-29.
- ²⁷ Y. Koizumi, M. Ide, A. Saeki, C. Vijayakumar, B. Balan, M. Kawamoto, and S. Seki, *Polym. Chem.*, **2013**, *4*, 484-494.
- ²⁸ G. Kim, S.-J. Kang, G. K. Dutta, Y.-K. Han, T. J. Shin, Y.-Y. Noh, and C. Yang, *J. Am. Chem. Soc.*, **2014**, *136*, 9477-9483.
- ²⁹ G. Kollenz, G. Penn, R. Theuer, W. M. F. Fabian, H. A. Abd El-Nabi, X. Zhang, K. Peters, E. M. Peters, and H. G. von Schnering, *Tetrahedron*, **1996**, *52*, 5427-5440.
- ³⁰ I. A. Livsedge, S. J. Higgins, M. Giles, M. Heeney, and I. McCulloch, *Tetrahedron Lett.*, **2006**, *47*, 5143-5146.

- ³¹ J. K. Park, J. Jo, J. H. Seo, J. S. Moon, Y. D. Park, K. Lee, A. J. Heeger, and G. C. Bazan, *Adv. Mater.*, **2011**, *23*, 2430-2435.
- ³² D. Veldman, S. C. J. Meskers, and R. A. J. Janssen, *Adv. Funct. Mater.*, **2009**, *19*, 1939-1948.
- ³³ E. G. Wang, Z. Ma, Z. Zhang, K. Vandewal, P. Henriksson, O. Inganäs, F. Zhang, and M. R. Andersson, *J. Am. Chem. Soc.* **2011**, *133*, 14244-14347.

Chapter 4.

High ambipolar charge carrier mobility in benzodipyrrolidone conjugated polymers*

A series of alternating donor-acceptor polymers, consisting of diphenylbenzodipyrrolidone (BDP) and oligothiophene was synthesized and used in top-gate bottom-contact organic field-effect transistors and solar cells. The BDP polymers exhibit ambipolar charge transport with high and balanced mobilities up to 0.21 cm²/Vs for holes and 0.18 cm²/Vs for electrons. Increasing the length of the oligothiophene reduces the electron mobility roughly by an order of magnitude per thiophene, but the hole mobility remains high. This behavior is explained using DFT calculations by a strong localization of the electrons on the BDP units. All polymer solar cells with a BDP polymer as acceptor could be made but maximum efficiencies only reach 0.33%.

* This chapter is based on G.W.P van Pruissen, E.A. Pidko, M.M. Wienk, and R.A.J. Janssen, *J. Mater. Chem. C*, **2014**, *2*, 731-735.

4.1 Introduction

In the dye and pigment industry benzodifuranones (BDF) (Figure 4.1) were developed as a new colorant for polyester textiles by ICI in the late '70s and early '80s after pioneering work by King and Newall on their synthesis.¹ The possible synthetic variations on the BDF theme were fully explored by making asymmetric substitutions,^{2,3} extending the benzene core to a naphthalene core⁴ and substituting the furanone by pyrrolidone to give benzodipyrrolidone (BDP).²

The BDF and BDP cores are strong electron acceptors due to the withdrawing carbonyl moieties that are in conjugation with the π -electron system, making it interesting candidates to apply in donor acceptor copolymers. In addition, the conjugated π -electrons of these molecules have a quinoid electronic ground state. Combining quinoid with aromatic monomers can reduce the bond length alternation resulting in small band gap polymers.^{5,6} In a recent density functional theory (DFT) study it was suggested that besides smaller band gaps also the reorganization energy upon excitation can be reduced using the quinoid-aromatic design principle,⁷ favoring high charge mobility according to Marcus theory.⁸ Figure 4.2 illustrates the role of aromatic and quinoid resonance structures for a BDP-based polymer compared to poly(3-alkylthiophene).

Although BDF was introduced into conjugated polymers like the PBDFTP in Figure 4.1,^{9,10} the lack of solubilizing side chains make it hard to obtain soluble polymers. Contrary the BDF, BDP has two synthetically easy accessible lactam rings that can be *N*-alkylated and hence give soluble polymers. This was recently shown with two BDP-based copolymers with benzene (PBDFP3P, Figure 4.1) and thiophene.¹¹

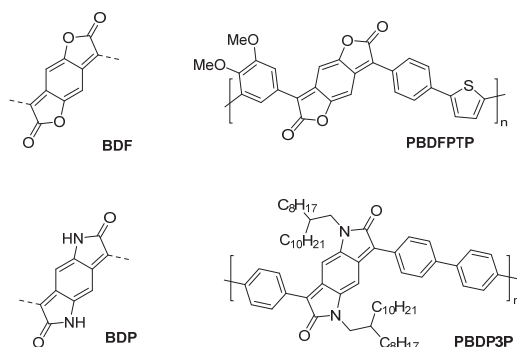


Figure 4.1 - Core structures of benzodifuranone (BDF) and benzodipyrrolidone (BDP) and two of the first conjugated polymers published incorporating these dyes.

The classical synthesis route of Greenhalgh² results in BDPs that are substituted by two phenyl groups in the 3 and 7 positions and that are twisted by 38° with respect to the BDP core in crystals of *N*-methylated monomers.¹¹ Despite this large twist, BDP-based polymers have onsets of absorption between 700 and 800 nm, and can be considered as small band gap materials.¹¹ Flanking BDP with two five-membered rings instead of two phenyl rings can reduce the twisting, thereby improving the conjugation along the backbone. The synthetically challenging 3,7-dithienyl-BDP monomer was recently reported by McCulloch *et al.*¹² and Wudl *et al.*¹³ and used to prepare small band gap polymers that show onsets of absorption up to 1500 nm. For dithienyl-BDP-based polymers charge carrier mobilities of 0.2 and 0.1 cm²/Vs for holes and electrons in OFETs with top gate bottom contact architecture have been reported.¹² OFETs based on diphenyl-BDP-based polymers have been reported, reaching charge carrier mobilities up to 0.03 cm²/Vs for holes¹⁴ and 0.012 cm²/Vs for electrons, the latter being measured in an *N*-acylated BDP polymer.¹⁵

BDP-based polymers were also used as electron donor in OPV with [6,6]-phenyl-C₆₁-butyric acid methyl ester (PC₆₀BM) as acceptor to give 2.6% power conversion efficiency.¹⁶ The low LUMO and good electron mobilities make it also an interesting candidate for all polymer bulk heterojunction solar cells. This subclass has been an interesting alternative for polymer:fullerene bulk heterojunctions for many years now as the synthetic options to tune the polymer structure and energy levels are virtually endless.¹⁷ In addition one can select two polymers with complementary absorption to maximize the total absorption of the active layer. All polymer solar cells always suffered from low PCEs (< 1%) until some recent examples showed significantly higher PCEs¹⁸⁻²² with a maximum of 5.7% in the scientific literature so far.²³ Together with certified higher efficiencies (6.4%, Polyera) with undisclosed materials this has revived the interest in all polymer solar cells as it now seems possible to bridge the gap with the highly efficient polymer:fullerene solar cells. The development of good acceptor polymers is crucial as until now only a few examples are known mainly based on naphthalenediimide,²¹ cyano-polyphenylenevinylene,^{17,24} benzothiadiazole fluorene copolymers²⁵⁻²⁷ or more recently with lactam-based acceptors such as isoindigo²⁸ and diketopyrrolopyrrole.^{20,29}

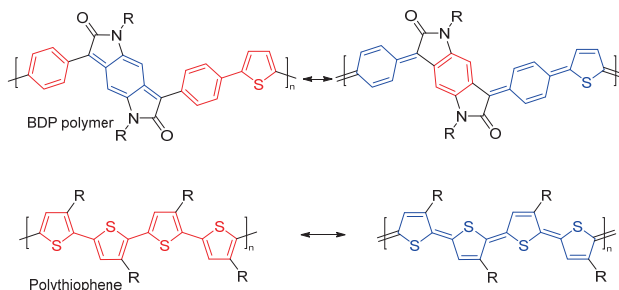


Figure 4.2 – Alternating quinoid (blue) and aromatic (red) segments in resonance structures of conjugated polymers with BDP in its backbone compared to fully quinoid and aromatic resonance structures of poly(3-alkylthiophene) as a conventional conjugated polymer.

4.2 Aim

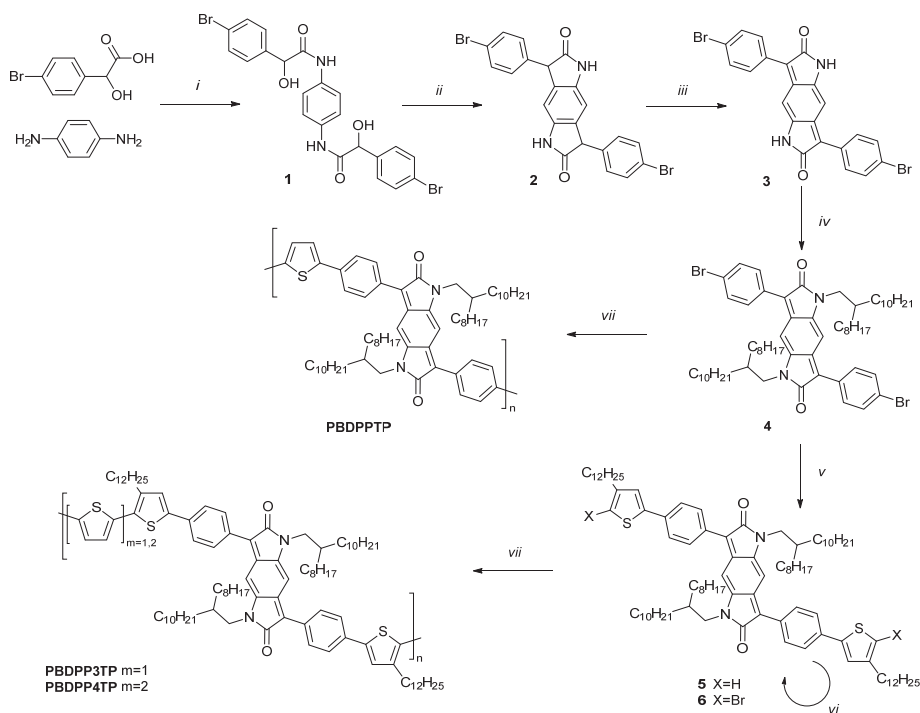
Based on these recent results it is of interest to understand how extended aromatic segments affect the hole and electron mobility in these BDP polymers. For the related DPP polymers it has been suggested that a low lying and widely delocalized LUMO is beneficial to achieve a high electron mobility. Here we report on the synthesis and properties of three conjugated polymers consisting of alternating diphenyl-BDP and oligothiophene units that afford mobilities for electrons and holes in OFETs that are higher by an order of magnitude compared to previous values^{14,15} and that are slightly improved with respect to the thiophene-flanked BDP-based polymers.¹² DFT calculations are used to investigate how the local geometrical properties and the length of the oligothiophene segments influence the electronic structure and, accordingly, the electron and hole mobility in these polymers.

4.3 Results and discussion

4.3.1 Synthesis

The phenyl-flanked BDP monomer **4** (Scheme 4.1) was synthesized according to known procedures,^{11,14,15} following the route developed by Greenhalgh *et al.*² Starting from 4-bromomandelic acid and benzene-1,4-diamine the *N,N'*-(1,4-phenylene)bis(2-(4-bromophenyl)-2-hydroxyacetamide (**1**) was synthesized by extensive heating. Consecutive stirring in concentrated sulfuric acid forms the bislactam by electrophilic aromatic substitution. The intermediate **2** was readily oxidized under alkaline conditions to give the quinoid 3,7-bis(4-bromophenyl)pyrrolo[2,3-f]indole-2,6(1*H*,5*H*)-dione (**3**). Branched side

chains were introduced on the amide by reaction of **3** with 9-(bromomethyl)nonadecane to give monomer **4**. Palladium catalyzed Stille polymerization of **4** with 2,5-bis(trimethylstannyl)thiophene afforded PBDPPTP ($M_n = 13.9$ kg/mol, PDI = 5.2). Because copolymers with bithiophene show very poor solubility and low molecular weights,¹⁴ **4** was extended with two 4-dodecylthiophen-2-yl rings via a Suzuki coupling to give **5**, introducing extra solubilizing side chains. Subsequent bromination with NBS resulted in the extended BDP monomer **6**. This extended monomer was polymerized with 2,5-bis(trimethylstannyl)thiophene and 5,5'-bis(trimethylstannyl)-2,2'-bithiophene via Stille coupling to give PBDPP3TP ($M_n = 28.9$ kg/mol, PDI = 2.3) and PBDPP4TP ($M_n = 30.6$ kg/mol, PDI = 2.1).



Scheme 4.1 – Synthesis of BDP-based polymers. (i) Chlorobenzene, 125 °C, 24 h. (ii) Concentrated H_2SO_4 , r.t., 15 h. (iii) 2 M KOH, hydrogen peroxide and ethanol, r.t., 2 h. (iv) 9-(Bromomethyl)nonadecane, K_2CO_3 , DMF, 125 °C, 15 h. (v) 2-(4-Dodecylthiophen-2-yl)-4,4,5,5-tetramethyl-1,3,2-dioxaborolane, K_3PO_4 , Aliquat 336, PPh_3 , Pd_2dba_3 , toluene/water (5/1), 110 °C, 15 h. (vi) NBS, DCM, 0 °C to r.t., 15 h. (vii) 2,5-Bis(trimethylstannyl)thiophene or 5,5'-bis(trimethylstannyl)-2,2'-bithiophene, Pd_2dba_3 PPh_3 , toluene/DMF (10/1), 115 °C, 15 h.

4.3.2 Optical and electrochemical properties

Optical absorption spectra of these polymers were measured in chloroform solution and as thin films on glass. All polymers show a broad absorption in the 350 – 800 nm region (Figure 4.3) with absorption maxima ranging from 580 to 615 nm. A second maximum is observed in all spectra at higher energy with an intensity that depends on the number of incorporated thiophenes. For all polymers a red-shift is observed going from solution to solid state thin films. This red-shift of the absorption is smaller for PBDPPTP (~25 nm) than for PBDPP3TP (~65 nm) and PBDPP4TP (~50 nm). The solubility of the latter two polymers is slightly better as a result of the extra dodecyl side chains on two thiophenes whilst PBDPPTP is more aggregated in solution. The steepness of the onset is also significantly different, both PBDPP3TP and PBDPP4TP show a more gradual increase of absorption with respect to PBDPPTP, both in solution and in the thin film state. From the onsets of absorption in the solid state the band gaps of these materials were estimated to be 1.69, 1.52 and 1.56 eV, respectively. With an increasing number of thiophenes the optical band gap is initially lowered but going from three to four thiophenes, the optical band gap moves to higher energy. This is rationalized by considering that by increasing length of the oligothiophene, the quinoid resonance structure increases in energy (Figure 4.2).

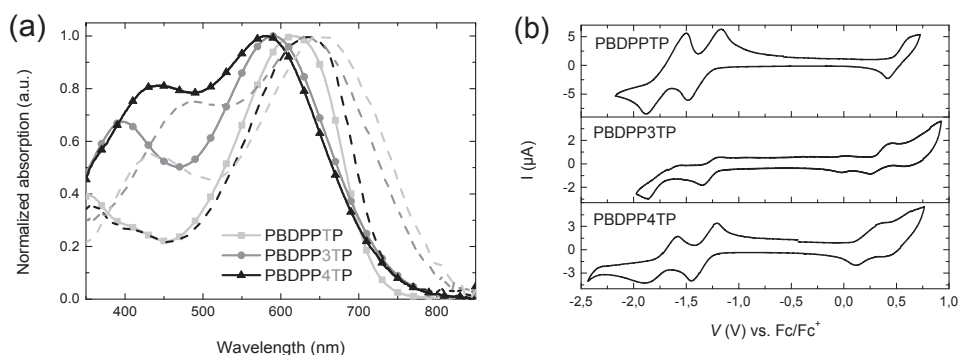


Figure 4.3 – (a) Normalized absorption for PBDPPTP, PBDPP3TP and PBDPP4TP in chloroform solution (solid lines) and in thin films on glass, spin coated from chloroform solutions (dashed lines). (b) Cyclic voltammograms of the BDP polymers.

The frontier orbital energy levels of the polymers were estimated using cyclic voltammetry. The polymers were dissolved in a 0.1 M TBAPF₆ *ortho*-dichlorobenzene (ODCB) electrolyte and measured against an Ag/AgCl reference electrode with ferrocene/ferrocenium as an internal standard (Figure 4.3). HOMO and LUMO levels were calculated from the onset of oxidation and reduction, respectively, using $E_{MO} = -5.23 - qE_{redox}$. The LUMO levels are nearly identical for all three polymers with $E_{LUMO} = -3.96$, -4.04 , and -3.99 eV for PBDPPTP, PBDPP3TP, and PBDPP4TP (Table 4.1). The HOMO levels increase with the number of thiophenes from $E_{HOMO} = -5.68$, via -5.53 , to -5.35 eV.

Table 4.1 – Optical and electrochemical characteristics

	M_n	PDI	λ_{onset}^{sol}	λ_{onset}^{film}	$E_g^{sol a}$	$E_g^{film a}$	$E_g^{cv b}$	E_{HOMO}^c	E_{LUMO}^c	$\mu_{h sat}$	$\mu_{e sat}$
	kg/mol		nm	nm	eV	eV	eV	eV	eV	cm ² /Vs	cm ² /Vs
PBDPPTP	13.9	2.3	720	735	1.72	1.69	1.72	-5.68	-3.96	2.1×10^{-1}	1.8×10^{-1}
PBDPP3TP	28.9	2.3	737	817	1.68	1.52	1.49	-5.53	-4.04	1.9×10^{-1}	5.4×10^{-2}
PBDPP4TP	30.6	2.1	732	796	1.69	1.56	1.35	-5.35	-3.99	1.0×10^{-1}	5.8×10^{-3}

$$^a E_g^{sol/film} = 1240/\lambda_{onset^{sol/film}} \cdot \quad ^b E_g^{cv} = q(E_{ox} - E_{red}). \quad ^c E_{Fc/Fc^+} \text{ taken as } -5.23 \text{ eV.}$$

This corroborates with a simple molecular orbital representation for donor-acceptor polymers in which the HOMO is mainly determined by the donor part and the LUMO mainly by the acceptor. In this case the BDP acceptor is the same in all polymers giving similar LUMO energies, while the donating character increases from one to four thiophene rings, resulting in a higher lying HOMO level. The HOMO levels are below -5.25 eV which can provide stability against oxidation in ambient conditions. The electrochemical band gaps calculated from the HOMO and LUMO levels are 1.72, 1.49, and 1.35 eV and resemble the ones measured optically, except for PBDPP4TP where the electrochemical band gap is 0.2 eV less compared to the optical band gap.

4.3.3 Characterization of OTFT devices

To evaluate charge transport properties of these materials top-gate bottom-contact OFETs were made by evaporating gold source and drain contacts on glass, spin coating the active layer and a Cytop dielectric layer followed by evaporation of a gold gate electrode. Transfer curves for all three polymers are shown in Figure 4.4 for positive and negative source-drain voltages (V_{SD}) and the mobility data are collected in Table 4.1. The BDP polymers exhibit ambipolar charge transport in OFETs. Each of the three polymers reaches

a saturated hole mobility of $\mu_h = 1\text{--}2 \times 10^{-1} \text{ cm}^2/\text{Vs}$, but the electron mobilities differ significantly. For the polymer with the longest oligothiophene, PBDPP4TP, the electron mobility is low ($\mu_e = 5.8 \times 10^{-3} \text{ cm}^2/\text{Vs}$), but it improves by an order of magnitude ($5.4 \times 10^{-2} \text{ cm}^2/\text{Vs}$) for PBDPP3TP, which has one thiophene less. The highest and best balanced mobilities are found for PBDPPTP, which has a single thiophene ring, and has $\mu_h = 2.1 \times 10^{-1}$ and $\mu_e = 1.8 \times 10^{-1} \text{ cm}^2/\text{Vs}$. These mobilities are the highest reported values for diphenyl-BDP-based polymers to date and similar to those of dithienyl-BDP-based materials.¹²

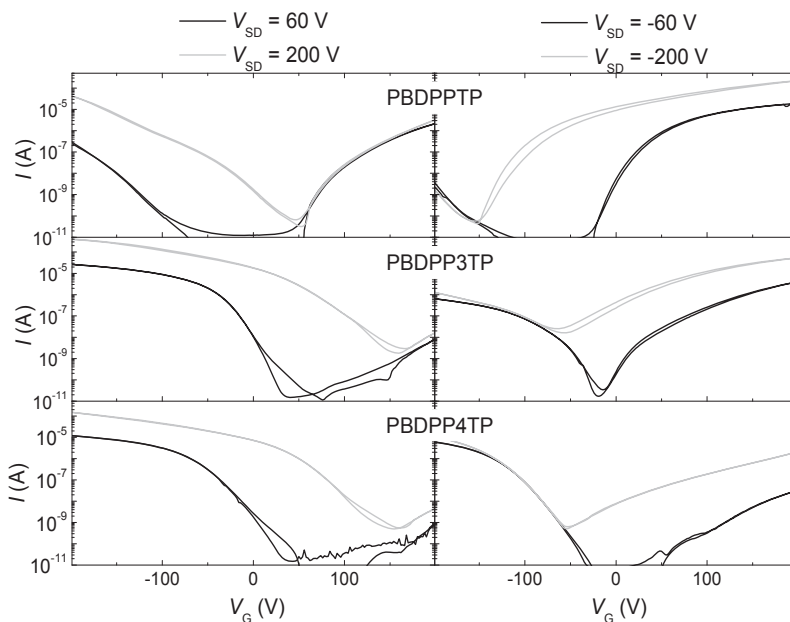


Figure 4.4 – Transfer curves for BDP polymer OFETs at different source drain voltages (± 60 and ± 200 V).

In general charge mobility is affected by molecular weight, purity, morphology, deposition process, and device architecture. The reason for the higher hole and electron mobilities of PBDPPTP found here compared to the values reported in Ref. 11 ($\mu_h = 3.5 \times 10^{-3}$ and $\mu_e = 6.4 \times 10^{-3} \text{ cm}^2/\text{Vs}$) can possibly be related to the higher molecular weight ($M_n = 13.9 \text{ kg/mol}$ vs. 8 kg/mol in Ref. 11) and a more optimal device architecture. In the bottom contact/top gate (staggered) configuration used here the contact resistance is reduced compared to the bottom contact/bottom gate (coplanar) configuration used in

Ref. 11. These differences however, do not explain the low $\mu_e = 5.3 \times 10^{-3} \text{ cm}^2/\text{Vs}$ for PBDPPTP reported in Ref. 15, because the reported $M_n = 49.0 \text{ kg/mol}$ is higher and the staggered FET configuration is similar to the work presented here.

The correspondence between charge mobility in polymers with diphenyl or dithienyl substituted BDP units is remarkable (see Ref. 14) and suggests –somewhat counter intuitively– that, compared to the more planar thiophene rings, the increased torsional twisting of the phenyl rings with respect to the central BDP unit, does not drastically decrease the charge mobility of BDP polymers.

4.3.4 Morphology

The morphology of the polymer layers was further investigated with X-ray diffraction (XRD) and atomic force microscopy (AFM) (Figure 4.5). XRD measured on drop cast films revealed a broad peak at $2\theta = 4.20^\circ - 4.55^\circ$, corresponding to a lamellar packing with a d -spacing distance of 1.94 – 2.10 nm. Upon thermal annealing all peaks sharpen and one higher order reflection becomes visible indicating increased crystallinity. Concomitantly the reflections shift slightly to lower angles, indicating that the d -spacing increases to 2.00 – 2.30 nm (see Table 4.2).

Table 4.2 – Diffraction data and associated distances for lamellar stacking.

	As cast		150 °C Annealed	
	Peak _{max}	d	Peak _{max}	d
	2θ	nm	2θ	nm
PBDPPTP	4.55	1.94	4.41	2.00
PBDPP3TP	4.20	2.10	3.88	2.28
PBDPP4TP	4.50	1.96	4.20	2.10

AFM reveals very smooth film surfaces that coarsen upon annealing at 150 °C. Especially the PBDPP3TP and PBDPP4TP layers exhibit an increased height and width of surface features, consistent the growth of small crystalline domains and the enhanced and narrowed XRD diffraction. The fact that this effect is the strongest in PBDPP3TP and PBDPP4TP can be explained by the extra dodecyl side chains allowing for structural rearrangement of the polymers upon heating.

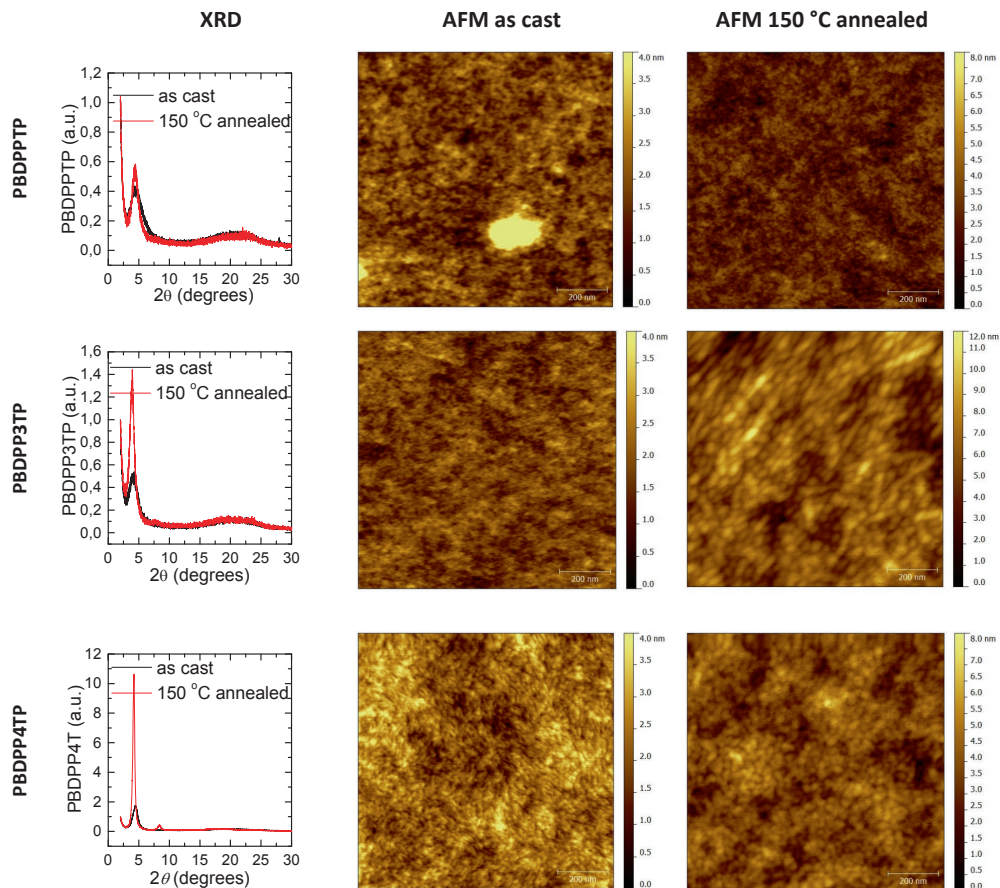


Figure 4.5 – In the left column the XRD diffraction of drop casted films of PBDPPTP, PBDPP3TP and PBDPP4TP on a silicon wafer before (black) and after annealing at 150 °C (red). All curves are normalized to the intensity at 2θ of 2.0 degrees in order to compare measurements. AFM images of spin coated layers of PBDPPTP, PBDPP3TP and PBDPP4TP on silicon substrates. In the middle column *as cast* and in the right column *annealed at 150 °C*. All samples are $1\ \mu\text{m} \times 1\ \mu\text{m}$ and have the height scale set between 0 – 4 nm for the as cast samples. The annealed samples differ in height scale and are 12 nm for PBDPP3TP and 8 nm for the others.

4.3.5 DFT calculations

To further investigate the electronic structures and geometries DFT calculations were performed at the B3LYP/6-311G(d) level of theory using the Gaussian 09 program.³⁰ Calculations were performed on acceptor-donor-acceptor model structures in which the long alkyl side chains were replaced by methyl groups because of the low influence of the

alkyl side-chains on the electronic structure of the conjugated back-bone. Figure 4.6 shows a representation of the HOMO and LUMO of the different Ph-BDP-Ph-oligothiophene-Ph-BDP-Ph molecules. For the shortest molecule, the HOMO is delocalized over a large part of the molecule, including the BDP units, but with increasing length of the oligothiophene the HOMO fully localizes on the (oligo)-thiophene moiety. In all structures, the HOMO remains delocalized over a significant part of the molecule. In a polymer thin film this ensures that holes can be transported because interactions between HOMOs on adjacent chains remain likely. On the other hand, a strong localization of the LUMO on the BDP units is observed for all models. With increasing length of the oligothiophene it covers only a small geometric part of the molecule. Such a strong LUMO localization hampers both intrachain and interchain transport of electrons. The results in Figure 4.6 suggest that this effect will be more pronounced for the polymers with longer oligothiophene moieties in line with the experimental observations. By increasing the donor part in these polymers the sites for electrons are effectively diluted and the average distance to the next possible site increases, hampering electron transport.

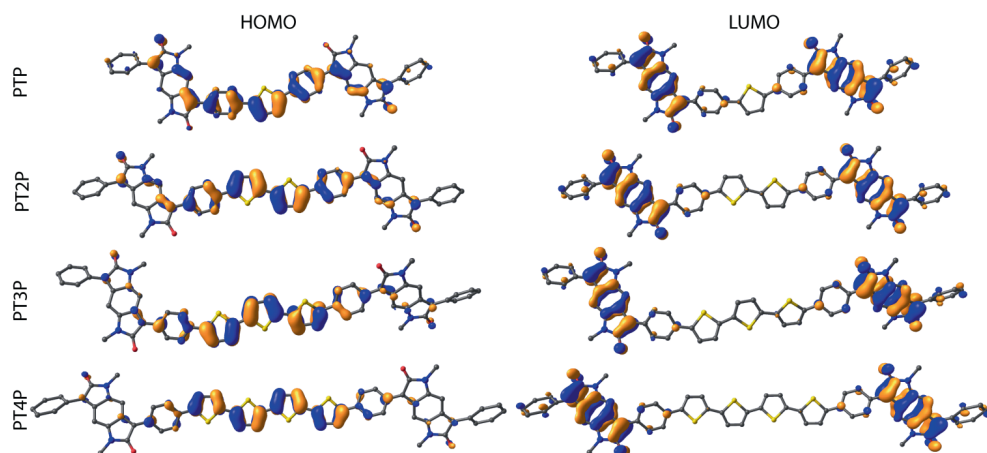


Figure 4.6 – HOMO and LUMO from DFT calculations for different phenyl-flanked Ph-BDP-Ph-oligothiophene-Ph-BDP-Ph systems.

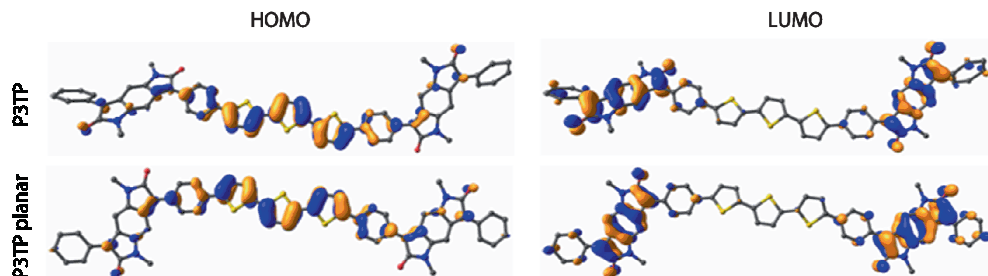


Figure 4.7 – Two different optimizations for Ph-BDP-Ph-3T-Ph-BDP-Ph. Top image shows HOMO and LUMO for the fully optimized molecule without any restrictions, bottom picture shows the results for HOMO and LUMO with fixed dihedral angles of 0° between BDP and phenyl rings.

To make sure that these characteristics correspond to the intrinsic properties of BDP as a quinoid acceptor rather than result of the hampered conjugation due to the calculated 30° twist of the phenyl rings with the BDP, the calculations were repeated with the dihedral angles set to 0° to enforce a planar structure but no significant differences in HOMO and LUMO were found (Figure 4.7). To further check the relevance of these results for polymeric systems, an extended BDP-donor-BDP-donor-BDP molecule with Ph-3T-Ph as donor part, was calculated. The HOMO is distributed over the donor part, while the LUMO, LUMO+1, and LUMO+2 are nearly degenerate (< 0.06 eV) and carry exclusively contributions from the three BDP units as can be seen in Figure 4.8. Therefore the HOMO and LUMO distribution of large polymeric systems are represented well by the molecules shown in Figure 4.6.

Table 4.3 – Comparison of optical characteristics from experiment and DFT for BDP polymers.

donor block	$\lambda_{\text{onset}}^{\text{DFT}}$	$\lambda_{\text{onset}}^{\text{sol}}$	$\lambda_{\text{onset}}^{\text{film}}$	$E_g^{\text{sol } a}$	$E_g^{\text{film } a}$	$E_g^{\text{cv } b}$	$E_{0 \rightarrow 1}^{\text{DFT}}$	$f_{\text{oscillator}}^{\text{DFT}}$	$\Delta E^{\text{DFT } c}$
	nm	nm	nm	eV	eV	eV	eV		eV
PTP	680	720	735	1.72	1.69	1.72	1.82	0.92	2.08
P2TP	713	-	-	-	-	-	1.74	1.36	1.98
P3TP	737	737	817	1.68	1.52	1.49	1.68	1.28	1.92
P4TP	758	732	796	1.69	1.56	1.35	1.64	1.34	1.85

$$^a E_g^{\text{sol/film/DFT}} = 1240/\lambda_{\text{onset}}^{\text{sol/film/DFT}}, \quad ^b E_g^{\text{cv}} = q(E_{\text{ox}} - E_{\text{red}}), \quad ^c \Delta E^{\text{DFT}} = E_{\text{HOMO}}^{\text{DFT}} - E_{\text{LUMO}}^{\text{DFT}}.$$

Time-dependent DFT (TD-DFT) calculations were employed to compute first excitation energy ($E_{0 \rightarrow 1}$). Besides general overestimation of the excitation energy the calculated values show similar trends as the observed optical and electrochemical data (Table 4.3).

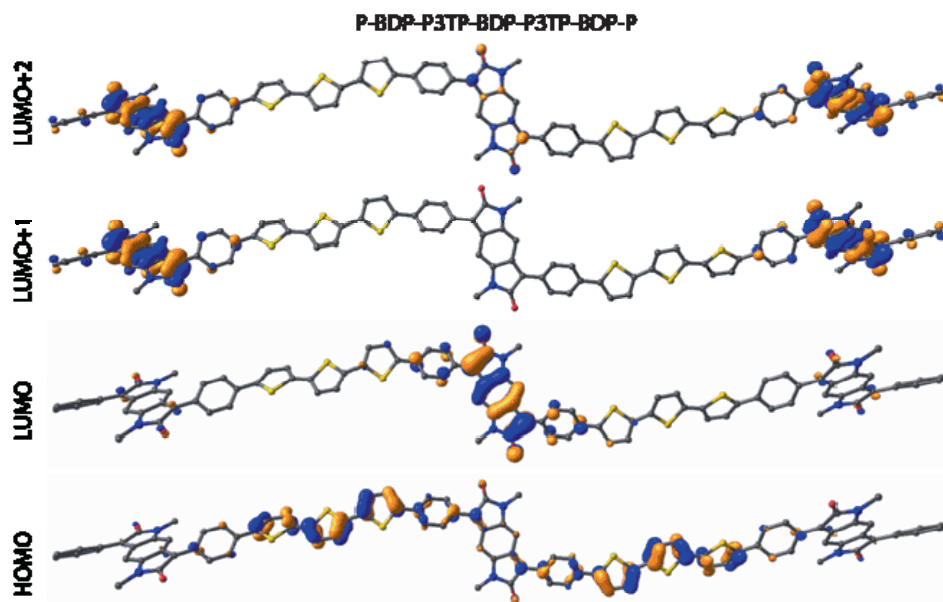


Figure 4.8 – HOMO and LUMO, LUMO+1, and LUMO+2 for the Ph-BDP-Ph-3T-Ph-BDP-Ph-3TP-BDP-Ph trimer showing the three nearly degenerate LUMO levels. LUMO+1 and LUMO+2 are respectively 0.05 and 0.06 eV higher.

4.3.6 Solar cells

4.3.6.1 Polymer:PCBM solar cells

Despite the low offset of the LUMO level of these polymers (-4.00 ± 0.04 eV) with respect to the LUMO of [6,6]-phenyl- C_{71} -butyric acid methyl ester PC₇₀BM (-4.15 eV) they were tested as donor material in solar cells. PC₇₀BM was used as acceptor since it has a stronger absorption coefficient in the visible range of the spectrum compared to PC₆₀BM, which has a formally forbidden HOMO – LUMO transition due to symmetry restrictions.³¹ Regular polarity ITO/PEDOT:PSS/active layer/LiF/Al devices were made with active layers spin coated from chlorobenzene (CB) with 2% v/v diiodooctane (DIO) and a polymer:PC₇₀BM ratio of 1:2 (12 mg/ml total concentration). The current density – voltage

($J - V$) characteristics of the optimized devices are shown in Figure 4.9 and the relevant solar cell parameters are collected in Table 4.4. The cells show relatively high open-circuit voltage (V_{oc}), but performed poorly because of very low short-circuit current densities that varied between $J_{sc} = 0.2$ and 1.8 mA/cm^2 going from PBDPPTP via PBDPP3TP to PBDPP4TP (Table 4.4). This is a direct result of the low LUMO of the BDP polymers, which is almost equal to that of PC₆₀BM (-4.15 eV).³² It has been suggested that a minimum energy difference of 0.3 eV is required for efficient charge separation and this criterion is not met in the case of the BDP polymers and PC₇₀BM.³³ The spectrally resolved external quantum efficiency (EQE) of PBDPP4TP:PC₇₀BM solar cells (Figure 4.9b) indicates that the photocurrent is exclusively generated by photons absorbed by PC₇₀BM, not by the polymer. In this case a hole transfer from the HOMO of the excited PC₇₀BM to the HOMO of the PBDPP4TP generates the charges. Energetically this hole transfer will be more favorable than electron transfer from the polymer, since the HOMO – HOMO offset estimated by CV measurements is larger (0.55 eV) than the LUMO – LUMO offset (0.16 eV). For the other polymers no EQE data were recorded, but the observed lower J_{sc} for these materials might be related to the fact that the HOMO energy levels become deeper with decreasing number of thiophene rings, which reduces the HOMO – HOMO energy offset to $\sim 0.4 \text{ eV}$ and $\sim 0.2 \text{ eV}$ for PBDPP3TP and PBDPPTP, respectively.

Table 4.4 – Solar cell characteristics for BDP polymers

Polymer	ratio	Solvent	J_{sc} mA/cm	V_{oc} V	FF	PCE %
PBDPPTP:PC ₇₀ BM	1:2	CB:DIO 2% (v/v)	0.21	0.954	0.344	0.07
PBDPP3TP:PC ₇₀ BM	1:2	CB:DIO 2% (v/v)	0.63	0.815	0.578	0.30
PBDPP4TP:PC ₇₀ BM	1:2	CB:DIO 2% (v/v)	1.82	0.808	0.617	0.91
PDPP5T:PBDPPTP	1:1	CHCl ₃ :ODCB 10% (v/v)	1.17	0.749	0.380	0.37

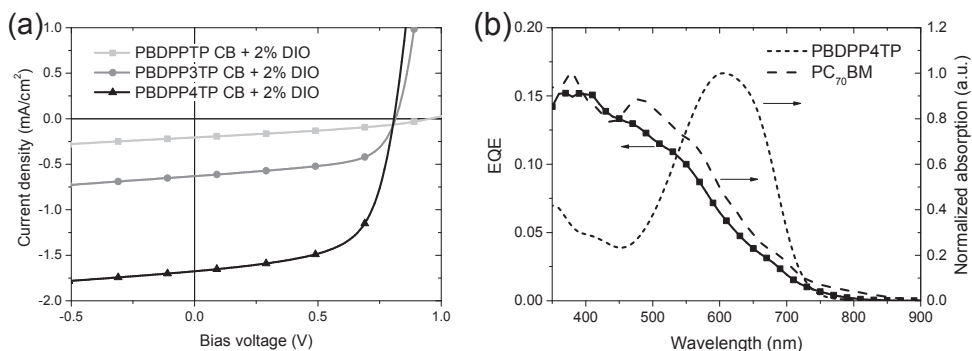


Figure 4.9 – (a) $J - V$ characteristics of solar cells from BDP polymers with PC₇₀BM. (b) EQE of the PBDPP4TP:PC₇₀BM solar cell showing exclusive contribution from the PC₇₀BM absorption.

The low LUMO energy levels of the BDP polymers render these materials ineffective as electron donor, but it may be turned to an advantage if the materials are used as electron acceptor, for example in all polymer solar cells, combining it with a suitable polymer as electron donor.

4.3.6.2 Polymer:polymer solar cells

The BDP polymers all show a low LUMO level making it suitable candidates to replace the fullerene as electron accepting polymer in polymer:polymer solar cells. As also electrons need to be transported through the acceptor polymer phase, high electron mobility is a prerequisite. This makes PBDPPTP the polymer of choice to be tested with a complementary donor polymer. A good complementary polymer should have sufficient LUMO – LUMO and HOMO – HOMO offsets (> 0.3 eV), and preferably absorb in a different range of the solar spectrum. PDPP5T^{20,34} (Figure 4.10) has shown a PCE of up to 5.3% as a donor polymer in a polymer:PC₆₀BM device. This polymer has a LUMO energy of -3.63 eV and a HOMO level of -5.23 eV with an optical band gap of 1.44 eV.³⁴ Hence, both offsets are expected to be sufficient for photoinduced charge generation when PDPP5T and PBDPPTP are mixed.

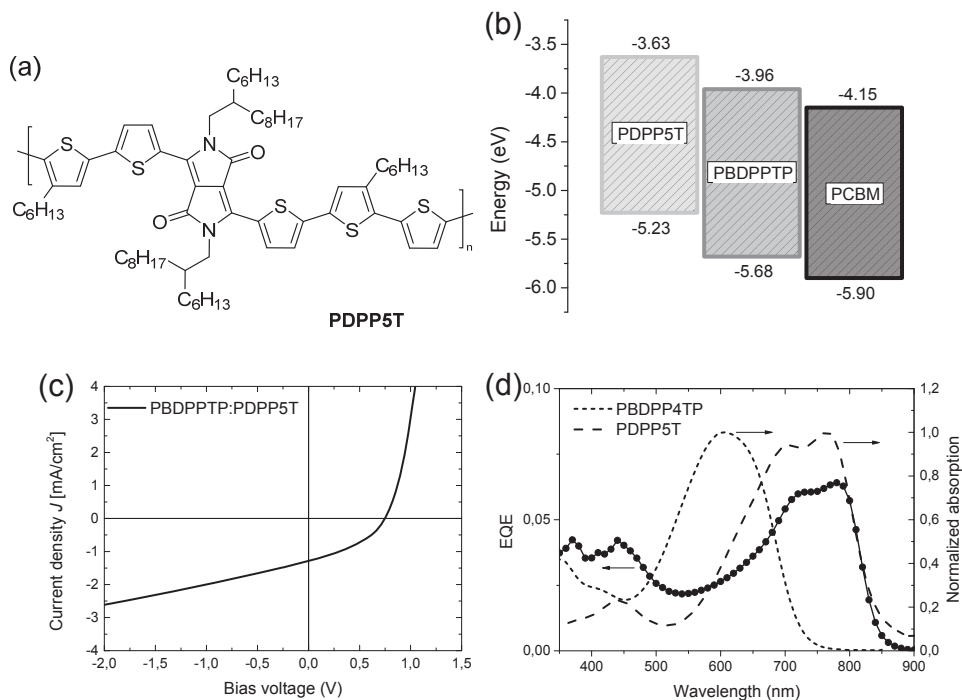


Figure 4.10 – (a) PDPP5T structure and (b) energy level diagram of the materials used in the solar cells. (c) $J - V$ curve for PDPP5T:PBDPPTP all polymer solar cells under illumination and (d) EQE of the same solar cell with the absorption spectra of the respective polymers for reference.

Combining these polymers in a 1:1 ratio and spin coating the active layer from a CHCl₃:10%ODCB solution in a regular polarity ITO/PEDOT:PSS/PDPP5T:PBDPPTP/LiF/Al configuration gave the best results after annealing at 100 °C for 3 min with $J_{sc} = 1.2$ mA/cm², $V_{oc} = 0.75$ V and FF = 0.38, and a PCE of 0.3%. The recorded photocurrent effectively proves that generation of charges and therefore exciton splitting does occur within this material combination. However, when the EQE spectrum is compared to the absorption spectra of the two polymers (Figure 4.10) it becomes clear that the collected charges originate exclusively from photons absorbed by the PDPP5T. The LUMO – LUMO offset is thus probably large enough to enable electron transfer. The fact that there is no contribution from the PBDPPTP absorption to the photocurrent suggests that there is no hole transfer from the HOMO of the PBDPPTP to the HOMO of the PDPP5T. This is somewhat unexpected because the estimated HOMO – HOMO offset is larger than the LUMO – LUMO offset. One possible alternative explanation is that the excitons in the BDP

polymers are very short lived and do not reach a donor acceptor interface within their lifetime.

The field-dependent photocurrent (Figure 4.10) and consequently moderate fill factor (FF = 0.38) indicate that charge separation or charge transport are a problem in these solar cells. As the electron and hole mobility in the pristine materials are sufficiently high the interpenetrating network of donor and acceptor phase must be sub optimal. This can lead to poor charge generation and to poor charge transport. Spin coating the active layer from chloroform solutions with different solvent additives such as DIO and 1-chloronaphthalene (CN) showed no improvement, also not with annealing.

4.4 Conclusions

Three soluble, high molecular weight push-pull polymers incorporating BDP as an acceptor and oligothiophene as a donor were synthesized via Stille polycondensation. The polymers possess deep lying HOMO and LUMO levels that are beneficial to the stability of this class of materials under ambient conditions. DFT calculations show that the HOMO and LUMO are highly localized on the donor and acceptor and that this is a result of intrinsic molecular properties rather than twisting in the conjugated backbone. The polymers show ambipolar charge transport with a high mobility for holes and an electron mobility that strongly depends on the length of the thiophene segment. Charge carrier mobility is nicely balanced in PBDPPTP with $\mu_h = 0.21 \text{ cm}^2/\text{Vs}$ and $\mu_e = 0.18 \text{ cm}^2/\text{Vs}$. These values are among the highest charge mobilities for BDP-based materials to date. Because both electrons and holes can be conducted BDP materials are able to function both as electron donor and electron acceptor material in OPV devices, but charge generation and collection are limited resulting in PCEs below 1%.

4.5 Experimental

4.5.1 General procedures, materials, and instruments

See paragraph 2.5.1. for details on NMR, UV-vis-NIR, MALDI-TOF, and CV equipment.

Molecular weights were determined by GPC using a PL-GPC 120 High Temperature Chromatograph with a Mixed-C (200 - 2.000.000 Da versus polystyrene standards) column using ODCB at 80 °C as mobile phase. XRD was measured on a Bruker D4 Endeavor diffractometer using Cu K α radiation with a wavelength of 0.15406 nm. Scans were done from 2 – 30 degrees (2 θ) with scan speed of 0.2 seconds/step and increments of 0.01 degree/step. Samples for XRD were prepared by drop casting 100 μl of a 10 mg/ml

polymer solution in chloroform on to a (911) surface of a silicon wafer. Samples were measured directly as cast and after annealing by placing the samples for 15 min. upside down on a glass plate that was placed on a 150 °C hot plate. AFM was performed in tapping mode on a Veeco Multimode SPM equipped with a Nanoscope IIIa SPM controller. PPPNCH-50 aluminum coated silicon tips from Nanosensors were used with scan rates of 2 Hz. Sample preparation was done using silicon wafers and a 5 mg/ml chloroform solution of polymers. Layers were spin coated at 1000 rpm and annealed by placing the samples directly on a 150 °C hot plate for 15 min.

DFT calculations were performed on the High Performance Computing cluster of the department of Chemical Engineering and Chemistry of the Eindhoven University of Technology, The Netherlands. It is equipped with 54 computing nodes each with 2x Quadcore AMD processors and has Grid Engine installed as the queuing system.

4.5.2 OFET fabrication and characterization

Field-effect transistors were fabricated on 3 x 3 cm glass substrates in a bottom-contact top-gate configuration. Substrates were cleaned prior to use with soap, demi-water and isopropanol. Gold (30 nm) electrodes were then evaporated with a preceding chromium adhesion layer (3 nm). Active layers were spin coated from a 5 mg/ml polymer chloroform solution at 1000 rpm to give approximately 30 nm active layers that were annealed at 200 °C for 30 min. to remove solvent residues. A Cytop dielectric was applied by spin coating at 1000 rpm and annealing at 120 °C for 45 min. to remove solvent residues and provide on average a 1350 nm thick layer. Devices were finalized by evaporation of a gold (50 nm) top gate electrode. Electric characterization was done using a vacuum probe station connected to a Keithley 2636. Channel length and width were 20 and 1000 μm respectively.

4.5.3 OPV fabrication and characterization

See paragraph 2.5.2 for details of device fabrication and measurement equipment.

4.5.4 Synthesis

***N,N'*-(1,4-phenylene)bis(2-(4-bromophenyl)-2-hydroxyacetamide) (1).**

1,2,4-Trichlorobenzene (50 ml) was added to 4-bromo-DL-mandelic acid (10.0 g, 43.3 mmol) and benzene-1,4-diamine (2.1 g, 19.7 mmol) before heating the solution to 150 °C. After 2 h the mixture was cooled and poured into methanol. The precipitate was filtered and washed with methanol to give 4.0 g (7.5 mmol, 38% yield) of the title compound after drying. ^1H NMR (400 MHz, DMSO- d_6 , ppm): δ 9.88 (s, 2H), 7.59 (s, 4H), 7.58 – 7.52 (m, 2H), 7.49 – 7.41 (m, 2H), 6.50 (d, J = 4.7 Hz, 2H), 5.08 (d, J = 4.7 Hz, 2H). ^{13}C NMR (100 MHz, DMSO- d_6 , ppm): δ 170.85, 140.70, 134.60, 131.41, 129.13, 121.17, 120.42, 73.66.

3,7-Bis(4-bromophenyl)pyrrolo[2,3-*f*]indole-2,6(1*H*,5*H*)-dione (3).

To **1** (4.0 g, 7.5 mmol) was added concentrated sulfuric acid (100 ml) and the mixture was stirred at room temperature overnight. The solution was then precipitated in a water and ice mixture, filtered and dried to give compound **2**, which was subsequently used in

the next reaction without further purification. The residue was re-dissolved in a mixture of ethanol, 2 M KOH and hydrogen peroxide (2.5:1:1) and stirred for 2 h at room temperature. Then water was added and the precipitate filtered off which was dried in vacuum to give 2.8 g of pale red **3** (5.6 mmol, 75%). The crude product was used in the next reaction as obtained.

3,7-Bis(4-bromophenyl)-1,5-bis(2-octyldodecyl)pyrrolo[2,3-f]indole-2,6(1H,5H)-dione (4).

Under an argon atmosphere **3** (700 mg, 1.4 mmol), 9-(bromomethyl)nonadecane (1.5 g, 4.2 mmol) and K_2CO_3 (0.9 g, 7 mmol) were dissolved in DMF, heated to 125 °C and stirred at that temperature overnight. After cooling, water was added and the mixture was extracted with ethyl acetate several times. The combined organic fractions were dried and concentrated *in vacuo*. Silica column chromatography with chloroform as mobile phase was used to isolate product **4**, which was subsequently recrystallized from ethanol (350 mg, 330 μ mol, 24%). 1H NMR (400 MHz, $CDCl_3$, ppm): δ 7.64 – 7.53 (m, 8H), 6.29 (s, 2H), 3.50 (d, J = 7.4 Hz, 4H), 1.76 (s, 2H), 1.41 – 1.15 (m, 64H), 0.87 (dt, J = 6.8, 2.7 Hz, 12H). ^{13}C NMR (100 MHz, $CDCl_3$, ppm): δ 169.54, 144.29, 134.47, 132.03, 130.91, 130.00, 126.31, 123.57, 97.14, 75.59, 44.01, 37.08, 31.91, 31.88, 31.74, 29.99, 29.76 – 29.48 (m), 29.43 – 29.21 (m), 26.67, 22.78 – 22.55 (m), 14.11. MALDI-TOF m/z : 1056.66 (M^+ , 100%).

3,7-Bis(4-(4-dodecylthiophen-2-yl)phenyl)-1,5-bis(2-octyldodecyl)pyrrolo[2,3-f]indole-2,6(1H,5H)-dione (5).

To **4** (200 mg, 189 μ mol) was added 2-(4-dodecylthiophen-2-yl)-4,4,5,5-tetramethyl-1,3,2-dioxaborolane (180 mg, 473 μ mol) and K_3PO_4 (212 mg, 1 mmol) and the mixture was put under an argon atmosphere. Toluene and water (5:1) were added with Aliquat 336 (1 drop) and argon was bubbled through for 15 min. Then Pd_2dba_3 (4.3 mg, 4.7 μ mol) and PPh_3 (4.9 mg, 18.8 μ mol) were added and the mixture was heated to 115 °C for 24 h. After cooling the mixture was precipitated in methanol and filtrated. Subsequent recrystallization from chloroform/ethanol mixture gave pure **5** (186 mg, 134 μ mol, 71%). 1H NMR (400 MHz, $CDCl_3$, ppm): δ : 7.79 – 7.64 (m, 8H), 7.24 (s, 2H), 6.92 (s, 2H), 6.40 (s, 2H), 3.53 (d, J = 7.0 Hz, 4H), 2.68 – 2.56 (m, 4H), 1.80 (br, 2H), 1.73 – 1.57 (m, 8H), 1.44 – 1.09 (m, 96H), 0.94 – 0.78 (m, 18H).

3,7-Bis(4-(5-bromo-4-dodecylthiophen-2-yl)phenyl)-1,5-bis(2-octyldodecyl)pyrrolo[2,3-f]indole-2,6(1H,5H)-dione (6).

In DCM (20 ml) was dissolved **5** (186 mg, 133 μ mol) and subsequently at 0 °C NBS (47.8 mg, 266 μ mol) in portions. After 1 h the mixture was allowed to warm to room temperature and stirred overnight. Precipitation in methanol and filtration followed by recrystallization from chloroform/ethanol afforded the title compound (186 mg, 119 μ mol, 90%) with high purity. 1H NMR (400 MHz, $CDCl_3$, ppm): δ 7.75 (d, J = 8.2 Hz, 4H), 7.60 (d, J = 8.2 Hz, 4H), 7.08 (s, 2H), 6.38 (s, 2H), 3.52 (d, J = 7.4 Hz, 4H), 1.79 (br, 2H), 2.58 (t, J = 7.8 Hz, 4H), 1.62 (p, J = 7.2 Hz, 4H), 1.45 – 1.13 (m, 100H), 0.86 (p, J = 6.8 Hz, 18H). ^{13}C NMR (100 MHz, $CDCl_3$, ppm): δ 169.78, 144.10, 143.45, 142.76, 134.25, 133.98, 130.67, 130.04, 126.46, 125.45, 124.55, 109.27, 97.45, 43.96, 37.13, 31.91, 31.87, 31.80, 30.02, 29.73, 29.78 – 29.53 (m), 29.58, 29.43, 29.46 – 29.24 (m), 29.27, 26.74, 22.68, 22.67, 14.11. MALDI-TOF m/z : 1556.90 (M^+ , 100%).

General polymerization procedure; PBDPPTP.

To **4** (50 mg, 47.3 μmol) and 2,5-bis(trimethylstannyl)thiophene (19.4 mg, 47.3 μmol) under argon atmosphere was added a toluene/DMF (10/1) mixture (2 ml, anhydrous). Argon was bubbled through for 15 min. before adding Pd_2dba_3 (0.65 mg, 0.7 μmol) and PPh_3 (0.74 mg, 2.8 μmol). The mixture was heated in a sealed tube for 24 h and then precipitated in methanol. The precipitate was subjected to Soxhlet extraction with acetone, hexanes, and chloroform. The latter fraction was concentrated and precipitated in methanol again to give the desired polymer as a dark solid (36 mg, 75% yield).

PBDPPTP. GPC (ODCB, 80 °C): $M_n = 13.9$ kg/mol, PDI = 5.2. $\lambda_{\text{max}} = 615$ nm.

PBDPP3TP. GPC (ODCB, 80 °C): $M_n = 28.9$ kg/mol, PDI = 2.3. $\lambda_{\text{max}} = 591$ nm.

PBDPP4TP. GPC (ODCB, 80 °C): $M_n = 30.6$ kg/mol, PDI = 2.1. $\lambda_{\text{max}} = 582$ nm.

4.6 Acknowledgements

I thank Dr. Evgeny Pidko for DFT calculations and discussions.

4.7 References

- ¹ T. J. King and C. E. Newall, *J. Chem. Soc.*, **1965**, 974-977.
- ² C. W. Greenhalgh, J. L. Carey, and D. F. Newton, *Dyes Pigm.*, **1980**, *1*, 103-120.
- ³ G. Hallas and C. Yoon, *Dyes Pigments*, **2001**, *48*, 107-119.
- ⁴ G. Hallas and C. Yoon, *Dyes Pigments*, **2001**, *48*, 121-132.
- ⁵ J. L. Brédas, *Synth. Met.*, **1987**, *17*, 115-121.
- ⁶ C. Kitamura, S. Tanaka, and Y. Yamashita, *Chem. Mater.*, **1996**, *8*, 570-578.
- ⁷ N. Bérubé, J. Gaudreau, and M. Côté, *Macromolecules*, **2013**, *46*, 6873-6880.
- ⁸ R. A. Marcus, *Rev. Mod. Phys.*, **1993**, *65*, 599-610.
- ⁹ K. Zhang and B. Tieke, *Macromolecules*, **2011**, *44*, 4596-4599.
- ¹⁰ K. Zhang, B. Tieke, J. C. Forgie, F. Vilela, and P. J. Skabara, *Macromolecules*, **2011**, *45*, 743-750.
- ¹¹ W. Cui, J. Yuen, and F. Wudl, *Macromolecules*, **2011**, *44*, 7869-7873.
- ¹² J. W. Rumer, M. Levick, S.-Y. Dai, S. Rossbauer, Z. Huang, L. Biniek, T. D. Anthopoulos, J. R. Durrant, D. J. Procter, and I. McCulloch, *Chem. Comm.*, **2013**, *49*, 4465-4467.
- ¹³ W. Cui and F. Wudl, *Macromolecules*, **2013**, *46*, 7232-7238.
- ¹⁴ W. Hong, C. Guo, Y. Li, Y. Zheng, C. Huang, S. Lu, and A. Facchetti, *J. Mater. Chem.*, **2012**, *22*, 22282-22289.
- ¹⁵ P. Deng, L. Liu, S. Ren, H. Li, and Q. Zhang, *Chem. Comm.*, **2012**, *48*, 6960-6962.
- ¹⁶ W. Yue, X. Huang, J. Yuan, W. Ma, F. C. Krebs, and D. Yu, *J. Mater. Chem. A*, **2013**, *1*, 10116-10119.
- ¹⁷ S. A. Jenekhe and S. Yi, *Appl. Phys. Lett.*, **2000**, *77*, 2635-2637.
- ¹⁸ A. Facchetti, *Mater. Today*, **2013**, *16*, 123-132.
- ¹⁹ T. Earmme, Y.-J. Hwang, N. M. Murari, S. Subramaniyan, and S. A. Jenekhe, *J. Am. Chem. Soc.*, **2013**, *135*, 14960-14963.
- ²⁰ W. Li, W. S. C. Roelofs, M. Turbiez, M. M. Wienk, and R. A. J. Janssen, *Adv. Mater.*, **2014**, *26*, 3304-3309.
- ²¹ N. Zhou, H. Lin, S. J. Lou, X. Yu, P. Guo, E. F. Manley, S. Loser, P. Hartnett, H. Huang, M. R. Wasielewski, L. X. Chen, R. P. H. Chang, A. Facchetti, and T. J. Marks, *Adv. Energy Mater.*, **2014**, *4*, 1300785.
- ²² D. Mori, H. Bente, I. Okada, H. Ohkita, and S. Ito, *Adv. Energy Mater.*, **2014**, *4*, 1301006.
- ²³ D. Mori, H. Bente, I. Okada, H. Ohkita, and S. Ito, *Energy Environ. Sci.*, **2014**, *7*, 2939-2943.
- ²⁴ T. Kietzke, H.-H. Hörhold, and D. Neher, *Chem. Mater.*, **2005**, *17*, 6532-6537.
- ²⁵ X. He, F. Gao, G. Tu, D. Hasko, S. Hüttner, U. Steiner, N. C. Greenham, R. H. Friend, and W. T. S. Huck, *Nano Lett.*, **2010**, *10*, 1302-1307.
- ²⁶ D. Mori, H. Bente, J. Kosaka, H. Ohkita, S. Ito, and K. Miyake, *ACS Appl. Mater. Interfaces*, **2011**, *3*, 2924-2927.
- ²⁷ A. C. Arias, J. D. MacKenzie, R. Stevenson, J. J. M. Halls, M. Inbasekaran, E. P. Woo, D. Richards, and R. H. Friend, *Macromolecules*, **2001**, *34*, 6005-6013.
- ²⁸ R. Stalder, J. Mei, J. Subbiah, C. Grand, L. A. Estrada, F. So, and J. R. Reynolds, *Macromolecules*, **2011**, *44*, 6303-6310.
- ²⁹ M.-F. Falzon, A. P. Zoombelt, M. M. Wienk, and R. A. J. Janssen, *Phys. Chem. Chem. Phys.*, **2011**, *13*, 8931-8939.
- ³⁰ Gaussian 09, Revision A.01, M. J. Frisch, G. W. Trucks, H. B. Schlegel, G. E. Scuseria, M. A. Robb, J. R. Cheeseman, G. Scalmani, V. Barone, B. Mennucci, G. A. Petersson, H. Nakatsuji, M. Caricato, X. Li, H. P. Hratchian, A. F. Izmaylov, J. Bloino, G. Zheng, J. L. Sonnenberg, M. Hada, M. Ehara, K. Toyota, R. Fukuda, J. Hasegawa, M. Ishida, T. Nakajima, Y. Honda, O. Kitao, H. Nakai, T. Vreven, J. A. Montgomery, Jr., J. E. Peralta, F. Ogliaro, M. Bearpark, J. J. Heyd, E. Brothers, K. N. Kudin, V. N. Staroverov, R. Kobayashi, J. Normand, K. Raghavachari, A. Rendell, J. C. Burant, S. S. Iyengar, J.

- Tomasi, M. Cossi, N. Rega, J. M. Millam, M. Klene, J. E. Knox, J. B. Cross, V. Bakken, C. Adamo, J. Jaramillo, R. Gomperts, R. E. Stratmann, O. Yazyev, A. J. Austin, R. Cammi, C. Pomelli, J. W. Ochterski, R. L. Martin, K. Morokuma, V. G. Zakrzewski, G. A. Voth, P. Salvador, J. J. Dannenberg, S. Dapprich, A. D. Daniels, Ö. Farkas, J. B. Foresman, J. V. Ortiz, J. Cioslowski, and D. J. Fox, Gaussian, Inc., Wallingford CT, **2009**.
- ³¹ M. M. Wienk, J. M. Kroon, W. J. H. Verhees, J. Knol, J. C. Hummelen, P. A. van Hal, and R. A. J. Janssen, *Angew. Chem., Int. Edit.*, **2003**, *42*, 3371-3375.
- ³² J. C. Bijleveld, M. Shahid, J. Gilot, M. M. Wienk, and R. A. J. Janssen, *Adv. Funct. Mater.*, **2009**, *19*, 3262-3270.
- ³³ M. C. Scharber, D. Mühlbacher, M. Koppe, P. Denk, C. Waldauf, A. J. Heeger, and C. J. Brabec, *Adv. Mater.*, **2006**, *18*, 789-794.
- ³⁴ V. S. Gevaerts, A. Furlan, M. M. Wienk, M. Turbiez, and R. A. J. Janssen, *Adv. Mater.*, **2012**, *24*, 2130-2134.

Chapter 5.

The effects of cross conjugation in copolymers of isoindigo and thienothiophene*

The influence of introducing cross conjugation on the optical and electrochemical properties of donor-acceptor copolymers is investigated. Isoindigo was used as electron-deficient unit because it can be conjugated or cross-conjugated to adjacent units via substitution at either the 6,6' or the 5,5' positions, respectively. Thiophene-flanked thieno[3,2-b]thiophene and thieno[2,3-b]thiophene were taken as conjugated and cross-conjugated electron-rich building blocks. By combining these donor and acceptor units four isomeric polymers were synthesized and their optical electrochemical properties were determined. The study reveals that introducing cross conjugation in isoindigo has only a small effect on the optical band gap and the HOMO and LUMO levels. The onset of absorption is always in the near infrared and also the electrochemical band gaps are very similar. The optical absorption spectra differ, however, strongly because cross conjugation in the isoindigo unit causes the transition to the lowest excited state to have small oscillator strength, resulting in a low-intensity absorption at the band gap. In a series of copolymers with a varying ratio of conjugated and cross-conjugated isoindigos, the intensity of the low energy electronic transition increases linearly with the fraction of conjugated units. Cross conjugation in thienothiophene exerts a different effect. It causes a moderate but distinct blue shift of the optical absorption and a deeper HOMO level. The experimental results are corroborated by DFT calculations.

* G.W.P. van Pruissen, K.H. Hendriks, M.M. Wienk and R.A.J. Janssen, *Manuscript in preparation*, 2014.

5.1 Introduction

The field of π -conjugated semiconducting polymers is attracting attention since their discovery¹ as a promising class of materials for flexible and cheap optoelectronic devices, based on earth-abundant elements with endless synthetic variety. Specialized conjugated polymers for organic light-emitting diodes (OLED),^{2,3} organic field-effect transistors (OFET),^{4,5} and organic photovoltaics (OPV)^{6,7} have been developed, each with their optical and electronic properties tuned to the respective device specific requirements. For bulk heterojunction polymer-fullerene solar cells, tuning the band gap of the polymer to match the solar spectrum and match the LUMO level to that of the fullerene acceptor is one such example.⁸ General design strategies such as reduction of the backbone twists and enlarging fused ring systems⁹⁻¹¹ are combined with the successful donor (D) – acceptor (A) approach^{12,13} or in some cases the aromatic – quinoid design¹⁴⁻¹⁶ to reduce the bond length alternation. In all cases it concerns conjugated polymers with alternating single and double bonds along the polymer backbone. Lately also polymers with so called 2D character, having an extended π -system perpendicular to the backbone, have been successfully introduced.^{7,17-19}

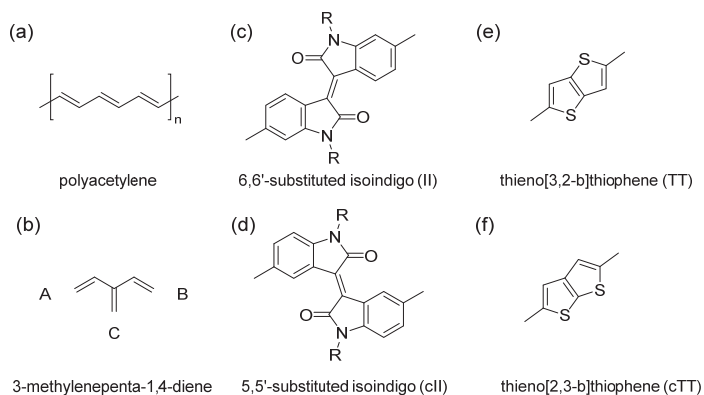


Figure 5.1 – (a) Polyacetylene as example of normal π -conjugation. (b) 3-Methylenepenta-1,4-diene, the basic example of a cross conjugation. (c) 6,6'-Substituted isoindigo (II) where substituents are fully conjugated and electronically connected to one another. (d) Cross-conjugated isoindigo (cII) with substituents on the 5,5' positions which are meta to the connecting central double bond. (e) Thieno[3,2-*b*]thiophene (TT) a fully conjugated electron rich molecule when connected on the 2,5 positions. (f) Thieno[2,3-*b*]thiophene (cTT) which has the methylenepenta-1,4-diene pattern in it and is a cross-conjugated analog of thieno[3,2-*b*]thiophene when 2,5 connected.

Incorporation of cross conjugation can be an interesting additional design principle to alter both optical and electronic properties without sacrificing planarity. Cross conjugation can be defined as a point substituted with three unsaturated groups of which two (A and B, see Figure 5.1) are conjugated to the third (C), but are not conjugated to each other.²⁰ This 3-methylenepenta-1,4-diene pattern can easily be introduced in numerous existing building blocks for conjugated polymers allowing for good comparison and potentially having wide applicability. Nevertheless, the influence of cross conjugation has been investigated mainly in small molecules and oligomeric systems,²¹⁻²³ but is seldom applied in polymeric systems.^{24,25} In most other cases where cross conjugation is applied it is either without specific intention²⁶ or cross conjugation arises as a byproduct of the polymerization mechanism.²⁷ Especially in D-A conjugated polymers the influence of cross conjugation is expected to be significant as it might (partially) block electronic communication between electron rich and poor parts. Although hampered, weak electronic communication through cross-conjugated bonds has been shown in donor acceptor substituted small molecules with different number of cross conjugations²⁸⁻³⁰. The influence of cross conjugation has, to the best of our knowledge, never been investigated systematically in the important class of materials formed by donor-acceptor conjugated copolymers.

5.2 Aim

Here the influence of cross conjugation on donor-acceptor copolymers is investigated in relation to the number and the position of the cross conjugations to develop design guidelines for the tuning of optical and electronic properties. Isoindigo is used as acceptor block. Several studies have shown high performing isoindigo-based polymers in OPV³¹⁻³⁴ of which one analog was taken as basis for this investigation. By changing the substitution pattern on isoindigo, in particular by changing the *para*-substitution in the 6,6'-isomer to the *meta*-substituted 5,5'-isomer, cross conjugation is introduced between the isoindigo unit (Figure 5.1) and its adjacent aromatic moieties. In this way isoindigo can be in full conjugation when substituted on the 6,6'-positions (II) and have two cross conjugation points when substituted on the 5,5'-positions (cII) as was investigated in detail for small molecules.³⁵ Thiophene-flanked thieno[3,2-*b*]thiophene (TT) and thieno[2,3-*b*]thiophene (cTT) were chosen as the donor building block, the latter has a cross-conjugated central double bond (Figure 5.1). These were previously used in a polythiophene-thienothiophene where a lowering of the HOMO with respect to the conjugated derivative was reported.²⁵

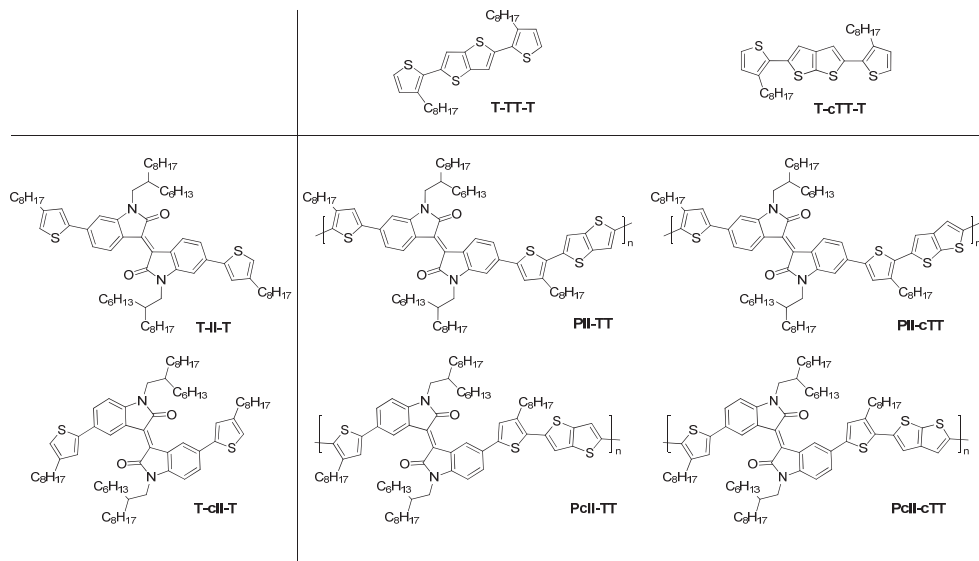


Figure 5.2 – Structures of the four molecules and four isomeric polymers that incorporate isoindigo and thienothiophene units in conjugated (II and TT) and cross-conjugated (cII and cTT) topologies.

The combination of the four building blocks shown in Figure 5.1 provides an interesting platform to study the effects of cross conjugation in donor-acceptor copolymers on optical band gap and frontier orbital levels by varying the number and position of cross conjugations with respect to the donor acceptor lattice. Four molecules were designed and four isomeric polymers with conjugated (II and TT) and cross-conjugated (cII and cTT) units as shown in Figure 5.2. The four isomeric polymers are chain extended combinations of the four molecules and allow investigating the effects of introducing cross conjugation in the isoindigo and thienothiophene units separately and in combination. These will first be assessed theoretically by DFT calculations and then be synthesized to compare with the experimental results.

5.3 Results and discussion

5.3.1 DFT calculations

To assess the influence of cross conjugation on frontier orbital energies and the optical transitions, DFT calculations were performed on the four molecules shown in Figure 5.2 at the B3LYP/6-31g (2d,p) level with the Gaussian09 A.02 package.³⁶ In the

calculations the long alkyl chains on isoindigo were replaced with methyl groups and the alkyl chains on the thiophene units were omitted. Following a full unrestricted geometry optimization time-dependent DFT (TD-DFT) was used to investigate the nature of the first three optical transitions.

Table 5.1 – DFT calculated energy levels and oscillator strengths of molecular building blocks

	E_{HOMO}	E_{LUMO}	E_g	ΔE	f	f_{exp}	Orbital contributions to vertical transition
	eV	eV	eV	eV			
T-II-T	-5.24	-2.72	2.52	2.21	0.59	0.47	HOMO \rightarrow LUMO (93.8%), HOMO -2 \rightarrow LUMO (5.8%)
				2.44	0.00		HOMO -1 \rightarrow LUMO (91.8%), HOMO -3 \rightarrow LUMO (7.1%)
				2.84	0.52		HOMO -2 \rightarrow LUMO (92.1%), HOMO \rightarrow LUMO (5.7%)
T-cII-T	-5.28	-2.74	2.54	2.03	0.03	0.11	HOMO \rightarrow LUMO (98.1%)
				2.04	0.00		HOMO -1 \rightarrow LUMO (98.7%)
				2.91	0.26		HOMO -2 \rightarrow LUMO (84.0%), HOMO -6 \rightarrow LUMO (13.6%)
T-TT-T	-5.13	-1.70	3.43	3.21	1.04	0.75	HOMO \rightarrow LUMO (99.6%)
				3.93	0.00		HOMO \rightarrow LUMO +1 (77.2%), HOMO-2 \rightarrow LUMO (21.2%)
				4.07	0.03		HOMO -1 \rightarrow LUMO (96.9%)
T-cTT-T	-5.20	-1.35	3.85	3.46	0.56	n.a. ^a	HOMO \rightarrow LUMO (93.7%), HOMO-1 \rightarrow LUMO +1 (5.1%)
				3.60	0.03		HOMO \rightarrow LUMO +1 (97.8%)
				3.99	0.67		HOMO -1 \rightarrow LUMO +1 (93.8%), HOMO \rightarrow LUMO (5.1%)

^a Due to peak overlap no reliable integral could be calculated from the molar extinction coefficient.

For T-II-T and T-cII-T the HOMO (-5.24 vs. -5.28 eV) and LUMO (-2.72 vs. -2.74 eV) are very similar. In T-II-T high oscillator strengths are found for the first electronic transition at 2.21 eV with $f = 0.59$ and the third transition at 2.84 eV with $f = 0.52$ (Table 5.1). In contrast, in T-cII-T the first electronic two transitions are very weak ($f = 0.03$ and $f = 0.00$), with only the third electronic transition at 2.91 eV having appreciable oscillator strength ($f = 0.26$). These results are very similar to those published recently by Brédas *et al.*³⁵

The HOMO orbital levels for T-TT-T and T-cTT-T are close (-5.13 vs. -5.20 eV) but their LUMO levels differ considerably (-1.70 vs. -1.35 eV). Also the electronic transitions differ. For T-TT-T the first transition is an almost pure HOMO \rightarrow LUMO excitation with a large oscillator strength ($f = 1.04$), but the second and third transitions are very weak. In T-cTT-T the first transition is predicted to be a mixed HOMO \rightarrow LUMO and HOMO-1 \rightarrow LUMO+1 transition with $f = 0.56$. The same orbitals also contribute to the third transition that has $f = 0.67$.

The DFT calculations on these four molecules reveal that cross conjugation in isoindigo strongly reduces the oscillator strength of T-cII-T compared to T-II-T of the lowest energy transition but that their frontier orbital levels are very similar. For cross conjugation in thienothiophene also the oscillator strength reduces, but the main effect is an increased energy for the first electronic transition.

In a next step DFT calculations were performed on the four isomeric polymers shown in Figure 5.2. For this purpose, a 1D lattice was constructed containing two repeat units in the unit cell. This allows for creating a continuous polymer structure without inconsistent twisting between adjacent rings. In these calculations all alkyl chains (i.e. both on isoindigo and thiophene) were replaced by methyl groups. The geometry optimization of the polymers is time intensive and preliminary results showed strongly curved and twisted polymer structures that failed to converge. To rule out differences in energy levels because of different twisting, all dihedral angles between adjacent aromatic rings were frozen and coplanarity was enforced for the aromatic units. To expedite the optimization, structures were optimized by extending the basis sets from STO-3G, to 3-21G, and finally 6-31G(2d,p). The resulting energy levels are collected in Table 5.2 and represented in Figure 5.3.

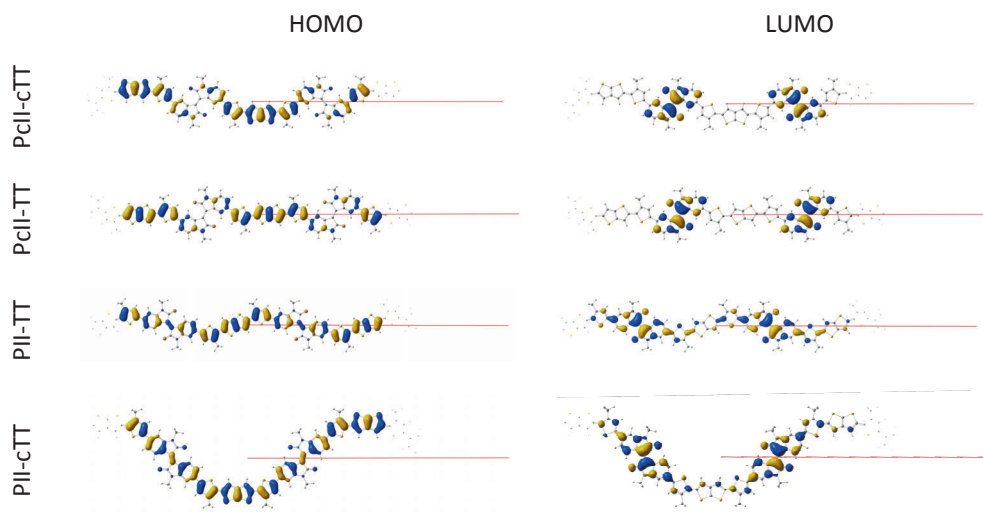


Figure 5.3 – HOMO and LUMO representations of all four isoindigo and thienothiophene copolymers as calculated with DFT. The red lines represent the repetition vector of the constructed 1D lattice. Blurred onsets of the next unit cell are shown.

For PII-TT and PII-cTT the HOMOs are rather uniformly distributed over the entire polymer chain (Figure 5.3) but the HOMO energy level is deeper for PII-cTT (−4.82 eV) than for PII-TT (−4.68 eV), likely as a consequence of the broken conjugation. The same rationale explains why the LUMO level of PII-cTT is calculated (−2.83 eV) to be higher than that of PII-TT (−2.91 eV). For PclI-TT and PclI-cTT, the LUMOs are entirely localized on the isoindigo unit and as a consequence the LUMO levels are virtually the same (−2.85 vs. −2.84 eV). The cross conjugation between the isoindigo acceptor and the thiophene donor hampers electron delocalization. Likewise, the HOMO localizes on the thiophene and thienothiophene donor with a small contribution of the phenyl ring of the isoindigo. With the HOMO levels of PclI-TT and PclI-cTT at −4.56 and −4.73 eV, respectively, increasing cross conjugation results in a deeper HOMO level as expected.

At present it is not possible for us to perform TD-DFT on the constructed open lattice systems for the polymers and hence the electronic transitions were not assessed theoretically in a direct way.

Table 5.2 – DFT calculated energy levels of polymers.

	E_{HOMO} eV	E_{LUMO} eV	E_g eV
PII-TT	−4.68	−2.91	1.77
PclI-TT	−4.56	−2.85	1.71
PII-cTT	−4.82	−2.83	2.00
PclI-cTT	−4.73	−2.84	1.88

The prime reason that the donor-acceptor design is so widely used for controlling the optical band gap in conjugated polymers is because it succeeds in counteracting the Peierls distortion via partial charge redistribution from the donor to the acceptor, therewith reducing the bond length alternation. Depending on the position of the cross conjugation this charge redistribution is hampered. Cross conjugations can therefore have significant influence on the bond length alternation. This effect can easily be visualized by monitoring the relative change in bond length of a number of specific bonds as determined from the DFT calculations. Figure 5.4 shows the effect for four characteristic bonds in the polymers: the central double bond of the isoindigos and thienothiophenes and the single bonds on either side of the thiophene linkers. The fully conjugated PII-TT is taken as a reference to show the relative changes in bond lengths. Cross conjugation increases the bond length alternation as the short double bonds become shorter and the

longer single bonds are elongated going from II to cII and from TT to cTT. The effect is strongest in close vicinity of the cross conjugations and is weaker or absent at longer distance. The central double bond in II and the single bond in II-T show large changes when replacing II by cII, while the central double bond in TT or cTT and the single TT-T and cTT-T bonds exhibit only small changes for the same II \rightarrow cII modification. A similar effect is found when going from TT to cTT. Here the central TT/cTT double bond becomes shorter and the single TT/cTT-T bond elongates, while the other bonds remain similar.

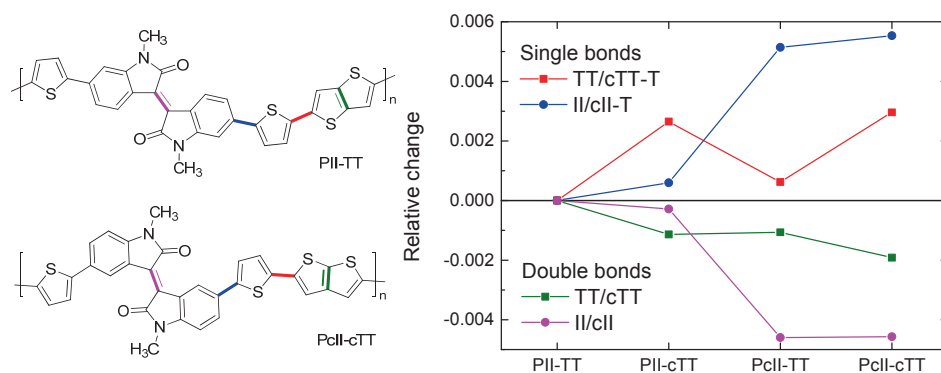


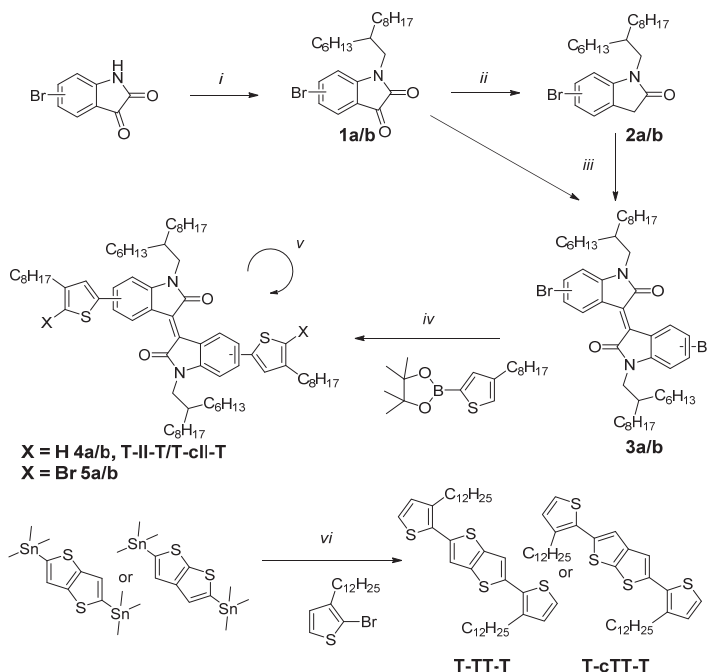
Figure 5.4 – Relative change in bond length of characteristic double and single bonds in cross-conjugated donor-acceptor polymers as inferred from DFT calculations. Specific bonds are color coded on the left in PII-TT and PclI-cTT as example. PII-TT is taken as reference. Introducing cross conjugation shortens double bonds and elongates single bonds. The effect is most pronounced for bonds closer to the point of cross conjugation.

5.3.2 Synthesis

The synthesis of the four molecules and the monomers for the four isomeric polymers is shown in Scheme 5.1. For the synthesis of T-II-T (**4a**) and T-clI-T (**4b**), a route via 6,6'-bisbromo-II (**3a**) and 5,5'-bisbromo-II (**3b**) was used. The synthesis of these intermediates has been adapted from literature procedures^{31,35} and started with 5-bromoisatin and 6-bromoisatin respectively that were alkylated with 1-bromo-2-hexyldecane using sodium hydride in DMF. Approximately half of the resulting products **1a/1b** were subsequently reduced with hydrazine in DMSO to give the *N*-alkylated 5- or 6-bromoindoles **2a/2b**. Combining the respective indole with the isatin in acetic acid gave isoindigos **3a/3b** in good yield. These isoindigos were extended with 4,4,5,5-tetramethyl-2-(4-octylthiophen-2-yl)-1,3,2-dioxaborolane using palladium catalyzed Suzuki coupling reactions to give **4a**

(T-II-T) and **4b** (T-cII-T). After bromination using NBS in DCM the extended monomers **5a** and **5b** were obtained that were used for polymerization reactions.

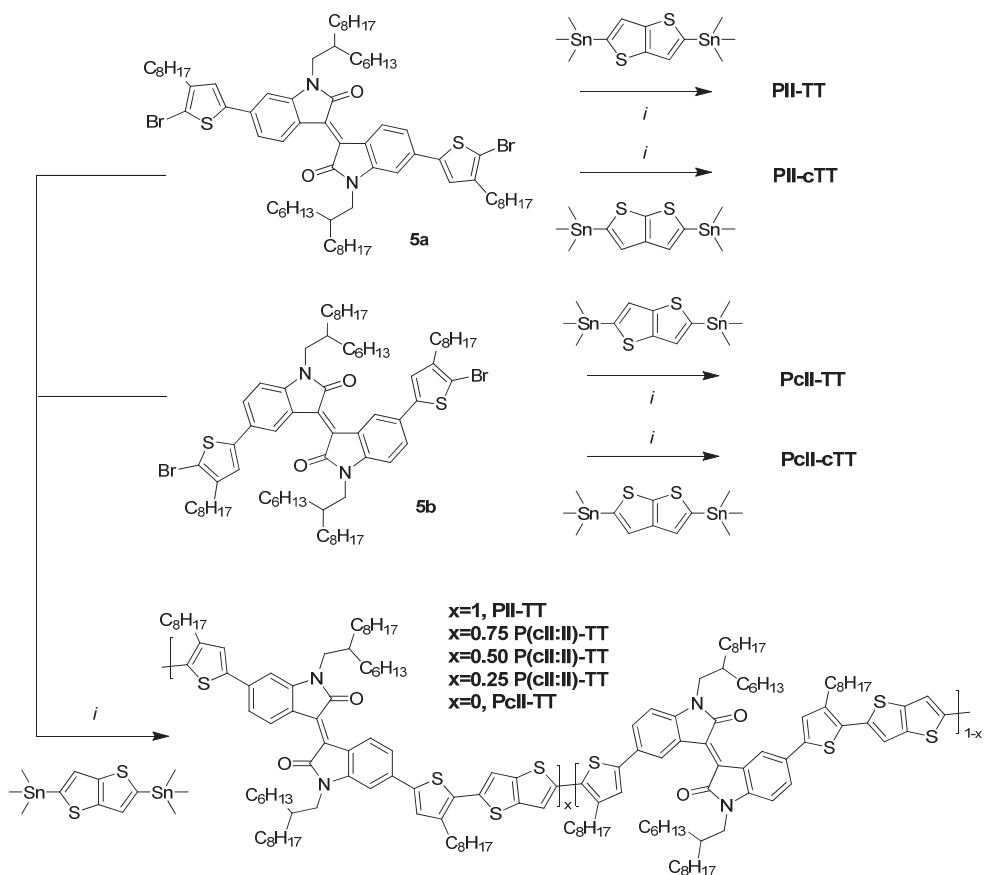
The route to the other two molecules, T-TT-T and T-cTT-T, is also shown in Scheme 5.1. The synthesis of 2,5-bis(3-dodecylthiophen-2-yl)thieno[3,2-*b*]thiophene (T-TT-T) has been described before.³⁷ Here we synthesized T-TT-T and 2,5-bis(3-dodecylthiophen-2-yl)thieno[2,3-*b*]thiophene (T-cTT-T) via Stille coupling from the bisstannylated TT and cTT derivatives with 2-bromo-3-dodecylthiophene (Scheme 5.1). The reagent for the first reaction, 2,5-bis(trimethylstannyl)thieno[3,2-*b*]thiophene, is available from commercial sources. 2,5-Bis(trimethylstannyl)thieno[2,3-*b*]thiophene was synthesized from thieno[2,3-*b*]thiophene with *n*-BuLi and chlorotrimethylstannane.



Scheme 5.1 – Synthesis of T-II-T (4a**), T-cII-T (**4b**), T-TT-T, T-cTT-T, and the isoindigo monomers **5a/5b**. (i) NaH, DMF, 0 °C to 65 °C, 24 h. (ii) H₄N₂, DMSO, 140 °C. (iii) AcOH, HCl, 120 °C, 24 h. (iv) Pd₂dba₃, PPh₃, 2 M K₃PO₄, toluene, 110 °C, 24 h. (v) NBS, DCM, 0 °C. (vi) Pd(PPh₃)₄, toluene, 115 °C, 24 h.**

The four isomeric donor-acceptor polymers and a series of copolymers with different II/cII ratios were synthesized using the Stille cross-coupling reaction as described in Scheme 5.2. As a catalytic system Pd₂dba₃/PPh₃ was used in toluene/DMF (9:1 v/v) at 115

°C. To determine the molecular weight of these polymers a super-heated chloroform GPC setup was used because several of these polymers aggregate strongly in solution. On regular GPC systems, using chloroform at room temperature or heated ODCB at 80 °C, polymer aggregates were measured or the polymers did not pass through the column at all. In super-heated chloroform temperatures up to 145 °C can be used to dissolve most of the aggregates as was previously shown for PII-TT.³⁸ Table 5.3 shows that the polymers have molecular weights (M_n) varying between ~20 and ~45 kg/mol.



Scheme 5.2 – Synthesis of the four isomeric donor acceptor copolymers PII-TT, PII-cTT, PClI-TT, and PClI-cTT using Stille coupling reactions. (i) Pd_2dba_3 , PPh_3 (1:4), toluene/DMF (9/1), 115 °C, 24 h. In similar way the P(cII:II)-TT copolymers with different II:cII ratios were synthesized.

Table 5.3 – Characteristics of cross-conjugated polymers

	M_n kg/mol	PDI	$\lambda_{\max}^{\text{sol}}$ nm	$\lambda_{\max}^{\text{film}}$ nm	$\lambda_{\text{onset}}^{\text{sol}}$ nm	$\lambda_{\text{onset}}^{\text{film}}$ nm	$E_g^{\text{sol } a}$ eV	$E_g^{\text{film } a}$ eV	$E_g^{\text{cv } b}$ eV	E_{HOMO}^c eV	E_{LUMO}^c eV
P(II-TT)	38.9	2.14	448, 650	449, 650	825	830±5	1.50	1.49	1.71	-5.62	-3.91
P(cII:II)-TT 25:75	43.9	2.11	439, 640	444, 639	785	790±5	1.60	1.57	1.61	-5.58	-3.97
P(cII:II)-TT 50:50	31.5	2.18	426, 622	438, 639	785	785±5	1.64	1.57	1.58	-5.56	-3.98
P(cII:II)-TT 75:25	30.7	2.01	422, 611	439, 625	785	785±5	1.64	1.57	1.60	-5.57	-3.97
PcII-TT	21.3	1.49	429	438	740	795±10	1.68	1.56±0.2	1.69	-5.59	-3.90
P(II-cTT)	38.5	1.94	386, 601	364, 613	765	815±10	1.62	1.52	1.89	-5.83	-3.94
PcII-cTT	19.0	1.70	390	370	720	795±20	1.72	1.56±0.4	1.78	-5.77	-3.99

^a $E_g^{\text{sol/film}} = 1240/\lambda_{\text{onset}}^{\text{sol/film}}$. ^b $E_g^{\text{cv}} = q(E_{\text{ox}} - E_{\text{red}})$. ^c $E_{\text{Fc}/\text{Fc}^+}$ taken as -5.23 eV.

5.3.3 UV-vis absorption

To evaluate the effect of cross conjugation the four molecules were first analyzed and compared (Figure 5.2). The absorption spectra of T-II-T and T-cII-T dissolved in toluene have been reported previously.³⁵ Because the transitions of T-TT-T and T-cTT-T are in the UV, the absorption spectra of all four compounds were recorded in heptane.

The conjugated T-II-T molecule exhibits a strong band maximizing at 533 nm with a molar absorption coefficient of 2×10^4 L/mol/cm (Figure 5.5). Based on the DFT calculations, this absorption is attributed to the HOMO \rightarrow LUMO transition with mainly π - π^* character. From the molar absorption coefficient the oscillator strength for the transition was calculated to be $f_{\text{exp}} = 0.47$ (Table 5.1). For the cross-conjugated T-cII-T molecule, the low-energy absorption band has a more than five-fold decreased intensity with maximum molar absorption coefficient of 3.5×10^3 L/mol/cm at 518 nm and a moderate oscillator strength of $f_{\text{exp}} = 0.11$. The dominant absorption of T-cII-T is at higher energies. The reduced oscillator strength for the HOMO \rightarrow LUMO transition of T-cII-T compared to T-II-T has been predicted by the DFT calculations. Despite the vastly different absorption spectra, the onsets of optical absorption in heptane are rather similar for both molecules: 637 nm (1.95 eV) for T-II-T and 665 nm (1.86 eV) for T-cII-T. Hence, introducing cross conjugation in the isoindigo unit (i.e. T-II-T \rightarrow T-cII-T) has a strong effect on the oscillator strength, but little or no influence on the optical band gap.

For T-TT-T and T-cTT-T a clear difference in the onset of absorption is observed of 400 nm versus 360 nm respectively. For T-TT-T an oscillator strength of $f_{\text{exp}} = 0.75$ was determined. For T-cTT-T the first absorption band has similar intensity as that of T-TT-T, but it seems composed of three overlapping transitions such that it is not possible to reliably determine the oscillator strength.

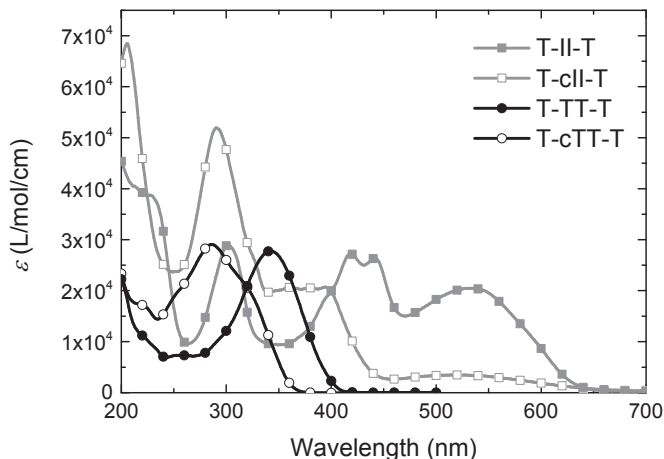


Figure 5.5 – UV-vis absorption spectra of T-II-T, T-cII-T, T-TT-T, and T-cTT-T in heptane solution.

For conjugated polymers it is common practice to determine the optical band gap as the onset of optical absorption. With increasing number of cross conjugations in the polymer backbone the absorption maxima shift to higher energies, from 651 nm for PII-TT, via 613 nm for PII-cTT, to 438 nm for PII-TT, and finally 390 nm for PII-cTT (Figure 5.6). Although there is large shift in the wavelength of maximum absorption, the onsets of the absorption bands are all at long wavelengths as can be seen in a semi-logarithmic plot (Figure 5.6b). While the onsets do not coincide, it is clear that all four polymers have optical absorption up to at least 750 nm. The large tailing of absorption spectra of the PII-TT and PII-cTT polymers into the red indicates that their main absorption bands in the 350 – 550 nm region are not due to the HOMO-LUMO transition but originate from higher energy transitions, e.g. $\text{HOMO} - x \rightarrow \text{LUMO}$ or $\text{HOMO} \rightarrow \text{LUMO} + y$. Best estimates for the onsets of absorption are collected in Table 5.3. The actual optical band gap is very similar for all four polymers ($\sim 1.55 \pm 0.05$ eV). We hypothesize, based on the DFT calculations, that due to the cross conjugation between the donor and acceptor, the transition dipole moment of the donor-acceptor charge-transfer absorption becomes weaker because the HOMO and LUMO become more localized at the donor and acceptor blocks, respectively. This would imply that the absorption properties arise essentially within one repeat unit.

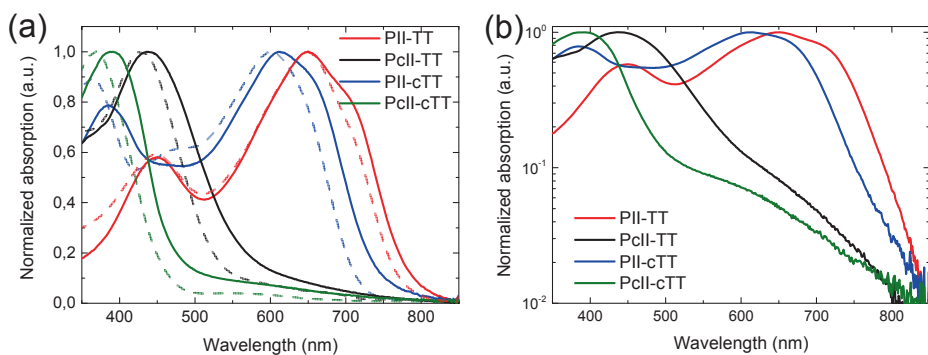


Figure 5.6 – Normalized UV-vis absorption spectra of PII-TT, PII-cTT, PclI-TT, and PclI-cTT in chloroform solution (dashed lines) and as thin films on glass (solid lines). (a) Linear scale. (b) Semi-logarithmic scale.

To investigate if interactions between donor and acceptor are limited to one repeat unit and not a function of the amount of cross conjugation in the polymer chain, a series of copolymers with different II:cII monomer ratios were synthesized with TT as a donor. As can be seen in Figure 5.7 the P(cII:II)-TT copolymers show two almost independent absorption bands for the conjugated segments at (~ 650 nm) and the cross-conjugated parts at ~ 440 nm. The ratio of the peak intensities of the low and high energy band is increasing almost linearly with the fraction of conjugated II vs. II+cII in the copolymers. Interestingly, there is only a small (~ 25 nm) shift of the wavelength of maximum absorption for the low-energy band and onset of absorption remains at ~ 800 nm.

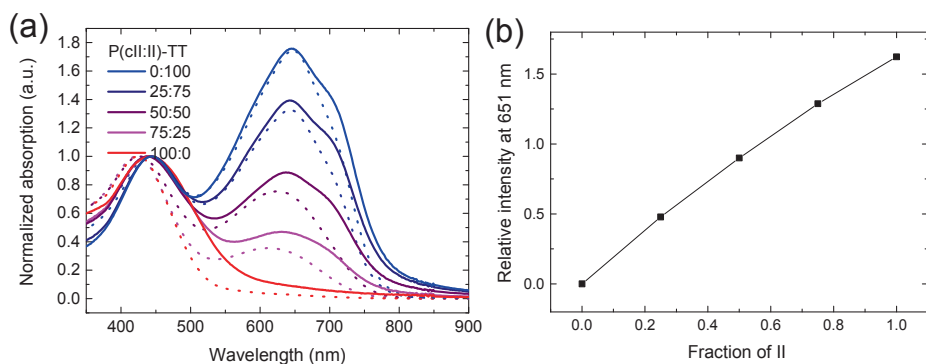


Figure 5.7 – (a) Normalized absorption of P(cII:II)-TT copolymers in chloroform solution (dashed lines) and in thin films on glass (solid lines). (b) The relative intensity of the band at ~ 651 nm vs. that of the band at ~ 440 nm as function of the fraction of II in the P(cII:II)-TT polymers.

Introduction of cTT has a different effect. The absorption spectra of PII-cTT and PClI-TT both shift to the blue when TT is replaced by cTT. This different behavior of the polymers with TT and cTT are attributed to the different nature of the cross conjugation. The cross conjugation in cTT does not hamper donor acceptor interaction but splits the donor block in two, creating two new donor parts with reduced donating strength interacting with the acceptor block. Because of the weaker donor, the HOMO is lowered and the charge transfer absorption shifts to higher wavelength.

5.3.4 Cyclic voltammetry

To determine the frontier orbital levels of the cross-conjugated polymers, the oxidation and reduction potentials were measured by cyclic voltammetry. As can be seen in Figure 5.8 and Table 5.3 the reduction potential is very similar for all polymers and the resulting LUMO levels are in a narrow range (-3.9 to -4.0 eV). This indicates that the LUMO is localized on the isoindigo units with only minor contributions from the donor surroundings. For both II and cII an irreversible oxidation takes place as evidenced by an extra peak at negative bias that has no matching reduction peak. Figure 5.8 shows that the HOMO levels differ for the TT (-5.56 to -5.62 eV) and cTT polymers (-5.77 to -5.83 eV). This can be rationalized by considering that in cTT the conjugation is broken compared to TT, such that the electron rich segment is split in two disconnected units. These results are qualitatively consistent with the changes in optical band gaps (despite a significant difference in oscillator strength) and the results of the DFT calculations in Table 5.2.

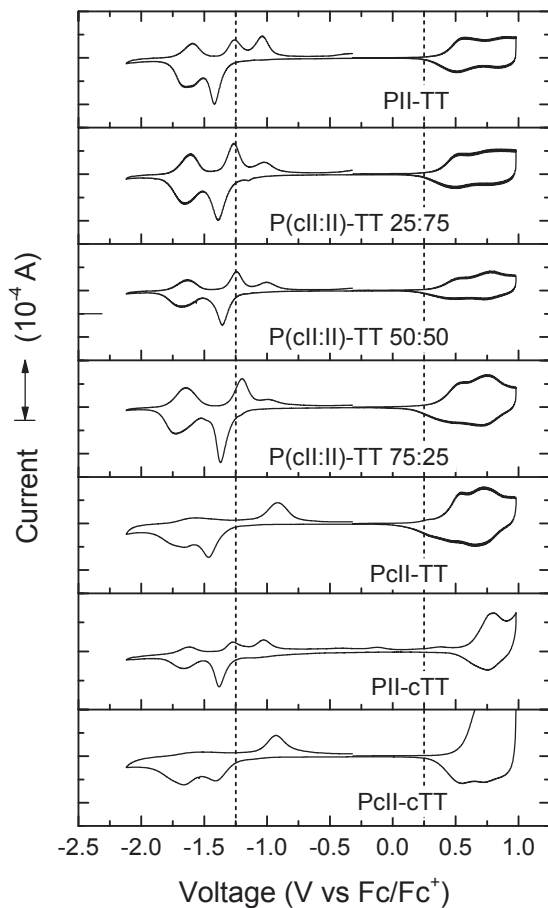


Figure 5.8. Cyclic voltammograms for PII-TT, P(cII:II)-TT, PclI-TT, PII-cTT, and PclI-cTT recorded as thin films on ITO. The vertical dashed lines at -1.25 and +0.25 V are guides to the eye. The onsets for oxidation and reduction potentials are very similar, except for PII-cTT and PclI-cTT that have a higher oxidation potential.

5.4 Conclusions

We have introduced cross conjugation in alternating donor acceptor copolymers of bis(2-thienyl)thienothiophene (T-TT-T) and isoindigo (II) via cross-conjugated cII and cTT units to investigate the tunability of the optical band gap and frontier orbital energy levels by adjusting the number and position of cross conjugations in the polymer chain.

Remarkably, the optical band gap of the fully conjugated PII-TT, the partially cross-conjugated PcII-TT and PII-cTT, and the fully cross-conjugated PcII-cTT showed comparatively little changes. The onsets of the optical absorption of these four isomeric polymers are all in the near infrared and the electrochemical band gaps are within 0.2 V from each other. The optical spectra differ however, significantly as a result of the fact that the lowest energy transition has a strongly reduced absorption coefficient for polymers that incorporate cross-conjugated isoindigo (cII) units. This result is corroborated by DFT calculations that predict very low oscillator strengths for the lowest electronic transitions in T-cII-T. The effect of cross conjugation in isoindigo on the intensity of the lowest electronic transition was verified in a series of copolymers in which II and cII are alternating with T-TT-T in different ratios. These P(cII:II)-TT polymers with cII:II = 0:100, 25:75, 50:50, 75:25, or 100:0 have very similar optical band gaps but show a nearly linear increase of the intensity of the low-energy electronic transition with the fraction of conjugated isoindigo in the polymer chain. Introduction of cTT in the PII and PcII polymers results in a small but distinct blue shift of the optical absorption and a lowering of the HOMO levels compared to those with TT.

Summarizing, the tunability of the opto-electronic properties of semi-conducting donor-acceptor polymers via cross conjugation is moderate, but using cross-conjugated isoindigo it is possible to strongly influence the oscillator strength of the π - π^* transition.

5.5 Experimental

5.5.1 General procedures, materials and instruments

See paragraph 2.5.1. for details on NMR, UV-vis-NIR, MALDI-TOF, and CV equipment.

Molecular weights were determined by GPC using superheated chloroform. This in home developed equipment is described in detail elsewhere.³⁹ In short it consists of an FD-53 oven (Binder, Tuttlingen, Germany) a LC-20 AD pump (Shimadzu, Kyoto, Japan), a heater exchanger made from a 1.5 m narrow-bore stainless steel tubing (1/16 in. (o.d.) × 0.004 in. (i.d.), Alltech-Grace, Lokeren, Belgium) located in the oven before the PLgel mixed-C column linear molecular weight range up to 2,000 kg/mol based on polystyrene (Agilent Technologies, Amsterdam, the Netherlands). Another piece of 1.2 m of narrow bore stainless steel tubing (1/16 in. (o.d.) × 0.004 in. (i.d.), Alltech-Grace) and the UV/Vis detector (SPD-20A, Shimadzu).

For details on DFT calculations see paragraph 4.4.1.

5.5.2 Synthesis

5-bromo-1-(2-hexyldecyl)isatin (**1a**).

Sodiumhydroxide 60% dispersion in mineral oil (850 mg, 21.4 mmol) was dispersed in dry DMF (100 ml) at 0 °C before addition of 5-bromoisatin (4.00 g, 17.7 mmol). After stirring for 30 minutes 1-bromo-2-hexyldecane (6.10 g, 20.0 mmol) was added and the mixture heated to 65 °C for 24h. After cooling the mixture was extracted with water and ethyl acetate and the organic fractions washed with brine and dried over MgSO₄. The crude oil was subjected to column chromatography using a 0% to 100% gradient of heptanes and chloroform as mobile phase to give 6.60 g of the pure title product in 82.8% yield. ¹H NMR (400 MHz, CDCl₃, ppm) δ 7.69 (s, 1H), 7.67 (d, *J* = 2.3 Hz, 1H), 6.81 – 6.74 (m, 1H), 3.58 (d, *J* = 7.4 Hz, 2H), 1.89 – 1.75 (m, 1H), 1.41 – 1.16 (m, 24H), 0.91 – 0.80 (m, 6H).

6-bromo-1-(2-hexyldecyl)isatin (**1b**).

Syntheses of **1b** was done in a similar fashion as **1a** starting from 6-bromoisatin (2.00 g, 8.85 mmol) and resulting in 3.00 g of a yellow orange oil (75.5%). ¹H NMR (200 MHz, CDCl₃, ppm) δ 7.46 (d, *J* = 7.8 Hz, 1H), 7.27 (dd, *J* = 7.9, 1.5 Hz, 1H), 7.03 (d, *J* = 1.6 Hz, 1H), 3.58 (d, *J* = 7.4 Hz, 3H), 1.84 (s, 1H), 1.41 – 1.16 (m, 24H), 0.96 – 0.79 (m, 6H).

5-bromo-1-(2-hexyldecyl)indolin-2-one (**2a**).

In a mixture of N₂H₄ (15 ml) and DMSO (30 ml) **1a** (4.0 g, 8.9 mmol) was dissolved and heated to 140 °C for 40 minutes. After cooling water/HCl (1/1) (50 ml) was added and the mixture was subsequently extracted with ethyl acetate. Organic fractions were combined and washed with brine and dried over MgSO₄ to give a yellow crude oil that was purified by silica column chromatography using heptane/chloroform (20/80) as mobile phase. The pure fractions were concentrated *in vacuo* to give 3.6 g of yellow oil (yield 93.3%). ¹H NMR (400 MHz, CDCl₃, ppm) δ 7.40 – 7.29 (m, 2H), 6.67 (d, *J* = 8.2 Hz, 1H), 3.55 (d, *J* = 7.4 Hz, 2H), 3.51 (s, 2H), 1.82 (m, 1H), 1.40 – 1.13 (m, 24H), 0.94 – 0.79 (m, 6H). ¹³C NMR (100 MHz, CDCl₃, ppm) δ 174.51, 144.10, 130.56, 127.53, 126.59, 114.62, 109.86, 65.70, 44.62,

35.96, 35.49, 31.85, 31.76, 31.56, 31.54, 29.93, 29.62, 29.49, 29.26, 26.45, 26.42, 22.65, 22.61, 14.09, 14.06.

6-bromo-1-(2-hexyldecyl)indolin-2-one (2b).

Synthesis of **2b** was done in a similar fashion as **2a** starting from **1b** (1.1 g, 2.4 mmol) and resulting in 400 mg of a yellow oil (37.5%). ¹H NMR (200 MHz, CDCl₃, ppm) δ 7.16 (dd, *J* = 7.9, 1.6 Hz, 1H), 7.09 (d, *J* = 7.8 Hz, 1H), 6.98 – 6.87 (m, 1H), 3.55 (d, *J* = 7.4 Hz, 2H), 3.46 (s, 2H), 1.84 (s, 1H), 1.42 – 1.16 (m, 24H), 0.87 (t, *J* = 6.6 Hz, 6H). ¹³C NMR (50 MHz, CDCl₃, ppm) δ 175.03, 146.42, 125.56, 124.77, 123.36, 121.25, 111.93, 44.59, 35.86, 35.30, 31.87, 31.79, 31.45, 29.97, 29.65, 29.53, 29.30, 26.35, 22.66, 14.12.

(E)-5,5'-dibromo-1,1'-bis(2-hexyldecyl)-[3,3'-biindolinylidene]-2,2'-dione (3a).

Hydrochloric acid (0.5 ml) was added to a solution of **1a** (2.0 g, 4.6 mmol) and **2a** (2.1 g, 4.6 mmol) in acetic acid (60 ml). This mixture was reacted at 120 °C for 24 h before quenching it by pouring the mixture over ice. The mixture was extracted with ethyl acetate and washed subsequently with a saturated NaHCO₃ solution and brine. The ethyl acetate fraction was dried over MgSO₄, filtered and concentrated before purifying by column chromatography with heptane/DCM (80/20) to give 3.7 g product in 80.4% yield. ¹H NMR (400 MHz, CDCl₃, ppm) δ 9.37 (d, *J* = 2.0 Hz, 2H), 7.45 (dd, *J* = 8.3, 2.0 Hz, 2H), 6.63 (d, *J* = 8.6 Hz, 2H), 3.63 (d, *J* = 7.4 Hz, 4H), 1.86 (hept, *J* = 7.0 Hz, 2H), 1.44 – 1.16 (m, 24H), 0.92 – 0.80 (m, 6H). ¹³C NMR (100 MHz, CDCl₃, ppm) δ 167.48, 144.18, 135.03, 133.19, 132.55, 122.86, 114.79, 109.46, 44.61, 36.08, 31.85, 31.79, 31.55, 29.97, 29.64, 29.53, 29.27, 26.46, 26.42, 22.65, 22.61, 14.09, 14.06.

(E)-6,6'-dibromo-1,1'-bis(2-hexyldecyl)-[3,3'-biindolinylidene]-2,2'-dione (3b).

¹H NMR (400 MHz, CDCl₃, ppm) δ 9.06 (d, *J* = 8.6, 2H), 7.15 (dd, *J* = 2.0, 8.6, 2H), 6.88 (d, *J* = 2.0, 2H), 3.60 (d, *J* = 7.4, 4H), 1.87 (s, 2H), 1.27 (m, 48H), 0.86 (t, *J* = 7.4, 12H). ¹³C NMR (100 MHz, CDCl₃): δ 168.07, 146.18, 132.53, 131.01, 126.64, 125.06, 120.36, 111.51, 44.67, 36.07, 31.85, 31.78, 31.48, 29.96, 29.62, 29.52, 29.27, 26.34, 26.31, 22.65, 22.62, 14.10, 14.07.

(E)-1,1'-bis(2-hexyldecyl)-5,5'-bis(4-octylthiophen-2-yl)-[3,3'-biindolinylidene]-2,2'-dione (4a).

To **3a** (0.94 g, 1.1 mmol) was added 4,4,5,5-tetramethyl-2-(4-octylthiophen-2-yl)-1,3-dioxolane (1.1 g, 3.3 mmol), Pd₂dba₃ (22.9 mg, 25 μmol) and PPh₃ (26.3 mg, 100 μmol) and put under argon in a Schlenk finger. Toluene (9 ml), 2 M K₃PO₄ aqueous solution (1 ml, degassed) and a drop of Aliquat 336 were added and argon was bubbled through the solution for 15 min. before heating it to 115 °C. The reaction progressed slowly and only after a week all starting material was consumed. The reaction mixture was poured into methanol and filtered. The residue was taken up in chloroform and used to impregnate silica for column chromatography using a heptane/chloroform gradient. The product containing fractions were combined, dried and recrystallized from an ethanol/chloroform mixture to give 334 mg of pure **4a** (yield 27.6%). ¹H NMR (400 MHz, CDCl₃, ppm) δ 9.52 (d, *J* = 2.3 Hz, 2H), 7.56 (dd, *J* = 8.2, 2.3 Hz, 2H), 7.14 (s, 2H), 6.82 (s, 2H), 6.75 (d, *J* = 8.2 Hz, 2H), 3.69 (d, *J* = 7.4 Hz, 4H), 2.66 – 2.58 (m, 4H), 1.99 – 1.85 (m, 2H), 1.66 (p, *J* = 7.8 Hz, 2H), 1.45 – 1.15 (m, 68H), 0.92 – 0.79 (m, 18H). ¹³C NMR (100 MHz, CDCl₃, ppm) δ 168.10, 144.36, 144.20, 144.08, 133.76, 129.73, 129.07, 127.28, 123.91, 122.04, 118.56, 108.25, 44.54, 36.24, 31.90, 31.85, 31.80, 31.61, 30.69, 30.43, 29.98, 29.65, 29.55, 29.47, 29.39,

29.28, 26.52, 26.48, 22.78 – 22.57 (m), 22.65, 22.61, 14.10, 14.09, 14.05. MALDI-TOF: 1099.82 m/z $[M+H]^+$ 100%.

(E)-1,1'-bis(2-hexyldecyl)-6,6'-bis(4-octylthiophen-2-yl)-[3,3'-biindolinylidene]-2,2'-dione (4b).

The procedure was similar to that of **4a** only with a reaction time of 24 h. After column chromatography and recrystallization 1.2 g of product was obtained in 57.9% yield. ^1H NMR (400 MHz, CDCl_3 , ppm) δ 9.13 (d, J = 8.6 Hz, 2H), 7.26 (dd, J = 10.1 Hz, 2H), 7.23 (d, J = 1.1 Hz, 2H), 6.93 (d, J = 5.5 Hz, 2H), 3.66 (d, J = 7.4 Hz, 4H), 2.67 – 2.58 (m, 4H), 1.96 – 1.85 (br, 2H), 1.66 (p, J = 7.6 Hz, 4H), 1.44 – 1.17 (m, 68H), 0.87 (dt, J = 14.4, 6.8 Hz, 18H). ^{13}C NMR (100 MHz, CDCl_3 , ppm) δ 168.62, 145.60, 144.66, 143.66, 137.94, 131.86, 130.07, 125.51, 120.89, 120.81, 119.00, 104.85, 44.39, 36.38, 31.88, 31.85, 31.76, 30.62, 30.46, 29.99, 29.66, 29.59, 29.44, 29.38, 29.30, 29.27, 26.63, 22.66, 22.63, 14.09, 14.07. MALDI-TOF: 1099.84 m/z $[M+H]^+$ 100%.

(E)-5,5'-bis(5-bromo-4-octylthiophen-2-yl)-1,1'-bis(2-hexyldecyl)-[3,3'-biindolinylidene]-2,2'-dione (5a).

To **4a** (499 mg, 454 μmol) in DCM (20 ml) was added NBS (161.5 mg, 907 μmol) at 0 °C. The reaction was followed with TLC to complete conversion. The solution was washed with water and brine, dried over MgSO_4 and filtered. The residue was purified over a short silica plug and recrystallized from ethanol with a little bit of chloroform to give 565 mg of monomer in 98.9% yield. ^1H NMR (400 MHz, CDCl_3 , ppm) δ 9.46 (s, 2H), 7.49 (d, J = 8.2 Hz, 2H), 6.98 (s, 2H), 6.76 (d, J = 8.2 Hz, 2H), 3.69 (d, J = 7.8 Hz, 4H), 2.57 (t, J = 7.6 Hz, 4H), 1.91 (dt, J = 11.6, 6.1 Hz, 2H), 1.63 (p, J = 7.2 Hz, 4H), 1.42 – 1.19 (m, 68H), 0.86 (dt, J = 15.2, 6.8 Hz, 18H). ^{13}C NMR (100 MHz, CDCl_3 , ppm) δ 168.04, 144.66, 143.77, 143.01, 133.71, 129.49, 128.28, 127.12, 123.34, 122.05, 108.40, 107.20, 77.31, 76.99, 76.67, 44.57, 36.23, 31.90, 31.84, 31.80, 31.59, 29.97, 29.77, 29.72, 29.65, 29.53, 29.42, 29.28, 29.26, 26.50, 26.46, 22.68, 22.65, 22.61, 14.11, 14.09, 14.06. MALDI-TOF: 1256.68 m/z M^+ (100%).

(E)-6,6'-bis(5-bromo-4-octylthiophen-2-yl)-1,1'-bis(2-hexyldecyl)-[3,3'-biindolinylidene]-2,2'-dione (5b).

The same procedure as for **5a** was used with similar yield. ^1H NMR (400 MHz, CDCl_3 , ppm) δ 9.14 (d, J = 8.6 Hz, 2H), 7.17 (dd, J = 8.4, 1.8 Hz, 2H), 7.07 (s, 2H), 6.83 (d, J = 1.9 Hz, 2H), 3.67 (d, J = 7.4 Hz, 4H), 2.62 – 2.53 (m, 4H), 1.90 (br, 2H), 1.62 (p, J = 7.2 Hz, 4H), 1.44 – 1.21 (m, 68H), 0.92 – 0.80 (m, 18H). ^{13}C NMR (100 MHz, CDCl_3 , ppm) δ 168.52, 145.74, 143.56, 143.23, 137.05, 131.93, 130.24, 124.94, 121.15, 118.63, 109.90, 104.50, 44.42, 36.37, 31.87, 31.74, 29.99, 29.75, 29.70, 29.66, 29.59, 29.38, 29.30, 29.24, 26.61, 22.65, 22.63, 14.09. MALDI-TOF: 1256.66 m/z M^+ (100%)

2,5-bis(trimethylstannyl)thieno[2,3-*b*]thiophene.

Thieno[2,3-*b*]thiophene (1.0 g, 7.13 mmol) was dissolved in anhydrous THF (20 ml) under argon and cooled to -78 °C. Over 15 min. *n*-BuLi (6.3 ml, 15.7 mmol) was added dropwise and the mixture was allowed to warm to room temperature and stir overnight. Upon cooling to -78 °C again chlorotrimethylstannane (3.55 g, 17.8 mmol) was added and the mixture stirred another 24 h while warming to room temperature. After that the reaction was quenched with water and extracted with ether twice. The organic fractions were washed with 1 M K_2CO_3 aq. twice and brine and eventually dried over MgSO_4 .

Filtration and concentration gave the crude product that after two recrystallizations from acetonitrile afforded 1.3 g of the desired product in 39% yield. ^1H NMR (400 MHz, CDCl_3 , ppm) δ 7.23 (s, 2H), 0.39 (s, 9H). ^{13}C NMR (100 MHz, CDCl_3 , ppm) δ 152.39, 147.72, 142.72, 126.32, 77.31, 76.99, 76.68, -8.20.

2,5-bis(3-dodecylthiophen-2-yl)thieno[3,2-*b*]thiophene.

To 2,5-bis(trimethylstannyl)thieno[3,2-*b*]thiophene (49 mg, 105 μmol) and 2-bromo-3-dodecylthiophene (77 mg, 230 μmol , 2.2 eq.) was added tetrakis(triphenylphosphine)palladium(0) ($\text{Pd}(\text{PPh}_3)_4$) (11.6 mg, 10 μmol , 10%) and toluene (2 ml) under argon atmosphere. The reaction was heated to 115 $^\circ\text{C}$ and stirred at that temperature overnight. The crude was precipitated in methanol and filtrated. Subsequent column chromatography with hexane gave the title compound as yellow-white solids. Yield was not determined. ^1H NMR (400 MHz, CDCl_3 , ppm) δ 7.24 (s, 2H), 7.21 (d, $J = 5.1$ Hz, 2H), 6.96 (d, $J = 5.4$ Hz, 2H), 2.84 – 2.73 (m, 4H), 1.65 (p, $J = 7.8$, 7.2 Hz, 4H), 1.44 – 1.17 (m, 36H), 0.87 (t, $J = 6.8$ Hz, 6H). ^{13}C NMR (100 MHz, CDCl_3 , ppm) δ 140.25, 139.11, 137.58, 130.69, 130.03, 124.31, 118.01, 77.31, 76.99, 76.67, 31.92, 30.81, 29.68, 29.65, 29.64, 29.59, 29.55, 29.47, 29.35, 29.22, 22.68, 14.12.

2,5-bis(3-dodecylthiophen-2-yl)thieno[2,3-*b*]thiophene.

To 2,5-bis(trimethylstannyl)thieno[2,3-*b*]thiophene (49 mg, 105 μmol) and 2-bromo-3-dodecylthiophene (77 mg, 230 μmol , 2.2 eq.) was added $\text{Pd}(\text{PPh}_3)_4$ (11.6 mg, 10 μmol , 10%) and toluene (2 ml) under argon atmosphere. The reaction was heated to 115 $^\circ\text{C}$ and stirred at that temperature overnight. The crude was precipitated in methanol and filtrated. Subsequent column chromatography with hexane gave the title compound as white solids. Yield was not determined. ^1H NMR (400 MHz, CDCl_3 , ppm) δ 7.22 (d, $J = 5.1$ Hz, 2H), 7.20 (s, 2H), 6.96 (d, $J = 5.1$ Hz, 2H), 2.82 – 2.73 (m, 4H), 1.65 (p, $J = 7.8$, 7.2 Hz, 4H), 1.41 – 1.18 (m, 36H), 0.88 (t, $J = 7.0$ Hz, 6H). ^{13}C NMR (100 MHz, CDCl_3 , ppm) δ 171.30, 146.30, 140.41, 138.45, 136.96, 130.47, 129.83, 128.53, 124.35, 118.96, 77.31, 77.00, 76.68, 31.92, 30.88, 29.68, 29.65, 29.65, 29.59, 29.53, 29.47, 29.35, 29.14, 22.69, 14.12.

General procedure for polymerizations.

Equimolar amounts of **5a** or **5b** or a combination **5a/5b** with 2,5-bis(trimethylstannyl)thieno[2,3-*b*]thiophene or 2,5-bis(trimethylstannyl)thieno[3,2-*b*]thiophene are combined with 2% Pd_2dba_3 and 8% PPh_3 in a toluene/DMF (9/1) mixture and heated to 115 $^\circ\text{C}$ overnight. The polymer was than precipitated in methanol and filtered through a Soxhlet thimble. Soxhlet extraction with subsequently acetone, hexane, dichloromethane and chloroform or 1,1,2-tetrachloroethane. After concentration the final fraction was precipitated in methanol and filtered over a PTFE filter and dried in a vacuum oven to give the desired polymer.

PII-TT: GPC(145 $^\circ\text{C}$, chloroform) $M_n = 38.9$ kg/mol, PDI = 2.14. $\lambda_{\text{max}} = 449, 650$ nm.

P(cII:II)-TT 25:75: GPC(145 $^\circ\text{C}$, chloroform) $M_n = 43.9$ kg/mol, PDI = 2.11. $\lambda_{\text{max}} = 444, 639$ nm.

P(cII:II)-TT 50:50: GPC(145 $^\circ\text{C}$, chloroform) $M_n = 31.5$ kg/mol, PDI = 2.18. $\lambda_{\text{max}} = 438, 639$ nm.

P(cII:II)-TT 75:25: GPC(145 $^\circ\text{C}$, chloroform) $M_n = 30.7$ kg/mol, PDI = 2.01. $\lambda_{\text{max}} = 439, 625$ nm.

PcII-TT: GPC(145 $^\circ\text{C}$, chloroform) $M_n = 21.3$ kg/mol, PDI = 1.49. $\lambda_{\text{max}} = 438$ nm.

P11-cTT: GPC(145 °C, chloroform) $M_n = 38.5$ kg/mol, PDI = 1.94. $\lambda_{\max} = 364, 613$ nm.

Pc11-cTT: GPC(145 °C, chloroform) $M_n = 19.0$ kg/mol, PDI = 1.70. $\lambda_{\max} = 370$ nm.

5.6 References

- ¹ H. Shirakawa, E. J. Louis, A. G. Macdiarmid, C. K. Chiang, and A. J. Heeger, *J. Chem. Soc.-Chem. Commun.*, **1977**, 578-580.
- ² J. H. Burroughes, D. D. C. Bradley, A. R. Brown, R. N. Marks, K. Mackay, R. H. Friend, P. L. Burns, and A. B. Holmes, *Nature*, **1990**, *347*, 539-541.
- ³ A. Kraft, A. C. Grimsdale, and A. B. Holmes, *Angew. Chem., Int. Ed.*, **1998**, *37*, 402-428.
- ⁴ H. Sirringhaus, *Adv. Mater.*, **2014**, *26*, 1319-1335.
- ⁵ I. Kang, H.-J. Yun, D. S. Chung, S.-K. Kwon, and Y.-H. Kim, *J. Am. Chem. Soc.*, **2013**, *135*, 14896-14899.
- ⁶ H. Zhou, L. Yang, and W. You, *Macromolecules*, **2012**, *45*, 607-632.
- ⁷ C. Cui, W.-Y. Wong, and Y. Li, *Energy Environ. Sci.*, **2014**, *7*, 2276-2284.
- ⁸ M. C. Scharber, D. Mühlbacher, M. Koppe, P. Denk, C. Waldauf, A. J. Heeger, and C. J. Brabec, *Adv. Mater.*, **2006**, *18*, 789-794.
- ⁹ W. Zhang, J. Smith, S. E. Watkins, R. Gysel, M. McGehee, A. Salleo, J. Kirkpatrick, S. Ashraf, T. Anthopoulos, M. Heeney, and I. McCulloch, *J. Am. Chem. Soc.*, **2010**, *132*, 11437-11439.
- ¹⁰ F. He, W. Wang, W. Chen, T. Xu, S. B. Darling, J. Strzalka, Y. Liu, and L. Yu, *J. Am. Chem. Soc.*, **2011**, *133*, 3284-3287.
- ¹¹ R. Mondal, H. A. Becerril, E. Verploegen, D. Kim, J. E. Norton, S. Ko, N. Miyaki, S. Lee, M. F. Toney, J.-L. Bredas, M. D. McGehee, and Z. Bao, *J. Mater. Chem.*, **2010**, *20*, 5823-5834.
- ¹² E. E. Havinga, W. Tenhoeve, and H. Wynberg, *Polym. Bull.*, **1992**, *29*, 119-126.
- ¹³ E. E. Havinga, W. Tenhoeve, and H. Wynberg, *Synthetic Met.*, **1993**, *55*, 299-306.
- ¹⁴ J. L. Brédas, *Synth. Met.*, **1987**, *17*, 115-121.
- ¹⁵ C. Kitamura, S. Tanaka, and Y. Yamashita, *Chem. Mater.*, **1996**, *8*, 570-578.
- ¹⁶ N. Bérubé, J. Gaudreau, and M. Côté, *Macromolecules*, **2013**, *46*, 6873-6880.
- ¹⁷ J. Hou, Z. a. Tan, Y. Yan, Y. He, C. Yang, and Y. Li, *J. Am. Chem. Soc.*, **2006**, *128*, 4911-4916.
- ¹⁸ L. Huo, S. Zhang, X. Guo, F. Xu, Y. Li, and J. Hou, *Angew. Chem., Int. Ed.*, **2011**, *50*, 9697-9702.
- ¹⁹ M. Bolognesi, D. Gedefaw, D. Dang, P. Henriksson, W. Zhuang, M. Tassarolo, E. Wang, M. Muccini, M. Seri, and M. R. Andersson, *RSC Adv.*, **2013**, *3*, 24543-24552.
- ²⁰ N. F. Phelan and M. Orchin, *J. Chem. Educ.*, **1968**, *45*, 633.
- ²¹ M. Gholami and R. R. Tykwinski, *Chem. Rev.*, **2006**, *106*, 4997-5027.
- ²² A. B. Ricks, G. C. Solomon, M. T. Colvin, A. M. Scott, K. Chen, M. A. Ratner, and M. R. Wasielewski, *J. Am. Chem. Soc.*, **2010**, *132*, 15427-15434.
- ²³ M. Bruschi, M. G. Giuffreda, and H. P. Lüthi, *Chem. Phys. Chem.*, **2005**, *6*, 511-519.
- ²⁴ T. Maeda, T. Tsukamoto, A. Seto, S. Yagi, and H. Nakazumi, *Macromol. Chem. Phys.*, **2012**, *213*, 2590-2597.
- ²⁵ M. Heeney, C. Bailey, K. Genevicius, M. Shkunov, D. Sparrowe, S. Tierney, and I. McCulloch, *J. Am. Chem. Soc.*, **2005**, *127*, 1078-1079.
- ²⁶ K. Zhang and B. Tieke, *Macromolecules*, **2011**, *44*, 4596-4599.
- ²⁷ R. S. Loewe and R. D. McCullough, *Chem. Mater.*, **2000**, *12*, 3214-3221.
- ²⁸ C. A. van Walree, B. C. van der Wiel, and R. M. Williams, *Phys. Chem. Chem. Phys.*, **2013**, *15*, 15234-15242.
- ²⁹ Y. M. Zhao, S. C. Ciulei, and R. R. Tykwinski, *Tetrahedron Lett.*, **2001**, *42*, 7721-7723.
- ³⁰ S. C. Ciulei and R. R. Tykwinski, *Org. Lett.*, **2000**, *2*, 3607-3610.
- ³¹ E. G. Wang, Z. F. Ma, Z. Zhang, K. Vandewal, P. Henriksson, O. Inganäs, F. L. Zhang, and M. R. Andersson, *J. Am. Chem. Soc.*, **2011**, *133*, 14244-14247.
- ³² L. Fang, Y. Zhou, Y.-X. Yao, Y. Diao, W.-Y. Lee, A. L. Appleton, R. Allen, J. Reinspach, S. C. B. Mannsfeld, and Z. Bao, *Chem. Mater.*, **2013**, *25*, 4874-4880.

- ³³ C.-C. Ho, C.-A. Chen, C.-Y. Chang, S. B. Darling, and W.-F. Su, *J. Mater. Chem. A*, **2014**, *2*, 8026-8032.
- ³⁴ Y. Deng, J. Liu, J. Wang, L. Liu, W. Li, H. Tian, X. Zhang, Z. Xie, Y. Geng, and F. Wang, *Adv. Mater.*, **2014**, *26*, 471-476.
- ³⁵ L. A. Estrada, R. Stalder, K. A. Abboud, C. Risko, J.-L. Brédas, and J. R. Reynolds, *Macromolecules*, **2013**, *46*, 8832-8844.
- ³⁶ Gaussian 09, Revision A.02, M. J. Frisch, G. W. Trucks, H. B. Schlegel, G. E. Scuseria, M. A. Robb, J. R. Cheeseman, G. Scalmani, V. Barone, B. Mennucci, G. A. Petersson, H. Nakatsuji, M. Caricato, X. Li, H. P. Hratchian, A. F. Izmaylov, J. Bloino, G. Zheng, J. L. Sonnenberg, M. Hada, M. Ehara, K. Toyota, R. Fukuda, J. Hasegawa, M. Ishida, T. Nakajima, Y. Honda, O. Kitao, H. Nakai, T. Vreven, J. A. Montgomery, Jr., J. E. Peralta, F. Ogliaro, M. Bearpark, J. J. Heyd, E. Brothers, K. N. Kudin, V. N. Staroverov, R. Kobayashi, J. Normand, K. Raghavachari, A. Rendell, J. C. Burant, S. S. Iyengar, J. Tomasi, M. Cossi, N. Rega, J. M. Millam, M. Klene, J. E. Knox, J. B. Cross, V. Bakken, C. Adamo, J. Jaramillo, R. Gomperts, R. E. Stratmann, O. Yazyev, A. J. Austin, R. Cammi, C. Pomelli, J. W. Ochterski, R. L. Martin, K. Morokuma, V. G. Zakrzewski, G. A. Voth, P. Salvador, J. J. Dannenberg, S. Dapprich, A. D. Daniels, O. Farkas, J. B. Foresman, J. V. Ortiz, J. Cioslowski, and D. J. Fox, Gaussian, Inc., Wallingford CT, **2009**.
- ³⁷ X. Zhang and A. J. Matzger, *J. Org. Chem.*, **2003**, *68*, 9813-9815.
- ³⁸ X. Lou, J. L. J. van Dongen, Y. Braeken, J. Brebels, G. W. P. van Pruissen, W. Li, M. M. Wienk, and R. A. J. Janssen, *Polym. Chem.*, **2014**, *5*, 558-561.
- ³⁹ X. Lou, J. L. van Dongen, and E. W. Meijer, *J. Chromatogr.*, **2012**, *1237*, 72-79.

Chapter 6.

Pentacyclic lactam as a building block for wide band gap materials*

A series of donor – acceptor copolymers was synthesized based on 4,10-dialkyl-4,10-dihydrothieno[2',3':5,6]pyrido[3,4-g]thieno[3,2-c]isoquinoline-5,11-dione, a pentacyclic bislactam (PCL) acceptor, alternating with co-monomers as donor that differ in size and electron rich character. The PCL-based copolymers show wide band gaps (E_g), ranging from 1.63 to 2.14 eV in thin films. Efficient wide band gap semiconducting polymers are required to further advance the performance of multi junction polymer solar cells. In combination with a fullerene derivative ($PC_{70}BM$) as electron acceptor the PCL-based copolymers show power conversion efficiencies (PCE) up to 5.6% in polymer solar cells. As a result of efficient charge generation and charge collection, a good performance (PCE = 5.5 ± 0.1 %) was found for copolymers in which the PCL unit alternates with thiophene, dithiophene, thieno[3,2-b]thiophene, or benzo[1,2-b:4,5-b']dithiophene. The PCE of these materials is largely limited by a relatively large energy loss ($E_g - qV_{oc}$) in the range of 0.78 to 0.97 eV. This loss seems largely redundant because solar cells with energy losses in the range of 0.6 to 0.7 eV are possible. However, when the energy loss was be reduced to ~ 0.8 eV by copolymerizing PCL with benzo[c][1,2,5]thiadiazole, the PCE did not improve because of a reduced photocurrent.

* G.W.P. van Pruissen, J.J. van Franeker, M.M. Wienk and R.A.J. Janssen, *Manuscript in preparation*, 2014.

6.1 Introduction

Over the past ten years the development and synthesis of new conjugated polymers has resulted in increased power conversion efficiencies (PCEs) for bulk heterojunction polymer solar cells comprising complementary electron donor and acceptor materials. The present record of PCE = 9.5%,¹ is already approaching the maximum achievable efficiency for a single junction OPV devices of around 10-12% that has been predicted within an empirical approach.²

One of the intrinsic losses is the thermalization of higher excited states to the optical band gap (E_g) where its excess energy is transferred as heat to the surrounding. For OPV the energy differences between E_g and the interfacial donor-acceptor charge-transfer (CT) state and between the CT state and the open-circuit voltage (V_{oc}) represent additional energetic losses. Overall this has resulted in estimates that at room temperature and under one sun illumination the energy loss defined as $E_g - qV_{oc}$ must be at least 0.6 eV to ensure efficient charge generation. In practice this is equivalent to the well-known criterion that the minimal offset of the LUMO levels of donor and acceptor in the photoactive layer is 0.3 eV.³

Tandem and multi-junction solar cells offer the potential to further increase the PCE by making more efficient use of the energy in the solar spectrum. In multi junctions thermalization losses can be reduced when high-energy photons are collected in a wide band gap photoactive layer affording current at a high V_{oc} , while the low-energy photons are transmitted to a subsequent absorber layer with a small band gap. Similar empirical estimates for tandem OPV devices show that PCEs of 15% might be possible.⁴

Key for successful multi-junction devices is the development of high performing materials with suitable complementary band gaps that have their LUMO level well aligned to the LUMO of PCBM. At present the choice for efficient wide band gap materials is limited but recently a pentacyclic lactam (PCL) unit was developed and introduced in a donor-acceptor copolymer.⁵ The copolymer of PCL alternating with thiophene (T) provides a relatively large optical band gap (E_g) of 1.86 eV and affords an impressive PCE = 7.8% in an inverted device configuration.⁵ Despite the wide band gap this PPCLT polymer provided a high short-circuit current density (J_{sc}) of 13.69 mA/cm² owing to an external quantum efficiency (EQE) exceeding 0.7 in the range of 435–640 nm.⁵ The V_{oc} of 0.87 V is already high, but might be further increased because the energy loss from the lowest optical band gap in the blend to qV_{oc} of ~ 0.9 eV ($E_{g,PCBM}$ (1.75 eV) < $E_{g,PPCLT}$ (1.86 eV)), so the energy loss is calculated as 1.75 – 0.87 = 0.88 eV) is significantly larger than the threshold of about 0.6

eV. The only other reported examples with this PCL unit are polymers with benzo-[1,2-*b*:4,5-*b'*]dithiophene ($E_g = 2.02$ eV) and dithieno[3,2-*b*:2',3'-*d*]silole ($E_g = 1.86$ eV) that show a maximum PCE of 5.3% and 3.6% with V_{oc} of 0.90 V and 0.91 V respectively for the optimized devices.⁶

6.2 Aim

Since PCL gives access to wide band gap polymers and provides high efficiencies in OPV devices it is an interesting candidate as electron donor in photoactive layer in the front cell of tandem and triple junction devices with improved efficiencies. The optical band gap of the published PPCLT polymer (1.86 eV) is wider than that of the common fullerene (PCBM) acceptor (1.75 eV) and induces an avoidable loss. Further, there is relatively large energy loss ($E_g - qV_{oc} = 0.88$ eV) in PPCLT:PCBM cells. These possible improvements warrant exploring the prospects of PCL-based conjugated polymers for OPV applications. Here a range of new PCL-based conjugated donor-acceptor copolymers is presented. These combine PCL with strong electron donors (thiophene, dithiophene, and thieno[3,2-*b*]thiophene), weaker electron donors (benzene and benzo[1,2-*b*:4,5-*b'*]dithiophene), and with an electron acceptor (benzo[*c*][1,2,5]thiadiazole) as shown in Figure 6.1.

Another approach to improving V_{oc} and reducing the energy loss is using a less strong acceptor, i.e. raising the LUMO of the fullerene acceptor. It is therefore of interest to test the PCL-based polymers with indene-*C*₆₀-*bis*-adduct (ICBA). ICBA is a well-known fullerene acceptor with a LUMO that is 0.2 eV higher than that of PCBM.^{7,8}

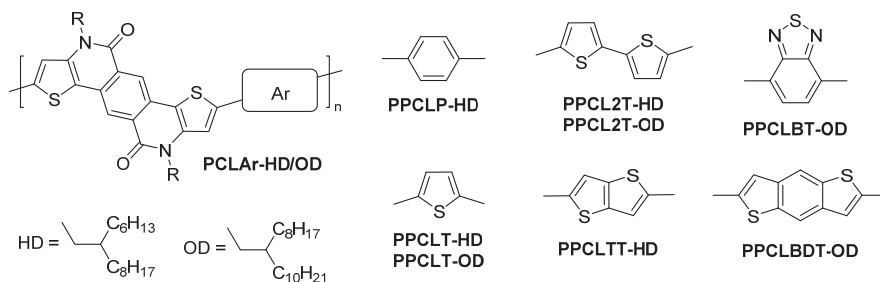


Figure 6.1 – Structure of PCL-based conjugated polymers studied.

6.3 Results and discussion

6.3.1 Synthesis

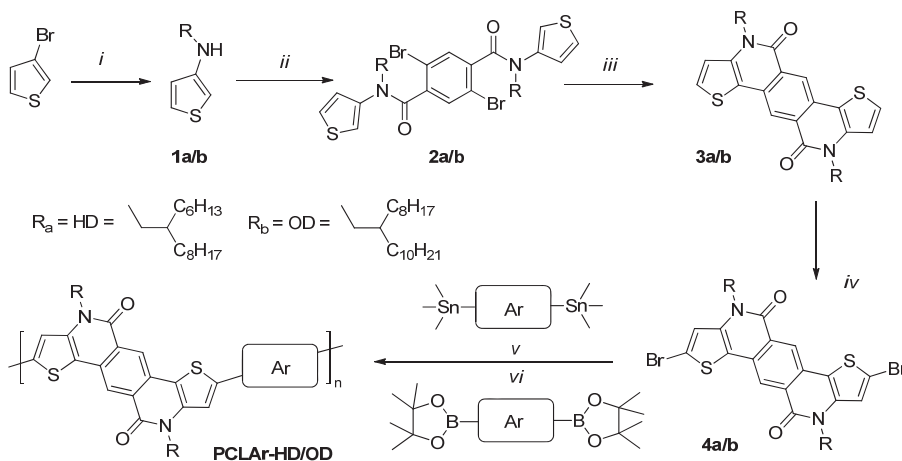
The route to the PCL-based conjugated polymers is shown in Scheme 6.1 and is based on the reported synthetic procedure.⁵ The synthesis of the PCL monomers started with an Ullmann coupling of 2-hexyldecylamine or 2-octyl-dodecylamine with 3-bromothiophene to give *N*-(2-hexyldecyl)thiophen-3-amine (**1a**) or *N*-(2-hexyldecyl)thiophen-3-amine (**1b**). All subsequent steps are similarly applied for both **1a** (HD) and **1b** (OD). The secondary amine was then reacted with 2,5-dibromoterephthaloyl dichloride to give **2a/b**. Ring closure was achieved via palladium catalyzed direct hetero arylation, forming the intramolecular benzene-thiophene bonds to give pentacyclic bislactam (PCL) (**3a/b**). This was brominated with NBS and recrystallized from ethanol with addition of small quantities chloroform to afford (**4a/b**) as a shiny yellow monomer.

With the PCL dibromo monomers **4a** and **4b** a series of copolymers (shown in Figure 6.1) was synthesized via Stille and Suzuki coupling with the appropriate aromatic bis-stannanes for thiophene derivatives or bis-pinacolato boronic esters for benzene derived co-monomers. The copolymer with thiophene (PPCLT-HD) as described in Ref. 5 was synthesized following the published procedure and our own standard protocol. In our hands only polymerization with Pd₂dba₃ and PPh₃ as catalytic system in concentrated solutions gave high molecular weight polymers (PPCLT-HD, $M_n = 96.4$ kg/mol and PPCLT-OD, $M_n = 72.0$ kg/mol) (Scheme 6.1, Table 6.1).

Fused and extended thiophene units are generally beneficial for charge transport and as therefore the thiophene donor was replaced with thieno[3,2-*b*]thiophene (PPCLTT-HD, $M_n = 11.3$ kg/mol) and with dithiophene (PPCL2T-HD). The latter turned out to be insoluble and therefore homolog with the longer 2-octyl-dodecyl side chains was synthesized (PPCL2T-OD, $M_n = 93.3$ kg/mol).

Because stronger donors can lower the band gap but raise the HOMO, copolymers with benzene (PPCLP-HD, $M_n = 27.4$ kg/mol) and benzo[1,2-*b*:4,5-*b'*]dithiophene (PPCLBDT-OD, $M_n = 35.4$ kg/mol) were synthesized. These weaker donors tend to give polymers with deeper HOMO levels. Lowering the HOMO also raises the band gap. To have a smaller band gap and a deep HOMO a copolymer with the strong acceptor benzothiadiazole was synthesized that lowers both the HOMO and the LUMO (PPCLBT-OD, $M_n = 40.7$ kg/mol).

The polydispersity (PDI) measured for these polymers significantly exceeds the standard polydispersity for a condensation polymerization (PDI = 2 vs. PDI > 3) (Table 6.1). This is attributed to bimodal distributions and tailing as a result of interaction with the GPC column despite the high temperature.



Scheme 6.1 – Synthesis of PCL monomers and subsequent PPCLX polymers. (i) 3-Bromothiophene, 2-hexyldecylamine or 2-octyldecylamine, CuI, K_3PO_4 , dimethylaminoethanol (DMAE), 90 °C, 2 d, 35%. (ii) 2,5-Dibromoterephthalic acid, SOCl_2 , DCM, 24 h, then, Et_3N , DCM, room temperature, overnight. (iii) $\text{Pd}(\text{OAc})_2$, PCy_3HBF_4 , K_2CO_3 , dimethylamine (DMA), 120 °C, overnight. (iv) NBS, DCM, 0 °C to room temperature, 2 h. (v) Pd_2dba_3 , PPh_3 , toluene/DMF (9/1), 115 °C, overnight. (vi) Pd_2dba_3 , PPh_3 , toluene/2 M K_3PO_4 (aq) (9/1) Aliquat 336, 110 °C, overnight.

6.3.2 Optical and electrochemical analysis

The UV-vis-NIR absorption spectra of the PPCLX polymers were measured both in thin film and in chloroform solution (Figure 6.2). The absorption spectra for PPCLT-HD, PPCLT-OD, PPCL2T-OD, and PPCLTT-HD are very similar and the optical band gap for the first three as determined from the onsets of optical absorption in thin films is 1.88 eV. PPCLTT-HD shows a slightly higher band gap of 1.93 eV. The polymers with weak electron donors have significantly higher band gaps of 2.04 eV for PPCLBDT-OD and 2.14 eV for PPCLP-HD. When combined with a strong acceptor like benzothiadiazole a large red-shift of the absorption with a corresponding reduced band gap of 1.63 eV is found for PPCLBT-OD. Table 6.1 summarizes these results.

The PPCLX polymers fluorescence when excited at 500 nm (Figure 6.2). PPCLP-HD shows a strong orange pink fluorescence that can be observed by eye. The fluorescence spectra show two vibronic transitions except for PPCLBT-OD, where the detector limit is reached.

Table 6.1 - Molecular weight and optical data of PPCLX polymers

Polymer	M_n kg/mol	PDI	$\lambda_{\text{onset}}^{\text{sol}}$ nm	$\lambda_{\text{onset}}^{\text{film}}$ nm	$\lambda_{\text{max}}^{\text{abs}}$ nm	$\lambda_{\text{max}}^{\text{emission}}$ nm	E_g^{sol} eV	E_g^{film} eV
PPCLP-HD	27.4 ^a	4.2 ^a	574	580	553	620	2.16	2.14
PPCLT-HD	96.4 ^a	4.4 ^a	651	660	603	659	1.90	1.88
PPCLT-OD	72.0 ^a	3.3 ^a	648	656	603	655	1.91	1.89
PPCL2T-OD	93.3 ^b	4.0 ^b	655	661	613	657	1.89	1.88
PPCLTT-HD	11.3 ^a	6.0 ^a	639	644	602	726	1.94	1.93
PPCLBT-OD	40.7 ^a	3.3 ^a	750	761	700	771	1.65	1.63
PPCLBDT-OD	35.4 ^a	5.0 ^a	605	608	526	696	2.05	2.04

^a GPC with ODCB at 140 °C. ^b GPC with ODCB at 80 °C.

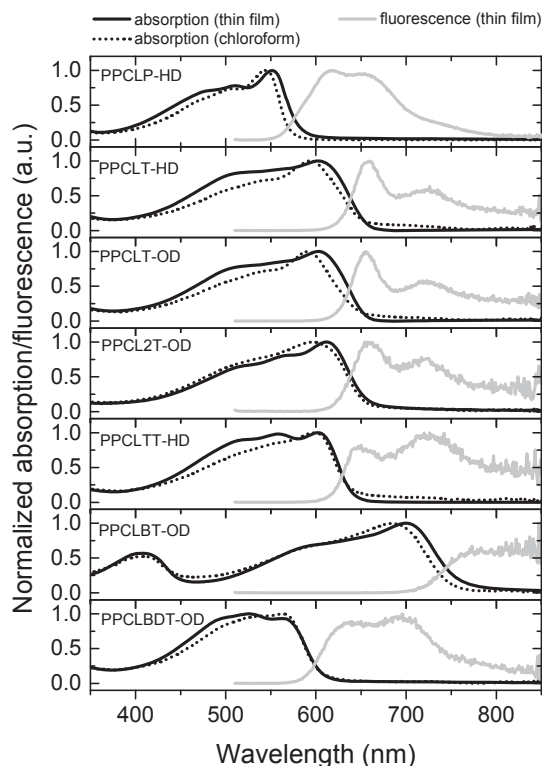


Figure 6.2 – UV-vis-NIR absorption spectra (black) for PPCLX polymers both in solution (dotted) as thin films (solid). In grey (solid) the respective normalized fluorescence spectra. The noise at wavelengths below 800 nm is due to reduced sensibility of the detector in that region.

The oxidation and reduction potentials of the PPCLX polymers were measured using cyclic voltammetry. The measurements were performed on spin-coated thin films on ITO covered glass substrates in acetonitrile containing 0.1 M TBAPF₆ as electrolyte. The results are collected in Table 6.2. The electrochemical band gap is significantly larger than the optical band gap. The HOMO levels are relevant for the V_{oc} . The HOMO levels of PPCLT-HD and PPCLT-OD are very similar value (−5.72 eV and −5.73 eV) and almost equal to those of PPCLBT-OD (−5.76 eV) and PPCLBDT (−5.75 eV). The polymers with extended electron rich thiophene units, PPCL2T-OD and PPCLTT-OD have HOMO levels that are about 100 meV higher (−5.63 and −5.62 eV respectively). Only for PPCLP-HD the HOMO level is significantly deeper (−5.80 eV).

Table 6.2 – Measured oxidation and reduction potentials for PPCLX polymers and calculated HOMO and LUMO energy thereof.

Polymer	E_{red} V	E_{ox} V	E_{HOMO}^a eV	E_{LUMO}^a eV	E_g^{CV} eV	E_g^{film} eV	$E_g^{CV} - E_g^{film}$ eV
PPCLP-HD	-2.09	0.57	-5.80	-3.14	2.66	2.14	0.52
PPCLT-HD	-1.99	0.49	-5.72	-3.24	2.48	1.88	0.60
PPCLT-OD	-2.03	0.50	-5.73	-3.20	2.53	1.89	0.64
PPCL2T-OD	-2.04	0.40	-5.63	-3.19	2.44	1.88	0.56
PPCLTT-HD	-2.05	0.39	-5.62	-3.18	2.44	1.93	0.51
PPCLBT-OD	-1.53	0.53	-5.76	-3.70	2.06	1.63	0.43
PPCLBDT-OD	-2.04	0.52	-5.75	-3.19	2.56	2.04	0.52

$$^a E_{HOMO/LUMO} = -5.23 - qE_{ox/red} \text{ eV}$$

Table 6.3 – Solar cell characteristics for PPCLX:PC₇₀BM solar cells

Polymer	ratio	Solvent additive	d nm	J_{sc} mA/cm ²	V_{oc} V	FF	PCE %	$E_g - qV_{oc}$ eV
PPCLP-HD	1:1.5	10% ODCB ^a	115	6.15	0.93	0.69	3.9	0.82 ^d
PPCLT-HD	1:2	2% DIO ^a	80	9.97	0.87	0.64	5.5	0.88 ^d
PPCLT-OD	1:1.5	3% DIO ^a	130	6.89	0.78	0.53	2.8	0.97 ^d
PPCL2T-OD	1:1.5 ^c	10% ODCB ^b	100	9.33	0.80	0.72	5.4	0.95 ^d
PPCLTT-HD	1:1.5	10% ODCB ^a	90	10.82	0.82	0.63	5.6	0.93 ^d
PPCLBT-OD	1:1	3% DIO ^a	110	7.45	0.85	0.54	3.4	0.78 ^e
PPCLBDT-OD	1:1.5	10% ODCB ^a	90	9.87	0.88	0.65	5.6	0.87 ^d

^aAdditive to CHCl₃. ^bAdditive to TCE. ^cWith PC₆₀BM. ^dBased on $E_g = 1.75$ eV for PC₇₀BM. ^eBased on $E_g = 1.63$ eV for PPCLBT-OD.

6.3.3 Solar cells

6.3.3.1 J-V characteristics

Solar cells of PPCLX polymers mixed with PC₇₀BM were made in a regular polarity configuration on glass substrates with ITO(80 nm)/PEDOT:PSS(35 nm)/PPCLX:PC₇₀BM/LiF(1 nm)/Al(150 nm). The active layers of PPCLX:PC₇₀BM were spin coated from chloroform or 1,1,2,2-tetrachloroethane with *ortho*-dichlorobenzene (ODCB) or diiodooctane (DIO) as

co-solvent. The performance of the best cells is summarized in Table 6.3 and the corresponding current density – voltage (J - V) characteristics and EQE spectra are shown in Figure 6.3.

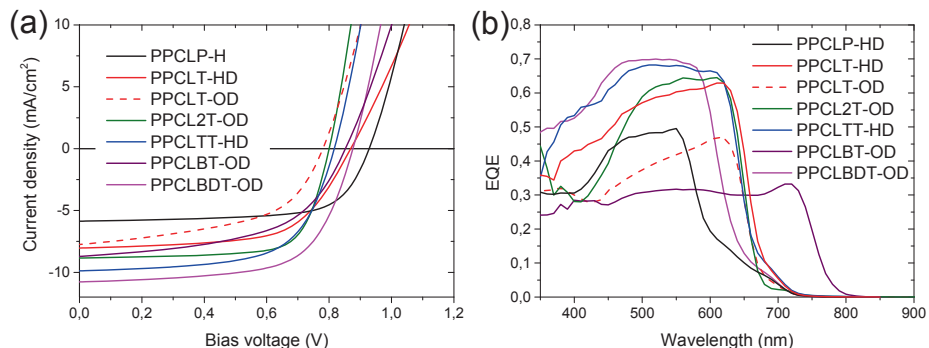


Figure 6.3 – (a) J – V characteristics and (b) EQE spectra of the PPCLX:PC₇₀BM solar cells.

PPCLT-HD for which PCE = 7.8% has been reported in literature⁵ gives a maximum PCE = 5.5% in our hands. The V_{oc} (0.87 vs. 0.87 V) and FF (0.64 vs. 0.66) are similar but the J_{sc} of $9.97 \text{ mA}/\text{cm}^2$ is significantly lower than the $13.69 \text{ mA}/\text{cm}^2$ reported in literature.⁵ This difference arises in part from the different layer thicknesses and the different device configuration. We find optimum performance for photoactive layers of $\sim 80 \text{ nm}$, whereas the photoactive layers are $\sim 180 \text{ nm}$ thick in the study reported by Cao *et al.*⁵ This thicker layer accounts for increased light absorption and higher currents. These devices constitute an optical cavity for which light absorption is affected by optical interference. For wide band gap photoactive layers maxima are expected around thicknesses of 80 and 200 nm.⁹ Attempts to optimize thicker cells did not yield higher efficiencies because the fill factor decreased for thick layers. All other cells were optimized in the first interference maximum. Also the regular device configuration may affect the maximum PCE. Cao *et al.* find a reduction of the PCE from 7.8% to 7.2% going from inverted to regular polarity devices.

Elongating the side chains from 2-hexyldecyl to 2-octyldecyl yielded lower performance; all solar cell parameters for PPCLT-OD decrease compared to PPCLT-HD. The decrease in performance for longer side chains likely results from a reduced tendency of the polymer to aggregate during processing. For PPCL2T the longer 2-octyldecyl side chains are necessary because PPCL2T-HD is insoluble. When spin coated from TCE:10%ODCB (v/v), PPCL2T-OD:PC₆₁BM cells give a very high fill factor of 0.72, $V_{oc} = 0.80$

V , and $J_{sc} = 9.33 \text{ mA/cm}^2$ leading to a good PCE of 5.4%. Changing thiophene to thieno[3,2-*b*]thiophene gives a sparingly soluble polymer but provides solar cells with increased $J_{sc} = 10.82 \text{ mA/cm}^2$ but lower $V_{oc} = 0.82 \text{ V}$ and $FF = 0.63$. The overall PCE of 5.6% is the best for this series.

For PPCLP-HD the deeper HOMO level results in a higher V_{oc} of 0.93 V compared to PPCLT-HD in combination with PC₇₀BM. As result of the high V_{oc} and high FF, PPCLP-HD still provides PCE = 3.9% despite the fact the wide optical band gap of 2.14 eV limits the photocurrent. PPCLBDT-OD with good $J_{sc} = 9.87 \text{ mA/cm}^2$, $V_{oc} = 0.88 \text{ V}$ and $FF = 0.65$ provide PCE = 5.6%. The high photocurrent results from a high EQE of almost 0.7 (Figure 6.3).

Despite the small band gap PPCLBT-OD shows a moderate $J_{sc} = 7.45 \text{ mA/cm}^2$ resulting in PCE of 3.4%. The EQE shows that the polymer is indeed absorbing up to almost 800 nm and contributing to the photocurrent, but the EQE is only ~ 0.3 which is much less than for the other PPCLX polymers (Figure 6.3). The low EQE is likely a consequence of a reduced generation of charges in the layer. This can be due to a reduced LUMO – LUMO offset between PPCLBT-OD (-3.70 eV) and PC₇₀BM (-4.15 eV) that gets below the 0.3 eV that is necessary for efficient charge separation.

6.3.3.2 Energy loss

For all polymers and the resulting solar cell characteristics an energy loss can be defined as lowest $E_g - qV_{oc}$ which incorporates all losses due to LUMO – LUMO offset and charge transport to the contacts (Table 6.3). The latter is empirically found to be 0.3 – 0.4 eV leaving the rest to LUMO – LUMO offset which is ideally 0.3 eV. Consequently ideal polymers should have an energy loss of around 0.6 – 0.7 eV as lower values will hamper efficient charge generation and collection while higher values mark unnecessary energy losses. This makes the energy loss an interesting parameter to easily assess the significance of the polymers. For all but one polymer the energy loss is found to be larger than 0.8 eV (Table 6.3). For PPCLBT-OD:PC₇₀BM the energy loss of 0.78 eV is lowest and should still be sufficient for efficient charge separation. This contradicts the low EQE and the LUMO – LUMO offset as determined by CV which both suggest that the LUMO – LUMO offset is slightly too low.

6.3.3.3 Morphology

An ideal morphology would consist of two interpenetrating networks of donor and acceptor material on the 10 nm scale. The optimized morphology of the active layers was studied by transmission electron microscopy (TEM) showing fiber-like structures for all polymer:PCBM layers (Figure 7.4). Different coarsening can be distinguished; a fine morphology for PPCLTT-HD, PPCL2T-OD and PPCLBDT-OD whereas PPCLT-HD, PPCLT-OD, and PPCLBT-OD show coarser structures with thicker fibers and PPCLP-HD is in between. For DPP-based polymers it has been established that the EQE decreases with the width of the fibers.¹⁰ Such relation is also seen here because the solar cells with high EQE generally correspond to the samples with finer fiber structure. However for PPCLT-HD (EQE > 0.6), shows thicker fibers than PPCLP-HD or PPCLBT-OD which both have significantly lower EQE_{max} values (~0.45 and ~0.30). This demonstrates that the width of the fibers is not the only criterion here. From a magnification of PPCLTT-HD (Figure 7.4 bottom-right) crystalline domains can be observed showing the lamellar stacking that is typically observed for all samples. The crystallinity of these samples can be beneficial for charge transport which is reflected in the good fill factors observed (Table 6.3).

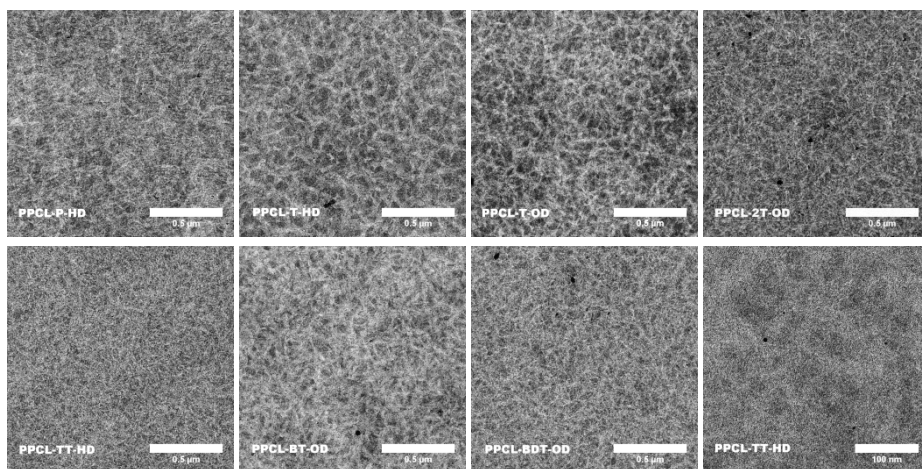


Figure 6.4 – Transmission electron microscopy (TEM) images showing the morphology of the optimized active layers for all PCL polymers. Bottom-right a magnification of PPCLTT-HD shows lamellar stacking and hence the crystallinity in the sample.

6.4 Conclusion

By testing PCL with different co-monomers materials with smaller and wider band gap could be obtained compared to the previously reported PPCLT-HD. For the wide band gap polymers PPCLP-HD and PPCLBDT-OD PCEs of 3.9% and 5.6% are obtained which is good considering the low amount of photons they absorb. Also for the polymers PPCL2T-OD and PPCLTT-HD similar PCEs are found with 5.4% and 5.6% respectively.

All these polymers show a too large band gap for an ideal front cell in tandem solar cell applications. Additionally their LUMO – LUMO offset is too large leading to high energy losses. Combining these polymers with IC₆₀BA can reduce the LUMO – LUMO offset but does not yield devices with higher PCE. Combining PCL with an acceptor can be a viable way to both reduce the band gap and lower the LUMO – LUMO offset as is shown by the PPCLBT-OD polymer. Although the energy loss of 0.78 eV suggests a sufficient offset the LUMO level of -3.91 eV determined by CV suggests it is on the low side of the limit. The low EQE obtained for solar cells based on PPCLBT-OD further supports this.

The fact that PPCLBT-OD is so close to ideal parameters makes it an interesting candidate to see if minor variations can make this a successful class of polymers in terms of thermodynamic efficiency and potentially as wide band gap front cells.

6.5 Experimental

6.5.1 General procedures, materials and instruments

See paragraph 2.5.1. for details on NMR, UV-vis-NIR, MALDI-TOF, and CV equipment.

6.5.2 Solar cell device fabrication and characterization

See paragraph 2.5.2 for details of device fabrication and measurement equipment.

6.5.3 Synthesis

***N*-(2-hexyldecyl)thiophen-3-amine (1a).**

A mixture of 3-bromothiophene (11.023 g, 67.6 mmol), 2-hexyldecan-1-amine (16.3 g, 67.6 mmol), CuI (1.3 g, 6.8 mmol) and grinded K₃PO₄ (43.0 g, 200 mmol) in dimethylaminoethanol (30 ml) was heated to 90 °C for 2 days under an argon atmosphere. The reaction was cooled to room temperature and filtered. The residue was washed with ethyl acetate and the filtrate concentrated and subjected to silica column chromatography (gradient heptane/dichloromethane 0 - 100%) to give 7.7 g (35.5%) of the desired air sensitive compound. ¹H NMR (400 MHz, CDCl₃, ppm): δ 7.13 (dd, *J* = 5.1, 2.9 Hz, 1H), 6.61

(dd, $J = 5.1, 1.5$ Hz, 1H), 5.91 (dd, $J = 3.0, 1.5$ Hz, 2H), 3.56 (s, 1H), 2.97 (d, $J = 6.0$ Hz, 2H), 1.70 – 1.52 (m, 1H), 1.45 – 1.12 (m, 24H), 0.88 (t, $J = 6.7$ Hz, 6H). ^{13}C NMR (100 MHz, CDCl_3 , ppm): δ 149.10, 124.94, 119.90, 94.76, 49.87, 37.82, 32.22, 32.21, 31.90, 31.88, 30.07, 29.74, 29.60, 29.33, 26.79, 26.76, 22.69, 22.68, 14.10.

***N*-(2-octylododecyl)thiophen-3-amine (1b).**

The same procedure as for **1a** but using an equivalent amount of 2-octylododecan-1-amine instead of 2-hexyldecan-1-amine. ^1H NMR (400 MHz, CDCl_3 , ppm) δ 7.14 (dd, $J = 5.1, 3.0$ Hz, 1H), 6.61 (dd, $J = 5.2, 1.5$ Hz, 1H), 5.91 (dd, $J = 3.1, 1.5$ Hz, 1H), 3.57 (s, 1H), 2.97 (d, $J = 6.1$ Hz, 2H), 1.59 (p, $J = 9.5, 4.6, 4.1$ Hz, 1H), 1.37 – 1.15 (m, 32H), 0.88 (t, $J = 6.9$ Hz, 6H). ^{13}C NMR (100 MHz, CDCl_3 , ppm): δ 149.10, 124.96, 119.91, 94.79, 77.31, 76.99, 76.67, 49.87, 37.80, 32.20, 31.91, 30.05, 29.66, 29.63, 29.60, 29.33, 26.78, 22.68, 14.11.

2,5-Dibromo-*N*¹,*N*⁴-di(2-hexyldeceyl)-*N*¹,*N*⁴-di(thiophen-3-yl)terephthalamide (2a).

2,5-Dibromoterephthalic acid (1.50 g, 4.63 mmol) was dissolved in dichloromethane (50 ml) with a few drops of DMF and SOCl_2 (3 ml) was added dropwise. The reaction was stirred at r.t. overnight and dried *in vacuo* to give the acid chloride that was redissolved in dichloromethane (15 ml). A solution of **1a** (3.75 g, 11.6 mmol) and Et_3N (2 ml) in dichloromethane (30 ml) was added dropwise and the reaction stirred overnight at r.t.. After addition of water the organics were extracted with chloroform and washed with brine, dried over MgSO_4 and purified via silica column chromatography to give 1.8 g (2.1 mmol) of the desired product (45% yield). ^1H NMR (400 MHz, CDCl_3 , ppm) δ 7.12 (dd, $J = 5.4, 3.1$ Hz, 2H), 7.08 (s, 2H), 6.84 (d, $J = 3.5$ Hz, 2H), 6.75 (dd, $J = 5.2, 1.4$ Hz, 2H), 3.75 (s, 4H), 1.54 (h, $J = 6.1$ Hz, 2H), 1.35 – 1.11 (m, 48H), 0.87 (td, $J = 6.8, 4.5$ Hz, 12H).

2,5-Dibromo-*N*¹,*N*⁴-di(2-octylododecyl)-*N*¹,*N*⁴-di(thiophen-3-yl)terephthalamide (2b).

The same procedure as for **2a** but using an equivalent amount of **1b** instead of **1a**. The product was directly continued in the next reaction.

4,10-Di(2-hexyldeceyl)-4,10-dihydrothieno[2',3':5,6]pyrido[3,4-*g*]thieno[3,2-*c*]isoquinoline-5,11-dione (3a).

The same procedure as for **3b** but using an equivalent amount of **2a** instead of **2b**. ^1H NMR (400 MHz, CDCl_3 , ppm) δ 8.88 (s, 2H), 7.49 (d, $J = 5.4$ Hz, 2H), 7.10 (d, $J = 5.4$ Hz, 2H), 4.24 (d, $J = 4.6$ Hz, 4H), 2.09 – 1.96 (m, 1H), 1.42 – 1.19 (m, 48H), 0.84 (t, $J = 7.0$ Hz, 12H).

4,10-Di(2-octylododecyl)-4,10-dihydrothieno[2',3':5,6]pyrido[3,4-*g*]thieno[3,2-*c*]isoquinoline-5,11-dione (3b).

Compound **2b** (8.2 g, 7.8 mmol) was dissolved in dimethylamine (100 ml) with $\text{Pd}(\text{OAc})_2$ (87.5 mg, 390 μmol), PCy_3HBF_4 (287 mg, 780 μmol) and K_2CO_3 (1.2 g, 8.6 mmol) and heated under argon to 120 °C overnight. The reaction was cooled and water was added. The organics were extracted with chloroform and washed with brine, dried over MgSO_4 and concentrated before column chromatography with chloroform/heptane gradient (0% to 100%). The product containing fractions were combined, concentrated and recrystallized from ethanol with a little addition of chloroform. Filtration and drying gave the title compound as yellow powder (1.47 g) in 21% yield. ^1H NMR (400 MHz, CDCl_3 , ppm) δ 8.86 (s, 2H), 7.48 (d, $J = 5.4$ Hz, 2H), 7.09 (d, $J = 5.4$ Hz, 2H), 4.23 (d, $J = 7.8$ Hz, 4H), 2.02 (q, $J = 7.4, 6.6$ Hz, 2H), 1.22 (d, $J = 3.5$ Hz, 64H), 0.85 (dt, $J = 6.6$ Hz, 10H). ^{13}C NMR (100 MHz, CDCl_3 , ppm) δ 161.58, 139.43, 129.99, 126.80, 126.09, 123.62, 117.94, 117.73,

77.31, 76.99, 76.67, 49.71, 37.11, 31.87, 31.84, 31.64, 29.95, 29.58, 29.55, 29.50, 29.30, 29.24, 26.66, 22.65, 22.62, 14.09, 14.06.

2,8-Dibromo-4,10-di(2-hexyldecyl)-4,10-dihydrothieno[2',3':5,6]pyrido[3,4-g]thieno[3,2-c]isoquinoline-5,11-dione (4a).

The same procedure as for **4b** but using an equivalent amount of **3a** instead of **3b**. ^1H NMR (400 MHz, CDCl_3 , ppm) δ 8.67 (s, 2H), 7.06 (s, 2H), 4.18 – 4.11 (m, 4H), 2.48 – 1.78 (m, 2H), 1.43 – 1.19 (m, 48H), 0.85 (t, $J = 6.8$ Hz, 12H). ^{13}C NMR (100 MHz, CDCl_3 , ppm) δ 161.10, 138.82, 129.32, 126.81, 123.38, 120.86, 118.80, 115.13, 77.32, 77.00, 76.68, 49.74, 36.98, 31.85, 31.79, 31.52, 31.48, 29.94, 29.64, 29.51, 29.27, 26.53, 26.51, 22.65, 22.62, 14.09, 14.08. MALDI-TOF m/z : 930.33 (M^+ , 100%).

2,8-Dibromo-4,10-di(-octyldodecyl)-4,10-dihydrothieno[2',3':5,6]pyrido[3,4-g]thieno[3,2-c]isoquinoline-5,11-dione (4b).

A mixture of **3b** (1.0 g, 1.13 mmol) dissolved in dichloromethane (50 ml) was cooled to 0 °C before adding NBS (402 mg, 22.26 mmol). As a precipitate formed chloroform was added after 2 h. Small portions of NBS were added until thin layer chromatography (TLC) showed full conversion. Column chromatography with chloroform/heptane gradient (0% to 100%) gave the desired product that was subsequently recrystallized from ethanol with a small amount of chloroform. After filtration and drying a shiny yellow compound was obtained (980 mg) in 83% yield. ^1H NMR (400 MHz, CDCl_3 , ppm) δ 8.59 (s, 2H), 7.03 (s, 2H), 4.12 (d, $J = 4.1$ Hz, 4H), 2.05 – 1.87 (m, 2H), 1.44 – 1.12 (m, 64H), 0.85 (dt, $J = 6.8$ Hz, 12H). ^{13}C NMR (100 MHz, CDCl_3 , ppm) δ 160.95, 138.78, 129.21, 126.70, 123.26, 120.82, 118.72, 115.07, 77.32, 77.00, 76.68, 49.71, 36.97, 31.89, 31.85, 31.50, 29.95, 29.61, 29.56, 29.51, 29.32, 29.27, 26.54, 22.66, 22.64, 14.10, 14.08. MALDI-TOF m/z : 1042.47 (M^+ , 100%).

2,6-Bis(trimethylstannyl)benzo[1,2-b:4,5-b']dithiophene.

In THF (20 ml) was dissolved benzo[1,2-*b*:4,5-*b'*]dithiophene (250 mg, 1.32 mmol) and cooled to -78 °C. Four equivalents of *tert*-butyllithium (1.6 M in hexanes, 3.30 ml, 5.28 mmol) was added dropwise. After 1 h the reaction was warmed to r.t. for a short period and cooled to -78 °C again before quenching the reaction with chlorotrimethylstannane (1.0 M in THF, 5.30 ml, 5.28 mmol). After addition the reaction was allowed to warm to r.t. and stirred for another 2 h. The reaction was then concentrated *in vacuo* and redissolved in heptane. The salts were filtered off and the procedure was repeated three times. The resulting product was then recrystallized from ethanol twice to give 186 mg of white crystals. ^1H NMR (400 MHz, CDCl_3 , ppm) δ 8.28 (s, 2H), 7.42 (s, 2H), 0.44 (s, 6H). ^{13}C NMR (100 MHz, CDCl_3 , ppm) δ 141.71, 141.30, 138.56, 130.92, 115.05, 77.32, 77.00, 76.68, -8.37.

Typical Suzuki polymerization: PPCLBT-OD.

To a Schlenk tube with **4b** (80.9 mg, 77.5 μmol), 4,7-bis(4,4,5,5-tetramethyl-1,3,2-dioxaborolan-2-yl)benzo[*c*][1,2,5]thiadiazole (30.1 mg, 77.5 μmol), Pd_2dba_3 (1.42 mg, 1.55 μmol) and PPh_3 (1.63 mg, 6.20 μmol) was added under argon atmosphere toluene (1.8 ml) and 2 M K_3PO_4 aqueous solution (0.2 ml) and a drop of Aliquat 336. Argon was bubbled through the mixture for 15 min. before heating it to 110 °C overnight. After cooling to r.t. the polymer was precipitated in methanol and filtered through a Soxhlet thimble. Extraction with acetone, heptane and dichloromethane gave only slightly colored fractions indicating poor solubility, so the final polymer was collected by cooking the thimble in TCE

and filter it hot. After concentration the polymer was precipitated in methanol again and filtered over a PTFE filter to give 57 mg.

PPCLBT-OD: Yield 57 mg, GPC (ODCB, 140 °C) $M_n = 40.7$ kg/mol, PDI = 3.3, $\lambda_{\max} = 700$ nm.

PPCLP-HD: Yield 69 mg, GPC (ODCB, 140 °C) $M_n = 96.4$ kg/mol, PDI = 4.4, $\lambda_{\max} = 553$ nm.

Typical Stille polymerization: PPCLT-OD.

Equimolar amounts of **4b** (80.9 mg, 77.5 μ mol) and 2,5-bis(trimethylstannyl)thiophene (31.8 mg, 77.5 μ mol) were put in a Schlenk tube with Pd₂dba₃ (1.42 mg, 1.55 μ mol) and PPh₃ (1.63 mg, 6.20 μ mol) and put under argon. The mixture is dissolved in toluene/DMF (9/1) (2 ml) and argon is bubbled through for 15 min. before heating the reaction to 115 °C overnight. After cooling the polymer is precipitated in methanol and filtered through a Soxhlet thimble. Soxhlet extraction with acetone, heptane and dichloromethane was used to wash residual catalyst and lower molecular weight fractions and the final polymer was extracted with chloroform and again precipitated in methanol and filtered over a PTFE filter to give 41 mg. GPC (ODCB, 140 °C) $M_n = 72.0$ kg/mol, PDI = 3.3, $\lambda_{\max} = 603$ nm.

PPCLT-HD: Yield 72 mg, GPC (ODCB, 140 °C) $M_n = 27.4$ kg/mol, PDI = 4.2, $\lambda_{\max} = 603$ nm.

PPCLTT-HD: Yield 51mg, GPC (ODCB, 140 °C) $M_n = 11.3$ kg/mol, PDI = 6.0, $\lambda_{\max} = 602$ nm.

PPCL2T-OD: Yield 68 mg. GPC (ODCB, 80 °C) $M_n = 93.3$ kg/mol, PDI = 4.0, $\lambda_{\max} = 613$ nm.

PPCLBDT-OD: Yield 50 mg. GPC (ODCB, 140 °C) $M_n = 35.4$ kg/mol, PDI = 5.0, $\lambda_{\max} = 526$ nm.

6.6 Acknowledgements

I thank Hans van Franeker for measuring TEM images.

6.7 References

- ¹ L. Ye, S. Zhang, W. Zhao, H. Yao, and J. Hou, *Chem. Mater.*, **2014**, *26*, 3603-3605.
- ² R. A. J. Janssen and J. Nelson, *Adv. Mater.*, **2013**, *25*, 1847-1858.
- ³ M. C. Scharber, D. Mühlbacher, M. Koppe, P. Denk, C. Waldauf, A. J. Heeger, and C. J. Brabec, *Adv. Mater.*, **2006**, *18*, 789-794.
- ⁴ G. Dennler, M. C. Scharber, T. Ameri, P. Denk, K. Forberich, C. Waldauf, and C. J. Brabec, *Adv. Mater.*, **2008**, *20*, 579-583.
- ⁵ J. Cao, Q. Liao, X. Du, J. Chen, Z. Xiao, Q. Zuo, and L. Ding, *Energy Environ. Sci.*, **2013**, *6*, 3224-3228.
- ⁶ Q. Liao, J. Cao, Z. Xiao, J. Liao, and L. Ding, *Phys. Chem. Chem. Phys.*, **2013**, *15*, 19990-19993.
- ⁷ N. C. Miller, S. Sweetnam, E. T. Hoke, R. Gysel, C. E. Miller, J. A. Bartelt, X. Xie, M. F. Toney, and M. D. McGehee, *Nano Lett.*, **2012**, *12*, 1566-1570.
- ⁸ M. A. Faist, S. Shoaee, S. Tuladhar, G. F. A. Dibb, S. Foster, W. Gong, T. Kirchartz, D. D. C. Bradley, J. R. Durrant, and J. Nelson, *Adv. Energy Mater.*, **2013**, *3*, 744-752.
- ⁹ A. J. Moulé, J. B. Bonekamp, and K. Meerholz, *J. Appl. Phys.*, **2006**, *100*, 094503.
- ¹⁰ W. Li, K. H. Hendriks, A. Furlan, W. S. C. Roelofs, S. C. J. Meskers, M. M. Wienk, and R. A. J. Janssen, *Adv. Mater.*, **2014**, *26*, 1565-1570.

Chapter 7.

Wide band gap TPD materials for tandem solar cells

Efficient wide band gap conjugated polymers are of interest for tandem polymer solar cells to convert photons from the high-energy part of the solar spectrum. Here, 4H-thieno[3,4-c]pyrrole-4,6(5H)-dione (TPD) is investigated as a moderate electron deficient unit for wide band gap conjugated polymers. In analogy with previous chapters thiophene-flanked TPD monomers were polymerized with benzene (P), thiophene (T), and thieno[3,2-b]thiophene (TT) based monomers in Suzuki and Stille reactions to afford PTPDXT polymers with band gaps of 2.11, 1.84, and 1.86 eV respectively. The power conversion efficiencies (PCEs) for these materials in single junction solar cells reached up to 4.7%, but either the open-circuit voltage ($X = T, TT$) or the short-circuit current density ($X = P, T$) were too low to be useful in a tandem cell. A polymer in which TPD alternates with an alkoxy substituted benzo[1,2-b:4,5-b']dithiophene (BDT-OEH) was found to have deeper HOMO and LUMO levels and a band gap of 1.84 eV. A PCE of 6.5% in single junction solar cells was obtained with this PTPDBDT-OEH polymer. In combination with an efficient small band gap conjugated polymer a tandem cell was designed with an expected PCE of 9.4%. Experimentally the best tandem solar cell was found to have a PCE of 7.2%, mainly due to lower than expected current density.

7.1 Introduction

Tandem polymer solar cells can enhance the efficiency of single junction cells by combining wide and small band gap photoactive layers in a stacked device configuration. For an efficient tandem cell, both the wide and small band gap sub cells must be efficient. Especially for wide band gap sub cells, the choice of materials is limited and hence it is of interest to explore new wide band gap materials. In the donor–acceptor approach for band gap control in conjugated polymers, a wide band gap copolymer can be obtained by combining moderately electron deficient with moderately electron rich units. For the former 4*H*-thieno[3,4-*c*]pyrrole-4,6(5*H*)-dione (TPD) is an interesting candidate because it fuses an electron rich thiophene with a single electron deficient imide. Thereby TPD slightly deviates from the acceptor units discussed in the previous chapters, where two amide bonds are responsible for the electron deficiency of the unit.

TPD was first synthesized just to prove the successful synthesis of thiophene-3,4-dicarboxylic acid¹ and later mainly tested for its biological activity as herbicides or insecticides.^{2,3} Zhang *et al.* were the first to incorporate TPD in donor–acceptor conjugated polymers in 1997^{4,5} but it would take more than ten years before the first TPD-based polymers were used in organic solar cells.^{6–11} The good efficiencies achieved with these first polymers led to a significant increase in the number of studies on TPD-containing polymers alternating with various donors. Next to oligothiophenes (*n*T),^{12–16} TPD was combined with different dithieno derivatives (DTX) and with benzodithiophenes (BDT) (Figure 7.1).

For the dithieno derivatives different hetero atoms have been introduced starting with nitrogen and then from carbon going down the 14th period of the Periodic Table to silicon and germanium. 4*H*-dithieno[3,2-*b*:2',3'-*d*]pyrrole (X = N) gives small band gap materials with moderate performance.^{17–21} Polymers incorporating 4*H*-cyclopenta[2,1-*b*:3,4-*b'*]dithiophene (X = C) have shown promising results^{22–25} with a highest PCE of 6.4% so far,²⁶ while copolymers with 4*H*-silolo[3,2-*b*:4,5-*b'*]dithiophene (X = Si)^{27–31} show PCE well over 7%.^{32,33} Some examples with 4*H*-germolo[3,2-*b*:4,5-*b'*]dithiophene (X = Ge)^{27,34–36} however, are highly efficient with PCEs > 8%^{37,38} and a record PCE of 8.5%.³⁹

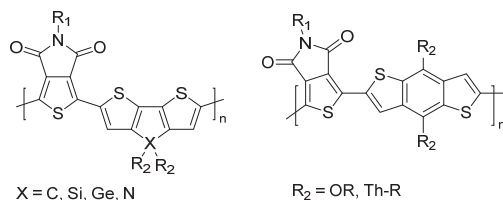


Figure 7.1 – The two successful classes of TPD-based polymers, left with dithieno derivatives and on the right with benzodithiophene derivatives.

The strong attention for BDT-TPD copolymers is based on the good PCE of 6.8% reported already in one of the first publications on this type of copolymer.¹¹ Although some examples with thiophene branching are reported to deepen the HOMO level,⁴⁰ most effort was put in optimization of the side chain length and branching for BDT alkoxy derivatives.^{10,41-43} This led to performances well over 7% PCE for polymers with 2-ethylhexyloxy side chains on BDT and a linear *n*-octyl side chain on TPD (PBDTPD-OEH).^{44,45} A significantly higher PCE of 8.5% for the same polymer with *n*-heptyl side chains on the TPD was found after tedious optimization.⁴³

7.2 Aim

The wide band gap (> 1.7 eV) of TPD-based copolymers and their excellent performance make them interesting candidates to form the active layer in front cells of tandem polymers solar cell. Two recent examples show the viability of this idea, providing PCEs of 7.5%⁴⁶ and 8.6%.⁴⁷

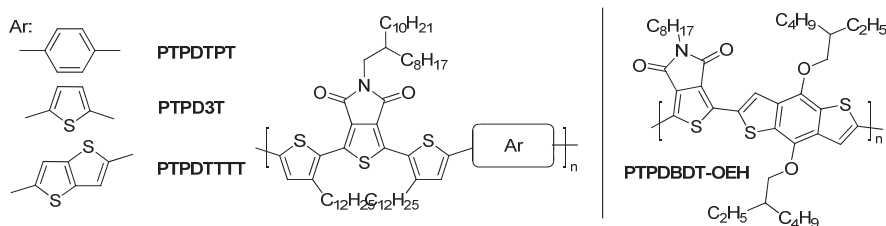


Figure 7.2 – Structures of the polymers studied in this chapter.

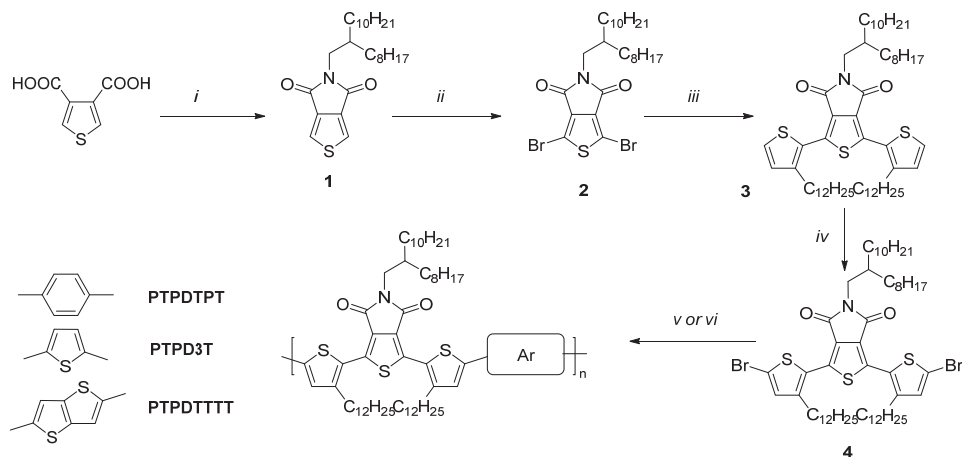
Here we aim to develop new efficient front cell materials combining TPD with the TXT donor structure that was successfully tested with lactam-based acceptors in previous chapters. By varying X from benzene (TPT) to thiophene (3T) and thieno[3,2-*b*]thiophene

(TTTT) (Figure 7.2) hopefully polymers with suitable band gap, good efficiency for charge generation with PCBM, and good stacking behavior for improving charge transport are acquired. Furthermore PTPDBDT-OEH (Figure 7.2), that showed almost ideal properties for tandem front cells, was resynthesized according to literature procedure⁴³ to test it with some of the existing small band gap polymer materials based on diketopyrrolopyrrole (DPP).^{48,49}

7.3 Results and discussion

7.3.1 Synthesis

The synthesis of the TPD polymers is outlined in Scheme 7.1. To synthesize the thiophene-flanked TPD monomer **4** reactions from several different literature procedures were applied mainly following the scheme as outlined by Guo *et al.*⁵⁰ Synthesis of the TPD monomer starts with thiophene-3,4-dicarboxylic acid that is converted into the anhydride using acetic anhydride and subsequently into the imide using 2-octyldodecyl-1-amine and 4-DMAP to form the *N*-alkylated-TPD **1** (Scheme 7.1). To brominate **1** with NBS, harsh conditions using concentrated sulfuric acid and trifluoroacetic acid are needed to give **2**. To extend **2** with thiophenes and to ensure solubility of the final polymers, 2-(3-dodecylthiophen-2-yl)-4,4,5,5-tetramethyl-1,3,2-dioxaborolane was used in a Suzuki type coupling reaction giving **3** that was reacted with NBS to give TPD monomer **4**. After recrystallization of the monomers polymerization with a Stille reaction for PTPD3T and PTPDTTTT and a Suzuki reaction for PTPDTPT, was performed with Pd₂dba₃ and PPh₃ as catalyst. Soluble polymers were obtained with good molecular weights (Table 7.1).



Scheme 7.1 – Synthesis of TPD monomers and polymers. (i) 1. Ac_2O , $75\text{ }^\circ\text{C}$, 2 h. 2. 2-octyldodecyl-1-amine, 4-DMAP, dioxane, $55\text{ }^\circ\text{C}$, overnight. 3. Ac_2O , $80\text{ }^\circ\text{C}$, 4 h. 19% (ii) NBS, $\text{H}_2\text{SO}_4/\text{TFA}$, 1 h. 39% (iii) 2-(3-Dodecylthiophen-2-yl)-4,4,5,5-tetramethyl-1,3,2-dioxaborolane, Pd_2dba_3 , PPh_3 , 2 M K_3PO_4 aq., Aliquat 336, toluene, $110\text{ }^\circ\text{C}$, overnight. 47% (iv) NBS, $\text{CHCl}_3/\text{AcOH}$, 77% (v) 2,5-bis(trimethylstannyl)thiophene, 2,5-bis(trimethylstannyl)thieno[3,2-*b*]thiophene, or (4,8-bis((2-ethylhexyl)oxy)benzo[1,2-*b*:4,5-*b'*]dithiophene-2,6-diyl)bis(trimethylstannane), Pd_2dba_3 , PPh_3 , toluene/DMF (9/1), $115\text{ }^\circ\text{C}$, overnight. (vi) 1,4-bis(4,4,5,5-tetramethyl-1,3,2-dioxaborolan-2-yl)benzene, Pd_2dba_3 , PPh_3 , 2 M K_3PO_4 aq., Aliquat 336, toluene, $110\text{ }^\circ\text{C}$, overnight.

7.3.2 Optical and electrochemical properties

UV-vis absorption spectroscopy of the PTPDXT polymers showed some distinct differences (Figure 7.3). PTPDTPT has a wide band gap of 2.11 eV in thin film. In solution the absorption onset shows an additional large shift to the blue of almost 100 nm. The blue shift is the result of twisting of the benzene ring with respect to the conjugated backbone hampering good conjugation and indicates that PTPDTPT is molecularly dissolved. In the solid state, however, the polymer aggregates and the benzene and thiophene rings are forced to become more coplanar due to stacking of the polymers. For PTPD3T and PTPDTTTT the absorption spectra in solution and in thin films almost overlap, suggesting strong aggregation already in solution. The optical band gaps of 1.84 eV and 1.86 eV for PTPD3T and PTPDTTTT respectively determined from the onset of the optical absorption are suited for use in the wide band gap sub cell of a tandem solar cell if the frontier orbitals are well aligned to those of the PCBM acceptor.

Table 7.1 – Materials properties for PTPDXTX polymers

Polymer	M_n kg/mol	PDI	$\lambda_{\text{onset}}^{\text{sol}}$ nm	$\lambda_{\text{onset}}^{\text{film}}$ nm	E_g^{sol} eV	E_g^{film} eV	E_{HOMO} eV	E_{LUMO} eV	E_g^{CV} eV
PTPDTP	33.2 ^a	1.9	513	587	2.42	2.11	-5.67	-3.11	2.56
PTPD3T	29.9	2.5	667	673	1.86	1.84	-5.59	-3.30	2.29
PTPDTTTT	64.1 ^a	2.9	665	667	1.86	1.86	-5.43	-3.51	1.92

^a GPC chloroform, 145 °C.

Cyclic voltammetry was used to determine the oxidation and reduction potentials versus the ferrocene/ferrocenium redox couple (Table 7.1) HOMO and LUMO levels were calculated to be -5.67 eV and -3.11 eV for PTPDTP, -5.59 eV and -3.30 eV for PTPD3T, and -5.43 eV and -3.51 eV for PTPDTTTT based on $E_{\text{HOMO/LUMO}} = -5.23 - qE_{\text{ox/red}}$. The LUMO levels of these polymers are relatively high which might lead to large LUMO – LUMO offsets with PCBM in OPV devices.

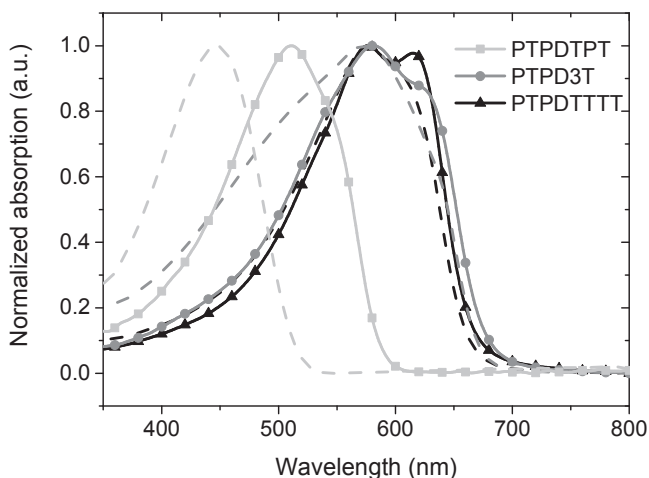


Figure 7.3 – UV-vis absorption spectra of PTPDXTX polymers with X = benzene, thiophene and thieno[3,2-*b*]thiophene (solid: thin film on glass, dashed: chloroform solution).

7.3.3 Solar cells

Solar cells of the three polymers with PC₇₀BM were constructed in a glass/ITO(115 nm)/PEDOT:PSS(35 nm)/PTPDTXT:PC₇₀BM/LiF(1 nm)/Al(100 nm) device configuration. Their performance was optimized with respect to the choice of solvent and co-solvent. Coincidentally, this resulted in the same processing conditions with chloroform (CF) and 2% diiodooctane (DIO) for all three polymers. The current density – voltage ($J - V$) characteristics and external quantum efficiencies (EQE) are shown in Figure 7.4 and the data are summarized in Table 7.2. The best performance (PCE = 4.7%) is found for PTPDTTTT:PC₇₀BM cells, where the short-circuit current density (J_{sc}) is 9.9 mA/cm² and the open-circuit voltage (V_{oc}) 0.68 V. The high fill factor (FF = 0.70) and EQE (up to 62%) show that charge generation and collection are good in this cell. For PTPD3T:PC₇₀BM cells a much lower PCE = 1.7% was achieved, despite exploring many different processing conditions. The V_{oc} (0.65 V) is similar to that of the PTPDTTTT:PC₇₀BM cell, but J_{sc} (4.9 mA/cm²) and FF (0.54) are much less. PTPDTPT:PC₇₀BM cells show a significantly enhanced V_{oc} of 0.92 eV, but the charge generation is limited as evidenced from a lower EQE, resulting in a lower J_{sc} and a PCE of 3.5%. For PTPDTPT:PC₇₀BM cells the EQE shows the individual contributions of PTPDTPT to ~600 nm and of PC₇₀BM in the 600 – 700 nm range.

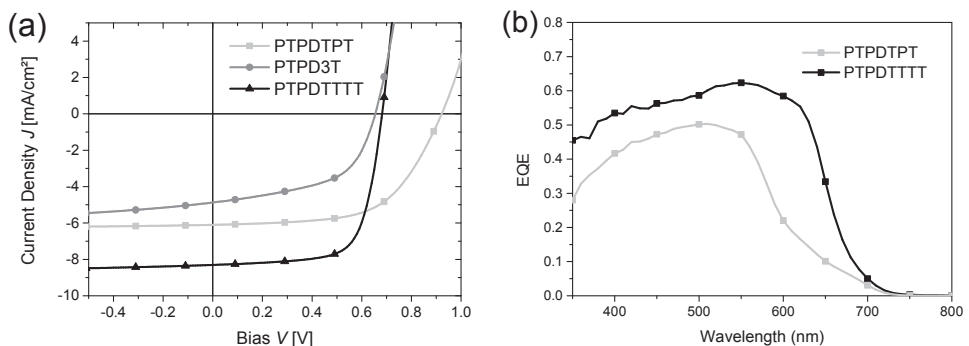


Figure 7.4 – (a) $J - V$ characteristics of solar cells with PTPDTXT polymers and PC₇₀BM. (b) The corresponding EQE spectra.

Table 7.2 – Solar cell characteristics on PTPDTXT polymers with PC₇₀BM as acceptor.

Polymer	ratio	Solvent additive	<i>d</i> nm	<i>J</i> _{sc} mA/cm ²	<i>V</i> _{oc} V	FF	PCE %	<i>E</i> _g – <i>qV</i> _{oc} eV
PTPDTPT	1:1.5	CF:2% DIO	105	6.4	0.92	0.60	3.5	0.83 ^b
PTPD3T	1:2	CF:2% DIO	n.a.	4.9	0.65	0.54	1.7 ^a	1.10 ^b
PTDPTTTT	1:1.5	CF:2% DIO	95	9.9	0.68	0.70	4.7	1.07 ^b

^a Uncorrected for spectral response. ^b Based on *E*_g = 1.75 eV for PC₇₀BM

When looking at these results it can be noted that the *V*_{oc} of the PTPDTTTT:PC₇₀BM cell of 0.68 V implies a significant photon energy loss (defined as *E*_g – *qV*_{oc}) of 1.07 eV. Without improving the *V*_{oc}, the material will not be able to fulfill the requirements for an efficient wide band gap cell in a tandem configuration. In terms of photon energy loss the PTPDTPT:PC₇₀BM cell is much better. Here *E*_g – *qV*_{oc} = 0.83 eV (taking *E*_g = 1.75 eV for PC₇₀BM), but the EQE is lower, especially in the range between 600 and 700 nm.

Table 7.3 – Optimized solar cells of PTPDTTTT:IC₆₀BA (1:1.5), spin coated from chloroform with different additives.

Solvent additive	<i>d</i> nm	<i>J</i> _{sc} mA/cm ²	<i>V</i> _{oc} V	FF	PCE %	<i>E</i> _g – <i>qV</i> _{oc} eV
1% DIO	90	7.0	0.96	0.58	3.9	0.74 ^a
2% DIO	110	7.3	0.95	0.56	3.9	0.75 ^a
4% DIO	80	6.8	0.96	0.60	3.9	0.74 ^a
20% ODCB	85	6.1	0.95	0.49	2.9	0.75 ^a

^a Based on *E*_g = 1.70 eV for IC₆₀BA.

To improve the *V*_{oc} and reduce the photon energy loss of PTPDTTTT-based solar cells, PC₇₀BM was replaced by indene-C₆₀-*bis*-adduct (IC₆₀BA, *E*_g = 1.70 eV⁵¹). Optimizing the processing conditions of PTPDTTTT:IC₆₀BA solar cells for solvent additive (testing different concentrations of ODCB and DIO in chloroform, Table 7.3), led to the same optimum conditions as for devices with PC₇₀BM. The *V*_{oc} of devices spin coated from chloroform with 2% DIO (v/v) showed a strong increase in *V*_{oc} from 0.68 V with PC₇₀BM up to 0.95 V with IC₆₀BA and had *J*_{sc} = 7.3 mA/cm² with FF = 0.56, and PCE = 3.9% (Figure 7.5). Devices from 1% and 4% DIO showed virtually the same PCE with minor differences in current and fill factor. For a device processed with 4% DIO a fill factor of even 0.60 was achieved showing that it is possible to get reasonable fill factors with IC₆₀BA and PTPDTTTT.

Comparison of the EQE spectra revealed that the decrease in J_{sc} going from PC₇₀BM to IC₆₀BA is mainly the result of a lower EQE in the region where PC₇₀BM absorbs.

Summarizing, the combination of IC₆₀BA with PTPDTTTT results in an enhanced V_{oc} but a reduced J_{sc} and no net improvement of the PCE.

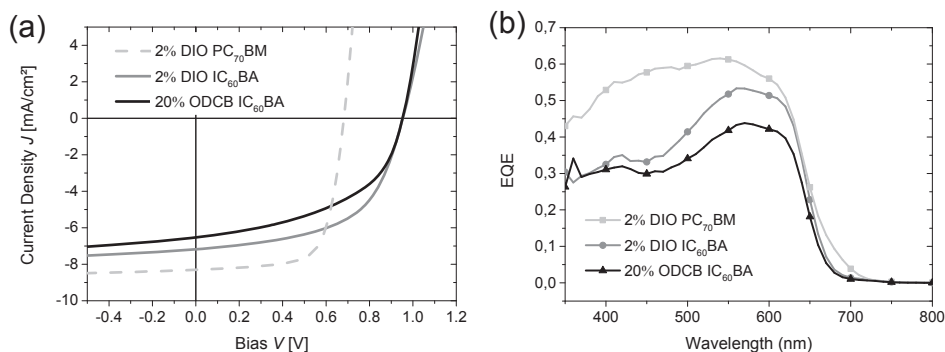
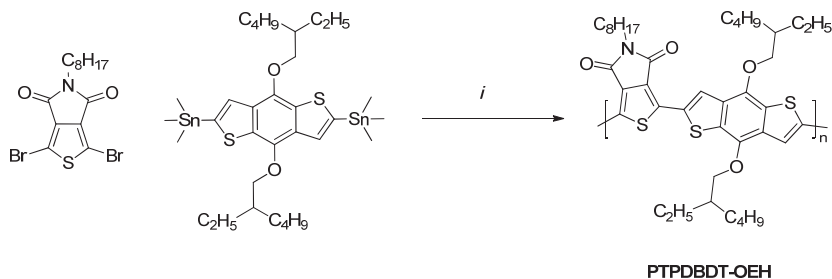


Figure 7.5 – $J - V$ characteristics (a) and EQE spectra (b) of PTPDTTTT with ICBA processed from chloroform with 2% DIO (solid grey) and 20% ODCB (solid black) as additive to chloroform. The $J - V$ characteristics and EQE of the best PTPDTTTT:PC₇₀BM device is added for reference (light grey).

7.3.4 PTPDBDT-OEH for tandem solar cells

The TPD derived materials synthesized so far failed to give a good voltage with PC₇₀BM or a high current density when combined with IC₆₀BA. A TPD-based copolymer with 4,8-bis((2-ethylhexyl)oxy)benzo[1,2-b:4,5-b']dithiophene (PTPDBDT-OEH) was shown to have ideal energy levels and showed a record 8.5% PCE with a linear heptyl side chain on the TPD and 7.5% PCE with an *n*-octyl side chain.⁴³ As the *n*-octyl TPD monomer was available it was combined with the commercial (4,8-bis((2-ethylhexyl)oxy)benzo[1,2-b:4,5-b']dithiophene-2,6-diyl)bis(trimethylstannane) to give the PTPDBDT-OEH polymer (Scheme 7.2). The Stille polymerization was done under slightly different conditions with Pd₂dba₃ and P(*o*-tolyl)₃ in chlorobenzene as compared to the standard procedure employed in this thesis with Pd₂dba₃ with PPh₃ in toluene/DMF. Polymers with reasonable molecular weight ($M_n = 17.6$ kg/mol) were obtained and a band gap of 1.84 eV as determined from the onset of absorption (Table 7.4 and Figure 7.6).



Scheme 7.2 – Synthesis of PTPDBDT-OEH. (i) Pd_2dba_3 , $\text{P}(o\text{-tolyl})_3$, chlorobenzene, 115 °C, overnight.

The performance of PTPDBDT-OEH was tested in glass/ITO(115 nm)/PEDOT:PSS(35 nm)/PTPDBDT-OEH:PC₇₀BM (110 nm)/LiF(1 nm)/Al(100 nm) solar cells. The photoactive layer was spin coated from chlorobenzene with 5% 1-chloronaphthalene (CN) as co-solvent. Due to the strong aggregation behavior of PTPDBDT-OEH it had to be processed from 115 °C hot solutions. Optimization led to a cell with $J_{\text{sc}} = 10.6 \text{ mA/cm}^2$, $V_{\text{oc}} = 0.93 \text{ V}$, and $\text{FF} = 0.67$, giving $\text{PCE} = 6.5\%$ (Table 7.5 and Figure 7.6) with a 1:1.5 ratio (w/w) of PTPDBDT-OEH vs. PC₇₀BM. With $\text{PCE} = 6.5\%$, the performance is significantly better than with either of the PTPDXT:PC₇₀BM layers. Although the photon energy loss has been reduced to $E_{\text{g}} - qV_{\text{oc}} = 0.82 \text{ eV}$, further tailoring of E_{g} and V_{oc} can still be beneficial. While $\text{PCE} = 6.5\%$ was obtained for the best device, the variance in the results was very large. From nine series of device fabrication under optimized conditions the average performance of the best cell in each series is shown in Table 7.5. Significant variations in short-current and fill factor demonstrate that it is hard to control the processing in a reproducible way. This is most likely due to the high temperature of the solution that leads to quick and difficult to control cooling during the layer deposition.

Table 7.4 – Materials properties for PTPDBDT-OEH

Polymer	M_n kg/mol	PDI	$\lambda_{\text{onset}}^{\text{sol}}$ nm	$\lambda_{\text{onset}}^{\text{film}}$ nm	$E_{\text{g}}^{\text{sol}}$ eV	$E_{\text{g}}^{\text{film}}$ eV	E_{HOMO} eV	E_{LUMO} eV	E_{g}^{CV} eV
PTPDBDT-OEH	17.6	3.3	666	673	1.86	1.84	-5.83	-3.37	2.46

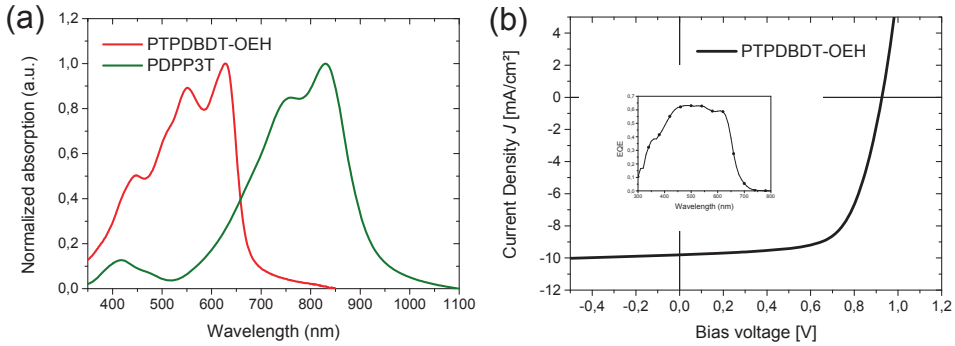


Figure 7.6 – (a) Absorption spectrum of PTPDBDT-OEH (red) and PDPP3T (green) as thin film on glass. (b) $J - V$ characteristic of PTPDBDT-OEH:PC₇₀BM (1:1.5) from chlorobenzene with 5% 1-chloronaphthalene.

Table 7.5 – Single junction solar cells with PTPDBDT-OEH:PC₇₀BM as active layer.

	d ratio	J_{sc} nm	J_{sc} mA/cm ²	V_{oc} V	FF	PCE %	$E_g - qV_{oc}$ eV
Best cell	1:1.5	110	10.59	0.93	0.67	6.5	0.82 ^a
Average ^b	1:1.5	-	10.03	0.92	0.61	5.6	-

^a Based on $E_g = 1.75$ eV for PC₇₀BM. ^b Average of the best cells out of nine series

7.3.4.1 Tandem solar cells

To construct the tandem solar cell several different small band gap materials were considered as a back cell with PTPDBDT-OEH:PC₇₀BM as front cell. To predict the $J - V$ characteristics of a tandem solar cell the refractive index and extinction coefficient for all layers in the device stack (Figure 7.7) were combined with the electrical behavior of the single junction solar cells at different thicknesses, following the procedure previously published by Gilot *et al.*⁵² For this optimization the cell configuration was glass/ITO/PEDOT:PSS/PTPDBDT-OEH:PC₇₀BM/ZnO/n-PEDOT/small band gap layer/LiF/Al.

The best result was expected for a back cell with PDPP3T:PC₆₀BM with a thickness of 170 nm. The structure of PDPP3T is shown in Figure 7.7b and has an optical band gap $E_g = 1.30$ eV (Figure 7.6).⁵³ The front cell with PTPDBDT-OEH:PC₇₀BM is preferably 150 nm thick. The predicted $J - V$ characteristics are shown in Figure 7.7c (dashed curves) for both the single junction sub cells and the tandem cell. A PCE of 9.4% is predicted for this tandem device with $J_{sc} = 9.3$ mA/cm², $V_{oc} = 1.58$ V, and FF = 0.64 (Table 7.6).

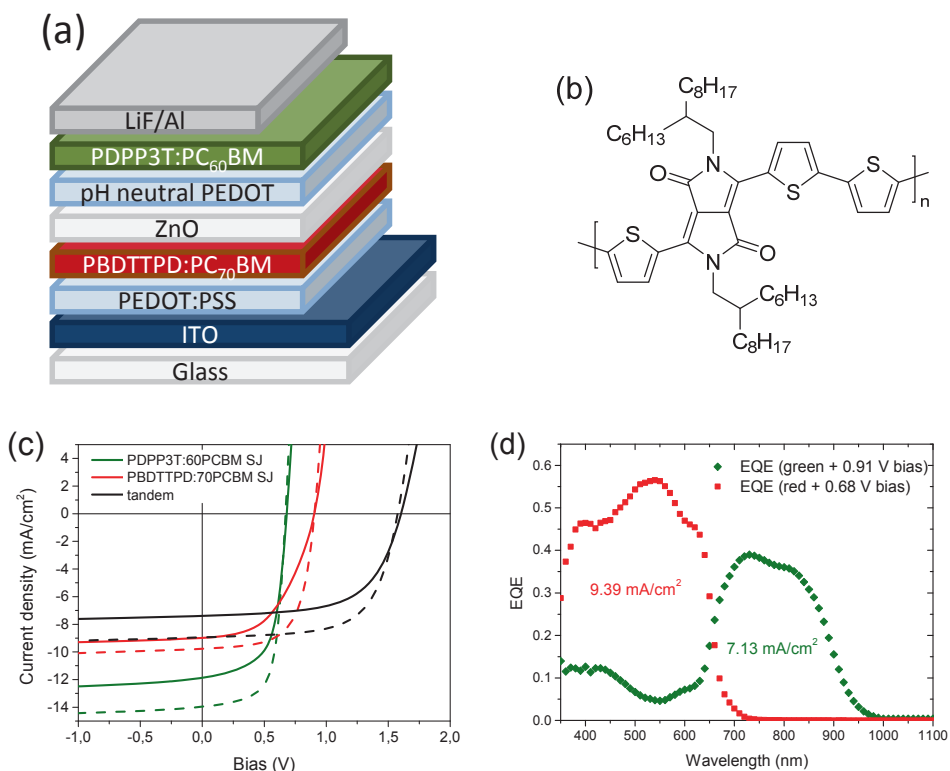


Figure 7.7 – (a) Schematic device stack for the tandem solar cell. (b) PDPP3T. (c) Modeled (dashed) and experimental (solid) $J-V$ characteristics for the single junctions and tandem solar cell. (d) EQE of the tandem solar cell, sub cells measured under red or green bias light.

Tandem solar cells were made with a glass/ITO/PEDOT:PSS/PTPDBDT-OEH:PC₇₀BM/ZnO/n-PEDOT/PDPP3T:PC₆₀BM/LiF/Al stack. Along with the tandem solar cell also both sub cells were fabricated as a single junction device with the same processing conditions. The $J-V$ characteristics for both sub cells and tandem solar cell are shown in Figure 7.7c (solid lines). The EQE for the tandem solar cell was measured according to a procedure previously outlined by Gilot *et al.* using a red and green laser to provide bias illumination and provide voltage bias compensation to maintain short circuit conditions.⁵⁴

The maximum PCE achieved was 7.2% for a tandem with $J_{sc} = 7.4 \text{ mA/cm}^2$, $V_{oc} = 1.60 \text{ V}$ and $FF = 0.61$. The V_{oc} of 1.60 V corresponds to the sum of the V_{oc} s of the two sub cells and reveals that the intermediate contact forms good Ohmic contacts. Compared to the predictions both J_{sc} and FF are lower. As can be seen from the single junctions the fill

factor of the front cell was low in this run and for both the front and back cells a significant lower J_{sc} was achieved than predicted. For the front cell, the variance between similar processed cells make it difficult to achieve tandem devices that are up to par with predictions based on the best cells with this material. The slight deviations in thickness compared to the modeled thicknesses would only give rise to a minor deviation of 0.2% and cannot be the reason for the underperformance.

Table 7.6 – Modeled and experimental solar cell characteristics for PTPDBDT-OEH:PC₇₀BM/PDPP3T:PC₆₀BM tandem solar cells and single junction sub cells.

		ratio	d nm	J_{sc} mA/cm ²	V_{oc} V	FF	PCE %
Modeled	Front cell	1:1.5	155	9.8	0.91	0.64	5.7
	Back cell	1:2	170	14.0	0.67	0.67	6.3
	Tandem			9.3	1.58	0.64	9.4
Experime	Front cell	1:1.5	150	9.0	0.90	0.50	4.0
	Back cell	1:2	140	12.1	0.68	0.62	5.1
	Tandem			7.4	1.60	0.61	7.2

7.4 Conclusions

Three donor-acceptor conjugated polymers with a TPD acceptor unit and a TXT (X = P, T, or TT) donor unit were synthesized as wide band gap materials for use as a front cell in tandem polymer solar cells. A maximum efficiency of PCE = 4.7% was achieved for PTPDTT:PC₇₀BM solar cells. The performance was mainly limited by the low open-circuit voltage compared to the optical band gap ($V_{oc} = 0.68$ V, $E_g = 1.84$ eV). Using IC₆₀BA instead of PC₇₀BM as a less strong electron acceptor resulted in a higher open-circuit voltage ($V_{oc} = 0.95$ V) but a lower short-circuit current density due to a loss of absorption going from a C₇₀ to a C₆₀ fullerene derivative, and an overall reduced performance with a PCE = 3.9%.

Both photocurrent and voltage can be improved when using PTPDBDT-OEH:PC₇₀BM solar cells. PTPDBDT-OEH:PC₇₀BM solar cells combine an $E_g = 1.84$ eV band gap with high $V_{oc} = 0.93$ V. As a result single junction cells with PCE = 6.5% have been achieved, but due to the high temperatures needed for processing this polymer it is difficult to reproduce this value, and the average PCE of 5.6% is less.

Combined optical-electrical modeling of tandem solar cells based on a PTPDBDT-OEH:PC₇₀BM front cell and a PDPP3T:PC₆₀BM back cell predicts tandem solar cell with PCE = 9.4%. Construction of the device resulted in a tandem with PCE = 7.2%. The tandem cell shows the expected V_{oc} but has J_{sc} and FF lower than predicted, in consequence of the difficulties encountered with processing PTPDBDT-OEH:PC₇₀BM cells.

Summarizing, TPD polymers remain interesting candidates as wide band gap solar cells. Future research directions could involve combining PTPDTT with IC₇₀BA or addressing the processing of PTPDBDT-OEH cells via modification of side chains or tuning the molecular weight.

7.5 Experimental

7.5.1 General

See paragraph 2.5.1. for details on NMR, UV-vis-NIR, MALDI-TOF, and CV equipment.

7.5.2 OPV fabrication and characterization

See paragraph 2.5.2 for details of single junction device fabrication and measurement equipment.

PTPDXT devices were spin coated from solutions with 3 – 6 mg/ml polymer concentration with the appropriate amount of PC₇₀BM or IC₆₀BA added. Active layers were spin coated both in air as in inert atmosphere. PTPDBDT-OEH devices were made from a 10 mg/ml polymer solution of CB with 5% (v/v) CN and PC₇₀BM added in a 1:1.5 ratio to the polymer. Solutions were stirred at 115 °C and spin coated hot under inert atmosphere. PDPP3T devices were made from 4 mg/ml solution of chloroform with 7.5% ODCB (v/v) and PC₆₀BM in a 1:2 ratio. Solutions were stirred at 90 °C and cooled for 10 minutes before spin coating. Tandem solar cells were made by spin coating ZnO nanoparticles⁵⁵ from a 10 mg/ml solution in isopropanol on top of the front cell active layer. A pH neutral PEDOT:PSS (Orgacon, AGFA) was diluted 1:1 with ultra-pure water. Then isopropanol was added up to 0.2 mg/ml concentration to improve wetting on the ZnO layer that is was sin coated on. Than the back cell active layer was spin coated and the device was finished similar to single junction devices.

External quantum efficiency was measured on a home-built set-up with modulated monochromatic probe light (Oriol Cornerstone 130 1/8 m, Newport) from a halogen lamp (Osram 64610) that was mechanically chopped at a frequency of 165 Hz with an optical chopper (SR 540, Stanford Research) and illuminated the sample via a 2 mm aperture. Illumination with a green (532 nm B&W, Tek Inc., 30 mW) and red (780 nm (B&W, Tek Inc., 21 mW) solid state laser was used to bias each sub cell independently. A lock-in-amplifier (SR 830, Stanford Research) with a load of 50 Ω was used to record all data via a

Labview program on a computer. The electrical bias over the tandem cell was provided by the lock-in-amplifier.

Optical modeling was performed with SETFOS 3 (Fluxim, Switzerland) and a home-built Python script in a way previously described.⁵² The optical constants were obtained via reflection and transmission measurements on a Perkin-Elmer Lambda 900 spectrometer equipped with an integrating sphere.

7.5.3 Synthesis

2-(3-Dodecylthiophen-2-yl)-4,4,5,5-tetramethyl-1,3,2-dioxaborolane.

To a solution of 2-bromo-3-dodecylthiophene (2.50 g, 7.54 mmol) in THF (60 ml) at $-50\text{ }^{\circ}\text{C}$ was added *n*-BuLi (10 M in hexane, 0.75 ml, 7.54 mmol) dropwise. After 10 min. of stirring at this temperature, 2-isopropoxy-4,4,5,5-tetramethyl-1,3,2-dioxaborolane (1.84 ml, 9.05 mmol) was added and the reaction was allowed to warm to room temperature. After 1 h the reaction was quenched with water and extracted with diethyl ether. The combined organic phases were washed with water, brine and dried over MgSO_4 before concentrating under reduced pressure to give a colorless oil (2.93 g, full conversion). ^1H NMR (400 MHz, CDCl_3 , ppm): δ 7.49 (t, $J = 7\text{ Hz}$, 1H), 7.02 (d, $J = 4.7\text{ Hz}$, 1H), 2.90 (m, 2H), 1.59 (m, 2H), 1.34 (m, 18H), 1.27 (m, 12H), 0.89 (t, $J = 6.8\text{ Hz}$, 3H).

5-(2-Octyldodecyl)-4H-thieno[3,4-c]pyrrole-4,6(5H)-dione (1).

A solution of thiophene-3,4-dicarboxylic acid (2.63 g, 15.3 mmol) in acetic anhydride (150 ml) was stirred at $75\text{ }^{\circ}\text{C}$ for 2 h. After cooling to room temperature, the solvent was evaporated and 4-DMAP (2.05 g, 16.8 mmol), 2-octyldodecylamine (5.00 g, 16.8 mmol) and dioxane (138 ml) were added to the residue. This mixture was stirred at $55\text{ }^{\circ}\text{C}$ for 20 h before adding acetic anhydride (88 ml). After stirring for 4 more hours at $80\text{ }^{\circ}\text{C}$, the mixture was cooled to room temperature, quenched with water and extracted with dichloromethane. The combined organic phases were washed with water, brine and dried over MgSO_4 . After evaporation of the solvent *in vacuo*, the crude mixture was purified by silica column chromatography (dichloromethane/hexane 7/3) and the compound was obtained as a pale yellow solid (1.23 g, 19%). ^1H NMR (400 MHz, CDCl_3 , ppm): δ 7.80 (s, 2H), 3.51 (d, $J = 7.4\text{ Hz}$, 2H), 1.84 (m, 1H), 1.26 (m, 32H), 0.87 (m, 6H).

1,3-Dibromo-5-(2-octyldodecyl)-4H-thieno[3,4-c]pyrrole-4,6(5H)-dione (2).

To a solution of **1** (1.03 g, 2.37 mmol) in TFA (13 ml) and concentrated sulfuric acid (4.3 ml) was added NBS (2.08 g, 11.84 mmol) over a course of 10 min. at room temperature. The reaction was quenched with ice water after one hour of stirring. The mixture was extracted with dichloromethane and the combined organic phases were washed with a saturated NaHCO_3 -solution and dried over MgSO_4 . After evaporation of the solvent under reduced pressure, the residue was purified by column chromatography (dichloromethane/heptane 7/3) and yielded a pale orange solid (0.55 g, 39%). ^1H NMR (400 MHz, CDCl_3 , ppm): δ 3.45 (d, $J = 7.4\text{ Hz}$, 2H), 1.79 (m, 1H), 1.22 (m, 32H), 0.84 (t, $J = 6.6\text{ Hz}$, 6H). ^{13}C NMR (100 MHz, CDCl_3 , ppm): δ 160.49, 134.73, 112.79, 43.03, 36.81, 31.91, 31.88, 31.43, 29.89, 29.62, 29.59, 29.54, 29.34, 29.28, 26.26, 22.68, 22.67, 14.12.

1,3-Bis(3-dodecylthiophen-2-yl)-5-(2-octyldodecyl)-4H-thieno[3,4-c]pyrrole-4,6(5H)-dione (3).

A solution of **2** (0.55 g, 0.92 mmol) and 2-(3-dodecylthiophen-2-yl)-4,4,5,5-tetramethyl-1,3,2-dioxaborolane (1.05 g, 2.76 mmol) in toluene (10 ml) was degassed for 20 min. After adding K_3PO_4 (2 M, 2.31 ml, degassed), Aliquat 336, Pd_2dba_3 (2%, 16.5 mg, 18 μ mol) and PPh_3 (8%, 19.4 mg, 74 μ mol), the mixture was stirred at 115 °C for 48 h, quenched with water, and extracted with dichloromethane. The combined organic phases were washed with water, brine and dried over $MgSO_4$. After evaporation of the solvent under reduced pressure, the residue was purified by column chromatography (chloroform/heptane 1/1) and yielded an orange solid (410 mg, 47%). 1H NMR (400 MHz, $CDCl_3$, ppm): δ 7.40 (d, J = 5.2 Hz, 2H), 7.01 (d, J = 5.2 Hz, 2H), 3.50 (d, J = 7.2 Hz, 2H), 2.79 (m, 4H), 1.85 (m, 1H), 1.65 (m, 4H), 1.24 (m, 68 H), 0.87 (m, 12H). MALDI-TOF m/z : 933.65 (M^+ , 100%).

1,3-Bis(5-bromo-3-dodecylthiophen-2-yl)-5-(2-octyldodecyl)-4H-thieno[3,4-c]pyrrole-4,6(5H)-dione (4).

To a solution of **3** (0.38 g, 0.41 mmol) in chloroform/acetic acid (1/1) (14 ml) at 0 °C was added NBS (0.14 g, 0.81 mmol) in small portions. After stirring for 10 min. at 0 °C, the solution was warmed to room temperature and was stirred for 4 days. The mixture was quenched with saturated $NaHCO_3$ -solution and extracted with dichloromethane. The combined organic phases were washed with water, brine and dried over $MgSO_4$. After evaporation of the solvent, the residue was purified by column chromatography (chloroform/heptane 3/7) followed by recrystallization from ethanol to give yellow crystals (343 mg, 77%). 1H NMR (400 MHz, $CDCl_3$, ppm): δ 6.97 (s, 2H), 3.49 (d, J = 7.4 Hz, 2H), 2.73 (t, J = 7.8 Hz, 4H), 1.83 (m, 1H), 1.61 (m, 4H), 1.24 (m, 68H), 0.87 (t, J = 6.6 Hz, 12H). ^{13}C NMR (100 MHz, $CDCl_3$, ppm): δ 162.34, 144.90, 135.39, 132.57, 130.65, 126.31, 115.40, 36.95, 31.91, 31.89, 31.56, 30.32, 30.00, 29.78, 29.68, 29.66, 29.65, 29.62, 29.56, 29.46, 29.40, 29.35, 26.35, 26.33, 22.68, 22.67, 14.10.

PTPDTPT.

1,4-Bis(4,4,5,5-tetramethyl-1,3,2-dioxaborolan-2-yl)benzene (21.2 mg, 64.1 μ mol), 1,3-bis(5-bromo-3-dodecylthiophen-2-yl)-5-(2-octyldodecyl)-4H-thieno[3,4-c]pyrrole-4,6(5H)-dione (70.0 mg, 64.1 μ mol) (**4**), toluene (1.4 ml) and Aliquat 336 were put together in a flask which was degassed for 20 minutes. Then, a degassed K_3PO_4 solution (2 M, 320.5 μ mol) was added to the mixture. After degassing for 5 more minutes, Pd_2dba_3 (2 mol%, 1.17 mg, 1.3 μ mol) and PPh_3 (8 mol%, 1.35 mg, 5.1 μ mol,) were added and the mixture was stirred overnight at 115 °C. Then, 4,4,5,5-tetramethyl-2-(thiophen-2-yl)-1,3,2-dioxaborolane (152.5 mg, 256.4 μ mol) was added to end cap the formed polymer for 1 h at 115 °C. Afterwards, 2-bromothiophene (0.082 ml, 513 μ mol) was added, after which the reaction was again stirred for 1 h at 115 °C, precipitated in methanol, and filtered through a Soxhlet thimble. The precipitate was purified via Soxhlet extraction with acetone, hexane and chloroform. The chloroform fraction was concentrated and precipitated in methanol. GPC (145 °C, chloroform): M_n = 33.2 kg/mol, PDI=1.9, λ_{max} = 511 nm. (59 mg, 91%).

PTPDTTTT & PTPD3T.

1,3-Bis(5-bromo-3-dodecylthiophen-2-yl)-5-(2-octyldodecyl)-4H-thieno[3,4-c]pyrrole-4,6(5H)-dione (70.0 mg, 64.1 μmol), 2,5-bis(trimethylstannyl)thieno[3,2-*b*]thiophene (29.9 mg, 64.1 μmol) or 2,5-bis(trimethylstannyl)thiophene (26.2 mg, 64.1 μmol) and toluene/DMF (10/1) (2 ml) were put in a flask and were degassed for 20 minutes. Pd_2dba_3 (2%, 1.17 mg, 1.3 μmol) and PPh_3 (8%, 1.35 mg, 5.1 μmol) were added and the mixture was stirred overnight at 115 °C. Then, tributyl(thiophen-2-yl)stannane (80 μl , 256 μmol) was added to end cap the formed polymer for 1 h at 115 °C. Afterwards, 2-bromothiophene (50 ml, 512 μmol) was added, after which the reaction was again stirred for 1 h at 115 °C, precipitated in methanol, and filtered through a Soxhlet thimble. The precipitate was purified via Soxhlet extraction with acetone, hexane, dichloromethane, and chloroform. The leftover in the thimble was boiled in TCE or ODCB to dissolve it and filtered before it was precipitated in methanol. The chloroform fraction was concentrated by evaporation under reduced pressure and precipitated in methanol as well.

PTPDTTTT: GPC (145 °C, chloroform): $M_n = 64.1$ kg/mol, PDI = 2.9 (chloroform fraction, 47 mg, 69%). GPC (145 °C, chloroform): $M_n = 106.2$ kg/mol, PDI = 2.1, $\lambda_{\text{max}} = 576$ nm. (TCE fraction, 13 mg, 19%).

PTPD3T: GPC (145 °C, chloroform): $M_n = 29.9$ kg/mol, PDI = 2.5, $\lambda_{\text{max}} = 581$ nm. (ODCB fraction, 38 mg, 59%).

PTPDBDT-OEH.

To freshly recrystallized 4,8-bis((2-ethylhexyl)oxy)benzo[1,2-*b*:4,5-*b'*]dithiophene-2,6-diyl)bis(trimethylstannane) (643.3 mg, 833 μmol) and 1,3-dibromo-5-octyl-4H-thieno[3,4-c]pyrrole-4,6(5H)-dione (363 mg, 858 μmol) were added chlorobenzene (13 ml) under an argon atmosphere. Pd_2dba_3 (22.9 mg, 25 μmol) and $\text{P}(o\text{-tolyl})_3$ (30.4 mg, 100 μmol) were added and argon was bubbled through the solution for 30 min. The reaction was heated to 110 °C for 2 days. After cooling diethyldithiocarbamic acid sodium salt (112.6 mg, 500 μmol) was added in chloroform with a drop of methanol. The polymer was then precipitated in methanol and filtered through a Soxhlet thimble. Soxhlet extraction with methanol, dichloromethane, chlorobenzene, and TCE yielded two fractions. Both the chlorobenzene fraction and the TCE fraction were precipitated in methanol, filtered, and dried. The chlorobenzene fraction is used in the experiments in this work. GPC (145 °C, chloroform): $M_n = 17.6$ kg/mol, PDI=3.3, $\lambda_{\text{max}} = 627$ nm. (CB fraction, 506 mg). GPC (145 °C, chloroform): $M_n = 20.5$ kg/mol, PDI=3.3, $\lambda_{\text{max}} = 627$ nm. (TCE fraction, 57 mg).

7.6 Acknowledgements

I thank Yasmine Braeken for her work on the synthesis and characterization of TPDTXT polymers and Alice Furlan for her work on the PTPDBDT-OEH-based tandem solar cells.

7.7 References

- ¹ J. Sicé, *J. Org. Chem.*, **1954**, *19*, 70-73.
- ² P. Münster, W. Freund, G. Steiner, H. Walter, K. O. Westphalen, and M. Gerber, BASF A.-G., Germany, **1992**, p. 49 pp.
- ³ S. Harmsen, H. M. M. Bastiaans, W. Schaper, J. Tiebes, U. Doller, D. Jans, U. Sanft, W. Hempel, and M.-T. Thonessen, Aventis CropScience GmbH, Germany, **2000**, p. 106 pp.
- ⁴ Q. T. Zhang and J. M. Tour, *J. Am. Chem. Soc.*, **1997**, *119*, 5065-5066.
- ⁵ Q. T. Zhang and J. M. Tour, *J. Am. Chem. Soc.*, **1998**, *120*, 5355-5362.
- ⁶ X. Guo, H. Xin, F. S. Kim, A. D. T. Liyanage, S. A. Jenekhe, and M. D. Watson, *Macromolecules*, **2010**, *44*, 269-277.
- ⁷ Y. Zou, A. Najari, P. Berrouard, S. Beaupré, B. Réda Aïch, Y. Tao, and M. Leclerc, *J. Am. Chem. Soc.*, **2010**, *132*, 5330-5331.
- ⁸ Y. Zhang, S. K. Hau, H.-L. Yip, Y. Sun, O. Acton, and A. K. Y. Jen, *Chem. Mater.*, **2010**, *22*, 2696-2698.
- ⁹ M.-C. Yuan, M.-Y. Chiu, S.-P. Liu, C.-M. Chen, and K.-H. Wei, *Macromolecules*, **2010**, *43*, 6936-6938.
- ¹⁰ G. Zhang, Y. Fu, Q. Zhang, and Z. Xie, *Chem. Commun.*, **2010**, *46*, 4997-4999.
- ¹¹ C. Piliago, T. W. Holcombe, J. D. Douglas, C. H. Woo, P. M. Beaujuge, and J. M. J. Fréchet, *J. Am. Chem. Soc.*, **2010**, *132*, 7595-7597.
- ¹² X. Guo, H. Xin, F. S. Kim, A. D. T. Liyanage, S. A. Jenekhe, and M. D. Watson, *Macromolecules*, **2011**, *44*, 269-277.
- ¹³ M.-C. Yuan, M.-Y. Chiu, S.-P. Liu, C.-M. Chen, and K.-H. Wei, *Macromolecules*, **2010**, *43*, 6936-6938.
- ¹⁴ G.-Y. Chen, Y.-H. Cheng, Y.-J. Chou, M.-S. Su, C.-M. Chen, and K.-H. Wei, *Chem. Commun.*, **2011**, *47*, 5064-5066.
- ¹⁵ J. Jo, A. Pron, P. Berrouard, W. L. Leong, J. D. Yuen, J. S. Moon, M. Leclerc, and A. J. Heeger, *Adv. Energy Mater.*, **2012**, *2*, 1397-1403.
- ¹⁶ P. Berrouard, A. Najari, A. Pron, D. Gendron, P.-O. Morin, J.-R. Pouliot, J. Veilleux, and M. Leclerc, *Angew. Chem., Int. Edit.*, **2012**, *51*, 2068-2071.
- ¹⁷ X. Hu, M. Shi, L. Zuo, Y. Nan, Y. Liu, L. Fu, and H. Chen, *Polymer*, **2011**, *52*, 2559-2564.
- ¹⁸ W. Yue, T. T. Larsen-Olsen, X. Hu, M. Shi, H. Chen, M. Hinge, P. Fojan, F. C. Krebs, and D. Yu, *J. Mater. Chem. A*, **2013**, *1*, 1785-1793.
- ¹⁹ E. Zhou, J. Cong, K. Tajima, C. Yang, and K. Hashimoto, *J. Phys. Chem. C*, **2012**, *116*, 2608-2614.
- ²⁰ E.-J. Zhou, J.-Z. Cong, K. Tajima, C.-H. Yang, and K. Hashimoto, *Macromol. Chem. Phys.*, **2011**, *212*, 305-310.
- ²¹ W. Vanormelingen, J. Kesters, P. Verstappen, J. Drijkoningen, J. Kudrjasova, S. Koudjina, V. Liegeois, B. Champagne, J. Manca, L. Lutsen, D. Vanderzande, and W. Maes, *J. Mater. Chem. A*, **2014**, *2*, 7535-7545.
- ²² Q. Zheng, G. Fang, R. C. Coffin, C. M. MacNeill, Y. Li, N. Sun, P. Qin, W. Nie, E. D. Peterson, X. Fan, F. Cheng, H. Huang, M. Wang, X. Zhao, and D. Carroll, *Sol. Energy Mater. Sol. Cells*, **2011**, *95*, 3114-3118.
- ²³ C. M. MacNeill, E. D. Peterson, R. E. Nofle, D. L. Carroll, and R. C. Coffin, *Synth. Met.*, **2011**, *161*, 1137-1140.
- ²⁴ Y. Zhang, J. Zou, H.-L. Yip, Y. Sun, J. A. Davies, K.-S. Chen, O. Acton, and A. K. Y. Jen, *J. Mater. Chem.*, **2011**, *21*, 3895-3902.
- ²⁵ Y.-R. Hong, J. Y. Ng, H. K. Wong, L. C. H. Moh, Y. J. Yip, Z.-K. Chen, and T. B. Norsten, *Sol. Energy Mater. Sol. Cells*, **2012**, *102*, 58-65.
- ²⁶ Z. Li, S.-W. Tsang, X. Du, L. Scoles, G. Robertson, Y. Zhang, F. Toll, Y. Tao, J. Lu, and J. Ding, *Adv. Funct. Mater.*, **2011**, *21*, 3331-3336.

- ²⁷ C. M. Amb, S. Chen, K. R. Graham, J. Subbiah, C. E. Small, F. So, and J. R. Reynolds, *J. Am. Chem. Soc.*, **2011**, *133*, 10062-10065.
- ²⁸ T.-Y. Chu, S.-W. Tsang, J. Zhou, P. G. Verly, J. Lu, S. Beaupre, M. Leclerc, and Y. Tao, *Sol. Energy Mater. Sol. Cells*, **2012**, *96*, 155-159.
- ²⁹ M.-C. Yuan, Y.-J. Chou, C.-M. Chen, C.-L. Hsu, and K.-H. Wei, *Polymer*, **2011**, *52*, 2792-2798.
- ³⁰ X. Guo, N. Zhou, S. J. Lou, J. W. Hennek, R. Ponce Ortiz, M. R. Butler, P.-L. T. Boudreault, J. Strzalka, P.-O. Morin, M. Leclerc, J. T. Lopez Navarrete, M. A. Ratner, L. X. Chen, R. P. H. Chang, A. Facchetti, and T. J. Marks, *J. Am. Chem. Soc.*, **2012**, *134*, 18427-18439.
- ³¹ Y.-R. Hong, H.-K. Wong, L. C. H. Moh, H.-S. Tan, and Z.-K. Chen, *Chem. Commun.*, **2011**, *47*, 4920-4922.
- ³² T. Y. Chu, J. P. Lu, S. Beaupré, Y. G. Zhang, J. R. Pouliot, S. Wakim, J. Y. Zhou, M. Leclerc, Z. Li, J. F. Ding, and Y. Tao, *J. Am. Chem. Soc.*, **2011**, *133*, 4250-4253.
- ³³ T.-Y. Chu, J. Lu, S. Beaupré, Y. Zhang, J.-R. Pouliot, J. Zhou, A. Najari, M. Leclerc, and Y. Tao, *Adv. Funct. Mater.*, **2012**, *22*, 2345-2351.
- ³⁴ J. R. Manders, S.-W. Tsang, M. J. Hartel, T.-H. Lai, S. Chen, C. M. Amb, J. R. Reynolds, and F. So, *Adv. Funct. Mater.*, **2013**, *23*, 2993-3001.
- ³⁵ H. Zhong, Z. Li, E. Buchaca-Domingo, S. Rossbauer, S. E. Watkins, N. Stingelin, T. D. Anthopoulos, and M. Heeney, *J. Mater. Chem. A*, **2013**, *1*, 14973-14981.
- ³⁶ H. Zhong, Z. Li, F. Deledalle, E. C. Fregoso, M. Shahid, Z. Fei, C. B. Nielsen, N. Yaacobi-Gross, S. Rossbauer, T. D. Anthopoulos, J. R. Durrant, and M. Heeney, *J. Am. Chem. Soc.*, **2013**, *135*, 2040-2043.
- ³⁷ S. Chen, C. E. Small, C. M. Amb, J. Subbiah, T.-h. Lai, S.-W. Tsang, J. R. Manders, J. R. Reynolds, and F. So, *Adv. Energy Mater.*, **2012**, *2*, 1333-1337.
- ³⁸ C. E. Small, S.-W. Tsang, S. Chen, S. Baek, C. M. Amb, J. Subbiah, J. R. Reynolds, and F. So, *Adv. Energy Mater.*, **2013**, *3*, 909-916.
- ³⁹ C. E. Small, S. Chen, J. Subbiah, C. M. Amb, S.-W. Tsang, T.-H. Lai, J. R. Reynolds, and F. So, *Nat. Photon.*, **2012**, *6*, 115-120.
- ⁴⁰ J. Yuan, Z. Zhai, H. Dong, J. Li, Z. Jiang, Y. Li, and W. Ma, *Adv. Funct. Mater.*, **2013**, *23*, 885-892.
- ⁴¹ B.-G. Kim, X. Ma, C. Chen, Y. Le, E. W. Coir, H. Hashemi, Y. Aso, P. F. Green, J. Kieffer, and J. Kim, *Adv. Funct. Mater.*, **2013**, *23*, 439-445.
- ⁴² S. Beaupre, A. Najari, and M. Leclerc, *Synth. Met.*, **2013**, *182*, 9-12.
- ⁴³ C. Cabanetos, A. El Labban, J. A. Bartelt, J. D. Douglas, W. R. Mateker, J. M. J. Frechet, M. D. McGehee, and P. M. Beaujuge, *J. Am. Chem. Soc.*, **2013**, *135*, 4656-4659.
- ⁴⁴ B. R. Aich, J. Lu, S. Beaupré, M. Leclerc, and Y. Tao, *Org. Electron.*, **2012**, *13*, 1736-1741.
- ⁴⁵ J. A. Bartelt, Z. M. Beiley, E. T. Hoke, W. R. Mateker, J. D. Douglas, B. A. Collins, J. R. Tumbleston, K. R. Graham, A. Amassian, H. Ade, J. M. J. Fréchet, M. F. Toney, and M. D. McGehee, *Adv. Energy Mater.*, **2013**, *3*, 364-374.
- ⁴⁶ A. R. bin Mohd Yusoff, S. J. Lee, J. Kim, F. K. Shneider, W. J. da Silva, and J. Jang, *ACS Appl. Mater. Interfaces*, **2014**, *6*, 13079-13087.
- ⁴⁷ J. Jo, J.-R. Pouliot, D. Wynands, S. D. Collins, J. Y. Kim, T. L. Nguyen, H. Y. Woo, Y. Sun, M. Leclerc, and A. J. Heeger, *Adv. Mater.*, **2013**, *25*, 4783-4788.
- ⁴⁸ W. Li, A. Furlan, K. H. Hendriks, M. M. Wienk, and R. A. J. Janssen, *J. Am. Chem. Soc.*, **2013**, *135*, 5529-5532.
- ⁴⁹ K. H. Hendriks, W. Li, M. M. Wienk, and R. A. J. Janssen, *J. Am. Chem. Soc.*, **2014**, *136*, 12130-12136.
- ⁵⁰ X. Guo, R. P. Ortiz, Y. Zheng, M.-G. Kim, S. Zhang, Y. Hu, G. Lu, A. Facchetti, and T. J. Marks, *J. Am. Chem. Soc.*, **2011**, *133*, 13685-13697.

- ⁵¹ D. Di Nuzzo, G.-J. A. H. Wetzelaer, R. K. M. Bouwer, V. S. Gevaerts, S. C. J. Meskers, J. C. Hummelen, P. W. M. Blom, and R. A. J. Janssen, *Adv. Energy Mater.*, **2013**, *3*, 85-94.
- ⁵² J. Gilot, M. M. Wienk, and R. A. J. Janssen, *Adv. Mater.*, **2010**, *22*, E67-E71.
- ⁵³ J. C. Bijleveld, A. P. Zoombelt, S. G. J. Mathijssen, M. M. Wienk, M. Turbiez, D. M. de Leeuw, and R. A. J. Janssen, *J. Am. Chem. Soc.*, **2009**, *131*, 16616-16617.
- ⁵⁴ J. Gilot, M. M. Wienk, and R. A. J. Janssen, *Adv. Funct. Mater.*, **2010**, *20*, 3904-3911.
- ⁵⁵ W. J. E. Beek, M. M. Wienk, M. Kemerink, X. Yang, and R. A. J. Janssen, *J. Phys. Chem. B*, **2005**, *109*, 9505-9516.

Summary

In the past decade diketopyrrolopyrrole (DPP) based conjugated polymers were successfully developed for organic photovoltaic (OPV) and organic field-effect transistor (OFET) applications. The cyclic amide structures, i.e. lactams, that define DPP, are highly colored due to the push-pull interaction of the nitrogen and carbonyl moieties with the conjugated π -electrons, are electron deficient, are flat and, are likely enhancing stacking via dipole interactions. Inspired by the good performance DPP and the fundamental benefits of lactam-based materials a number of derivatives is explored in this thesis. The highlights are summarized here.

Isoindigo (II) based materials were shown to have ideal positioned energy levels for application in organic photovoltaics (OPV). Chapter 2 assesses the influence of incorporating fused aromatic ring systems (X = thiophene, thieno[3,2-*b*]thiophene, or benzo[1,2-*b*:4,5-*b'*]dithiophene) as electron rich unit in alternating copolymers with II as electron deficient unit. An increased aggregation behavior, decreased solubility, and lower molecular weight is found when increasing the fused ring system. The polymers were used as electron donor in polymer solar cells in combination with a fullerene derivative and power conversion efficiencies up to 5.6% were achieved for a polymer with thieno[3,2-*b*]thiophene, displaying the most balanced solubility; sufficiently poor to enhance π - π stacking, improve the electronic properties of the material, and generate a favorable morphology; yet sufficiently good to allow processing from hot 1,1,2,2-tetrachloroethane.

In Chapter 3 a structural derivative of isoindigo is synthesized with an electron rich thiophene moiety replacing the benzene ring enhancing intermolecular donor acceptor interactions. At the same time planarity is enhanced by elimination of the steric hindrance of the benzene proton with the carbonyl of the lactam. Copolymers alternating with combinations of benzene, thiophene, and carbazole show extremely small band gaps from 1.52 eV to 0.87 eV. The semiconducting properties of these TII copolymers were established in bottom-gate bottom-contact field-effect transistors that provide exclusively hole mobilities in the range of 10^{-3} to 10^{-2} cm²/Vs.

A series of alternating donor-acceptor polymers, consisting of diphenyl-benzodipyrrolidone (BDP) and oligothiophene (*n*T) was synthesized and used in top-gate bottom-contact organic field-effect transistors and solar cells in Chapter 4. The BDP

polymers exhibit ambipolar charge transport with high and balanced mobilities up to 0.21 cm²/Vs for holes and 0.18 cm²/Vs for electrons. Increasing the length of the oligothiophene reduces the electron mobility roughly by an order of magnitude per thiophene, but the hole mobility remains high. This behavior is explained using DFT calculations by a strong localization of the electrons on the BDP units, hence the similar low LUMO level observed for all three polymers (~-4.0 eV). For polymer:PC₇₀BM solar cells results in low LUMO – LUMO offset and only hole transfer from PC₇₀BM absorption contributing to the photocurrent and hence very low efficiency (PCE < 1%). The low LUMO and high electron mobility however make these materials suitable candidates for acceptor polymers in all polymer solar cells. A solar cell with a BDP polymer as acceptor and a DPP polymer as donor could be made but maximum efficiencies only reached 0.33%.

In Chapter 5 the influence of cross conjugation on the optical and electrochemical properties of donor-acceptor copolymers is investigated. Electron-deficient isoindigo was combined with electron-rich thiophene-flanked thienothiophenes. By substituting the isoindigo at either the 6,6' or the 5,5' positions, and using thieno[3,2-*b*]thiophene or thieno[2,3-*b*]thiophene cross conjugations were introduced. Optical and electrochemical analysis of the four combinatorial polymers reveals that introducing cross conjugation in isoindigo has only a small effect on the optical band gap and the HOMO and LUMO levels. The onset of absorption is always in the near infrared and also the electrochemical band gaps are very similar. The optical absorption spectra differ, however, strongly because cross conjugation in the isoindigo unit causes the transition to the lowest excited state to have small oscillator strength, resulting in a low-intensity absorption at the band gap. In a series of copolymers with a varying ratio of conjugated and cross-conjugated isoindigos, the intensity of the low energy electronic transition increases linearly with the fraction of conjugated units. Cross conjugation in thienothiophene exerts a different effect. It causes a moderate but distinct blue shift of the optical absorption and a deeper HOMO level. The experimental results are corroborated by DFT calculations.

Chapter 6 addresses a series of donor – acceptor copolymers based on 4,10-dialkyl-4,10-dihydrothieno[2',3':5,6]pyrido[3,4-*g*]thieno[3,2-*c*]isoquinoline-5,11-dione, a pentacyclic bislactam (PCL) acceptor. Copolymers alternating with donors that differ in size and electron rich character show wide band gaps ranging from 1.63 to 2.14 eV. Efficient wide band gap semiconducting polymers are required to further advance the performance of multi junction polymer solar cells. In combination with PC₇₀BM as electron acceptor PCL-based copolymers with thiophene, dithiophene, thieno[3,2-*b*]thiophene, or

benzo[1,2-*b*:4,5-*b'*]dithiophene, show PCEs up to $5.5 \pm 0.1\%$ in polymer solar cells. The PCE of these materials is largely limited by a relatively large energy loss ($E_g - qV_{oc}$) in the range of 0.78 to 0.97 eV. This loss seems largely redundant because solar cells with energy losses in the range of 0.6 to 0.7 eV are possible. However, when the energy loss was reduced to ~ 0.8 eV by copolymerizing PCL with benzo[*c*][1,2,5]thiadiazole, the PCE did not improve because of a reduced photocurrent.

Finally, 4*H*-thieno[3,4-*c*]pyrrole-4,6(5*H*)-dione (TPD) is investigated as a moderate electron deficient unit for wide band gap conjugated polymers in Chapter 7. In analogy with previous chapters thiophene-flanked TPD monomers were polymerized with benzene, thiophene, and thieno[3,2-*b*]thiophene in Suzuki and Stille reactions. Band gaps of 2.11 eV, 1.84 eV, and 1.86 eV were respectively obtained. The PCEs for these materials in single junction solar cells with PC₇₀BM acceptor, reached up to 4.7%, but either the open-circuit voltage (thiophene and thieno[3,2-*b*]thiophene) or the short-circuit current density (benzene and thiophene) were too low to be useful in a tandem cell. A polymer in which TPD alternates with an alkoxy substituted benzo[1,2-*b*:4,5-*b'*]dithiophene (BDT-OEH) was found to have deeper HOMO and LUMO levels and a band gap of 1.84 eV giving a PCE of 6.5% in a single junction solar cell. In combination with an efficient small band gap conjugated polymer a tandem cell was designed with an expected PCE of 9.4%. Experimentally the best tandem solar cell was found to have a PCE of 7.2%, mainly due to lower than expected current density.

Samenvatting

In het afgelopen decennium zijn geconjugeerde polymeren met diketopyrrolopyrrool (DPP) met succes ontwikkeld voor toepassingen in organische zonnecellen (*organic photovoltaic* - OPV) en organische veldafhankelijke transistoren (*organic field-effect transistors* - OFET). DPP wordt gevormd door twee cyclische amidestructuren ofwel lactams. De sterke lichtabsorptie van DPP is een gevolg van de elektronenstuwende en elektronenzuigende interacties van het stikstofatoom en de carbonylgroep met de geconjugeerde π -elektronen. De lactamring maakt DPP elektronenarm, plat en versterkt de pakking via dipoolinteracties. Geïnspireerd door de uitstekende prestaties van DPP materialen in OPV en OFET applicaties en de te verwachten fundamentele voordelen van lactams, worden een aantal structurele variaties verkend in dit proefschrift. De belangrijkste resultaten zijn hier samengevat.

Het was reeds bekend dat op isoindigo (II) gebaseerde materialen ideale energieniveaus kunnen hebben voor toepassing in OPV. Hoofdstuk 2 onderzoekt de invloed van het invoegen van gefuseerde aromatische ringen (thiofeen, thieno[3,2-*b*]thiofeen, en benzo[1,2-*b*:4,5-*b'*]dithiofeen) als elektronenrijk comonomeer in alternerende copolymeren met II als elektronenarme groep. Met het vergroten van het aantal gefuseerde ringen werden een toename van de aggregatie, een afname van de oplosbaarheid en lagere molgewichten gevonden. Deze polymeren zijn vervolgens gebruikt als elektronendonor in combinatie met een fullereen in OPV en lieten een maximale efficiëntie van 5.6% zien voor het polymeer met thieno[3,2-*b*]thiofeen. Deze is nog net genoeg oplosbaar om uit 1,1,2,2-tetrachloorethaan verwerkt te worden, de π - π stapeling te bevorderen, de elektronische eigenschappen van het materiaal te verbeteren en een goede morfologie te vormen.

In hoofdstuk 3 wordt een structuurafgeleide van isoindigo gesynthetiseerd waarbij de benzeenring is vervangen door een elektronenrijke thiofeenring die de intermoleculaire donor-acceptor interacties versterkt. Dit molecuul is platter doordat de sterische hinder tussen het waterstofatoom van de benzeenring en de carbonyl van de lactam is verdwenen. Copolymeren met combinaties van benzeen, thiofeen en carbazool laten extreem smalle bandafstanden zien van 1.52 eV tot 0.87 eV. De halfgeleidende eigenschappen van deze thienoisoindigo-copolymeren zijn vervolgens vastgesteld met

behulp van veldafhankelijke transistoren en laten gatenmobiliteiten in de orde van 10^{-3} tot 10^{-2} cm^2/Vs zien.

Een serie van alternerende donor-acceptor polymeren, bestaande uit dibenzeen-benzodipyrrolidon (BDP) en oligothiofeen (*n*T) werd gesynthetiseerd en gebruikt in organische veldeffect transistoren in hoofdstuk 4. De BDP polymeren laten een ambipolair ladingstransport zien met hoge mobiliteiten die vergelijkbaar zijn voor gaten ($0.21 \text{ cm}^2/\text{Vs}$) en elektronen ($0.18 \text{ cm}^2/\text{Vs}$). Met elke verlenging van het oligothiofeensegment neemt de elektronenmobiliteit af terwijl de gatenmobiliteit onveranderd hoog blijft. Dit gedrag wordt verklaard met behulp van DFT-berekeningen die een sterke lokalisatie van elektronendichtheid laat zien op de BDP, wat de lage en vergelijkbare LUMO-niveaus (~ -4.0 eV) van alle polymeren verklaard. Voor polymeer:PC₇₀BM zonnecellen geeft dit een laag LUMO – LUMO verschil waardoor alleen gatenoverdracht van PC₇₀BM tot stroom leidt bij belichting en dientengevolge de efficiëntie laag blijft (PCE < 1%). De lage LUMO en hoge mobiliteit voor elektronen maken deze polymeren echter geschikte kandidaten als acceptorpolymeer in polymeer:polymeer zonnecellen. Een zonnecel met een BDP-polymeer als acceptor en een DPP-polymeer als donor geeft uiteindelijk een maximale efficiëntie van 0.33%.

In hoofdstuk 5 wordt de invloed van kruisconjugatie onderzocht op de optische en elektrochemische eigenschappen van donor-acceptor polymeren. Elektronenarm isoindigo wordt hierin gecombineerd met elektronenrijk thienothiofeen. Door isoindigo op de 6,6' of de 5,5' posities te substitueren en thieno[3,2-*b*]thiofeen of thieno[2,3-*b*]thiofeen te gebruiken worden kruisconjugaties in de polymeerketen geïntroduceerd. Optische en elektrochemische analyse van de vier mogelijke combinaties van monomeren laat zien dat de introductie van kruisconjugatie slechts een minimaal effect heeft op de bandafstand en de HOMO- en LUMO-niveaus. Absorptie begint altijd in het nabije infrarood en elektrochemisch worden vergelijkbare oxidatie- en reductiepotentialen gevonden. De absorptiespectra verschillen echter wel degelijk sterk van elkaar omdat kruisconjugatie ervoor zorgt dat de overgang van de laagste aangeslagen toestand in isoindigo slechts een lage oscillatorsterkte heeft, wat resulteert in een lage absorptie rond de bandafstand. In een serie van copolymeren met variabele ratio van geconjugerd en kruisgeconjugerd isoindigo varieert de intensiteit van de laag energetische overgang lineair met de hoeveelheid geconjugerd isonindigo in het polymeer. Kruisconjugatie in de thienothiofeen sorteert een heel ander effect, het geeft een matige maar duidelijk

waarneembare blauwverschuiving in de absorptie en een dieper liggend HOMO-niveau. Deze experimentele resultaten worden ondersteund door de DFT-berekeningen.

In hoofdstuk 6 staat een serie van donor-acceptor polymeren met 4,10-dialkyl-4,10-dihydrothieno[2',3':5,6]pyrido[3,4-*g*]thieno[3,2-*c*]isoquinoline-5,11-dion, een pentacyclische bislactam acceptor (PCL), centraal. Copolymeren met alternerende donoren met verschillende grootte en elektronenrijkheid laten bandafstanden zien van 1.63 eV tot 2.14 eV. Efficiënte polymeren met brede bandafstand zijn nodig om de efficiëntie van multi-junctie zonnecellen verder te verhogen. In combinatie met PC₇₀BM als elektronenacceptor laten op PCL-gebaseerde copolymeren met thiofeen, dithiofeen, thieno[3,2-*b*]thiofeen en benzo[1,2-*b*:4,5-*b'*]dithiofeen, efficiënties zien van $5.5 \pm 0.1\%$ in OPV. De efficiëntie van deze materialen wordt beperkt door een relatief hoog energieverlies ($E_g - qV_{oc}$) van ongeveer 0.78 tot 0.97 eV. Dit verlies is grotendeels onnodig aangezien succesvolle zonnecellen met een energieverlies van 0.6 tot 0.7 eV mogelijk zijn. Met benzo[*c*][1,2,5]thiadiazol werd het energieverlies beperkt tot ~ 0.8 eV, echter ging de efficiëntie niet omhoog omdat de fotostroom flink lager werd.

In het laatste hoofdstuk 7 wordt 4*H*-thieno[3,4-*c*]pyrrool-4,6(5*H*)-dion (TPD) onderzocht als elektronenarm monomeer voor polymeren met een brede bandafstand. In analogie met vorige hoofdstukken wordt TPD geflankeerd met thiofenen en gecopolymeriseerd met thiofeen, benzeen en thieno[3,2-*b*]thiofeen met Suzuki en Stille reacties. Bandafstanden van 2.11, 1.84, and 1.86 eV zijn het resultaat. De efficiëntie van deze materialen in zonnecellen met een enkele junctie en PC₇₀BM als acceptor bereikt maximaal 4.7%, maar ofwel de open-klemspanning (thiofeen en thieno[3,2-*b*]thiofeen) ofwel de kortsluitstroombichtheid (benzeen and thiofeen) waren te laag om van toegevoegde waarde in tandem zonnecellen te zijn. Een polymeer met TPD alternerend met een alkoxy gesubstitueerde benzo[1,2-*b*:4,5-*b'*]dithiophene (BDT-OEH) liet een veel dieper HOMO- en LUMO-niveau zien bij een bandafstand van 1.84 eV wat leidde tot een efficiëntie van 6.5% in een enkele junctie zonnecel. In combinatie met een efficiënt polymeer met een smalle bandafstand lukte het om een goede tandem zonnecel te maken met een verwachte efficiëntie van 9.4%. De beste experimenteel gerealiseerde zonnecel had echter een lagere efficiëntie van 7.2%, voornamelijk door een lager dan verwachte stroombichtheid.

Curriculum Vitae

Gijs van Pruissen was born on the 17th of March 1984 in Tilburg, the Netherlands. After passing his MAVO D exams in 2002 at the Vrije School Eindhoven, the Netherlands, he obtained his VWO degree one year later at the ROC Tilburg, the Netherlands, and started to study Natural Sciences at the Radboud University in Nijmegen, the Netherlands. In 2010 he graduated *bene meritum* within the Molecular Materials group of prof.dr. Alan Rowan on the synthesis and analysis of donor-acceptor block copolymers for organic solar cells.



Within this project he visited the group of dr. Vincenzo Palermo at the Institute for Organic Synthesis and Photoreactivity of the National Research Council in Bologna, Italy, where he investigated self assembled systems with porphyrin trimers and fullerenes. From 2010 he started a PhD project at the Eindhoven University of Technology, the Netherlands, in the Molecular Materials and Nanosystems group of prof.dr.ir. René Janssen on the synthesis of lactam based π -conjugated polymers for opto-electronic applications of which the results are presented in this dissertation.

List of publications

Peer-reviewed publications:

Cross-conjugation in donor-acceptor conjugated polymers as a new design principle to independently tune absorption and frontier orbital levels

Gijs W.P. van Pruissen, Jeroen Brebels, Koen H. Hendriks, Martijn M. Wienk, and René A.J. Janssen, manuscript in preparation

Homo-coupling defects in diketopyrrolopyrrole based co-polymers and their effect on photovoltaic performance

Koen H. Hendriks, Weiwei Li, Gaël H. L. Heintges, Gijs W. P. van Pruissen, Martijn M. Wienk, and René A. J. Janssen, *J. Am. Chem. Soc.*, **2014**, *136*, 11128-11133.

High balanced ambipolar charge carrier mobility in benzodipyrrolidone conjugated polymers

Gijs W. P. van Pruissen, Evgeny A. Pidko, Martijn M. Wienk and René A. J. Janssen, *J. Mater. Chem. C*, **2014**, *2*, 731-735.

Superheated high-temperature size-exclusion chromatography with chloroform as the mobile phase for π -conjugated polymers

Xianwen Lou, Joost L. J. van Dongen, Yasmine Braeken, Jeroen Brebels, Gijs W. P. van Pruissen, Weiwei Li, Martijn M. Wienk and René A. J. Janssen, *Polym. Chem.*, **2014**, *5*, 558-561.

Wide band gap diketopyrrolopyrrole-based conjugated polymers incorporating biphenyl units applied in polymer solar cells

Weiwei Li, Alice Furlan, W. S. Christian Roelofs, Koen H. Hendriks, Gijs W. P. van Pruissen, Martijn M. Wienk, and René A. J. Janssen, *Chem. Commun.*, **2014**, *50*, 679-681.

Synthesis and properties of small band gap thienoisindigo based conjugated polymers

Gijs W. P. Van Pruissen, Fatemeh Gholamrezaie, Martijn M. Wienk and René A. J. Janssen, *J. Mater. Chem.*, **2012**, 22, 20387-20393.

Direct backbone structure determination of polyisocyanodipeptide using solid-state nuclear magnetic resonance

Chandrakala M. Gowda, Ernst R. H. van Eck, Arend M. van Buul, Erik Schwartz, Gijsbrecht W. P. van Pruissen, Jeroen J. L. M. Cornelissen, Alan E. Rowan, Roeland J. M. Nolte, and Arno P. M. Kentgens, *Macromolecules*, **2012**, 45, 2209-2218.

Poster presentations:

Amide and imide derived acceptors for conjugated D-A polymers in OPV's

Gijs W.P. van Pruissen, Yasmine Braeken, Jeroen Brebels, Martijn M. Wienk, and René A.J. Janssen, *Hybrid and Organic Photovoltaics Conference*, **2013**, Sevilla, Spain

New DPP derived acceptors for conjugated D-A polymers in OPV's

Gijs W.P. van Pruissen, Martijn M. Wienk, and René A.J. Janssen, *VIII International Krutyn Summer School 2011, Frontiers in Organic, Dye-sensitized and Hybrid Solar Cells*, **2011**, Krutyn, Poland

New DPP derived acceptors for conjugated D-A polymers in OPV's

Gijs W.P. van Pruissen, Martijn M. Wienk, and René A.J. Janssen, *Photovoltaics at the Nanoscale Conference*, **2011**, Hasselt, Belgium

Dankwoord

Hier ligt mijn proefschrift dan, glanzend, af, en vooral op tijd te zijn. Dat laatste heeft mij, en wellicht meer mensen, toch verbaasd. Ik had dat ook zeker niet alleen kunnen doen en wil de mensen die direct en indirect aan dit resultaat hebben bijgedragen daarom graag bedanken.

Het streven naar mijn ideaalbeeld van overvloedige en goedkope zonne-energie heeft de afgelopen jaren mijn keuzes voor studie en deze promotie bepaald. De passie voor duurzaamheid heb ik voor een belangrijk deel te danken aan mijn onlangs overleden oom, Henk Kuiper. Hij kon je als geen ander de schoonheid van de natuur in alle eenvoud en kwetsbaarheid laten zien en zich onbaatzuchtig inzetten voor het behoud ervan. Zijn aanstekelijke idealisme is op mij overgeslagen waarvoor ik hem altijd dankbaar zal zijn.

Ik wil graag mijn promotor en copromotor bedanken voor het vertrouwen dat ze me de afgelopen vier jaar hebben gegeven. René, bedankt voor de kans, de ideeën, de helpende hand en het dwingende duwtje in de rug op de beslissende momenten. Zonder franje leid jij een groep waarin iedereen, ondanks je volle agenda, het gevoel heeft de aandacht en tijd te krijgen die hij/zij nodig heeft. Mijn bewondering voor je kan ik het best omschrijven met je eigen stopwoordje: Halleluja! Halleluja voor je wetenschappelijke kennis én je mensenkennis, je geheugen, je correcties en je antwoorden op *referees*. Maar vooral halleluja voor de vanzelfsprekendheid en het plezier waarmee je elke dag weer bergen werk verzet. Ik had me geen betere promotor kunnen wensen. Martijn bedankt voor je heerlijke realiteitszin. Jij wist altijd alles terug te brengen tot de essentie. Eerst begrijpen wat je doet, om dan kleine stapjes vooruit te kunnen zetten, het liefst één voor één. Nieuwe meetresultaten kon ik met jou altijd verklaren en in retrospectief had ik de afgelopen jaren eigenlijk nog veel meer van je kennis en ervaring gebruik willen maken.

I would like to thank my defense committee members Martin Heeney, Alan Rowan, Dirk Vanderzande, Albert Schenning and Jef Vekemans for their proof reading, useful comments, and final approval of this thesis and for participating in the defense ceremony.

Een deel van dit proefschrift bevat werk van de twee masterstudenten die ik gedurende mijn promotie heb mogen begeleiden. Jeroen, je werk aan isoindigo's met grotere π -geconjugeerde systemen was een flinke synthetische uitdaging. Die ben je aangegaan en heeft met succes tot de synthese van (semi)naftaleen-isoindigo geleid. Die

hebben het proefschrift uiteindelijk niet gehaald maar hoofdstuk 2 rust zwaar op isoindigo polymeren van jouw hand met prachtige efficiëntie tot 5.5%, terecht iets om trots op te zijn. Bedankt voor je inzet en heel veel succes met je eigen promotietraject in Hasselt. Yasmine, jouw werk aan TPD is voor een deel verwerkt in hoofdstuk 7. Ondanks dat we de nodige tegenslagen hadden met moeilijke monomeren of dat goede ideeën een week later door anderen gepubliceerd werden, heb ik nooit een onvertogen woord over je lippen horen komen. Je hebt zelfstandig en consciëntieus doorgewerkt met als resultaat een mooie serie polymeren met interessante eigenschappen en een goede efficiëntie van 4.8%. Ook jij bedankt voor je toewijding en harde werken, ik wens je heel veel succes met je eigen promotietraject in Hasselt.

Met sommige collega's heb ik de afgelopen jaren nauw samengewerkt. Koen, vanuit Nijmegen hebben we geheel toevallig bijna identieke paden bewandeld. Bedankt voor het samen optrekken op conferenties, samen ideeën ontwikkelen voor superefficiënte zonnecellen en het delen van kennis en materialen. Wie weet waar onze paden elkaar ooit weer kruisen. Weiwei, it was a pleasure working with you in the lab. Besides your incredible speed in making and testing new materials you are also a very nice person. Thank you very much for your help and good collaboration, I am sure you will make a good professor in Beijing and I hope to visit you someday. Mindaugas, I want to thank you for the many useful discussions we had, both on scientific and other topics. Hopefully we still get to publish the work on Pechmann dyes. Alice, thank you for your cheerful vibe in the office and off course your work on the tandem solar cells of chapter 7. Hans, bedankt voor de prachtige TEM plaatjes in hoofdstuk 6. Ik ben blij dat we door jouw onderzoek ook eindelijk echt zinnige dingen over morfologie kunnen zeggen.

My publications would have never been possible without the help of several people. Evgeny, I want to thank you for the initial DFT calculations which are in chapter 4, later you taught me how to perform my own calculations. It has been very useful throughout my thesis. Fatemeh, thank you for introducing me to OFET device making and measuring as many of my new materials proved to be more interesting in OFET rather than OPV. Also Christian and Youngyu deserve credits for that. Lou and Ralf, thank you for all the tedious GPC and Maldi measurements, even when it was on short notice and for difficult analyses. It was a pleasure working with you. Stefan, stille kracht met een geweldige stem en kennis, bedankt voor de inzichtelijke uitleg over symmetrieën, transitieën en het proeflezen en becommentariëren van mijn proefschrift.

My office mates during the past four years: Bram, Dominique, Marie-France, Stefan O, Daniele, Dhritiman, Rateesh, Wenshan, Weiwei, Alice, Robin, Gael, Andreanne, Ruurd and Dario. Thank you for making the biggest office not only a place to work but also a place with fun conversation where the strangest things could happen: movie watching, juggling and beer drinking to name a few.

My other M2N colleagues Veronique, Sandra, Serkan, Benjamin, Mike, Chunhui, Fallon, Jolanda M, Martina and Nora, as well as Bram P, Daan, and Janus and all the SMO/MST colleagues, I would like to thank you for the great atmosphere in the lab and creating this top level scientific environment. Jolanda S, jou wil ik apart bedanken voor onze samenwerking bij het organiseren van vier Nolte-Meijer Cups en de gezamenlijke interesse in volleybal, waarbij je ook buiten werk om met interesse mijn prestaties volgde.

Het V-woord is gevallen. In de afgelopen achttien jaar heb ik veel tijd besteed aan volleyballen, zowel op het strand als in de zaal. Daarbij heb ik een ongelooflijk grote groep mensen leren kennen die het tot een waar feest hebben gemaakt: Erik en Wietske, Imke, Manon, Joop, Renske, Dennis en Manon, Lotte, David en Marloes, Michiel, Sue, Niels, Sander, Benno, Jaapjan, Torsten en Wieneke. Maar ook mijn oud-studiegenootjes Isabel, Steven, Tim, Maarten, Jur, Yvonne, Inge, Tanneke, Bram en Nan. Ik heb het velen van jullie vast al eens persoonlijk verteld, maar ik prijs me gelukkig zulke lieve vrienden te hebben.

Rogier, het bovenstaande geldt natuurlijk ook voor jou, met het verschil dat wij samen Pobeka Solar hebben opgericht. Zeker niet altijd eenvoudig (vooral niet tijdens het schrijven van een proefschrift), maar wel ontzettend tof om te doen. Zowel als vriend en als zakenpartner ben je goud waard. Het zou mooi zijn als we dat nu ook echt gaan verdienen.

Lieve Papa en Mama, jullie boven al, maar ook Anna, Willem, Sebastiaan, Elisabeth en Thijmen, bedankt voor de onbezorgde jeugd waarin jullie er altijd voor me waren. Jullie onvoorwaardelijke steun heeft mij altijd het gevoel gegeven dat ik voor het geluk in de wieg gelegd ben en de hele wereld aan kan. Een gevoel dat ik met liefde aan ieder van jullie wil geven als het in mijn macht ligt. Ik hou van jullie.

Lieve Myrte, eigenlijk komt bijna al het voorgaande samen in jou. Je steunt me in mijn idealen, brengt structuur in mijn chaos en helpt me als dat nodig is. Ik hou van onze simpele dingen samen, maar ook van de avonturen, samen in de zomer het strand op, samen mooie reizen maken, letterlijk mijn grenzen verleggen. En welke richting de reis vanaf nu ook gaat, ik weet zeker dat ik hem samen met jou wil maken. Niet alleen ben je mijn beste vriend maar bovenal de liefde van mijn leven. Met jou wil ik oud worden!

